UNIVERSIDAD DE GRANADA
FACULTAD DE CIENCIAS
DEPARTAMENTO DE MICROBIOLOGÍA

APLICACIÓN DE TECNOLOGÍAS ÓMICAS PARA LA CARACTERIZACIÓN CELULAR Y MOLECULAR DE LA RESISTENCIA MICROBIANA A URANIO Y SELENIO EN LA CEPA *STENOTROPHOMONAS BENTONITICA* BII-R7

APPLICATION OF OMICS TECHNOLOGIES FOR CELLULAR AND MOLECULAR CHARACTERIZATION OF MICROBIAL RESISTANCE TO URANIUM AND SELENIUM IN THE STRAIN *STENOTROPHOMONAS BENTONITICA* BII-R7

Programa de Doctorado en Biología Fundamental y de Sistemas

María Pinel Cabello

TESIS DOCTORAL

Granada, 2021

Editor: Universidad de Granada. Tesis Doctorales
Autor: María Pinel Cabello
ISBN: 978-84-1306-888-6
URI: http://hdl.handle.net/10481/69076

Esta Tesis Doctoral ha sido realizada en el Departamento de Microbiología (Facultad de Ciencias) de la Universidad de Granada durante los años 2016-2021 dentro del grupo de investigación Mixobacterias (BIO 103).

Para realizar este trabajo la doctoranda disfrutó de una beca F.P.U (Formación de Profesorado Universitario) con referencia FPU 15/04284 del Ministerio de Ciencia, Innovación y Universidades.

Además, esta Tesis Doctoral también ha sido financiada a través del proyecto europeo MIND (*Microbiology In Nuclear Waste Disposal),* financiado por el programa *"Euroatom research and training program 2014-2018 under Grant Agreement no. 661880 (H2020 Programme)*, con el Dr. Mohamed Larbi Merroun como investigador principal de dicho proyecto en la Universidad de Granada. La realización de este trabajo también ha recibido financiación del *"European Regional Development Fund (ERDF)-co-financed Grant"* CGL2014-59616-R y RTI2018.101548.B.I00 del Ministerio de Ciencia e Innovación.

El doctorando también ha disfrutado de dos Ayudas a la movilidad para estancias breves y traslados temporales FPU (EST 17/00739 y EST 18/00610) del Ministerio de Ciencia, Innovación y Universidades para la realización de estancias en centros de investigación extranjeros:

- Estancia breve de tres meses en el Hospital de la Universidad Otto-von-Guericke en la ciudad de Magdeburg (Alemania). Fechas de la estancia: 20/09/2018-20/12/2018.
- Estancia breve de tres meses en el "*Institute de Biosciences et Biotechnologies"* de la *"Commissariat à l'Energie Atomique et aux Energies Alternatives"* (CEA-Cadarache) en Francia. Fechas de la estancia: 20/09/2019-19/12/2019.

Los resultados obtenidos a lo largo de esta Tesis Doctoral han sido publicados o están siendo preparados para su publicación como artículos científicos en revistas de impacto.

Artículos científicos publicados o en proceso de publicación con los resultados de esta Tesis Doctoral:

- **Pinel-Cabello M.,** Jroundi F., López-Fernández M., Geffers R., Jarek M., Jauregui R., Link A., Vílchez-Vargas R., Merroun M.L. 2021.Multysistem combined uranium resistance mechanisms and bioremediation potential of *Stenotrophomonas bentonitica* BII-R7: Transcriptomics and microscopic study. *J Hazard Materials*. 403, 123858.

- **Pinel-Cabello M.,** Chapon, V., Ruiz-Fresneda M.A., Alpha-Bazin B., Berthomieu C., Armengaud J., Merroun M.L. Delineation of cellular stages and identification of key proteins for reduction and biotransformation of Se(IV) in *Stenotrophomonas bentonitica* BII-R7. *J Hazard Materials*. En revision.

Parte de los resultados obtenidos también han sido publicados en congresos nacionales e internacionales:

- **Pinel-Cabello M.** [*]**,** Chiguen-nou I., Martín-Sánchez I., Merroun M.L. Comunicación oral. Mecanismos moleculares y genéticos de resistencia microbiana a metales pesados. III Jornadas Doctorales de la Universidad de Murcia, Murcia, España, 2017.

- **Pinel-Cabello M.,** [*] Merroun M.L. Comunicación oral. Mecanismos moleculares y genéticos de resistencia microbiana a metales pesados. II Congreso de Jóvenes Químicos y Bioquímicos Terapéuticos "II QuimBioQuim", Universidad Rey Juan Carlos, Móstoles, España, 2017.

- **Pinel-Cabello M.** [*]**,** Jroundi F., Sánchez-Castro I., Merroun M.L. Comunicación oral. Biomineralización de uranio (VI) por *Stenotrophomonas bentonitica* sp. nov BII-R7. III Jornadas/I Congreso Nacional de

Investigadores en Formación: Fomentando la Interdisciplinariedad (JIFFI). Universidad de Granada, Granada, España, 2018.

- Sánchez-Castro I., Martínez-Rodríguez P*., **Pinel-Cabello M.,** Bosch-Estévez G., Phrommavanh V., Descostes M., Merroun M.L. Póster. Bacterial strain *Microbacterium* sp. Be9: variable behaviour in presence of uranium. Geomicrobiology Network. University of Strathclyde, Glasgow, Escocia. 2018.

- Sánchez-Castro I. *, Martínez-Rodríguez P., **Pinel-Cabello M.,** Bosch-Estévez G., Phrommavanh V., Descostes M., Merroun M.L. Póster. Versatile behaviour of bacterial strain *Microbacterium* sp. Be9 in presence of uranium and its bioremediation potential. 7th European Bioremediation Conference/11th International Society for Environmental Biotechnology Conference. Technical University of Crete, Grecia. 2018

- **Pinel-Cabello M. *,** Sánchez-Castro I., Merroun M.L. Póster. Removal of uranium induced by phosphatase activity in *S. bentonitica* sp. nov BII-R7. 17th International Symposium on Microbial Ecology. Leipzig, Alemania. 2018.

- **Pinel-Cabello M. *,** Vílchez-Vargas R., Jroundi F., Geffers R., Jarek M., Jauregui R., Merroun M.L. Comunicación oral. Response of *S. bentonitica* BII-R7 to uranium: transcriptomic and microscopic studies. 7th International Symposium on Metallomics. Varsovia, Polonia. 2019.

- Sánchez-Castro I. *, Martínez-Rodríguez P., **Pinel-Cabello M.,** Bosch-Estévez G., Descostes M., Merroun M.L. Póster. Effect of Be9, a microbial strain isolated from mining porewaters, on the biogeochemical cycle of uranium. 8th Congress of European Microbiologists FEMS2019. Glasgow, Escocia. 2019.

- **Pinel-Cabello M. *,** Vílchez-Vargas R., Jroundi F., López-Fernández M., Geffers R., Jarek M., Jauregui R., Merroun M.L. Comunicación oral.

Transcriptomic studies of bacterial tolerance to uranium. Goldschmidt 2019. Barcelona, España. 2019.

*Conferenciante

RELACIÓN DE ACRÓNIMOS

BSA: Bovine Serum Albumin

MIC: Minimal Inhibitory Concentration

EDX: Energy Dispersive X-Ray

LPS: Lipopolysaccharide

ESEM: Environmental Scanning Electron Microscopy

FFT: Fast Fourier Transform

STEM/HAADF: High Angle Annular Dark Field Scanning Transmission Electron Microscopy

ICP-MS: Inductively Coupled Plasm-Mass Spectrometry

LB: Luria-Bertani

SAED: Selected-Area Electron Difraction

TRLFS: Time-Resolved Laser-induced Fluorescence Spectroscopy

TMM: Tris Minimal Medium

G2P: Glycerol-2-phosphate

4-MUB-P: 4 methylumbelliferone phosphate di-Na salt

MOPS: 3-(*N*-morpholino)propanesulfonic acid

IAEA: International Atomic Energy Agency

TPM: Transcripts per million

NCBI: National Centro for Biotechnology Information

BLAST: Basic Local Alignment Search Tool

ENA: European Nucleotide Archive

NGS: Next Generation Sequencing

DNA: Deoxyribonucleic acid

mRNA: Messenger ribonucleic acid

rRNA: Ribosomal ribonucleic acid

SDS-PAGE: Sodium dodecyl sulfate polyacrylamide gel electrophoresis

NanoLC-MS/MS: Nanoscale Liquid Chromatography coupled to tandem Mass Spectrometry

MS/MS: Mass Spectrometry

RND: Resistance-nodulation-cell division

ABC: ATP-binding cassette

GSH: Glutathione

GR: Glutathione reductase

GS: Glutathione synthetase

OYE: Old yellow enzymes

ROS: Reactive oxygen species

TEM: Transmission Electron Microscopy

RAST: Rapid Annotation using the SEED-based method of Subsystem Technology

ÍNDICE

RESUMEN

La creciente demanda de recursos y la rápida industrialización durante las últimas décadas ha provocado la aparición de metales pesados a concentraciones tóxicas en el medio ambiente a escala global. Estos compuestos inorgánicos no pueden degradarse ni química ni biológicamente, lo que los convierte en contaminantes persistentes de alto riesgo acumulándose, tanto en el ambiente como en los organismos, a través de la cadena trófica. La gravedad del problema se ve incrementado con el vertido de radionúclidos presentes en los residuos radiactivos, cuya peligrosidad procede de su toxicidad tanto química como radiológica. Entre los residuos radiactivos, destacan los de alta actividad, ya que contienen radioisótopos que requieren hasta miles de años para que la radiación que emiten decaiga hasta niveles equiparables a los que encontramos de manera natural en el ambiente.

Entre los metales pesados y radionúclidos destacan el uranio (U) y el selenio (Se), ya que ambos se encuentran formando parte de productos de desecho de diversas industrias. Además, muchos de estos procesos industriales dependen de la extracción minera de estos elementos, lo que lleva a su acumulación en el ambiente. Su toxicidad depende, entre otros factores, de la especiación química en la que se encuentren. En la naturaleza, el U aparece principalmente en su forma oxidada y tóxica U(VI), altamente soluble y móvil. Por otro lado, el Se se encuentra como Se(VI), Se(IV), Se(0) y Se(-II), siendo las especies de Se(VI) y Se(IV) las que presentan mayor toxicidad.

Las técnicas de remediación actuales se basan en métodos físicos y químicos, que a menudo son costosos, difíciles de aplicar a gran escala y conllevan la generación de productos secundarios indeseados con consecuencias medioambientales. El biorremedio es una estrategia alternativa a la metodología tradicional, basada en el uso de sistemas biológicos para eliminar o transformar contaminantes, ya sean tanto orgánicos como inorgánicos. Es bien sabido que los microorganismos son capaces de tolerar e incluso crecer en presencia de altas concentraciones de metales pesados y radionúclidos, a través de mecanismos de interacción, tales como biosorción, biotransformación (oxidación/reducción), bioacumulación y/o biomineralización. Dichos mecanismos le permiten atenuar los daños ocasionados por la exposición al metal tóxico, mediante su inmovilización en una forma menos soluble y, por tanto, menos biodisponible, lo que los convierte en herramientas interesantes desde el punto de vista del biorremedio. Además, el uso de microorganismos como agentes de biorremedio presenta una serie de ventajas

que permiten el desarrollo de estrategias respetuosas con el medio ambiente y de bajo coste económico. Para ello, los microorganismos deben cumplir tres criterios interrelacionados entre sí: (1) presentar una elevada resistencia a metales pesados y/o radionúclidos, (2) poseer una alta diversidad metabólica, y, por tanto, (3) que lleven a cabo mecanismos de interacción que den lugar a la formación de especies inmóviles y menos tóxicas del metal. La aplicación segura y eficiente de esta alternativa requiere conocer en profundidad las bases de los mecanismos de resistencia y los factores que los afectan.

Esta Tesis Doctoral tiene como objetivo la caracterización de los mecanismos de resistencia llevados a cabo por la cepa *Stenotrophomonas benotnitica* BII-R7 en respuesta a U y Se a nivel genético y molecular. La capacidad de esta cepa para tolerar altas concentraciones de U y Se se ha demostrado anteriormente, y el conocimiento de la respuesta celular ante estos elementos permite la evaluación de su potencial como agente de biorremedio.

En el primer capítulo, mediante el uso de técnicas analíticas, microscópicas y espectroscópicas se consiguió determinar del tipo de mecanismo de interacción establecida entre la cepa objeto de estudio y el U(VI). El conjunto de análisis demostró la alta capacidad de BII-R7 de eliminar el U(VI) soluble en el medio, encontrando además diferencias según el pH y el estado fisiológico de las células. Así, los mayores porcentajes de eliminación se obtuvieron a pH neutro, especialmente en condiciones de crecimiento, donde además el proceso va acompañado de la liberación paulatina de fosfato inorgánico (P_i) como consecuencia de la actividad fosfatasa durante las primeras horas de incubación. En ausencia de crecimiento, estudios espectroscópicos (*time-resolved laser-induced fluorescence spectroscopy*, TRLFS) revelaron la formación de complejos de U(VI) con fosfatos orgánicos a pH 5.5, mientras que a pH 7 los resultados sugieren un proceso previo de biosorción del U(VI) en la pared celular a través de fosfatos orgánicos, seguido de su biomineralización al interaccionar con P_i procedente de la actividad de enzimas fosfatasa, dando lugar a fases minerales similares a meta-autunita. El análisis microscópico mediante STEM/HAADF (*high-angle anular dark field scanning transmission electron microscopy*) confirmó este proceso al demostrar la presencia de acúmulos extracelulares y en la superficie celular compuestos de U y P.

En el siguiente paso (capítulo II), se determinó la respuesta celular de *S. bentonitica* al U(VI) mediante estudios transcriptómicos, aportando conocimiento acerca de los mecanismos de resistencia a nivel celular y molecular. El metal provocó la

extensión de la fase de adaptación, en la cual las células se encontraban muy activas metabólicamente, poniendo en marcha diversos mecanismos que coexisten para contribuir al desarrollo de tolerancia. El análisis del transcriptoma revela una alteración de la homeostasis de la membrana, al activarse diversos mecanismos de señalización y proteínas de membrana para intentar restaurarla. Dicha alteración podría provocar cambios en la permeabilidad de la membrana, permitiendo la entrada de iones del metal, por lo que el incremento en la expresión de transportadores como sistemas RND (*resistance-nodulation-cell division*) podría eliminar el U(VI) que ha alcanzado el citoplasma. De forma simultánea, la cepa es capaz de incrementar la cantidad de ligandos para secuestrar el metal a nivel de la membrana, mediante la síntesis de estructuras como LPS. La inducción de la expresión de enzimas fosfatasa tanto ácida (PAP2) como alcalina (fosfoetanolamina transferasa) concuerdan con los datos de las pruebas bioquímicas y de liberación de P_i al medio. Estas observaciones, junto con los precipitados observados mediante STEM/HAADF, sugieren de nuevo un mecanismo bifásico de biosorción rápida del U(VI) a nivel de la membrana celular, seguido de la biomineralización por la acción de enzimas fosfatasa.

En conjunto, estos estudios ponen de manifiesto el impacto que tienen los factores fisiológicos y físico-químicos en el rendimiento de los procesos de interacción, así como la capacidad de *S. bentonitica* de llevar a cabo la biomineralización de fosfatos de U(VI) como mecanismo de resistencia frente a este metal pesado. La formación de una fase mineral como meta-autunita, estable durante largos periodos de tiempo, enfatiza el potencial que posee la cepa de estudio como agente de biorremedio de ambientes contaminados con U(VI).

También se abordó el estudio de los mecanismos celulares de resistencia en presencia de Se. Basados en investigaciones previas, que pusieron de manifiesto la capacidad de reducir tanto Se(VI) como Se(IV) por parte de *S. bentonitica*, estudios proteómicos y transcriptómicos fueron llevados a cabo para un conocimiento de las interacciones en mayor profundidad. Al igual que en el caso del U(VI), la prolongación de la fase de adaptación, junto con la mayor actividad metabólica, indican la activación de mecanismos para hacer frente a la toxicidad tanto del Se(VI) como del Se(IV). En ambos casos, además, el metal también provoca daños a nivel de la membrana, como indica la inducción de proteínas tales como la lipocalina Bcl o la bactofilina CcmA, ocasionados probablemente al interaccionar con la misma.

La observación de nanoesferas amorfas (a-Se) intracelulares mediante STEM/HAADF indica que la reducción de Se(IV) tiene lugar en el citoplasma, siendo por tanto la captación del metaloide un paso previo necesario. En el caso de *S. bentonitica*, dicha captación podría tener lugar mediante sistemas de transporte como la lipoproteína de tipo NodT, el transportador de magnesio MgtE o la porina OprP. Una vez en el citoplasma, enzimas como la 3-oxoacil-ACP reductasa FabG o los grupos tiol, especialmente el glutatión (GSH), llevarían a cabo la reducción a Se(0). Simultáneamente, el pool de glutatión reducido se repone por la acción de la glutamato—cisteína ligasa, glutatión reductasa (GR) y glutatión sintetasa (GS). Además del GSH, enzimas como la tioredoxina reductasa llevan a cabo un paso más de reducción de parte del Se(0) formado a Se(-II), que, junto con la actividad de metiltransferasas, da lugar a la formación de especies volátiles de dimetil diseleniuro (DMDSe) y dimetil selenil disulfuro (DMSeDS), previamente detectadas en esta cepa. Tanto la reducción como la presencia de las nanoesferas provocan un incremento en la producción de especies reactivas de oxígeno, activando mecanismos enzimáticos para mitigar los daños del estrés oxidativo. Las nanoesferas amorfas aumentarían de tamaño hasta salir al espacio extracelular mediante lisis. Los análisis microscópicos y estructurales (*Fast Fourier Transform*, FTT, *selected-area electron diffraction*, SAED) confirman un proceso de biotransformación de a-Se intracelulares hacia nanoestructuras cristalinas de *t*-Se extracelulares de diferentes tamaños y formas, pasando por una fase intermedia de *m*-Se. La presencia de S en estas estructuras sugiere la posible influencia de grupos tiol, que se adhieren probablemente durante el proceso de reducción y/o lisis celular.

En el caso del Se(VI), el transcriptoma de BII-R7 reveló una gran inducción génica ante la exposición a concentraciones del mismo de 50 mM. Los resultados indican que la captación del metaloide en este estado de oxidación podría tener lugar a través de la lipoproteína NodT, y de los transportadores de nitrato/nitrito NarK y/o de grupos tiol CydD. En la fase de adaptación, enzimas con actividad oxidorreductasa llevarían a cabo la reducción en el citoplasma. El operón *ars* también podría estar implicado en la reducción a Se(VI) mediante ArsC, así como del transporte del Se(IV) formado al exterior de la célula a través de ArsB. Por otro lado, la enzima nitrato reductasa respiratoria parece ser la implicada en el proceso de reducción a Se(VI) una vez se alcanza el crecimiento exponencial. Al igual que el Se(IV), se produce un incremento del estrés oxidativo, que activa mecanismos de detoxificación de especies reactivas de oxígeno, así como de enzimas que apoyan esta actividad oxidante. Sin embargo, la ausencia de cambio de color

en los cultivos indica que la reducción a Se(0) en esta concentración no es significativa, o bien la formación de especies biometiladas volátiles.

La elevada toxicidad causada por la presencia de 200 mM de Se(VI) provocó la disminución de la expresión génica respecto a los tratamientos control. No obstante, los análisis microscópicos (*environmental scanning electron microscopy*, ESEM y STEM/HAADF) mostraron la formación de nanotubos de Se(0) intracelulares y embebidos en la matriz de estructuras flagelares tras 24 h de incubación. La caracterización estructural (FFT y SAED) de los nanotubos indicaron que, al igual que las observadas en presencia de Se(IV), se trataban de *m*-Se y *t*-Se, encontrándose también la acumulación de S en las mismas mediante EDX. Sin embargo, los resultados sugieren un proceso de biotransformación totalmente distinto al propuesto para el Se(IV), ya que, en el caso del Se(VI), la agregación y síntesis de nanoestructuras parece ocurrir con mayor rapidez, y sin llegar a provocar la lisis de la célula. Estudios posteriores a tiempos más cortos de incubación son necesarios para esclarecer las posibles fases de la biotransformación hasta nanotubos. Hasta donde nosotros conocemos, la formación de nanotubos de *t*-Se a partir de Se(VI) ha sido descrita en este estudio por primera vez.

En conjunto, estos hallazgos sugieren que la resistencia de *S. bentonitica* a Se(IV) y Se(VI) se basa en tres mecanismos celulares concurrentes: la reducción de las formas reducidas del metaloide, la mitigación de los daños provocados por el estrés oxidativo, y la formación de nanoestructuras de *m*-Se y *t*-Se. Dada la menor toxicidad y movilidad de las especies de *t*-Se, estos estudios demuestran la capacidad de *S. bentonitica* para disminuir de forma eficiente las especies tóxicas del metaloide, y, por tanto, los efectos perjudiciales que conlleva su presencia en el medio ambiente.

Los estudios llevados a cabo en esta Tesis Doctoral revelan genes y proteínas clave en los procesos de resistencia microbiana frente a metales pesados y radionúclidos, proporcionando puntos de partida para el desarrollo de técnicas efectivas de bioremedio, así como una alternativa ecológica al desarrollo de nanoestructuras con fines industriales.

SUMMARY

The increasing demand of resources and the rapid industrialization during the last decades has led to the emergence of toxic concentrations of heavy metals in the environment at a global scale. Since these inorganic compounds cannot be neither chemically nor biologically degraded, they are extremely persistent contaminants of high risk due to their accumulation both in the environment and the inhabiting organism, through the food chain. The problem is exacerbated with the discharge of radionuclides from radioactive wastes, which cause detrimental effects arising from their chemical and radiological toxicity. The high-level radioactive wastes are of particular interest since they are composed by radioisotopes that requires even thousands of years until their radioactivity decrease until natural levels.

Among the most environmentally hazardous heavy metals and radionuclides, it is worth to mention uranium (U) and selenium (Se), as they appear as part of the waste products of several industrial activities. Furthermore, many industrial processes rely on the mining of these elements, which leads to their accumulation in the environment. Their toxicity depends on the chemical species, among other factors. In nature, U can be found mainly in its oxidized and toxic form U(VI), which is highly soluble and mobile. In case Se, it appears at Se(VI), Se(IV), Se(0) and Se(-II), being Se(VI) and Se(IV) the most toxic species.

Current remediation techniques are based on physical and chemical methods, that are often expensive, hardly applied on a large scale and produce undesirable secondary products with environmental impact. Bioremediation is an alternative strategy to the conventional methodology based on the use of biological systems to remove o transform both organic and inorganic contaminants. It is well known that microorganisms are able to tolerate and even grow in presence of high concentration of toxic heavy metals and radionuclides, due to the presence of interaction mechanisms such as biosorption, biotransformation (oxidation/reduction), bioaccumulation and/or biomineralization. These mechanisms enable the mitigation of the damage caused by the toxic metal exposure, through its immobilization into a less soluble, and hence, less available form. This feature makes the microbes an interesting tool from a bioremediation point of view. In addition, the use of microorganism as bioremediation agents offers a number of benefits that lead to the development of eco-friendly and cost-effective strategies. For this purpose, microorganisms must meet three main criteria: (1) to show high heavy metal

and/or radionuclide resistance, (2) to have high metabolic diversity, and hence, (3) to perform interaction mechanisms that result in the formation of immobile and less toxic metal species. To be safe and efficiently applied, this alternative requires in-depth knowledge of the bases of the resistance mechanisms, as well as the factors influencing the process.

The objective of this Doctoral Thesis is the characterization of the resistance mechanisms performed by the strain *Stenotrophomonas bentonitica* BII-R7 in response to U and Se at genetic and molecular levels. The capability of the strain to resist high concentration of U and Se has been previously demonstrated, and the knowledge of the cellular response against these elements allow us to evaluate the its potential as bioremediation agent.

In the first chapter, the use of analytic, microscopic and spectroscopic techniques enabled the determination of the type of interaction mechanism established between the studied strain and U(VI). The combination of the analyses showed the high ability of BII-R7 to remove the soluble U(VI) from the media, finding differences as function of pH and physiological state of the cells. Hence, the highest U(VI) removal efficiencies were observed at neutral pH, specifically under growing-conditions, which, moreover, the process is accompanied by the gradual release of inorganic phosphate (P_i) as a result of the activity of phosphatase enzymes during the first hours of incubation. Under non-growing conditions, spectroscopic studies (*time-resolved laser-induced fluorescence spectroscopy*, TRLFS) revealed the formation of U(VI)-organic phosphates complexes at pH 5.5, while results obtained at pH 7 suggest a previous biosorption process of U(VI) in the organic phosphates of the bacterial cell wall, followed by the biomineralization through the interaction with P_i from the phosphatase activity, resulting in mineral phases similar to meta-autunite. Microscopic analysis by STEM/HAADF (*high-angle anular dark field scanning transmission electron microscopy*) showed the presence of U-P accumulates located extracellularly and at the cell surface.

In the next step (chapter II), cellular response of *S. bentonitica* to U(VI) was determined by transcriptomics analyses, providing information about the resistance mechanisms at molecular and cellular levels. The metal triggered an elongation of the lag phase, in which high metabolic activity was detected in the cells, activating co-existing mechanisms that contribute for the development of tolerance to U(VI). The transcriptome evinces an alteration on membrane homeostasis, as diverse signaling mechanisms and membrane proteins to restore the damage were found. Such alteration could result in

changes of membrane permeability, allowing the entrance of metal ions. Therefore, the up-regulation of transporters such as RND (*resistance-nodulation-cell division*) could generate an efflux of the U(VI) that reached the cytoplasm. Simultaneously, the strain is able to increase the number of ligands at the cell membrane level, through the synthesis of structures such as LPS. The induction of both acid (PAP2) and alkaline phosphatase enzymes match with the results of biochemical analyses and the P_i released to the medium. These findings, along with the precipitates observed by STEM/HAADF, suggest again a biphasic mechanism of rapid biosorption of U(VI) to the cell surface, followed by the biomineralization mediated by phosphatase activity.

In summary, these studies reveal the impact of physiological and physico-chemical factors in the yielding of the interaction processes, as well as the ability of *S. bentonitica* to perform the biomineralization of U(VI)-phosphate complexes as resistance mechanism against metal toxicity. The formation of a long-term stable mineral such as meta-autunita, highlight the potential of the strain as bioremediation agent for U(VI) contaminated environments.

The resistance mechanisms performed in presence of Se were also addressed. Based on previous investigations that showed the capability of *S. bentonitica* to reduce both Se(VI) and Se(IV), transcriptomics and proteomics studies were performed in order to obtain a deeper understanding of the interaction mechanisms. Similarly to U(VI), the prolongation of the lag phase, along with the increased high metabolic activity, suggest the activation of mechanisms to cope with toxicity of both Se(VI) and Se(IV). Furthermore, the contact of the two of them with the cell also caused membrane damage, as indicated by the induction of proteins like lipocalin Bcl or CcmA bactofilin.

The appearance of intracellular amorphous nanospheres (a-Se) observed by STEM/HAADF suggest that the reduction of Se(IV) takes place in the cytoplasm, being necessary the previous uptake of the metalloid. In case of *S. bentonitica,* this uptake could be performed by transport systems like NodT-type lipoprotein, magnesium transport MgtE or the porin OprP. Once in the cytoplasm, enzymes such as 3-oxoacil-ACP reductase FabG or thiol groups, specially glutathione (GSH), could reduce the Se(IV) to Se(0). At the same time, the pool of reduced GSH is replenished by the activity of the glutamate—cysteine ligase, glutathione reductase (GR) and glutathione synthetase (GS). Apart from GSH, other enzymes like thioredoxin reductase could carry out a further reduction step from Se(IV) to Se(-II). Then, the action of methyltransferases could produce volatile dimethyl selenide (DMDSe) and dimethyl selenil disulphide (DMSeDS),

detected in previous studies in this strain. Both reduction of Se(IV) and the presence of the nanospheres trigger an increase of reactive oxygen species, activating enzymatic mechanisms to mitigate the damage from oxidative stress. The a-Se would increase their size until being released to the extracellular media via cellular lysis. Microscopic and structural analyses (*Fast Fourier Transform,* FTT, *selected-area electron diffraction,* SAED) confirmed a biotransformation process from a-Se to extracellular crystalline *t*-Se nanostructures of different size and shape, with *m*-Se as intermediate form. The presence of S in these structures suggest the possible influence of thiol groups, probably attached to the nanospheres during reduction or lysis.

In case of Se(VI), the BII-R7 transcriptome evinced the high gene induction against the exposure of 50 mM of the metalloid. According to the results, the uptake of Se(VI) could occur via NodT lipoprotein, nitrate/nitrite NarK and/or thiol groups transporters. During the lag phase, NAD(P)H-oxidoreductases enzymes would carry out the reduction in the cytoplasm. *ars* operon could also be involved in Se(VI) reduction by ArsC, as well as the efflux of Se(IV) outside the cell via ArsB, along with NodT and NarK. On the other hand, respiratory nitrate reductase seems to be implicated in Se(VI) once the cells reach the exponential growth. Similar to Se(IV), an increase of oxidative stress would occur, which triggers the activation of mechanisms for reactive oxygen species detoxification, as well as enzymes to support antioxidant activity. However, the absence of reddish coloration in this treatment suggest that no significant reduction to Se(0) occur, or the formation of volatile biomethylated species.

The high toxicity caused by the presence of 200 mM of Se(VI) led to the down-regulation of the gene expression regarding control treatments. Nevertheless, microscopic analyses (*environmental scanning electron microscopy,* ESEM and STEM-HAADF) showed the presence of nanotubes of Se(0) located intracellularly and embedded in the matrix of flagella-like structures after 24 h of incubation. Structural characterization (FFT y SAED) of the nanotubes indicated *m*-Se and *t*-Se structures as observed with Se(IV), showing also the accumulation of S by EDX. However, the results suggest a different biotransformation process from that described to Se(IV), since aggregation and synthesis of the nanostructures seems to be faster in presence of Se(VI), and without the lysis. Further studies of the products of Se(VI) reduction at shorter incubation times are needed in order to elucidate the possible stages of biotransformation to nanotubes. As far as we know, the formation of *t*-Se nanotubes from the reduction of Se(VI) is reported here for the first time.

Ultimately, these findings suggest that *S. bentonitica* resistance to Se(VI) and Se(IV) is based in three cellular mechanisms that occur simultaneously: bioreduction of reduced forms of the metalloid, mitigation of the damage caused by oxidative stress, and the formation of *m*-Se and *t*-Se nanostructures. Given the less mobility and toxicity of the *t*-Se species, these studies demonstrate the ability of *S. bentonitica* to efficiently reduce the toxic species of the metalloid, and hence, the detrimental effect produced by its presence in the environment.

The investigation of this Doctoral Thesis reveal genes and proteins with a key role in processes of microbial resistance to heavy metals and radionuclides, providing starting points for the development of effective bioremediation techniques, as well as an eco-friendly alternative to the synthesis of nanostructures with biotechnological purposes.

INTRODUCCIÓN

1. Metales pesados en el ambiente

Aunque no existe una definición estandarizada, el término "metal pesado" hace referencia a elementos metálicos que presentan una alta densidad, peso o número atómico elevado (Briffa et al., 2020; Duffus, 2002). El criterio usado depende del contexto en el que se use el término, encontrando incluso una alta variabilidad dentro de cada uno. Por ejemplo, si usamos el criterio de la densidad específica para determinar si un metal se encuentra dentro de este grupo, es posible considerar como tales aquellos con una densidad superior a 3,5, 5, 6 o 7 g/cm^3 según los autores que lo definan. Por otro lado, y según el número atómico, algunas definiciones incluyen, entre los metales pesados, algunos metaloides como el arsénico (As), selenio (Se) o teluro (Te) (Duffus, 2002; Nieboer and Richardson, 1980). Así, debido a la falta de consenso, algunos elementos considerados como metales pesados no cumplen con los criterios previamente establecidos, como el caso del zinc (Zn), que presenta una baja densidad (Pourret, 2018).

En muchas ocasiones, el concepto de metal pesado se ha relacionado con metales y metaloides que presentan una potencial toxicidad o eco-toxicidad (Duffus, 2002). No obstante, esta referencia tampoco sería precisa, ya que algunos de ellos juegan un papel importante a nivel fisiológico y bioquímico en los sistemas biológicos (Ali et al., 2019). Es el caso del zinc (Zn) o el hierro (Fe), que son micronutrientes clave para múltiples procesos metabólicos al ser necesarios para la actividad catalítica de numerosas enzimas (Osredkar, 2011). Así, los metales pesados se clasifican en dos grupos en base a su papel fisiológico:

- Metales esenciales: se incluyen en esta categoría aquellos que cumplen una función biológica en el organismo al formar parte de biomoléculas como las enzimas. Estos metales tienen efectos beneficiosos a concentraciones muy bajas pero, sin embargo, ejercen un efecto tóxico a concentraciones elevadas. Ejemplos de este tipo de metales son el cobre (Co), níquel (Ni), manganeso (Mn) o magnesio (Mg), además de los previamente citados (Ali et al., 2019).
- Metales no esenciales: se trata de metales que no presentan función biológica alguna, siendo tóxicos para los seres vivos incluso en concentraciones bajas (Ali et al., 2019; Singh Sidhu, 2016). En este grupo encontramos radionúclidos como el uranio (U) o metales nobles como el paladio (Pd).

En las últimas décadas, la concentración de metales pesados en el ambiente se ha incrementado considerablemente. Esto supone un gran problema, ya que su acumulación en el medio lleva a sobrepasar los límites en los que se compromete el equilibrio de los ecosistemas, así como la salud de los organismos que lo componen. Esto ocurre también en el caso de los metales esenciales. Pese a ser necesarios en concentraciones traza, los metales esenciales también tienen efectos tóxicos cuando sobrepasan determinados límites, como ocurre con el Se. Por este motivo, es de vital importancia gestionar correctamente los metales para evitar que se alcancen concentraciones que pongan en riesgo la integridad de los ecosistemas, asegurando, además, en el caso de los metales esenciales, que se alcance la ingesta apropiada (Nancharaiah and Lens, 2015). La distribución de los metales pesados en el ambiente está determinada, principalmente, por procesos naturales y por los derivados de la actividad humana.

1.1. Fuentes naturales:

Los metales pesados están presentes de manera natural en el ambiente, mayoritariamente en la corteza y el manto terrestre, formando parte de rocas magmáticas, metamórficas o en sedimentos. De hecho, la actividad volcánica emite grandes cantidades de metales y metaloides a la atmósfera en forma de compuestos volátiles, tales como Se, As, Te o mercurio (Hg), y otros como cadmio (Cd), Zn, etc., que varían dependiendo del tipo de volcán. Así, se ha observado que en conos volcánicos de naturaleza basáltica, la liberación de metales como el Cd, plomo (Pb), Se o cobre (Cu) puede alcanzar flujos de hasta 10^3-10^4 kg por día (Edmonds et al., 2018). Otros procesos, como la erosión de minerales y rocas o los incendios forestales, provocan la liberación de estos elementos, pudiendo llegar a alcanzar ecosistemas acuáticos donde serían movilizados aguas abajo o depositados en sedimentos (Bradl, 2005; Gautam et al., 2016; Singh Sidhu, 2016). Aunque en ocasiones las concentraciones derivadas de fuentes naturales son tóxicas, por lo general se trata de procesos lentos en los que, una vez liberados, los metales quedan relativamente inmovilizados durante largos periodos de tiempo, por lo que no contribuyen en gran medida a la contaminación ambiental (Amiro, 2001; Gautam et al., 2016).

1.2. Fuentes antropogénicas:

El rápido incremento de la industrialización durante el último siglo ha llevado a la explotación masiva de los recursos naturales, causando la emisión de contaminantes de toxicidad elevada entre los que se encuentran los metales pesados (Briffa et al., 2020;

Gautam et al., 2016). Diversos procesos industriales como la minería, la agricultura o la depuración de aguas residuales, entre otros, constituyen la principal causa de contaminación al alterar la distribución de los metales pesados presentes en el medio ambiente. Por ejemplo, los fertilizantes y pesticidas contienen cantidades variables de metales pesados como Cd o Pb, Cromo (Cr), Ni o Zn, y el uso continuado de estos agroquímicos lleva a su acumulación en el suelo (Singh Sidhu, 2016). De los procesos citados, cabe destacar la minería, ya que contribuye enormemente a la contaminación del suelo, el agua y la atmósfera por la liberación de grandes cantidades de metales pesados (Gautam et al., 2016; Qu et al., 2012). Asimismo, algunas fuentes antropogénicas producen residuos radiactivos que contienen radioisótopos, como U o plutonio (Pu). Esto supone un problema adicional ya que los efectos perjudiciales, derivados de su presencia en el ambiente, provienen de su toxicidad tanto química como radiológica. Pese a que el uso de material radiactivo está extendido en sectores como la medicina, la investigación o la actividad minera, el proceso industrial más relevante en la producción de estos desechos radiactivos es la producción de energía nuclear (IAEA, 2018).

La liberación de estos metales al medio ambiente, en una forma soluble y biodisponible, los convierte en elementos potencialmente tóxicos, lo que supone un serio problema por la magnitud del daño que producen a nivel medioambiental. Además de alterar la funcionalidad de ecosistemas terrestres y acuáticos, los metales pesados pueden afectar gravemente la salud humana al alcanzar la cadena trófica.

1.2.1. *La actividad minera*

Pese los beneficios socioeconómicos derivados de la minería, se trata de una de las actividades que contribuyen en mayor medida a la contaminación de ecosistemas por metales pesados a nivel mundial (Pan et al., 2015; Wei et al., 2018). Procesos de la industria minera como la excavación, transporte, fundición y refinado de recursos minerales genera grandes cantidades de residuos enriquecidos de estos contaminantes inorgánicos, tales como Cd, Hg, As, Se o Zn (Etteieb et al., 2020; Li et al., 2018). Un ejemplo son los drenajes ácidos, procedentes de la oxidación de minerales de sulfuros como pirita (Equeenuddin et al., 2013; Simate and Ndlovu, 2014; Zhuang et al., 2009). La liberación de estos residuos, sin tratamiento previo, ha ocasionado la contaminación de ambientes circundantes, con riesgo de alcanzar tierras de cultivo y/o recursos de agua para uso doméstico (Liao et al., 2016).

De entre los países con mayor actividad minera cabe destacar China, que posee el 12% de los recursos minerales a nivel global, siendo los mayores productores y consumidores de metales como antimonio (Sb), Fe, Pb, Mn, estaño (Sn), tungsteno (W) o Zn (Li et al., 2014). Esto ha derivado en un total de 960 millones de hectáreas de residuos con altas concentraciones de metales pesados, que aparecen en cantidades que superan varias veces las permitidas en los alrededores (Zhuang et al., 2009). Como consecuencia, durante las últimas dos décadas, numerosos estudios se han centrado en la evaluación de la magnitud de este problema y de su potencial riesgo para la salud humana (Li et al., 2018).

Dada la diversidad geológica del territorio, España también posee una importante actividad minera de minerales metálicos, como Cu, Zn, Sn, tántalo (Ta) oro (Au), plata (Ag) o Pb, situándose entre el segundo y tercer productor de mineral de Cu a nivel europeo. Cabe destacar el distrito minero de Almadén (Ciudad Real), muy importante a nivel mundial en la producción de Hg (García-Ordiales et al., 2016). En Andalucía, la extracción de minerales metálicos se corresponde con casi el 39% del valor total de la minería española (MITECO, 2018), principalmente en las regiones del sector occidental (entre Sevilla y Huelva). Un ejemplo son las minas de pirita (FeS_2) de Alnazcóllar (Sevilla) donde, además, el 25 de abril de 1998 se produjo la liberación accidental del contenido de la balsa de decantación de una mina (Figura 1). Los graves daños producidos a nivel medioambiental por aquel accidente fueron devastadores, ya que dio lugar a un vertido de agua ácida y lodos tóxicos con altas concentraciones de metales como As, Cu, Zn, Cd y Pb (Sarria Carabalí et al., 2015), lo que provocó el cierre de la mina hasta el año 2015.

Figura 1. Zona de rotura de la balsa minera de Aznalcóllar (https://elpais.com/ccaa/2012/05/22/andalucia/1337692996_148522.html)

A mediados del siglo pasado se produjo también el mayor desarrollo de la minería de U en España, ya que las reservas de U españolas se estiman en 4.650 toneladas siendo, en importancia, el segundo país europeo, con Francia en cabeza. Desde el inicio de las actividades de explotación mineras para la obtención de U hasta el año 1998, las minas de Don Benito (Badajoz) y Ciudad Rodrigo (Salamanca) cubrieron el 25% de las necesidades totales del Parque Nuclear español. De entre las minas de U españolas, destaca la de Saelices El Chico (Figura 2), también en Salamanca, operativa desde 1974 hasta el año 2000, cuando se iniciaron los procesos de restauración del espacio natural afectado (https://www.enusa.es).

El U extraído es utilizado para satisfacer la demanda de combustibles nucleares para la producción de electricidad en centrales nucleares. La fábrica de elementos combustibles de Juzbado (Salamanca) a cargo de la empresa ENUSA, operativa desde 1985, es responsable del abastecimiento de dicha demanda en España, aunque parte del combustible generado también se destina a la exportación a otros países europeos como Francia, Suecia, Bélgica, Finlandia o Alemania (https://www.enusa.es; https://www.nuclenor.org/aula/222_07/capitulo9.htm).

Figura 2. Antigua mina de uranio de Saelices el Chico ubicada en Salamanca (https://www.enusa.es).

1.2.2. *La tecnología nuclear y producción de desechos*

1.1.1.1. Historia de la energía nuclear

El desarrollo de la tecnología nuclear se inició en la década de 1940 y, con la llegada de la Segunda Guerra Mundial, los progresos en este campo se destinaron de

manera exclusiva a la fabricación de armas nucleares. Durante las investigaciones en este campo, los científicos advirtieron que la gran cantidad de calor generada en el proceso de fisión de átomos de determinados elementos también podía usarse para la obtención de energía eléctrica. De esta forma, el primer reactor nuclear diseñado para estos fines fue puesto en marcha en el Laboratorio Nacional Argonne (Idaho, EEUU) en diciembre de 1951, aunque la cantidad de energía producida era muy limitada. En 1953 el gobierno de Estados Unidos propuso el programa llamado "Atoms for Peace", en el que se promovía la reorientación de la energía nuclear para el uso civil, teniendo lugar el comienzo de la comercialización de la energía nuclear en la década de 1960 (IAEA, 2009). Sin embargo, la aplicación de este programa a nivel internacional no ocurrió hasta principios de la década de 1970. Desde entonces, y hasta 1985, dio comienzo la época de mayor desarrollo de esta tecnología, con lo que además del incremento en el número de reactores nucleares, también se produjo una gran mejora de la capacidad de producción de energía (Prăvălie, 2018) . Este rápido desarrollo se debió en parte a la crisis de petróleo que tuvo lugar durante la década de 1970, lo que impulsó a los países de occidente a apostar por la energía nuclear. De hecho, el Primer Ministro francés lanzó el llamado "Messmer Plan" en 1974, cuyo objetivo consistía en el completo abastecimiento de las necesidades energéticas de Francia mediante este tipo de tecnología (Albino, 2014) . Además, el avance en el ámbito de la energía nuclear no se limita a la producción de electricidad, sino que ha supuesto importantes logros en otros campos de gran relevancia como la medicina, contribuyendo a mejorar tanto el diagnóstico como el tratamiento de diversas enfermedades.

No obstante, el desarrollo de la tecnología nuclear no ha sido lineal, sino que la aparición de una serie de riesgos e inconvenientes ha limitado su uso. Varios incidentes como el que ocurrió en Pennsylvania en 1979, o el conocido desastre de Chernóbil en 1986 (Figura 3), provocaron una disminución en el interés de los gobiernos por el desarrollo de la energía nuclear, que se acentuó con la bajada del precio del petróleo en la misma década. El impacto de estos acontecimientos provocó que países como Reino Unido o Alemania frenaran la producción de energía nuclear, con medidas como la detención de la construcción de centrales nucleares o la desautorización del uso de energía nuclear (Pravalie y Bandoc, 2018). Otro accidente más reciente a destacar es el de la central de Fukushima Daiichi en Japón (2011), que también provocó la liberación de elevadas cantidades de isótopos radiactivos al medio ambiente, como ^{137}Cs (Pravalie y Bandoc, 2018).

Figura 3. Fotografía de la central nuclear de Chernóbil tras el accidente en abril de 1986 (https://www.ebrd.com/ebrds-mission-in-chernobyl-gallery.html).

1.1.1.2. Residuos radiactivos y efectos perjudiciales

Hoy en día, el rápido incremento de la población mundial, junto con el impacto medioambiental derivado del uso de combustibles fósiles, han llevado a la necesidad de encontrar fuentes de energía alternativas que permitan hacer frente en el futuro, de forma sostenible, a la creciente demanda energética (Verbruggen and Laes, 2015). La tecnología nuclear permite generar grandes cantidades de energía usando poco combustible, por lo que está llamando de nuevo la atención como estrategia a escala global generando una menor emisión de CO_2 a la atmósfera que otras tecnologías. A finales de 2019 442 reactores de centrales nucleares, operativos en más de 30 países, y esta expansión continúa incrementándose con la construcción de nuevos reactores en China, Irán, Rusia y Reino Unido (World Nuclear Association, 2020).

Como consecuencia, la producción de residuos radiactivos es uno de los grandes inconvenientes que surgen actualmente de la industria nuclear. Estos residuos engloban tanto materiales radiactivos como materiales contaminados por radiactividad (IAEA, 2018). Aunque la cantidad de residuos generada por esta industria es relativamente baja, la peligrosidad de los mismos reside en la presencia de isótopos radiactivos en su composición. Los isótopos radiactivos o radionúclidos son aquellos que emiten energía en forma de radiación (alfa, beta o gamma) como consecuencia de la inestabilidad de su núcleo, desintegrándose de manera espontánea hasta isótopos de mayor estabilidad. Estas radiaciones tienen suficiente energía para ionizar materiales y romper enlaces moleculares, ya que, al ser absorbidas por los tejidos, ocasionan daños por generación de

radicales libres y por alteración estructural de biomoléculas, tales como el ADN (Amiro, 2001).

La radiactividad es un proceso natural al que estamos expuestos continuamente. Los radionúclidos aparecen de forma natural por la incidencia de la energía cósmica en la atmósfera, como es el caso del ^{14}C a consecuencia de la interacción de estos rayos con el nitrógeno (N) atmosférico. Otra fuente natural se encuentra en la corteza terrestre, los llamados radionúclidos primordiales (Kónya and Nagy, 2018; Porcelli, 2018). Sin embargo son, de nuevo, los producidos artificialmente en el proceso de fisión (p. ej., el ^{131}I) los que suponen un mayor riesgo en la actualidad. Como se ha mencionado anteriormente, pese a que la producción de energía nuclear es el proceso que más contribuye a la generación de residuos radiactivos, también surgen de la actividad de otras industrias de gran relevancia, por lo que prácticamente la totalidad de Estados han desarrollado una normativa que regula su tratamiento de forma segura acorde a los criterios de la Agencia Internacional de Energía Atómica (IAEA, de las siglas en inglés *International Atomic Energy Agency*) (IAEA, 2018).

La composición de este tipo de desechos los hace potencialmente tóxicos para los ecosistemas y la salud, por lo que deben ser gestionados de manera adecuada para evitar su liberación al medio ambiente. A diferencia de otros residuos, la radiactividad de los elementos decae con el tiempo. Sin embargo, la vida media de algunos radionúclidos, como el ^{137}Cs o el ^{90}Sr, hace necesario el uso de sistemas de contención y almacenamiento durante largos periodos. Así, los residuos radiactivos se clasifican en diversos tipos en función del tiempo de desintegración y la actividad de los radionúclidos que los componen, aplicando un tratamiento acorde a cada tipo. Los más preocupantes son los denominados desechos de alta actividad. Estos residuos suponen únicamente el 3% de los residuos radiactivos, pero son responsables del 95% de la radioactividad de los mismos. Están compuestos por productos de fisión y elementos transuránicos altamente radiactivos procedentes del U (isótopo 235) y Pu que se generan en las operaciones de los reactores. Presentan compuestos tanto de vida media corta como larga, siendo en ocasiones persistentes en el ambiente por periodos de hasta 100.000 años, lo que dificulta enormemente su almacenamiento de forma segura (Horvath and Rachlew, 2016; Prăvălie, 2018) . Además, la desintegración del núcleo de los radionúclidos genera una cantidad considerable de calor, haciendo que se incremente significativamente la temperatura de los alrededores, siendo necesario el uso de sistemas de enfriamiento, lo que también conlleva un alto coste económico.

Hoy en día tanto la energía nuclear, como otras actividades antropogénicas, dependen de la industria minera de extracción de metales como U o Se. Este hecho conduce a la aparición de estos elementos en concentraciones elevadas, y, por tanto, requieren de tratamientos de remediación para evitar efectos perjudiciales en la salud humana y medioambiental.

2. Remediación de ambientes contaminados con metales pesados y radionúclidos

A diferencia de otros contaminantes orgánicos como herbicidas o pesticidas, los metales pesados no pueden ser química ni biológicamente degradados, por lo que persisten en el ambiente. Los metales pesados presentes en el suelo y agua pueden ser ingeridos a través de la cadena trófica, acumulándose en el organismo (Ali et al., 2019; Briffa et al., 2020). Los efectos perjudiciales derivados de la exposición a concentraciones tóxicas de estos contaminantes dependerán de parámetros físico-químicos como el metal, su especiación química, la dosis, la vía de exposición, así como de factores genéticos y nutricionales del individuo afectado (Tchounwou et al., 2012). La acumulación de metales pesados en el organismo ocasiona efectos perjudiciales de manera directa mediante la interacción de los mismos con biomoléculas (componentes celulares, enzimas del metabolismo, etc.), o indirecta como consecuencia de la generación de radicales libres (Briffa et al., 2020) (Figura 4). Esto conlleva efectos negativos en el ADN relacionados con la carcinogénesis (Wang and Shi, 2001). Estas características hacen que sean reconocidos como uno de los tipos de contaminantes inorgánicos más importantes (Thayer and Brinckman, 1982). Por ello, el desarrollo de tecnologías que permitan reducir la concentración de metales pesados en ambientes contaminados constituye una prioridad entre la comunidad científica en las últimas décadas. Las diferentes técnicas se pueden diferenciar en dos tipos, en función de si el tratamiento se realiza en la zona original (técnicas *in situ*) o si, para su tratamiento, el material afectado se traslada a otras instalaciones (técnicas *ex situ*). Debido al carácter no degradable de los metales pesados, estas técnicas se basan principalmente en eliminar o reducir la fuente de contaminación, o en bloquear las vías de exposición (Gavrilescu et al., 2009).

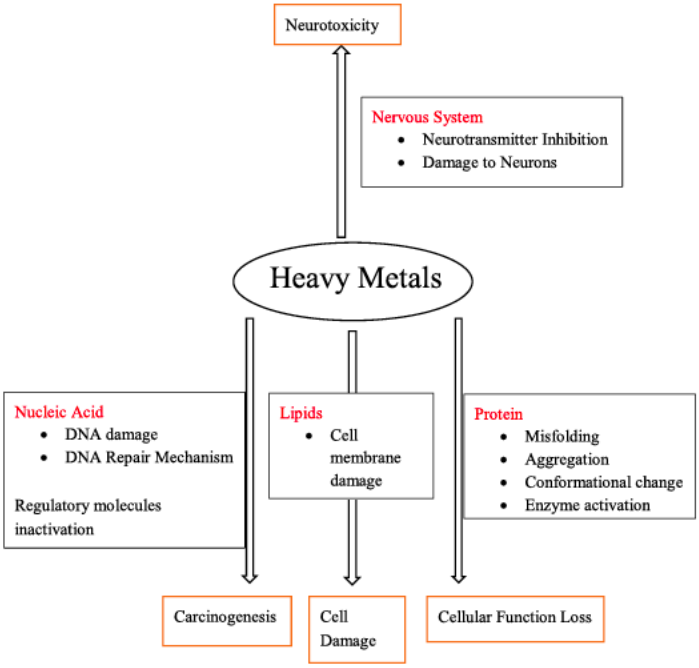

Figura 4. Esquema de la toxicidad generada en el organismo por los metales pesados (Briffa et al., 2020)

2.1.Técnicas convencionales

Se trata de un conjunto de técnicas en las que la atenuación de los metales se produce mediante métodos físicos o químicos. El tratamiento a emplear dependerá de factores como el tipo de las características de la zona a tratar, el grado de contaminación, etc., que, previamente, deben ser analizados en profundidad.

Los métodos físicos engloban procesos como la contención, lavado y reemplazo de suelos, vitrificación, flujo de calor, almacenamiento y drenaje de aguas, solidificación, solubilización y transporte de solutos (Gavrilescu et al., 2009; Khalid et al., 2008).

La contención es una estrategia para el caso de los residuos radiactivos. Mediante una serie de barreras impermeables, se evita la movilización de los radionúclidos y la infiltración de aguas. Aunque esta técnica es efectiva, no limita la fuente contaminante ni atenúa la toxicidad de los desechos (Gavrilescu et al., 2009). Por otro lado, las técnicas químicas conllevan la transformación, volatilización, reacciones de óxido/reducción, o adsorción o desorción de los metales. En esta categoría se incluyen procesos de lixiviación química, fijación o precipitación química, entre otros (Gautam et al., 2016; Sharma et al., 2018).

Pese a su uso, estas técnicas presentan una serie de inconvenientes que disminuyen su efectividad. Algunos de ellos son la falta de aplicabilidad *in situ,* dificultando su uso a gran escala la falta de especificidad hacia los metales contaminantes, lo que disminuye la eficiencia de la técnica ante la presencia de otros iones, o su alto coste. Por otra parte, presentan un problema adicional: el impacto medioambiental asociado. Así, el uso de productos químicos puede dar lugar a la formación de compuestos secundarios indeseables y, en el caso de la utilización de métodos físicos, tras su aplicación, es necesario un posterior reprocesamiento de los contaminantes (Sharma et al., 2018). Además, técnicas como la vitrificación en suelos implica el calentamiento del área a tratar para volatilizar los contaminantes, llegando a temperaturas de entre 1.400-2.000 ºC (Singh Sidhu, 2016). Como consecuencia de los problemas asociados, se ha limitado el uso de estas técnicas, surgiendo la necesidad de sustituirlas por otras más efectivas, de bajo impacto medioambiental y que, además, supongan un bajo coste.

2.2. Técnicas de biorremedio

El biorremedio o remediación biológica es un método biotecnológico que surge como alternativa a los tratamientos tradicionales mencionados anteriormente. Se define como el uso de sistemas biológicos para eliminar, reducir, transformar y/o degradar los contaminantes presentes en ecosistemas naturales. Esta estrategia puede incluir organismos vivos como plantas (lo que se conoce como fitorremediación o biorremediación botánica) o microorganismos, o componentes de los mismos, como sistemas enzimáticos o componentes celulares (Gautam et al., 2016; Sharma et al., 2018).

De hecho, se ha observado que determinados organismos son capaces de tolerar, e incluso crecer, en presencia de contaminantes, incluyendo los metales pesados. Esto se debe al desarrollo de mecanismos que les permiten protegerse de la toxicidad ejercida por estos compuestos otorgándoles, en ambientes contaminados, ventaja frente a los organismos que carecen de estos sistemas. De este modo, el fundamento de las técnicas de biorremedio se basa en la optimización de los procesos que ocurren naturalmente en el ambiente, lo que reduce los problemas derivados de la metodología tradicional (Shukla et al., 2017).

De entre los organismos comúnmente estudiados para estos fines, cabe mencionar los microorganismos, como bacterias y hongos. Efectivamente, hay multitud de microorganismos descritos que destacan por su capacidad para sobrevivir en ambientes extremos, donde las condiciones son tan inhóspitas que se creía que ningún ser vivo era

capaz de desarrollarse. Su descubrimiento llamó la atención de los investigadores, que pronto se interesaron por conocer los mecanismos celulares que subyacen tras dicho fenómeno. Un ejemplo a destacar es la bacteria *Deinococcus radiodurans*, que ha sido extensamente estudiada por su potente mecanismo de reparación de daños en el ADN y de eliminación de especies reactivas de oxígeno, lo hacen altamente radioresistente (Jin et al., 2019; Krisko and Radman, 2013). Por ello, el uso de microorganismos en diferentes procesos es un enfoque muy atractivo debido al gran número de beneficios que ofrece, entre los que cabe destacar (Selvakumar et al., 2018; Shukla et al., 2017; Wei et al., 2019):

- Se trata de procesos muy efectivos. Muchos de los mecanismos que otorgan tolerancia son mecanismos desarrollados evolutivamente como detoxificación, por lo que ofrecen una alta especificidad.

- Diversos procesos biotecnológicos a gran escala basados en procesos microbianos generan grandes cantidades de biomasa como desecho, que puede reutilizarse para fines de biorremedio, abaratando los costes.

- La posibilidad de usar organismos naturalmente presentes en estos hábitats reduce los posibles efectos adversos y, por tanto, se mejora la capacidad de regeneración del ecosistema tras el tratamiento.

- Son organismos fácilmente manipulables desde el punto de vista genético, lo que permite mejorar el rendimiento del proceso para el que se utilicen.

Por estos motivos, el aislamiento y caracterización de microorganismos capaces de soportar altas concentraciones de contaminantes, tanto orgánicos como inorgánicos, ha llevado en las últimas décadas a su consideración como agentes de biorremedio.

Existen tres abordajes principales en función de la comunidad microbiana para este tipo de tratamiento con microorganismos:

- Atenuación natural: esta técnica consiste en el uso de microorganismos autóctonos del área contaminada, ya sean aerobios o anaerobios, sin realizar ningún tipo de intervención. De este modo, este abordaje se basa únicamente

en la capacidad intrínseca de los microorganismos para llevar a cabo la remediación de forma natural (Francis y Nancharaiah, 2015).

- Bioestimulación: en este abordaje se introducen determinadas modificaciones en el medio contaminado, como pueden ser nutrientes (Wang et al., 2014), con el fin de potenciar la actividad de los microorganismos autóctonos.
- Bioaumentación: se trata de la adición, en el medio a tratar, de microorganismos especializados en el bioremedio eficaz de los metales contaminantes (Wang et al., 2014).

Para ser usados como agentes de biorremedio de metales pesados y radionúclidos los microorganismos tienen que cumplir una serie de criterios, los cuales podemos resumir en tres: (1) presentar una alta resistencia a estos contaminantes inorgánicos, (2) poseer una alta diversidad metabólica, y, como consecuencia, (3) se establezcan mecanismos de interacción que conduzcan a la inmovilización del metal en una forma menos tóxica.

Estos criterios están interrelacionados entre sí, ya que la alta diversidad metabólica es la característica que permite llevar a cabo diferentes interacciones con los metales pesados, que en última instancia confieren la resistencia a los mismos. Por tanto, el estudio de los mecanismos de resistencia conlleva al conocimiento de las interacciones que se establecen. La aplicación de técnicas de biorremedio de forma segura y efectiva requiere la caracterización detallada de estos mecanismos, así como de las variables que los condicionan.

3. Mecanismos de resistencia microbianos a metales pesados y radionúclidos

Hoy en día se sabe que los microorganismos juegan un papel clave en los ciclos biogeoquímicos de multitud de elementos químicos. Esto es debido a la alta variabilidad metabólica que poseen, y es de gran relevancia en términos medioambientales, ya que condicionan los procesos de movilización e inmovilización de nutrientes fundamentales para la vida como el C, el N o el azufre (S). Un ejemplo de ello es la liberación de compuestos como ácidos orgánicos, que pueden producir la solubilización de los minerales o rocas que los retienen.

Del mismo modo, la actividad microbiana también afecta a la distribución de los metales pesados, determinando su concentración y biodisponibilidad (Francis, 2007; Zammit et al., 2014). Como ya se ha mencionado anteriormente, numerosas cepas microbianas filogenéticamente diversas han demostrado su capacidad para crecer en presencia de concentraciones elevadas de metales pesados y radionúclidos preocupantes desde el punto de vista ambiental. Algunos de ellos incluso han sido aislados de ambientes contaminados, como minas o los alrededores de Chernóbil (Gallois et al., 2018; Sánchez-Castro et al., 2020). La exposición a estos compuestos ha permitido el desarrollo de mecanismos de interacción que les permiten hacer frente a su toxicidad (Figura 5).

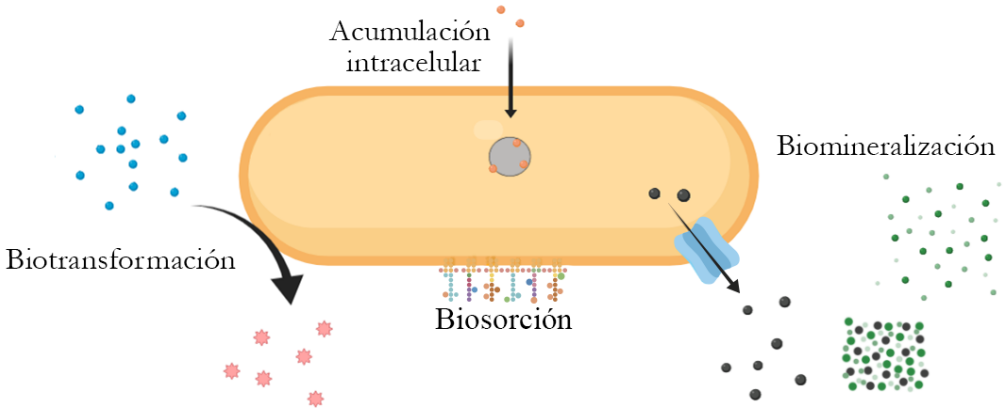

Figura 5. Esquema de los mecanismos de interacción establecidos entre los microorganismos y metales pesados y radionúclidos.

El tipo de interacción y el resultado de la misma está condicionado por las condiciones ambientales, por lo que es necesario el conocimiento detallado de las bases de cada una para diseñar estrategias de biorremedio efectivas. Estos mecanismos, que otorgan resistencia frente a la toxicidad de metales pesados, han sido agrupados en dos tipos principales según el estado metabólico en el que se encuentra la célula en el momento de la interacción (López-Fernández et al., 2020; Yang et al., 2015):

- Independientes del metabolismo: se trata de procesos que no requieren la viabilidad de la célula, ocurriendo principalmente por interacciones físicas. Este grupo incluye la biosorción.

- Dependientes del metabolismo: engloba las interacciones que requieren que las células microbianas estén activas desde un punto de vista metabólico, ya que dependen del funcionamiento de procesos celulares, como pueden ser los

sistemas enzimáticos. Es el caso de la bioacumulación, biotransformación o biomineralización/bioprecipitación.

Normalmente, ambos tipos de procesos tienen lugar en células viables (Yang et al., 2015), y aunque son ampliamente estudiados en la actualidad, los mecanismos dependientes del metabolismo son más atractivos en términos de biorremediación, ya que, en el caso de las interacciones independientes del metabolismo, determinados cambios en las condiciones ambientales pueden revertir el proceso.

En ocasiones, estos mecanismos están determinados por genes específicos de resistencia a iones tóxicos, como el caso del mercurio (Hg^{+}), Arsénico (AsO_2^{-}, AsO_4^{3-}), o plomo (Pb^{2+}), entre otros (Ji and Silver, 1995). Como consecuencia de algunas interacciones, se produce la generación de especies metálicas insolubles, lo que disminuye su biodisponibilidad y, por tanto, ayuda a los microorganismos a lidiar con la toxicidad de los metales. Esto es importante desde el punto de vista del biorremedio, ya que disminuye la probabilidad de contaminación de ecosistemas circundantes.

3.1. Mecanismos de resistencia microbiana a uranio

El U es un radionúclido naturalmente distribuido en el ambiente, encontrándose en concentraciones bajas como parte de algunos minerales, como la pechblenda (U_3O_8) o la uraninita (UO_2) (Celik et al., 2018; Selvakumar et al., 2018). Este último compuesto también forma parte de los anteriormente citados residuos radiactivos junto con otros radionúclidos como Pu y otros metales pesados tóxicos (IAEA, 2018), originándose en diferentes pasos del ciclo de combustible nuclear, como la fabricación o reprocesamiento, además de en otros procesos industriales (Selvakumar et al., 2018). La producción de grandes cantidades de estos residuos, junto con una gestión inadecuada de los mismos, genera un impacto medioambiental severo al afectar ecosistemas acuáticos, suelos y otras áreas. La vida media de los isótopos naturales es de 7×10^8 años para el ^{235}U, mientras que alcanza los $4{,}4 \times 10^9$ años en el caso del ^{238}U (The Royal Society, 2001). Así, se trata de un contaminante muy persistente con graves efectos adversos tanto a nivel ambiental como en la salud por su toxicidad química y radiológica.

La forma oxidada y soluble que encontramos con frecuencia en la naturaleza es el U(VI) en forma de ion uranilo (UO_2^{2+}). Esta especie es considerada altamente tóxica debido a su elevada solubilidad y movilidad, especialmente a pH alcalinos. Por el contrario, la forma reducida U(IV) da lugar a complejos insolubles muy estables en

condiciones anóxicas, que pueden ser reoxidadas en contacto con oxígeno u otros oxidantes (Lakaniemi et al., 2019; Lopez-Fernandez et al., 2020). Entre las interacciones microbianas con U relevantes desde un punto de vista biotecnológico, destacan la biorreducción de U(VI) a U(IV) y la biomineralización de U(VI), además de mecanismos pasivos de biosorción (Lopez-Fernandez et al., 2020). Estos dos mecanismos de interacción con el U, biomineralización y reducción, son también usados por células microbianas como procesos de resistencia frente a este radionúclido.

La biorreducción forma parte de procesos de resistencia usados por células microbianas en condiciones anaerobias para reducir la toxicidad del metal. Se trata de interacciones de biotransformación, que se definen como la modificación estructural de un compuesto químico mediada por microorganismos o sistemas enzimáticos (Singh, 2017). A menudo estas modificaciones conllevan una alteración en el estado de oxidación del compuesto, tratándose de reacciones de óxido-reducción que generan cambios en la solubilidad de los metales pesados o radionúclidos, dando lugar a formas insolubles y menos tóxicas, (Francis y Nancharaiah, 2015). La reducción de radionúclidos como el Pu(VI) ha sido descrita con anterioridad en especies como *Geobacter metallireducens* GS15 o *Shewanella oneidensis* MR1, generando como resultado fases sólidas altamente insolubles de Pu(IV) (Boukhalfa et al., 2007). En el caso del U, numerosas especies microbianas, como bacterias hierro- y sulfato-reductoras, son capaces de utilizar U(VI) como aceptor final de electrones en condiciones anaerobias, con la subsecuente precipitación de U(IV) (Lakaniemi et al., 2019; López-Fernández et al., 2020). Este proceso fue descrito por primera vez por Woolfolk y Whiteley (1962) en *Micrococcus lactilyticus* (especie posteriormente reclasificada como *Veillonella alcalescens*), extendiéndose su descripción a partir de ese momento a géneros muy diversos, como *Geobacter, Shewanella, Clostridium, Pseudomonas* o *Salmonella* (Lakaniemi et al., 2019). También se ha observado la formación de fases no cristalinas de U tetravalente, que surgen tanto de manera biótica como abiótica (Bone et al., 2017; Loreggian et al., 2020). Sin embargo, la estabilidad de estas formas reducidas se ve afectada por factores como la presencia de especies reactivas de oxígeno o FeS, que pueden llevar a la rápida reoxidación a la forma soluble U(VI)(Banala et al., 2021; Loreggian et al., 2020). Aunque la bioreducción de U(VI) es ampliamente estudiada para el biorremedio de ambientes anaerobios contaminados con este radionúclido, como sedimentos, la posibilidad de reoxidación es una de las limitaciones de su aplicación (Selvakumar et al., 2018).

A diferencia del mecanismo anterior, la resistencia a través de la biomineralización de U(VI) ofrece una aplicación prometedora en este ámbito del biorremedio, ya que se basa en la generación de especies de mayor estabilidad bajo un amplio rango de condiciones físico-químicas, lo que garantiza su aplicabilidad a largo plazo (Sowmya et al., 2014). Concretamente, la biomineralización o bioprecipitación hace referencia al proceso de transformación biológica de iones solubles en formas insolubles mediante la liberación de ligandos al medio o por unión a la superficie celular, distinguiéndose específicamente como biomineralización cuando el proceso tiene como resultado la formación de un mineral (Banala et al., 2021; Kolhe et al., 2018; Shukla et al., 2017). A diferencia de lo que ocurría con la precipitación a causa de la reducción de los metales, descrita en el apartado anterior, la forma insoluble generada mediante este proceso no implica modificaciones en el estado de oxidación. Los metales pesados y radionúclidos pueden ser precipitados en formas insolubles relativamente estables, comúnmente hidróxidos, carbonatos, fosfatos o sulfuros (López-Fernández et al., 2020; Merroun y Selenska-Pobell, 2008). La precipitación de U(VI) en forma de minerales de fosfatos mediada por microorganismos ha sido ampliamente reportada. Este mecanismo está basado en la actividad de enzimas fosfatasas, tanto ácidas como alcalinas, que liberan grupos fosfato al medio extracelular. Dichos grupos actúan como ligandos del ion UO_2^{2+}, dando lugar a minerales de fosfatos de U(VI) como autunita o meta-autunita (López-Fernández et al., 2020; Merroun y Selenska-Pobell, 2008), como es el caso de *Bacillus* sp. dwc-2 (Li et al., 2017). La eficiencia de la precipitación depende del pH, la actividad enzimática intrínseca o la disponibilidad de la fuente de fosfato (López-Fernández et al., 2020; Banala et al., 2021). A menudo este proceso se ha relacionado con la biosorción como paso previo, en el que los iones cargados positivamente se adhieren a los grupos funcionales de carga negativa presentes en la superficie de la pared celular microbiana (Figura 6) (Prakash et al., 2013). Al ser un mecanismo pasivo, este sucede de forma muy rápida, tan sólo unos minutos después del contacto de las células con el metal (Yang et al., 2015).

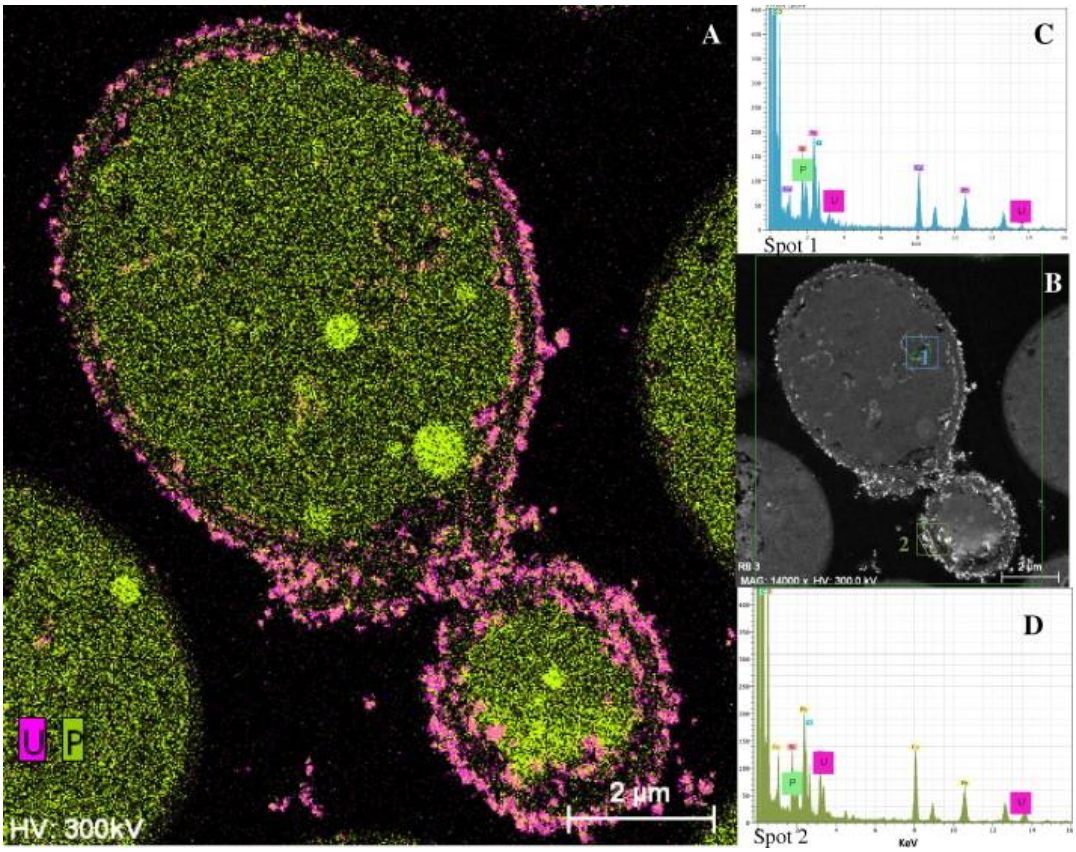

Figura 6. Micrografías de biosorción de U en la superficie celular de *Rhodotorula mucilaginosa* BII-R8 (A y B), junto con espectros de análisis por energía dispersiva de rayos X (EDX) (C y D) (López-Fernández et al., 2014)

El proceso de biosorción puede ser directo, a través de la interacción de los cationes de metales pesados con grupos funcionales (p. ej., fosfato, amino, carboxilo e hidroxilo, entre otros), o indirecto cuando la interacción tiene lugar a nivel de estructuras extracelulares como el lipopolisacárido extracelular (LPS) o la capa S (Shukla et al., 2017; Banala et al., 2021). En este caso, la biomineralización ocurre en la superficie celular, y el lugar concreto donde se produce se conoce como sitio de nucleación (Shukla et al., 2017). La unión del U(VI) a grupos funcionales de la superficie celular proporciona un sitio de nucleación donde se forma el mineral tras la liberación de grupos fosfato por parte del microorganismo (Banala et al., 2021; Merroun y Selenska-Pobell, 2008). Algunos géneros de especies bacterianas involucradas en el proceso son *Acinetobacter*, *Serratia*, *Bacillus*, *Sphingomonas o Stenotrophomonas* (Chandwadkar et al., 2018; Merroun et al., 2011; Sánchez-Castro et al., 2020; Tu et al., 2019). Recientemente también se ha demostrado la eficiencia de miembros del género *Stenotrophomonas*, como *S. bentonitica* BII-R7 y *Stenotrophomonas* sp. Br8 (Figura 7) (Pinel-Cabello et al., 2021; Sánchez-Castro et al., 2020). También cabe destacar la participación en este proceso de

especies fúngicas, como *Saccaromyces cerevisiae* (Gadd and Fomina, 2011; Shen et al., 2018).

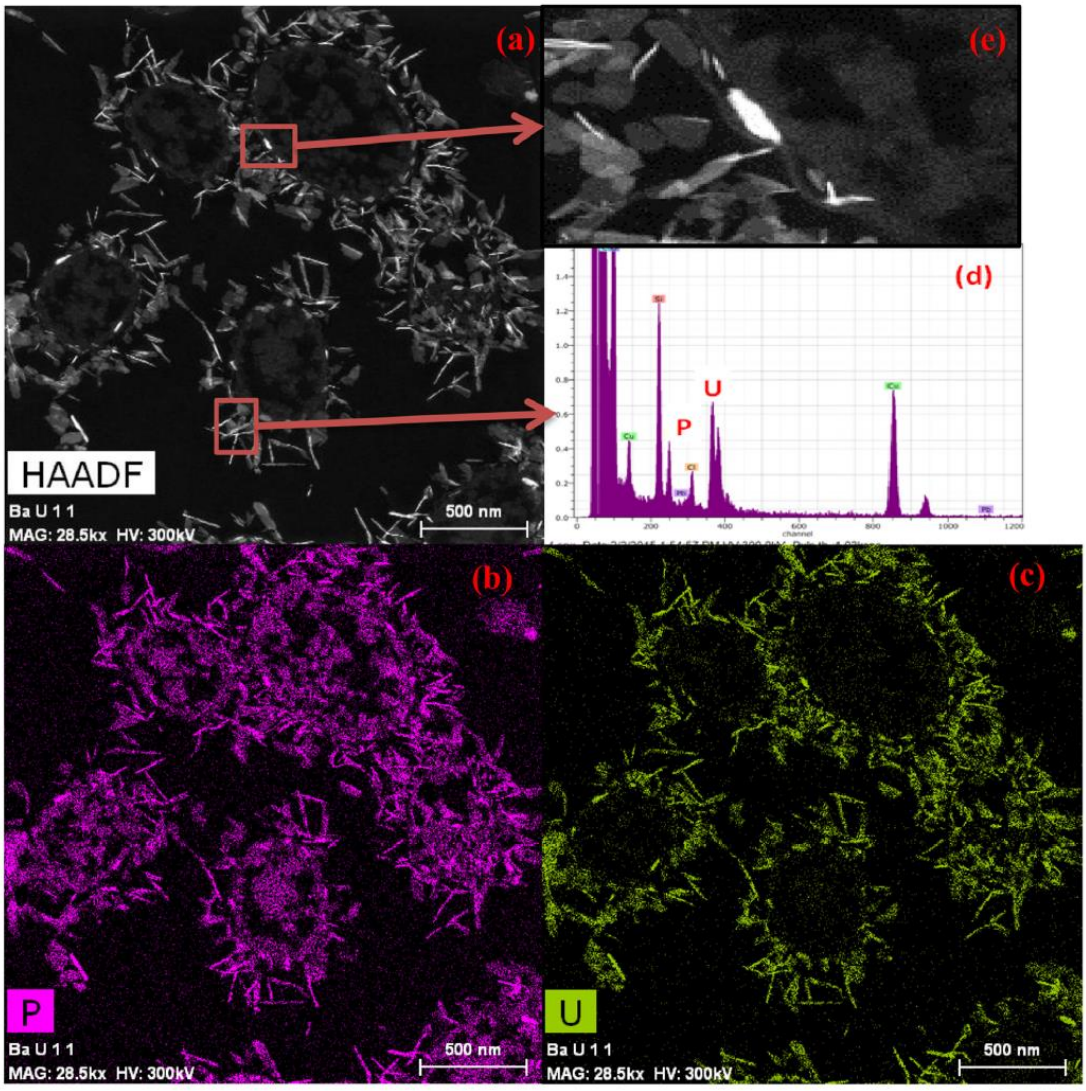

Figura 7. Fosfatos de U(VI) producidos a nivel de la pared celular en *Stenotrophomonas* sp. Br8 (Sánchez-Castro et al., 2020).

Para finalizar, la biomineralización también puede tener lugar a nivel del citoplasma, estando ligada a un mecanismo de acumulación intracelular. Según Tabak et al. (2005), se define como la retención y concentración de una sustancia, en este caso el U, en el interior de la célula. Al contrario de lo que ocurre en la biosorción, se trata de un proceso lento. La bioacumulación puede ser dependiente o independiente del metabolismo (Shukla et al., 2017). Al carecer de función biológica, el U podría ser captado a través de transportadores de elementos esenciales estructuralmente similares, o bien de forma pasiva por alteraciones en la permeabilidad de la membrana celular a consecuencia de daños severos en la pared celular, ocasionados por la presencia del metal

tóxico (López-Fernández et al., 2020; Merroun y Selenska-Pobell, 2008). Una vez en el interior, el metal queda retenido por biomoléculas o en sistemas de almacenamiento, tales como los gránulos de polifosfatos (Acharya and Apte, 2013; Mishra and Malik, 2013).

3.2. Mecanismos de resistencia microbiana al selenio

El Se es un micronutriente de gran importancia para la vida, ya que forma parte de diversas biomoléculas, como es el caso del aminoácido selenocisteína (Sec). Este aminoácido es un constituyente de las llamadas selenoproteínas, con funciones cruciales para el metabolismo y la mitigación del estrés oxidativo en todos los organismos vivos (Duntas and Benvenga, 2015). Sin embargo, el rango que separa los niveles tolerables y las concentraciones tóxicas es muy estrecho (Nancharaiah y Lens, 2015). De hecho, la presencia de este elemento, ampliamente usado por su multitud de aplicaciones biotecnológicas (Ojeda et al., 2020), por encima de niveles seguros supone un problema de interés creciente. Las principales fuentes de Se en el ambiente provienen de la industria metalúrgica, fabricación de vidrio, producción de pigmentos, aplicaciones en la electrónica o en la agricultura (Piacenza et al., 2018). Además, radioisótopos de vida media larga como el ^{79}Se (3,7 x 10^5 años) también son generados durante el proceso de fisión de radionúclidos como el ^{239}Pu, formando parte de los residuos radiactivos de alta actividad (Atwood, 2010; Ikonen et al., 2016).

De manera natural, el Se se encuentra en bajas concentraciones a diferentes estados de oxidación. En ambientes oxidantes, predominan las especies solubles Se(VI) y Se(IV), mientras que en condiciones reductoras encontramos mayoritariamente Se(0) y Se(-II) insolubles. Estas últimas presentan una menor movilidad, y por lo tanto, son los estados de oxidación Se(VI) y Se(IV) los que suponen una mayor peligrosidad (Schilling et al., 2020; Winkel et al., 2015). La capacidad de los microorganismos para alterar la especiación química de las distintas formas de Se está condicionada principalmente por procesos de biotransformación, que incluyen reacciones de reducción, oxidación, metilación y desmetilación (Che et al., 2018). La reducción biológica del Se(VI) y Se(IV) a especies insolubles de Se(0) y Se(-II) es considerada como un eficiente mecanismo de resistencia a este metaloide, ya que genera formas de menor toxicidad. Es por ello que el interés en la bioreducción microbiana de especies oxidadas de Se a formas reducidas e insolubles se ha convertido en un fenómeno creciente durante los últimos 20 años (Tugarova y Kamnev, 2017), especialmente en el caso del Se(IV).

La capacidad de producir nanopartículas de Se(0) por la reducción de Se(IV) ha sido descrita en multitud de bacterias y hongos (Ojeda et al., 2020; Tan et al., 2016; Zhang et al., 2019). Especies como *Stenotrophomonas maltophilia* SeITE02, *Proteus mirabilis* o *Bacillus selenitireducens*, entre otras, reducen Se(IV) al usarlo como aceptor de electrones alternativo (metabolismo asimilatorio o desasimilatorio), o bien como mecanismo de detoxificación en condiciones aerobias o anaerobias (Lampis et al., 2017; Wang et al., 2018; Wells et al., 2019). Como producto de este mecanismo se da la formación de precipitados rojizos de Se(0), en forma de nanopartículas amorfas, e incluso se forman nanoestructuras de las modificaciones alotrópicas de Se(0) monoclínico (*m*-Se) o trigonal (*t*-Se), que se acumulan dentro de la célula y/o en el espacio extracelular (Ruiz Fresneda et al., 2018; Ruiz-Fresneda et al., 2020; Tugarova and Kamnev, 2017). Además, esta última es de especial interés ya que se trata de la forma más estable de Se. Este hecho es de gran relevancia, ya que se ha demostrado la menor movilidad de las nanoestructuras de Se al tener una menor estabilidad coloidal y mayor eficiencia de sedimentación presentando, por tanto, una menor toxicidad en relación al resto de formas del metaloide (Jain et al., 2017). Entre las numerosas enzimas relacionadas con este proceso se encuentran la fumarato reductasa, las NAD(P)H deshidrogenasas o y la nitrito reductasa (Hunter, 2014; Piacenza et al., 2018; Song et al., 2017; Tan et al., 2018). También parecen estar involucrados los grupos tiol, especialmente el glutatión (GSH) (Lampis et al., 2014; Wang et al., 2018). Sin embargo, el conocimiento de microorganismos que llevan a cabo la reducción de Se(VI) es muy escaso. Uno de los mecanismos más estudiados es el de la enzima periplásmica selenato reductasa (Ser) descrita por primera vez en *Thaurera selenatis*, que permite la respiración anaerobia de Se(VI) (Schröder et al., 1997). Más tarde, el descubrimiento de otras Ser se extendió en diferentes microorganismos, como en *Bacillus selenatarsenatis* SF-1, tratándose en este caso de una proteína de membrana (Kuroda et al., 2011). Con posterioridad, también se ha descrito la reducción en condiciones aerobias en géneros como *Pseudomonas, Stenotrophomonas, Comamonas, Herbaspirillum* o (Che et al., 2019; Chen et al., 2020; Otsuka and Yamashita, 2020; Ruiz Fresneda et al., 2018; Ruiz-Fresneda et al., 2020). Además de con bacterias en cultivo puro, la reducción de Se(VI) también se ha estudiado en consorcios microbianos y lodos activados (Shi et al., 2020b; Yan et al., 2020; Z. Zhang et al., 2018). Por otra parte y, aunque también puede darse la oxidación de especies de Se insolubles, este fenómeno no es de gran relevancia debido a la baja tasa a la que ocurre (Eswayah et al., 2016).

La amplia diversidad metabólica relacionada con este proceso ocasiona que las nanopartículas sean muy variables en cuanto a sus características físico-químicas, lo que influye en la estabilidad y movilidad de las mismas. Normalmente las nanoestructuras producidas biológicamente presentan un recubrimiento orgánico, compuesto principalmente de polisacáridos y proteínas (Figura 7). Se ha demostrado que esta capa de materia orgánica juega un papel importante en la formación de las nanopartículas, influyendo en parámetros como el tamaño (Buchs et al., 2013; Dobias et al., 2011). Es por ello que se han dedicado grandes esfuerzos a conocer los mecanismos que determinan dichas características, ya que afectan a la eficacia de la técnica de biorremedio (Buchs et al., 2013). Por otra parte, el conocimiento detallado de este mecanismo no sólo tiene interés desde el punto de vista del biorremedio, sino que es objeto de creciente atención como método de biosíntesis de nanopartículas para su uso en aplicaciones industriales, por generar un menor impacto medioambiental en relación con la metodología estándar (Ojeda et al., 2020; Staicu et al., 2015).

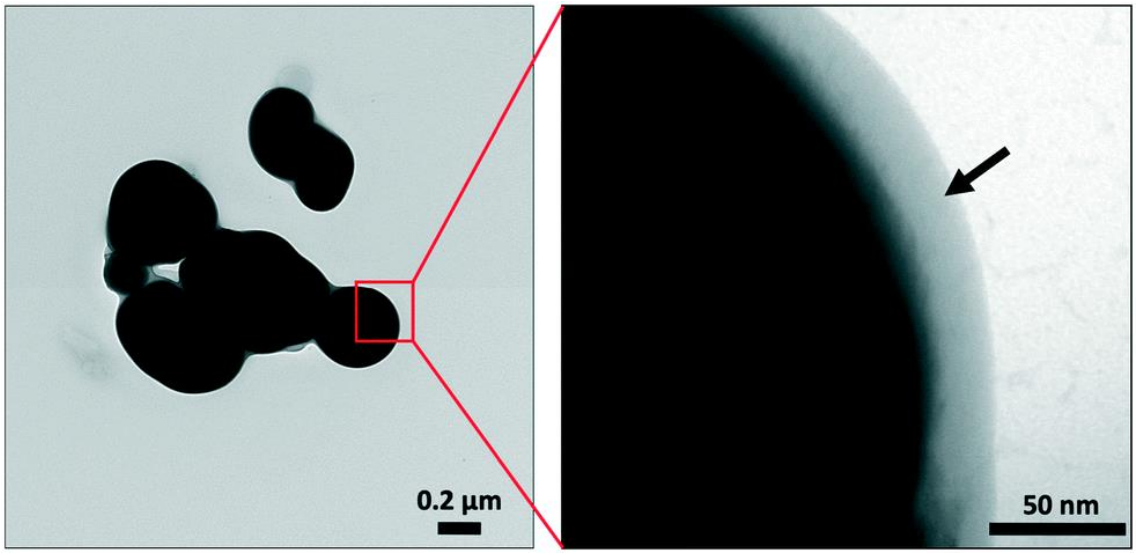

Figura 8. Nanoesferas de Se(0) sintetizadas por *Stenotrophomonas bentonitica* BII-R7 en presencia de Se(IV), recubiertas de una capa orgánica (derecha) (Ruiz-Fresneda et al., 2020).

Otro proceso de resistencia microbiana frente al Se y de interés como estrategia de biorremedio es la formación de especies volátiles de selenio. La formación de especies de dimetil seleniuro (DMSe) y dimetil diseleniuro (DMDSe) parece estar relacionada también con la detoxificación de este metaloide (Eswayah et al., 2016). Aunque aún queda mucho por conocer, la ruta de síntesis de especies volátiles conlleva la reducción y metilación del Se (Eswayah et al., 2016). Kessi (2006) demostró la relación entre el

metabolismo del GSH y la síntesis de estos compuestos en *Rhodospirillum rubrum* y *Rhodobacter capsulatus* al observar que la inhibición de la síntesis de GSH se traducía en una menor cantidad de especies volátiles. Algunas enzimas implicadas en la transferencia de grupos metilo también han sido identificadas en el proceso, como la tiopurina metiltransferasa de *Pseudomonas syringae*, que utiliza S-adenosilmetionina como molécula donadora de los grupos metilo formando DMSe y DMDSe al expresarse en *Escherichia coli* (Ranjard et al., 2002). Del mismo modo, la expresión en *E. coli* del gen *amtA*, que codifica para una metiltransferasa de *Hydrogenophaga* sp., también llevó a la detección de especies metiladas de Se (Ranjard et al., 2004).

3.3.Perspectivas futuras de estudios de resistencia microbiana a metales pesados: uso de técnicas ómicas

Pese a que los procesos de resistencia son muy estudiados, apenas existe conocimiento acerca de las bases genéticas y moleculares que los dirigen. Las tecnologías multi-ómicas son una herramienta muy útil para estudiar estos mecanismos a nivel molecular, ya que proporcionan gran cantidad de información sobre la respuesta celular que genera la exposición al contaminante, identificando así posibles rutas metabólicas, enzimas o genes implicados en los procesos de resistencia que sirven como dianas específicas para estudios posteriores. Sin embargo, mientras el uso de estas técnicas está extendido en el ámbito de investigación biomédica, no ha recibido mucha atención en el biorremedio de estos metales.

Gallois et al. (2018) llevaron a cabo el estudio del proteoma de *Microbacterium oleivorans* A9, aislada de suelo de una zona contaminada cerca de la central nuclear de Chernóbil, observando una perturbación del metabolismo del Fe y P por la exposición a U. Wang et al. (2019) identificaron genes específicos implicados en la resistencia a U mediante análisis transcriptómicos comparativos entre cepas de *Bacillus atrophaeus* tolerantes y sensibles al radionúclido. En el caso del Se, Fischer et al. (2020) realizaron análisis proteómicos de las proteínas adheridas a las nanopartículas de Se(0) producidas por *Bacillus safensis* JG-B5T. Del mismo modo, González-Gil et al. (2016) estudiaron las proteínas de nanopartículas, pero en este caso eran generadas por una comunidad microbiana de lodos granulares anaerobios en un reactor de aguas residuales. Sin embargo, pocos estudios proporcionan información acerca de la respuesta general a la exposición a los metales. Esto es de gran importancia, ya que es el conjunto de

mecanismos que se activan en la totalidad de la célula el que actúa conjuntamente para hacer frente a la toxicidad de los metales pesados y radionúclidos.

OBJETIVOS

El interés, tanto en la caracterización de las especies químicas de metal formadas como resultado de las interacciones microbianas con uranio (U) y selenio (Se), como en los procesos celulares subyacentes, ha crecido recientemente en el ámbito biotecnología ambiental. Las tecnologías ómicas son una estrategia prometedora para el estudio de dichas interacciones, otorgando gran cantidad de información acerca de la respuesta a nivel celular que genera la exposición de microorganismos a metales pesados y radionúclidos. Sin embargo, la aplicación de esta de metodología para fines de bioremedio está poco extendida, y poco se conoce aún acerca de los mecanismos moleculares específicos responsables de la resistencia a U y Se.

En base a estas premisas, esta tesis doctoral pretende estudiar las bases moleculares y genéticas de la respuesta de la cepa bacteriana *Stenotrophomonas bentonitica* BII-R7 a U y Se, con el fin de evaluar su potencial como agente de bioremedio de ambientes contaminados con estos elementos.

Los objetivos específicos propuestos para ello son:

1. Evaluación del efecto de factores fisicoquímicos y fisiológicos sobre la capacidad de la cepa *S. bentonitica* BII-R7 para llevar a cabo la biomineralización de U(VI), con la caracterización microscópica y espectroscópica de los precipitados generados.

2. Estudio de las bases genéticas de la resistencia microbiana a U(VI) y Se(VI) mediante técnicas de análisis transcriptómico en células de *S. bentonitica* BII-R7.

3. Análisis proteómico de la respuesta celular de *S. bentonitica* BII-R7 en presencia de Se(IV) e identificación de proteínas clave en el proceso de reducción y formación de nanoestructuras de Se(0).

MATERIALS AND METHODS

1. Biomineralization of U(VI) by *Stenotrophomonas bentonitica*

1.1. Bacterial strain and growth conditions

The newly described bacterial strain *S. bentonitica* BII-R7, isolated from bentonite clay formations from the south-east of Spain ("El cortijo de Archidona, Cabo de Gata" Natural Park Almería) (Sánchez-Castro et al., 2017a), was used in this Doctoral Thesis. Its recent characterization in our research group revealed a high tolerance to U, being able to grow even at 6 mM of the radionuclide (López-Fernández et al., 2014). Furthermore, whole genome analysis of BII-R7 identified interesting enzymes related to heavy metal resistance, as well as phosphatase enzymes, potentially involved in biomineralization of U(VI) in form of U(VI)-phosphates (López-Fernández et al., 2014, 2015; Sánchez-Castro et al., 2017b). The cells were grown and maintained aerobically in Luria-Bertani broth medium (tryptone 10 g/L, yeast extract 5 g/L, and NaCl 10 g/L, pH 7.0 ± 0.2) at 28 ºC on a rotatory shaker at 180 rpm.

1.2. Preparation of Uranium (VI) stock solution

A stock solution of uranyl nitrate ($UO_2(NO_3)_2 \cdot 6H_2O$) was prepared at a concentration of 1 M in 0.1 M of $NaClO_4$. This stock solution was filter-sterilized using nitrocellulose filters of 0.22 μm, then stored at 4 ºC until used.

1.3. Chemical speciation of U(VI) in the culture media

The software Visual Minteq (version 3.1) was used to obtain the chemical speciation of U(VI) in the culture media. Some organic compounds (xylose and tryptone) could not be considered in the calculations since they are not included in the databases of the software.

1.4. U(VI) removal experiments

Evaluation of the capability of cells of *S. bentonitica* to remove U(VI) was evaluated by estimating the concentration of U(VI) remaining in the culture medium after incubation with the bacterium. To that end, supernatant from U(VI)-cells suspensions were collected at different incubation times, and acidified with HNO_3. The amount of U(VI) was determined by using inductively coupled plasm-mass spectrometry (ICP-MS). Quantification of residual U(VI) was carried out with Arsenaze III method (Jauberty et

al., 2013). For that purpose, Arsenazo reagent was mixed with each sample and the absorbance was measured after 30-60 s at 651 nm (Genesys 10S UV-Vis; Thermo Scientific, MA, USA).

The amount of U adsorbed to the cells was calculated by subtracting the amount obtained in the supernatant from the initial U concentration. Solutions of U without cells of cells were used as control.

1.5 Biomineralization of U(VI) under growing conditions

The study of the effect of the physiological state of the cells in the effectiveness of the biomineralization of U(VI) process was addressed by growing cells of *S. bentonitica* in a optimized minimal medium.

1.5.1 Optimization of the culture medium for biomineralization assays

Evaluation of the biomineralization capability in growing conditions required the use of a salt minimal medium, in order to avoid possible abiotic precipitation of U(VI) that could affect to the interpretation of the results. The Tris Minimal Medium (TMM) from Choudhary and Sar (2011) was selected, althoug some modification were performed to obtain an optimal growth of BII-R7.

Cultures of *S. bentonitica* previously grown for 24h in diluted LB (10% final concentration) served to inoculate different variations of the medium amended with glucose, sodium acetate, gluconic acid, malic acid and D-(+)-Xylose. The level of growth was determined in microplates by reading the OD_{600} in Infinite Nanoquant M200 Pro. The final version of the TMM was composed by Tris-HCl, 6.06 g; NaCl, 4.68 g; KCl, 1.49 g; NH_4Cl, 1.07 g; Na_2SO_4, 0.43 g; $MgCl_2$, 0.03 g (pH 7.3-7.4), supplemented withβ-Glycerol phosphate disodium salt pentahydrate, 1.4 mM, sodium acetate, 15 mM, D-(+)-Xylose (2%) and tryptone (0.02%) in 1L of distilled water. For U(VI) assays, the cultures were amended with 100 and 250 μM of U(VI) from the stock solution.

1.5.2 Effect of U(VI) in S. bentonitica growth

Kinetic of the growth of *S. bentonitica* in liquid cultures of TMM amended with 100 and 250 μM of U(VI) was assessed by measuring the OD_{600} at 3-hour intervals.

1.5.3. Free inorganic phosphate (P_i) measurements

Free inorganic phosphate in the medium was estimated according to the methodology described by Murphy and Riley (1962). For that purpose, the samples were mixed with the reagent and absorbance was measured at 380 nm after 30 min. Abiotic

treatments (cultures amended with U(VI) but not inoculated with the bacterium) were used as controls.

1.5.4. Phosphatase activity in cells exposed to U(VI)

Determination of phosphatase activity of cultures of BII-R7 incubated with 100 and 250 μM of U(VI) was performed by using 4 methylumbelliferone (MUB)-phosphate di-Na salt (4-MUB-P) as substrate for phosphatase enzymes (German et al., 2011). Briefly, samples were collected by centrifugation at different incubation times, washed twice in NaCl (0.9%) and resuspended in $NaClO_4$ buffer at pH 5. Different concentrations of MUB used as standards and the samples were dissolved in $NaClO_4$ in a microplate. Excitation and emission were measured spectrophotometrically (Infinite Nanoquant M200 Pro) at 360 and 465 nm, respectively, and the data obtained were used to calculate the emission and quench coefficient of each sample as described in German et al., (2011).

1.6.Biomineralization of U(VI) under non-growing conditions

The biomineralization ability of *S. bentonitica* in non-growing conditions was assessed in 3-(*N*-morpholino)propanesulfonic acid (MOPS) buffer (20 mM) at two different pH (5.5. and 7) relevant for environmental contamination of U(VI). An appropriate amount of U(VI) from the stock solution was dissolved in the buffer to a final concentration of 100 μM. Glycerol-2-phosphate (G2P) (5 mM) was added as organic phosphate source. The medium was inoculated with BII-R7 cells at a final Optical Density (O.D) of 0.5.

The pH of the solutions was adjusted by addition of small volumes of acid ($HClO_4$) or base (NaOH) using an InLab Solids combination pH puncture electrode (Mettler-Toledo, Giessen, Germany) and sterilized by filtration through 0.22 μm nitrocellulose filters.

1.6.1. TRLFS spectra of complexes formed by S. bentonitica with U(VI)

Time-resolved laser fluorescence spectroscopy (TRLFS) is an advanced spectroscopic technique that enables to obtain speciation information on actinide and lanthanides metal ions at environmentally significant concentrations (micromolar to picomolar) (Collins et al., 2011). It is based on the analysis of the excitation and emission spectra and decay lifetimes of fluorescent metal ions irradiated with laser pulses (Figure 1). Since changes in the chemical speciation can alter the fluorescence, spectra and decay

lifetimes, this technique allows the identification of variations in the metal ions generated in different biogeochemical processes (Collins et al., 2011; Saito et al., 2010). Furthermore, it is also possible to determine the number of molecules or functional groups bound to the metal, through the number of water molecules present in the first coordination sphere (Saito et al., 2010).

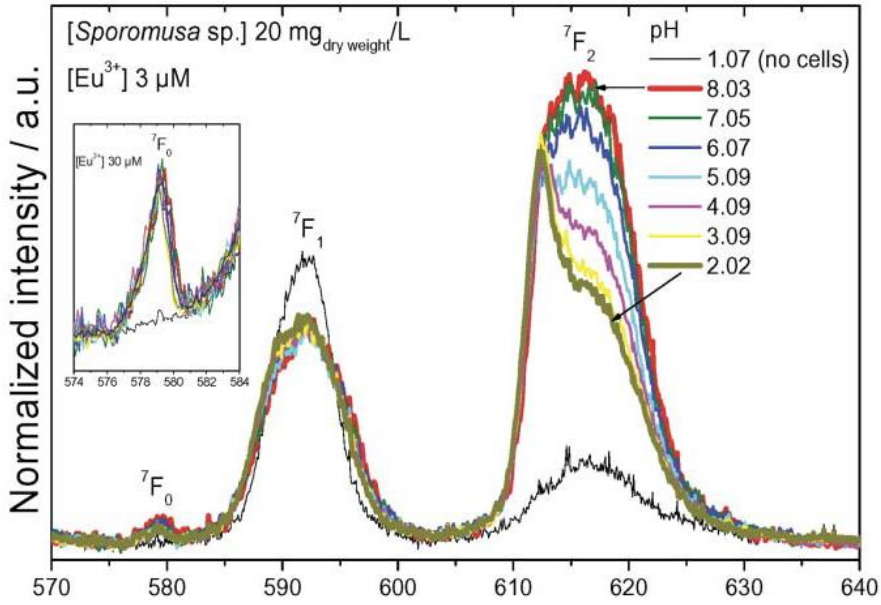

Figure 1. TRLFS spectra of curium (III) and europium (III) in *Sporomusa* sp. MT-2.99 as a function of pH (Moll et al., 2014).

This technique has showed to be very useful in determining the chemical speciation in solid and aqueous phases or to identify the coordination environment at molecular level of ions associated to minerals or the surface of bacterial strains (Collins et al., 2011). For this reason, the application of TRLFS analysis in this study would allow the detection of modifications of the in the chemical speciation of U(VI) at different incubation times, providing additional details about the functional groups at which U(VI) can be attached in the cell. To this effect, U(VI) was excited at 25°C using a pulsed Nd-YAG laser (Continuum, San Jose, USA) with laser pulses at 266 nm and an average pulse energy of about 250 µJ. The luminescence emissions were detected using an iHR 550 spectrograph (HORIBA Jobin Yvon, Bensheim, Germany) in combination with an ICCD camera (HORIBA Jobin Yvon, Bensheim, Germany). The luminescence spectrum of each sample was recorded from 370 to 670 nm by averaging 100 single spectra using a gate time of 2 µs. For time-resolved measurements a digital delay generator (DG535, Stanford Research Systems, Sunnyvale, CA, USA) was used. Subsequently, 51 U(VI) luminescence spectra were recorded at delay times between 0.05 and 50.05 µs with step sizes of 1 µs. Computer control over the entire system was ensured by the software

Labspec 5 (HORIBA Jobin Yvon, Edison, New York, USA). The obtained luminescence data were processed by using Origin 8.0 (Origin Lab Corporation, Northampton, MA, USA) including peak fitting module.

2. Mechanisms of interaction of *Stenotrophomonas bentonitica* in presence of selenium

2.1.Bacterial strain and growth conditions

Cells of *S. bentonitica* BII-R7 were cultured as previously indicated in section 1.1.

2.2. Se(VI) and Se(IV) stock solutions

Stock solutions from sodium selenite (Na_2SeO_3) and sodium selenate (Na_2SO_4) powder (Sigma-Aldrich) were prepared by dissolving the appropriate amount in Mili-Q water. The stock solutions were filter-sterilized by using 0.22 μM nitrocellulose filters, and then stored at 4º C.

2.3.Effect of Se(VI) on the growth of S. bentonitica

The effect of Se(VI) on cell growth was evaluated by quantification of total proteins in cells of *S. bentonitica*. For that purpose, 1 mL of cultures of BII-R7 exposed to 50 and 200 mM of Se(VI) were taken by centrifugation at different incubation times. Protein cells extracts were obtained by resuspending the pellets in extraction buffer (composed by SDS 99%, Na2HPO4, Triton X-100 and β-Mercaptoethanol 99%) and stored at -20 ºC for 24 h. Cells were then sonicated using Vibra cell™ sonicator at 30% of amplitude for 7 cycles of 15 sec with 10 sec intervals between cycles. Samples were centrifugated at 9000 rpm for 20 min at 4ºC, and total protein content was quantified using Bradford method (Bradford, 1976) with BSA as standard.

3. Microscopic analyses of uranium and selenium bioprecipitates

3.1 High-angle annular dark field scanning transmission electron microscopy (HAADF-STEM)

The determination of the morphology, size, amount and cellular location of U(VI) and Se products was performed in HAADF-STEM coupled to energy dispersive X-ray (EDX) spectrometry analyses. The nature of the minerals formed was determined by selected-area electron diffraction (SAED). In case of Se, further structural characterization of the nanostructures formed was carried out with high resolution TEM with fast Fourier transform (FFT). Samples were prepared as described in Merroun et al.,

(2005), and analysed in HAADF-STEM FEI TITAN G2 80-300 and Thermo Fisher Scientific TALOS F200X at the Centro de Instrumentación Científica (CIC) from University of Granada. To minimize sample contamination, prior to analysis the TEM specimen holders were cleaned by plasma.

3.2. Environmental scanning electron microscopy (ESEM)

Environmental scanning electron microscopy (ESEM) (Figure 2) with circular backscatter (CBS) and secondary (ETD) detectors allowed to characterize the formed in cultures of *S. bentonitica* with Se(VI) and to detect the presence of organic material around them. Cells were fixed in glutaraldehyde (2.5%) in cacodylate buffer (0.1M, pH 7.2) for 24 h. The pellets were fixed in 1% OsO_4 in cacodylate buffer and then dehydrated in ethanol solutions and the critical point method. Samples were analysed in ESEM FEI QUEMSCAN 650F equipped with X-ray microanalysis device Dual EDS XFlash Bruker with XFlash 6/30 detector at CIC from University of Granada.

Figure 2. Environmental scanning electron microscope from "Centro de Instrumentación Científica" of the University of Granada.

4. Molecular characterization of interactions with U and Se

4.1. Transcriptomics analyses of cells grown with U(VI) and Se(VI)

Transcriptomics analyses in cells of *S. bentonitica* enable to determine the cellular response to the presence of U(VI) and Se(VI). For this purpose, extraction of total RNA was performed using RNeasy Bacteria Mini kit (Qiagen). RNA sequencing was carried

out in the Helmholtz Centre for Infectious Diseases (Braunschweig, Germany). The detailed procedure is described in Pinel-Cabello et al. (2021) and chapter IV.

Transcriptomic-based approaches are revolutionary next generation sequencing (NGS) tools that provide the rapid generation of high quantities of information about the differential gene expression in biological systems, either an entire organism or in a given cell type. Their wide use in different biotechnological fields allowed a better understanding of biological, functional and molecular processes, which led to important progresses in disease mechanisms and diagnosis, therapies or microbial resistance to antibiotics. In addition, the application of these techniques in environmental biotechnology and bioremediation is gaining momentum, as more information about the specific metabolic pathways involved in degradation and resistance of pollutants is needed for the optimization of microorganisms-based bioremediation strategies.

4.2. Next generation proteomics of cells exposed to Se(IV)

Next generation proteomics is a powerful tool based on the high-throughput identification and quantification of the complete proteome of biological systems under specific physiological conditions. This technology is coupled with the biophsysical technique on tamden mass spectrometry. This approach has shown to be very useful determining the key proteins in process of biotechnological relevance, which provides new perspectives for metabolic engeenering (Armengaud, 2016). The technique can be addressed by the previous proteolysis of the total proteins in fragments, wich the later identification of peptide sequences by tandem mass spectrometry (bottom-up proteomics), or by the direct analysis of native proteins without previous digestion, with the fragmentation in the mass spectrometer for determination of the partial sequence (top-down).

Initially applied for medical research, it is currently used for characterization of biological processes mediated by microorganisms with biotechnological purposes. Although this approach has barely applied in microbial strains for bioremediation technologies, it offers a new perspective in the study of environmental samples. The response of *S. bentonitica* cells to Se(IV) exposure at specific incubation times was determined by differential label-free proteomics. Culture of BII-R7 in presence of 2 mM of Se(IV) and the proteomic shotgun experiments were performed during a short stay in the centers of Commissariat à l'Energie Atomique et aux Energies Alternatives (CEA) in

Cadarache and Marcoule (France). The specific details of the experimental procedure are described in the chapter III.

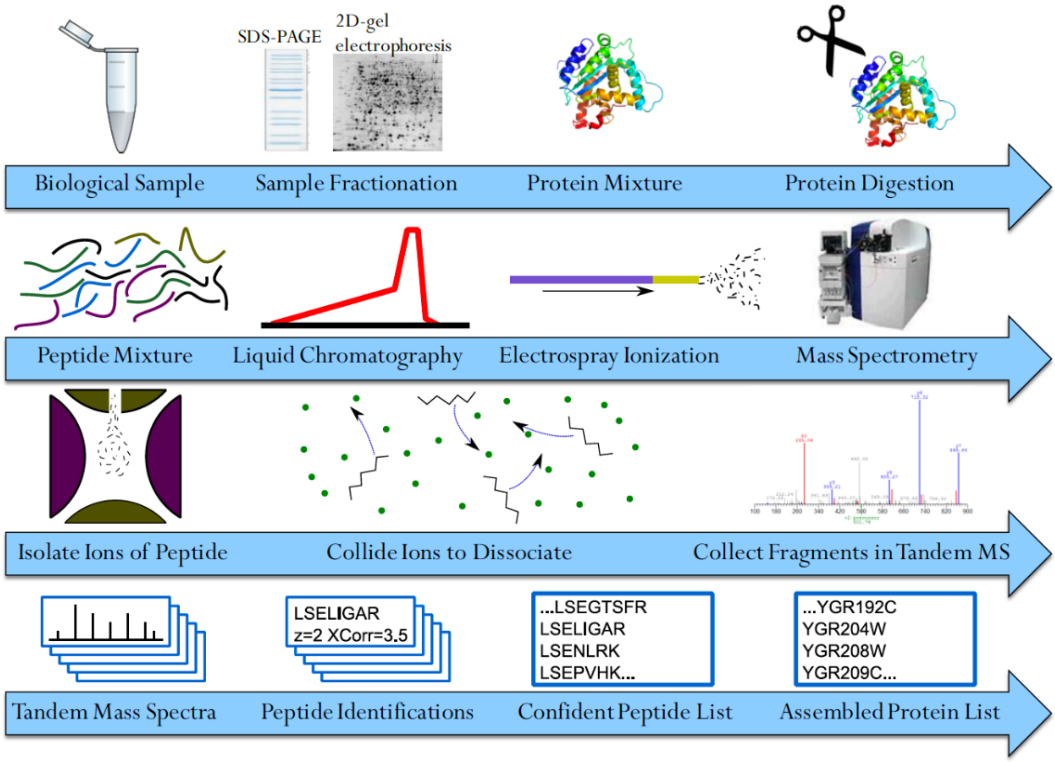

Figure 3. Workflow of shotgun proteomics analysis (Cheng et al., 2012).

CHAPTER I

Role of growth conditions and physico-chemical factors controlling the removal and biomineralization of U(VI) in *Stenotrophomonas bentonitica* BII-R7

María Pinel-Cabello[1], Miguel A. Ruiz-Fresneda, Iván Sánchez-Castro[1], Hannes Brinkmann[2], Henry Moll[2], Andrea Cherkouk[2], Margarita López-Fernández[1], Mohamed L. Merroun[1]

[1]Department of Microbiology, University of Granada, Granada, Spain

[2]Institute of Resource Ecology, Helmholtz-Zentrum Dresden-Rossendorf e.V., Dresden, Germany

Abstract

Production of radioactive wastes containing radionuclides such as U and Pu, is a matter of great concern given the persistence of these contaminants in the environment, leading to severe health and ecological damage. In the last decades, research in bioremediation of radionuclides have focused in the biomineralization capability of U-resistant microbes, and even environmental factors affecting the process, such as pH, have been addressed. However, little is known about the biological processes that determine the efficiency of the interactions between U and microorganisms. The present work studies the influence of pH and physiological state on the mechanisms of interaction with U(VI) in the newly described bacterial species *Stenotrophomonas bentonitica* BII-R7. To that end, a multidisciplinary approach combining analytic, spectroscopic, biochemical and microscopic techniques was performed under bacterial growing and non-growing conditions in presence of U(VI). The results showed that BII-R7 is able to precipitate insoluble U(VI)-phosphate through a biomineralization mechanism. The process showed to be more effective at neutral pH, and the U(VI) removal efficiencies were even higher when the cells were grown in an optimized minimal medium. Location of the precipitates by STEM-HAADF, along with TRLFS analyses, suggested a two-stage process involving two interaction mechanisms with U: firstly, a fast-passive biosorption process of U(VI) to organic phosphate groups of the cell surface, which would be later biomineralized in form of inorganic phosphate-(UVI) precipitates, probably with a structure similar to meta-autunite. Therefore, the results evince the key role of the physiological factors in the effectiveness of the biomineralization process, but also the suitability of *S. bentonitica* for the long-term removal of U(VI) for bioremediation purposes.

Key words: uranium, biomineralization, *Stenotrophomonas*, phosphatase enzymes

1. Introduction

Radioactive wastes are widely produced by anthropogenic activities associated to medicine, research, agriculture, mining and milling, and nuclear industry (different steps of production and enrichment of uranium (U), fabrication and reprocessing of fuel from nuclear fuel cycle for electricity production). Although radioactivity decreases over time, these residues must be correctly managed, since some of them require even thousands of years before reaching safety levels of radiation. It is the case of high-level wastes, composed by activation and fission products, plutonium (Pu) and U, among others (IAEA, 2018) . As a consequence of the massive production of nuclear wastes, long-term environmental contamination of U and other radionuclides has become a matter of great concern. U remaining in the radioactive wastes, along with other radionuclides such as thorium and toxic heavy metals, can be mobilized to soil and water environments, where cause severe ecosystems damage with the risk of reaching the food chain (Brugge and Buchner, 2011; Shukla et al., 2017). In addition, the lasting half-life of this inorganic contaminant makes it especially hazardous, persisting in the environment for long periods of time (Brugge and Buchner, 2011; IAEA, 2018). The most stable oxidation states of U in nature are the U(VI) and U(IV), depending on the environmental conditions (Banala et al., 2021; Shukla et al., 2017). These forms are also the most hazardous species of U due to their solubility, specially U(VI), and can cause severe impact on human health when safety levels are exceeded, due to its radiological and chemical toxicity (Brugge and Buchner, 2011). Among the negative effects attributed to U exposure are included kidney damage, hepatotoxicity, decreased fertility, several types of cancer, and even it can accumulate in bone tissue (Bjørklund et al., 2020).

The interest of understanding how microorganisms interact with radionuclides have increased over the recent decades, since microbial activity can affect the solubility of heavy metals and radionuclides, which determines their mobility to the surrounding environment (Zammit et al., 2014). Microbial/radionuclide interaction mechanisms include biosorption at the cell surface, bioaccumulation, biomineralization and redox reactions (Lopez-Fernandez et al., 2020; Yang et al., 2015). Many microorganisms have been reported to be able to survive under toxic concentrations of U through these processes (Shukla et al., 2017), and their use as bioremediation agents have become an attractive approach due to the several benefits that offers (high biomass availability, low cost, less negative environmental consequences and use of native microbial species) (Bhakat et al., 2019; Wei et al., 2019; Yang et al., 2015a). While biosorption occurs as

simple electrostatic forces between the cell surface and the metal, this mechanism is highly dependent on the physicochemical conditions (*e.g.* pH) (Yang et al., 2015). Hence, metabolism-dependent mechanisms are more interesting in terms of bioremediation, as usually produce the long-lasting immobilization of the metal in less bioavailable forms (Merroun and Selenska-Pobell, 2008; Newsome et al., 2014).

Although intracellular bioaccumulation has been studied for U(VI) remediation in contaminated sites, this method may hinder the metal recovery (Yang et al., 2015). On the other hand, biomineralization is an alternative that allows the long-term reduction of the mobility of the radionuclide, yielding stable products with potential applications (Sun et al., 2016). While reductive precipitation of U(IV) is more stable in absence of oxygen, biomineralization of U(VI) occurs mainly under aerobic conditions (Acharya, 2015). Nonreductive biomineralization consist in the precipitation of insoluble forms of U(VI) by interaction of the radionuclide with ligands (phosphate or sulfide) produced via microbial enzymatic activity, but it can also occur by alkalinization at the cell surface level (Acharya, 2015; Newsome et al., 2014). The ligand remains near the cell, where components of the bacterial surface provide a nucleation site for precipitation of U(VI) in different forms of uranyl phosphate, which limits the dispersion of the radionuclide and facilitates metal recovery with regard to chemical precipitation in dilute solutions (Lloyd and Macaskie, 2000; Newsome et al., 2014). In presence of an organic phosphate source, many bacterial species are able to release inorganic phosphate (P_i) via alkaline and/or acid phosphatase activity (Merroun and Selenska-Pobell, 2008). Macaskie et al. (2000) described the ability of a *Citrobacter* sp. (lately reclassified as *Serratia* sp. (Pattanapipitpaisal et al., 2002)) to form uranyl phosphate crystals bound to the LPS as a result of the activity of the acid phosphatase PhoN. Biomineralization has been also widely described in several species of *Bacillus* under different conditions, such as in presence of organic acids or humic substances as competitive ligands of P_i in nature (Tu et al., 2019a, 2019b). Furthermore, different pH values lead to changes in the yield and location of the minerals precipitated. *Microbacterium oxydans* SW-3 and *Stenotrophomonas maltophilia* JG-2 showed U(VI)-phosphate precipitates at pH 4.5, but no minerals were observed when U exposure occurred at pH 2 (Merroun and Selenska-Pobell, 2008). Similarly, *Serratia* sp. OT II 7 was able to form extracellular calcium uranyl phosphate minerals at pH 7 and 9, while U(VI)-phosphate accumulated intracellularly at pH 5 (Chandwadkar et al., 2018). However, challenges such as the low rate of biomineralization limit the performance of the method in natural environments

(Song et al., 2019). Many studies assess the microbial interactions with U(VI) under non-growing conditions (Banala et al., 2021; Song et al., 2019), but growing cells in a culture medium could have a different impact in biomineralization since it could affect processes such as LPS production or phosphatase activity. Furthermore, the nutrient deficiency could also have a negative effect in the performance of microbial-U(VI) interactions.

The present work is aimed to determine the role of the pH and physiological state of cells of *Stenotrophomonas bentonitica* BII-R7 in biomineralization of U(VI), through a combination of robust analytic, biochemical, spectroscopic and microscopic techniques. This strain was isolated from bentonite formations from the south-east of Spain (Sánchez-Castro et al., 2017b), selected as artificial barrier for Spanish geological repository of nuclear wastes. Previous studies revealed the ability to grow at high concentrations of U(VI), with a minimal inhibitory concentration (MIC) of 6 mM, as well as the high presence of endogenous acid and alkaline phosphatase activity (Lopez-Fernandez et al., 2014, 2015; Pinel-Cabello et al., 2021; Sánchez-Castro et al., 2017). Hence, this study involves the knowledge of the interactions of *S. bentonitica* with U(VI) under non-growing and growing conditions, as well as the influence of the pH, in order to assess the biological and environmental factors controlling the biomineralization process. The results obtained here will provide a starting point for the parameters to consider for further investigation to improve the U(VI) bioremediation strategies.

2. Materials and methods

2.2.Bacterial growth and culture conditions

The strain used in the present work was *S. bentonitica* BII-R7, isolated from Spanish bentonite formation located in "El Cortijo de Archidona, Cabo de Gata" Natural Park (Sánchez-Castro et al., 2017b). The cells were grown and maintained in Luria Bertani (LB) broth medium (tryptone 10g/L, yeast extract 5 g/L and NaCl 10 g/L, pH 7.0 ± 0.2) at 28ºC under shaking at 180 rpm for 24 h.

2.3.. Preparation of Uranium (VI) stock and working solution

A stock solution of U(VI) was prepared by dissolving uranyl nitrate in sterile distilled water to a final concentration of 0.01 M. A U(VI) working solution was prepared by diluting the U stock solution in MOPS buffer (20 mM). The pH of the solutions was adjusted by addition of small volumes of acid ($HClO_4$) or base (NaOH) using an InLab Solids combination pH puncture electrode (Mettler-Toledo, Giessen, Germany) and sterilized by filtration through 0.22 μm nitrocellulose filters.

Chemical speciation of U(VI) in MOPS and Tris Minimal Medium was obtained using the software Visual MINTEQ v. 3.1. In case of TMM, some organic compounds (xylose and tryptone) could not be considered in the calculations since they are not included in the databases of the software.

2.4.. Cellular localization of U(VI) precipitates by STEM/HAADF

The celular location and characterization of the precipitates formed was performed by microscopic analyses. Samples under growing and non-growing conditions were collected at different incubation times by centrifugation. The resultant pellets were washed twice and re-suspended in $NaClO_4$ and subsequently prepared as described in Merroun et al. (2005). The cellular location of U was examined under a TEM LIBRA 120 PLUS Carl Zeiss SMT microscope and a high-angle annular dark field scanning transmission electron microscope (STEM/HAADF) Thermo Fisher Scientific TALOS F200X equipped with energy dispersive X-ray (EDX) for elemental composition analysis. EDX analysis was performed at 300 kV using a spot size of 4 Å and a live counting time of 50 s. STEM specimen holders were cleaned by plasma prior to STEM analysis to minimize contamination.

2.5. Biomineralization of U(VI) under growing conditions

2.5.1. Minimal medium optimization for growing conditions assays

Growth of *S. bentonitica* in presence of U(VI) was performed in TMM (Choudhary and Sar, 2011). This medium was tested and modified in order to guarantee the correct growth of the bacterium and to avoid abiotic precipitation during U(VI) assays. Composition of TMM consisted of (1 L of distilled water) Tris-HCl, 6.06 g; NaCl, 4.68 g; KCl, 1.49 g; NH_4Cl, 1.07 g; Na_2SO_4, 0.43 g; $MgCl_2$, 0.03g; glycerol-2-phosphate (G2P), 0.432 g (1.4 mM); glucose, 5 g (pH 7.3-7.4). β- Sodium acetate, gluconic acid, malic acid and D-(+)-Xylose were also tested as carbon source, and tryptone (0.02%) was added as nitrogen source. All minimal media variations were inoculated with a 24 h-old culture of *S. bentonitica* at an initial Optical Density (OD_{600}) of 0.1, incubated for 48 h at 28ºC under shaking in microplates. Growth was evaluated by reading the OD_{600} using Infinite Nanoquant M200 Pro.

Final composition of optimized TMM consisted of (1 L of distilled water) Tris-HCl, 6.06 g; NaCl, 4.68 g; KCl, 1.49 g; NH_4Cl, 1.07 g; Na_2SO_4, 0.43 g; $MgCl_2$, 0.03 g (pH 7.3-7.4), supplemented with G2P, 1.4 mM, sodium acetate, 15 mM, D-(+)-Xylose (2%) and tryptone (0.02%). Glycerol phosphate and xylose were filter-sterilized using

nitrocellulose filters of 0.22 μm. Sodium acetate and tryptone were sterilized separately prior addition to the medium.

2.5.2. Quantification of residual U(VI) and free inorganic phosphate (P_i) in the culture medium

The amount of U removed biologically by *S. bentonitica* was determined by growing the strain in TMM modified as described in the section 2.4.1. Cells previously grown for 24 h in diluted LB liquid medium (10% final concentration), were harvested by centrifugation (11,000 rpm for 10 min), washed twice with NaCl 0.9% (w/v) and aliquots were inoculated in flask containing TMM at an initial O.D. of 0.05 (OD_{600}) (Genesys 10S UV-Vis; Thermo Scientific, MA, USA). For treated cells, TMM was amended with U to a final concentration of 100 and 250 μM. Three biological replicates were performed for each treatment.

Cells were collected at 15 min, 24, 48 and 72 h of incubation by centrifugation at 11,000 rpm for 5 min, and supernatants were stored at -20 ºC. Residual U in the supernatants was measured using Arsenazo III method (Jauberty et al., 2013). For that purpose, 1 mL of Arsenazo reagent was mixed with 250 μL of each sample and wait for 30 to 60 s before measuring the absorbance at 651 nm. Abiotic controls were also measured to detect and quantify possible abiotic precipitation of the radionuclide. Measurements using inductively coupled plasm-mass spectrometry (ICP-MS) were also performed in order to obtain more accurate data of this parameter. To that end, 3 mL of each sample were mixed with 4% of nitric acid, and quantified using NexION 300D (PerkinElmer) equipment.

Quantification of free inorganic phosphate (P_i) released by the strain was determined as described by Murphy and Riley (1962). Briefly, 280 μL of sample were diluted in 400 μL of distilled water, and 320 μL of reagent were added and incubated for 30 min. Absorbance was measured at 850 nm.

2.5.3. Determination of phosphatase activity of S. bentonitica in presence of U(VI)

Quantification of phosphatase activity of the strain was measured according to German et al. (2011) based on the use of 4 methylumbelliferone (MUB)-phosphate di-Na salt (4-MUB-P) as a substrate. For that purpose, 10 mL of each sample were taken by centrifugation at 11,000 rpm for 10 min at lag, exponential and stationary phases (1, 24

and 48 h of incubation, respectively). Cells were washed twice with NaCl 0.9% and resuspended in 5 mL of $NaClO_4$ buffer (pH 5). Samples (200 µL) and MUB standards (0.16 µM, 0.625 µM, 1.25 µM and 2.5 µM) were dissolved in $NaClO_4$ in a microplate in order to estimate the emission and quench coefficients of the samples, and read at 360 nm excitation and 465 nm emission (Infinite Nanoquant M200 Pro). An estimation of the phosphatase activity was made as described by German et al. (2011).

2.6. Biomineralization of U(VI) under non-growing conditions

2.6.1. Kinetics of U(VI) precipitation by the bacterium

S. bentonitica cells were collected at the exponential phase of growth by centrifugation (10,000 x g; 10 min). The resultant pellet was washed three times with 0.1 M $NaClO_4$ and resuspended therein to obtain a final biomass concentration of 0.2 g/L (0.5 O.D). Afterwards, the samples were contacted aerobically with 100 µM U(VI) working solution under different pH conditions (5.5 and 7) and incubated at 120 rpm on a rotator shaker at room temperature. G2P (5 mM) was added as organic phosphate source into the cultures. The U-bacteria suspensions were harvested by centrifugation (10000 x g; 10 min) after different incubation times (2, 24, and 48h). Then, 1 mL of the resultant supernatant was acidified with HNO_3 and measured by ICP-MS to estimate the U concentration. The amount of U adsorbed to the cells was calculated by subtracting the amount obtained in the supernatant from the initial U concentration. U solution (100 µM) without addition of cells was employed as control. All samples were performed in triplicate.

2.6.2. TRLFS spectra of complexes formed by S. bentonitica with U(VI)

Cells of *S. bentonitica* were brought into contact with 100 µM U(VI) under different pH conditions (5.5 and 7) and incubating times (2, 24, and 48h), and subsequently collected as described in section 2.4.1. The obtained pellets were washed twice and subsequently re-suspended in 0.1 M $NaClO_4$. Finally, TRLFS-measurements were performed in 1 cm single-use polystyrene cuvettes (Carl Roth, Karlsruhe, Germany).

The samples were put on a special sample holder and were positioned in the laser beam. U(VI) was excited at 25°C using a pulsed Nd-YAG laser (Continuum, San Jose, USA) with laser pulses at 266 nm and an average pulse energy of about 250 µJ. The luminescence emissions were detected using an iHR 550 spectrograph in combination with an ICCD camera (HORIBA Jobin Yvon, Bensheim, Germany). The luminescence

spectrum of each sample was recorded from 370 to 670 nm by averaging 100 single spectra using a gate time of 2 µs. For time-resolved measurements a digital delay generator (DG535, Stanford Research Systems, Sunnyvale, CA, USA) was used. Subsequently, 51 U(VI) luminescence spectra were recorded at delay times between 0.05 and 50.05 µs with step sizes of 1 µs. Computer control over the entire system was ensured by the software Labspec 5 (HORIBA Jobin Yvon, Edison, New York, USA). The obtained luminescence data were processed by using Origin 8.0 (Origin Lab Corporation, Northampton, MA, USA) including peak fitting module.

3. Results

3.1 Chemical speciation of U(VI) in the culture media

Chemical speciation of U was theoretically determined in MOPS supplemented with 5 mM of G2P and in TMM medium (with xylose and acetate as carbon source). The most predominant U(VI) species found in all treatments was $(UO_2)_3(OH)_5^+$, followed by $(UO_2)_4(OH)_7^+$. However, differences in the proportion of these species were observed with regard to the pH and initial U(VI) concentration (Table 1).

The 71.5 % of U is present as $(UO_2)_3(OH)_5^+$ in MOPS at pH 5.5 and 64.6 % at pH7, while $(UO_2)_4(OH)_7^+$ represents 12.5 and 33.9% respectively. On the other hand, the 60.8 and 54.8% of U correspond to $(UO_2)_3(OH)_5^+$ in TMM amended with 100 and 250 µM of U(VI), against the 37.2 and 43.9 % for $(UO_2)_4(OH)_7^+$ in these conditions.

3.2. Biomineralization of U(VI) by S. bentonitica under growing conditions

The effect of growing cells of *S. bentonitica* on the speciation of U(VI) was studied using minimal culture medium at two different U concentration (100 and 250 µM). Evaluation of the U(VI) biomineralization capability of *S. bentonitica* required the use of minimal media in order to minimize abiotic precipitation due to the interaction of the metal with medium components.

Table 1. Chemical speciation of U(VI) in MOPS and TMM as function of metal concentration and pH

% of total concentration					
MOPS			**TMM**		
pH 5.5	pH 7		100 μM	250 μM	
3.77	0.014	UO_2^{+2}	0.383	0.201	UO_2OH^+
5.547	0.555	UO_2OH^+		0.027	$(UO_2)_2(OH)_2^{+2}$
5.295	0.059	$(UO_2)_2(OH)_2^{+2}$	60.809	54.793	$(UO_2)_3(OH)_5^+$
71.479	64.629	$(UO_2)_3(OH)_5^+$	37.205	43.945	$(UO_2)_4(OH)_7^+$
12.463	33.882	$(UO_2)_4(OH)_7^+$	0.536	0.483	$(UO_2)_3(OH)_7^-$
1.22	0.041	$(UO_2)_3(OH)_4^{+2}$	0.031	0.028	$(UO_2)_3(OH)_4^{+2}$
0.019	-	$(UO_2)_2OH^{+3}$	0.151	0.079	$UO_2(OH)_3^-$
0.207	0.621	$UO_2(OH)_2$ (aq)	0.703	0.368	$UO_2(OH)_2$ (aq)
-	0.145	$(UO_2)_3(OH)_7^-$	0.046	0.024	UO_2-$(Acetate)_3^-$
-	0.055	$UO_2(OH)_3^-$	0.047	0.024	UO_2-$(Acetate)_2$ (aq)
				0.02	UO_2-$Acetate^+$

3.2.1. Optimization of minimal medium for U(VI) assays

The growth of BII-R7 was assessed in TMM (Choudhary and Sar, 2011), previously used in studies of bacterial interaction with U (Choudhary et al., 2012; Islam and Sar, 2016), prior to U exposure, and was adapted according to the nutritional requirements of the strain (Sánchez-Castro et al., 2017b).

Preliminary assays were focused on evaluating the cell growth (measured as $O.D_{600}$) in the original composition of TMM (see section 2.3.1). However, no significant

growth of *S. bentonitica* was detected under these conditions (data not shown). The lack of growth in TMM was probably due to two main reasons: the presence of glucose as carbon source and the low efficiency to obtain N from NH_4Cl. Therefore, the main changes performed in this medium were focused on addressing these matters. Based on the carbon sources more efficiently used by the strain (Sánchez-Castro et al., 2017), malic acid, xylose, gluconic acid and sodium acetate were selected. Therefore, four variations of the medium were performed, one for each carbon source, added at a final concentration of 5%. The challenge regarding the N source was addressed by adding tryptone at 0.02%.

Treatments supplemented with xylose and sodium acetate showed the higher $O.D_{600}$, followed by gluconic acid. Despite the fact that previous biochemical characterization of *S. bentonitica* demonstrated its ability to use malic acid as carbon source, this treatment showed the lowest cell growth. For this reason, the use of malic acid was not considered for further assays. Although there was some growth, it is expected that the presence of U(VI) negatively impact the viability of the cells, being necessary to obtain higher $O.D_{600}$ to conduct U(VI) assays. In order to improve these results, the next step consisted in the use of different concentrations of gluconic acid and sodium acetate (5 and 15 mM) combined with 2% of xylose. Original composition of TMM was used as control. The greater $O.D_{600}$ was reached in both treatments amended with acetate, particularly in those with 15 mM, suggesting a synergic effect of both xylose and acetate (Fig. 1). Hence, TMM supplemented with 2% of xylose, 0.02% of tryptone and 15 mM of sodium acetate was selected to perform U(VI) biomineralization assays.

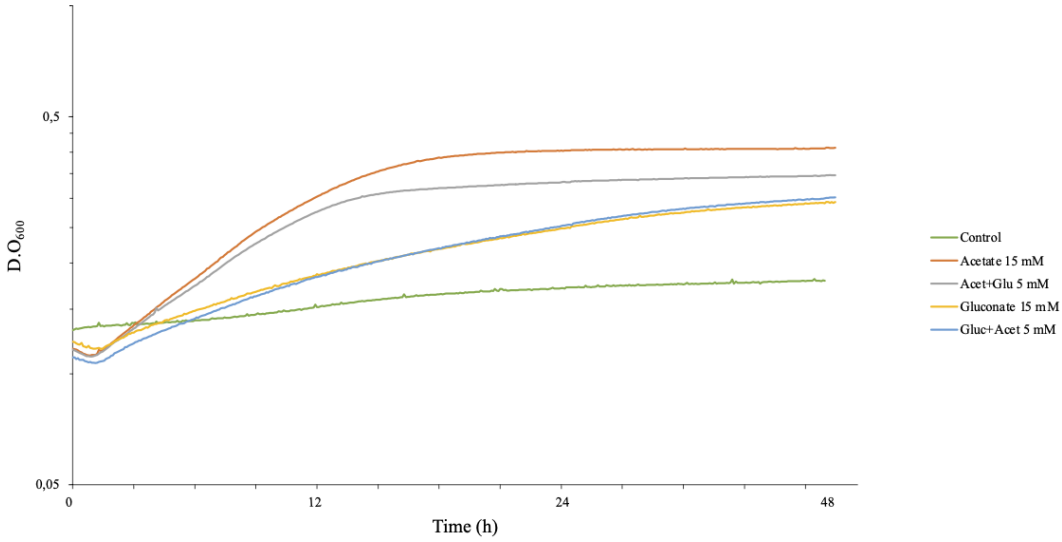

Fig. 1. Growth curves of *S. bentonitica* in Tris Minimal Medium (TMM) supplemented with different carbon sources. A treatment with the original composition of the TMM was used as control.

3.2.2. Quantification of residual U and free inorganic phosphate (P_i) in the culture medium

In order to evaluate U(VI) biomineralization of *S. bentonitica* in TMM, the concentration of soluble U(VI) in supernatants of cultures of the strain in TMM amended with 100 and 250 μM was measured at 15 min, 24, 48 and 72 h of incubation by Arsenazo III method. Fig. 2 shows that *S. bentonitica* was able to reduce progressively the quantity of soluble U(VI) throughout the incubation time at both tested U(VI) concentrations. During the first 24 h of contact with the metal, a quick reduction of 93.1±0.7 and 95.7±1.8% of the soluble U(VI) at 100 and 250 μM was detected, respectively, followed by a slower decrease in the later hours until reach up to 98±1.1% of U(VI) removed at both concentrations. Abiotic controls (medium amended with $UO_2(NO_3)_2{\cdot}6H_2O$ without bacteria) confirmed the key role of BII-R7 in the biomineralization process, as only a maximum of 13±9.6 and 21.8±8.3% of U(VI) was abiotically removed in the medium at 100 μM and 250 μM U, respectively.

The samples corresponding to 15 min, 24 and 72 h were also analyzed by ICP-MS, to determine the concentration of U(VI) more accurately. Fig. S1A shows the residual concentration of U(VI) in the supernatant of the samples in mg/L. From an initial concentration of 23.8 mg/L for 100 μM and 59.5 mg/L for 250 μM, the amount of U(VI) measured after 72 h of incubation with BII-R7 was 0.2±0.1 and 0.5±0.1 mg/L, respectively, which corresponded to 99±0.2% of U(VI) removed at both concentrations (Fig. S1B). These findings indicate that initial concentration of U(VI) did not impact the

biomineralization capability of the strain. On one hand, the concentration of U(VI) remained constant in abiotic controls for treatments with 100 μM, with around 10% of abiotic precipitation. On the other hand, a slight reduction in U(VI) concentration for abiotic controls with 250 μM was observed, with 30±1.9% of precipitation at 72 h. However, these percentages are much lower than those observed in treatments with U(VI) and the bacterium. These results were highly consistent with those obtained with Arsenazo III, corroborating the reliability of the method.

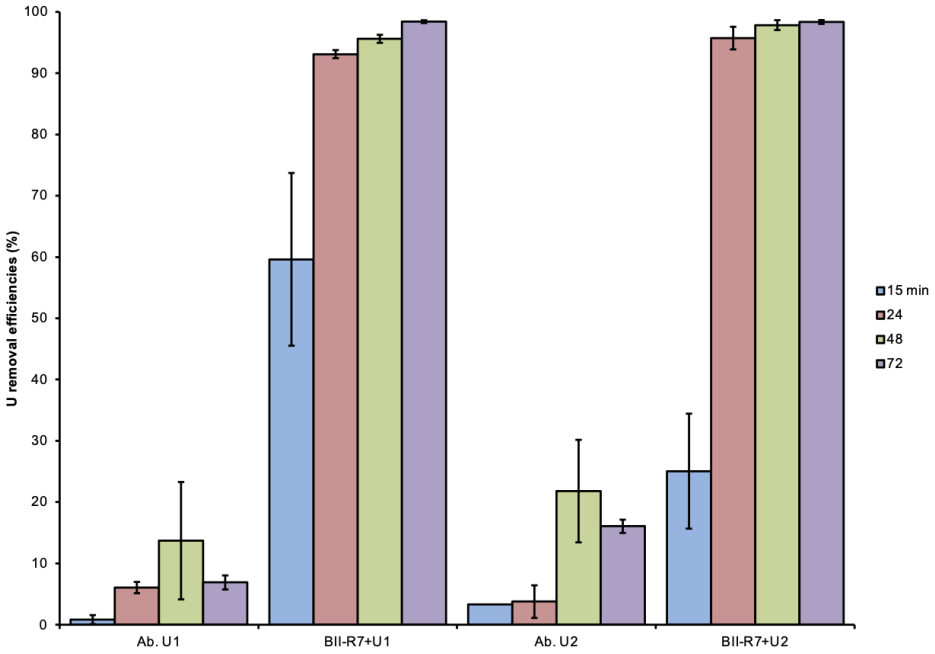

Fig. 2. U(VI) removed as % measured with Arsenazo III method at 100 (U1) and 250 (U2) μM. Abiotic controls (Ab. U1 and U2) were also performed.

Free inorganic phosphate (P_i) was also measured in the supernatant, to investigate whether the decrease in U(VI) concentration was produced by biomineralization in form of U(VI)-phosphate as a consequence of endogenous phosphatase activity of the strain. The amount of P_i released to the medium in % is showed in Fig. 3. The P_i increased gradually throughout the incubation time. No differences were found neither between treatments with 100 and 250 μM U nor between treated and non-treated cells, indicating that the amount of P_i released is not influenced by the initial concentration of the metal. Moreover, the concentration of P_i did not increase in abiotic controls, and remained constant at very low levels in all sampling time tested, which suggest that BII-R7 plays a key role in this process. The maximum percentage of P_i transferred from the G2P was around 25%, which indicates that the G2P was in excess in the culture medium despite

the reduction of its concentration in TMM with regard to the non-growing conditions (1.4 mM in TMM against the 5 mM in MOPS).

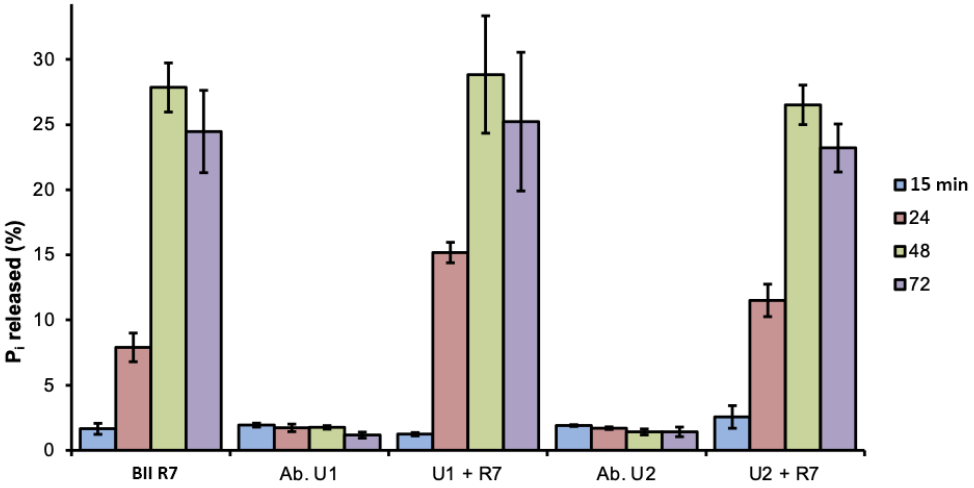

Fig. 3. Percentage of Pi released to the culture medium after 15 min, 24 h, 48 h and 72 h of incubation of *S. bentonitica* in TMM amended with 100 (U1) and 250 (U2) µM of U(VI).

3.2.3 Phosphatase enzymatic activity in S. bentonitica

Phosphatase activity of *S. bentonitica* growing in TMM amended with 100 and 250 µM of uranyl nitrate was measured after 1, 24 and 48 h of incubation as described above. BII-R7 showed the highest phosphatase activity at 1 h at both U(VI) concentrations tested, while no significant levels of activity were detected in the following times (Fig. 4). However, no enzymatic activity was detected in non-treated samples at any incubation time, suggesting a possible induction of the phosphatases in *S. bentonitica* by the metal.

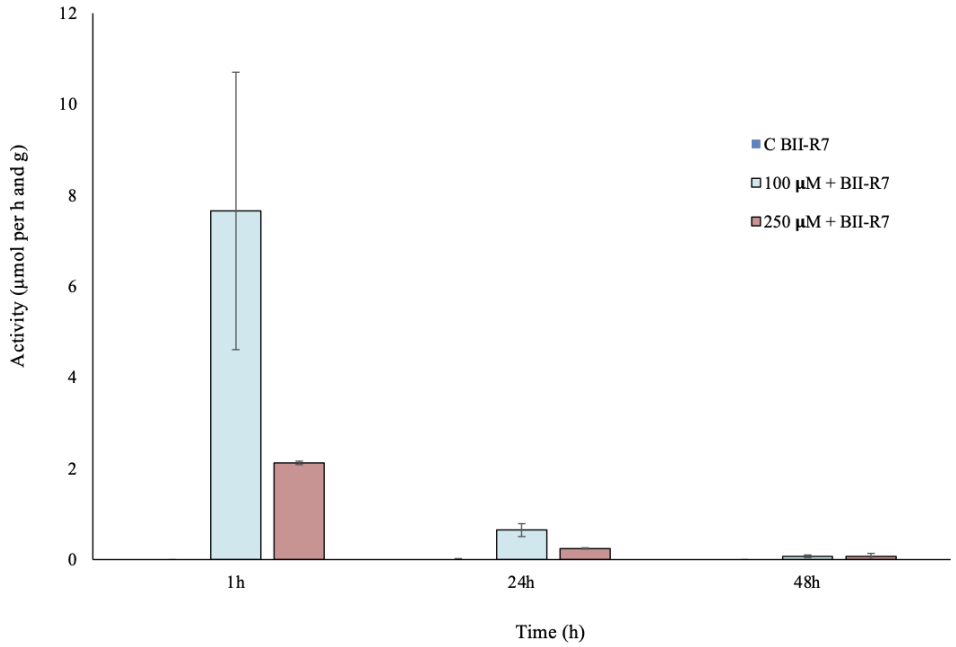

Fig. 4. Maximum levels of phosphatase activity over time in *S. bentonitica* BII-R7 at different U(VI) concentrations for a substrate concentration of 37.2 **µ**M.

3.2.4 Cellular location of U(VI) precipitates by STEM/HAADF

Microscopic analyses were carried out in order to determine the location of the U(VI)-accumulates formed in cells of *S. bentonitica*. STEM/HAADF micrographs showed the occurrence of needle-shape electron-dense accumulates in cells grown in TMM as of 24 h of incubation. These precipitates seemed to be mainly located at the extracellular media, and some of them were also attached to the cell surface (Fig. 5). Analysis of the composition also revealed the presence of U(VI) and P in the structure of the minerals. The number of precipitates at the cell surface decreased with time, finding even more in the extracellular media after 48 h of incubation (Fig. 6 and S5).

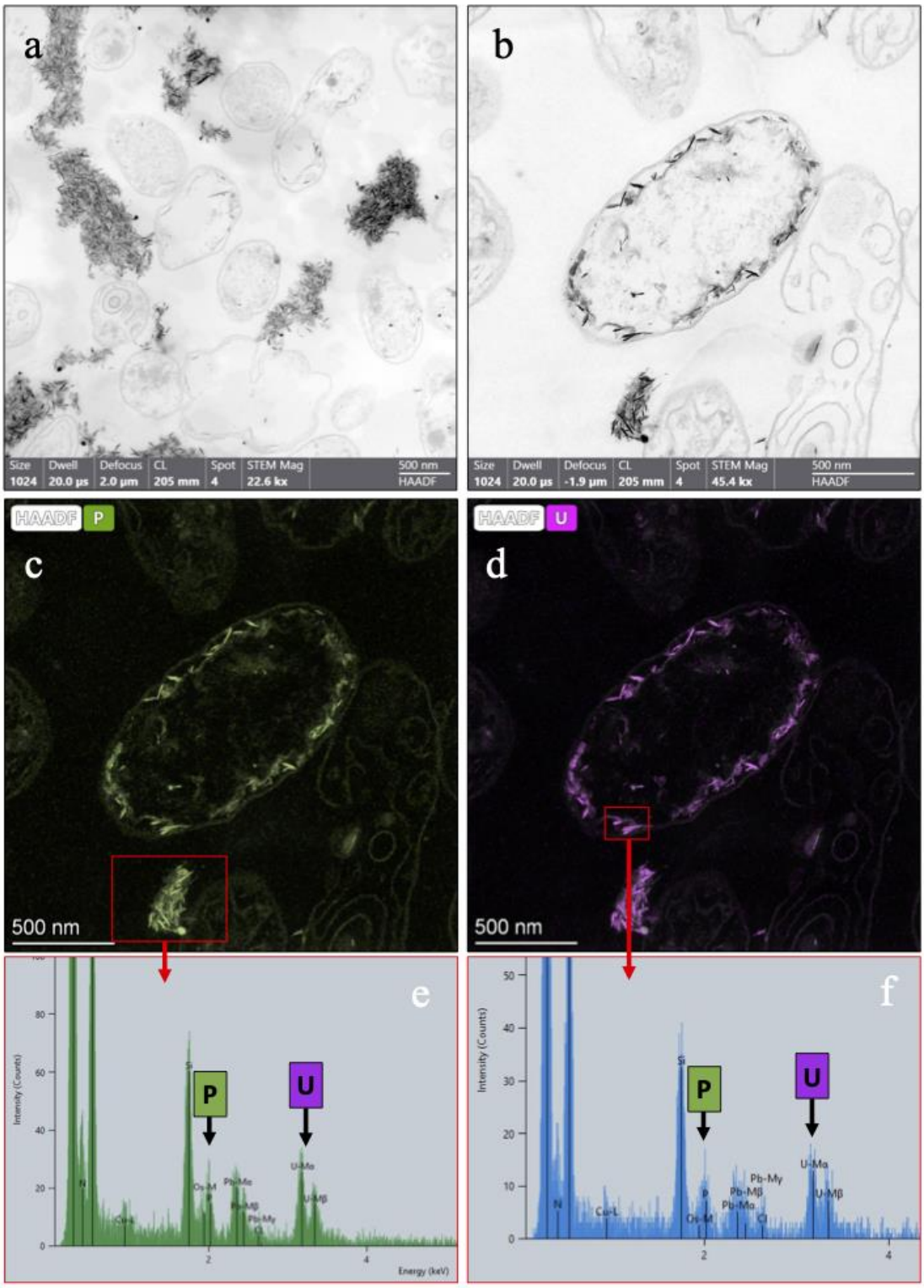

Fig. 5. Extracellular (a) and membrane-bound U-phosphate precipitates after 24 h of incubation with 100 **µ**M of U(VI) in TMM. Elemental mapping (c, d) and EDX (e, f) were applied to elucidate the composition.

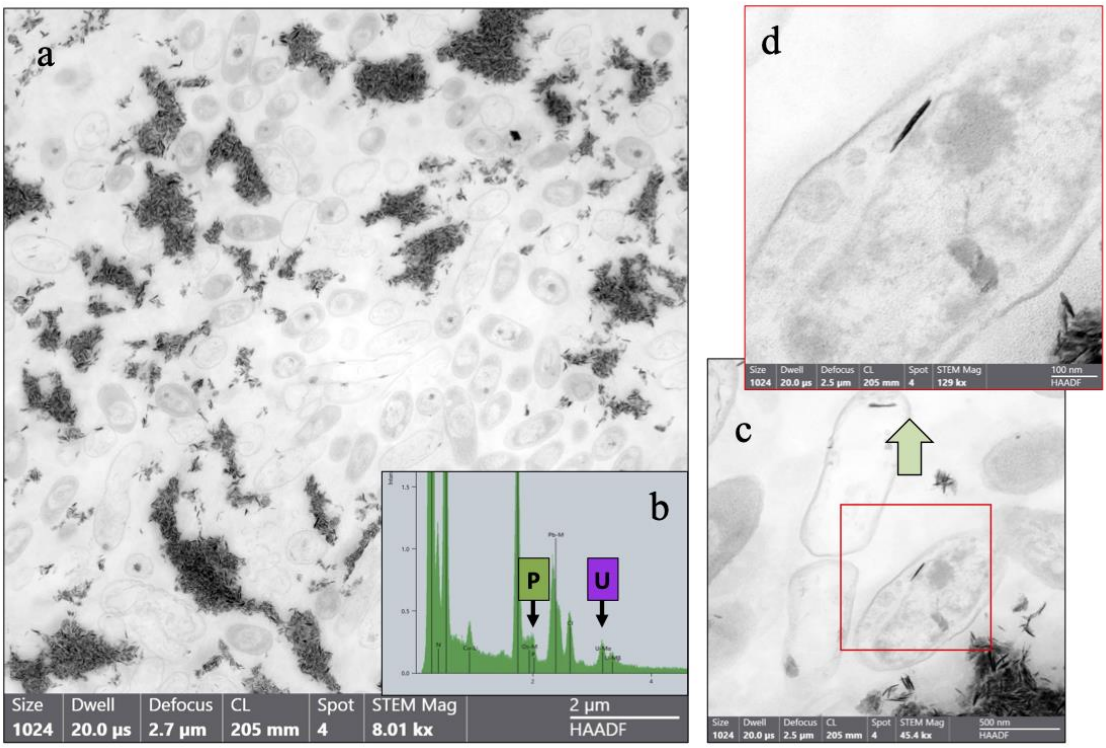

Fig. 6. Micrographs of extracellular precipitates after 48 h of incubation in TMM amended with 100 **µ**M of U(VI). The precipitates are mainly distributed in the extracellular media (a), with only a few cells showing some of them at the cell surface (b).

3.3.Biomineralization of U(VI) by S. bentonitica under non-growing conditions

After confirming U(VI) precipitation in growing conditions, the U biomineralization ability of the strain BII-R7 under non-growing conditions was studied using MOPS buffer supplemented with G2P at two different pH (5.5 and 7) and an initial U(VI) concentration of 100 µM. These two pH values are representative of uranium contaminated sites (Beazley et al., 2007).

3.3.1. U(VI) removal ability of the bacterium

U removal by *S. bentonitica* cells was measured as a function of time (2, 24 and 48h) and pH (5.5 and 7) in presence of G2P and 100 µM U, as is shown in Fig. 7. The results indicate that U(VI) removal increased gradually increasing contact time regardless of the pH, reaching the highest value at 48 h of incubation at pH 7. On one hand, a maximum of around 59.5 ± 3.2 mg of U(VI)/g of dry biomass was observed at pH 5.5 (Fig. S4), which corresponded to 53.9 ± 2.9 % of U(VI) removed from the total amount tested (Fig. 7). On the other hand, BII-R7 accumulated 105.8 ± 0.6 mg of U(VI)/g of dry biomass at pH 7, corresponding to 96.1 ± 0.6 % of the initial concentration of 100 µM. During the first 2 h, low levels of U, up to 18 and 24%, were removed from metal solution

at pH 5.5 and 7, respectively. These findings suggest that the bacterium biomineralizes U(VI) more effectively at pH 7, being removed almost in its totality after 48 h of incubation with the metal.

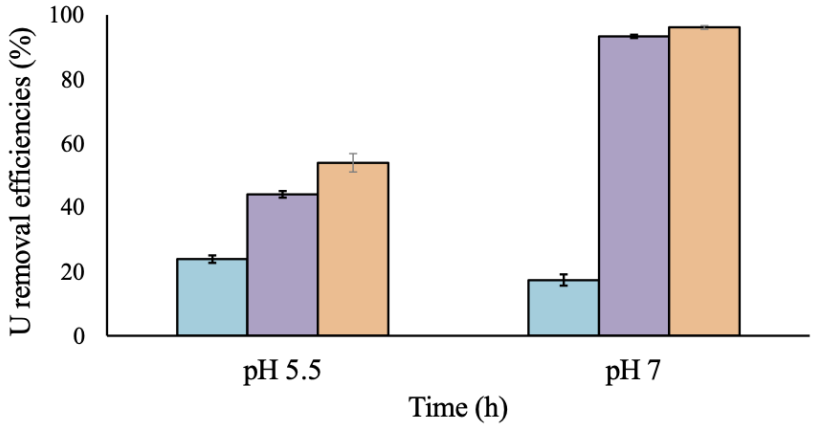

Fig. 7. Time dependence in the amount of U(VI) removed as percentage by *S. bentonitica* aerobically at pH 5.5 and 7.

3.3.2. TRLFS spectra of complexes formed by S. bentonitica with U(VI)

TRLFS approach was performed to shed light on the fluorescence parameters (life time and fluorescence emission bands) of the U complexes formed by the cells of *S. bentonitica* under different pH conditions (5.5 and 7) after 2, 24 and 48h. The luminescence data obtained would help to determine the nature of U species associated with the cells (organic/inorganic phosphates, carboxylates, etc.). The luminescence spectra recorded by TRLFS and the corresponding luminescence parameters (emission maxima and lifetimes) are shown in Fig. 8 and Table 2, respectively. The luminescence parameters found for the blanks (Table 2) were characteristic for different U(VI) species ($(UO_2)_3(OH)_5^+$, $(UO_2)_3(OH)_7^+$) identified as main U species in the absence of bacteria by theoretical speciation calculations and are confirmed by results reported by other authors (G. Geipel et al., 2000; Lütke et al., 2012; Morcillo et al., 2014). The main emission fluorescence bands for the experiment samples were detected around 494-496 nm, 517-518, and 539-542 nm (for pH 5.5), and 495-500, 518-523, and 542-548 (for pH 7) depending on the incubation time. The different parameters obtained between the blanks

and the samples was a clear indication of the key role of the bacterial cells of *S. bentonitica* in the U(VI) complex formation.

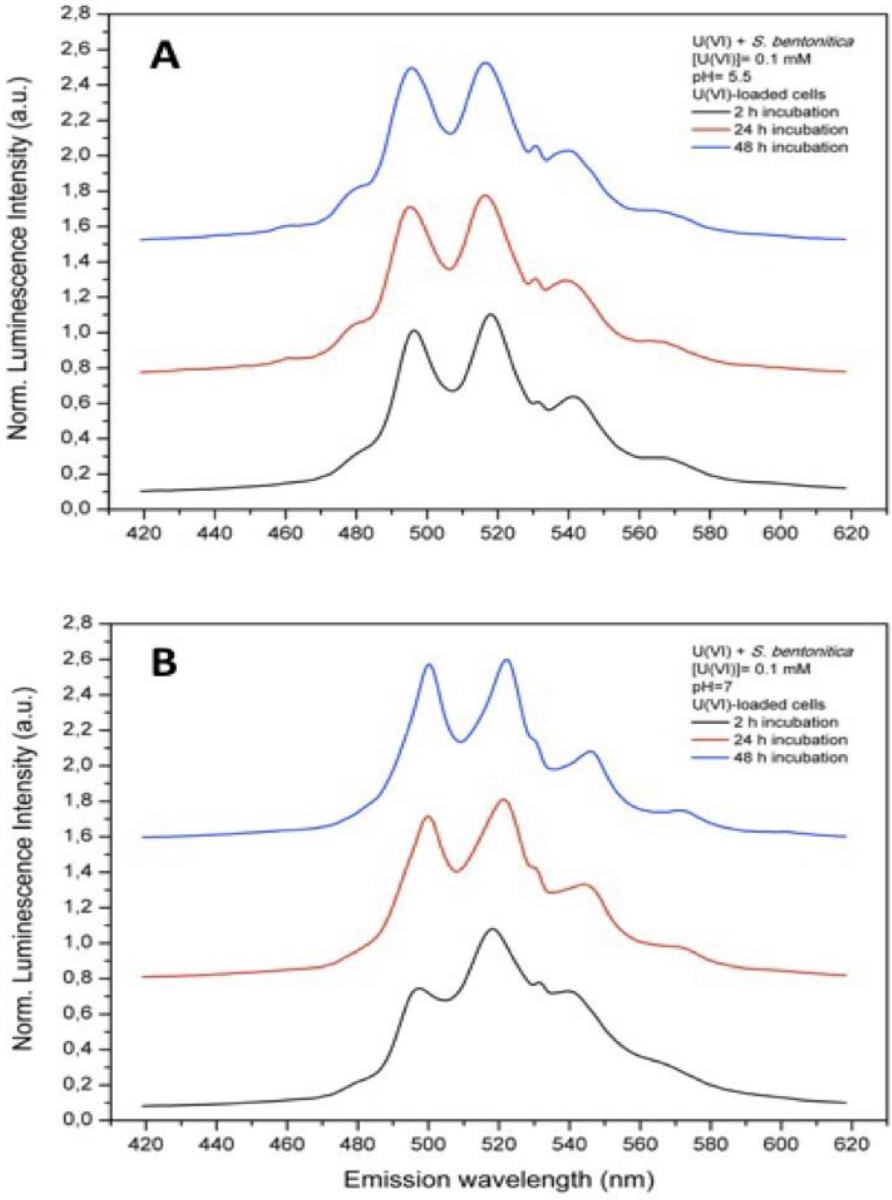

Fig. 8. Luminescence spectra of U(VI) complexes formed by *S. bentonitica* in NaClO4 after different incubation times (2, 24, and 48h) with 0.1 mM U(VI) at pH 5.5 (A) and 7 (B).

Table 2. Luminescence emission maxima an lifetimes of U(VI) complexes formed by *S. bentonitica* cells in $NaClO_4$ after different incubatio comparison to literature data.

Sample	**Emission peak maximum (nm)**					**Lifetime (µs)**	
U(VI)-Blanks ($NaClO_4$) pH 5.5		494.5	517.5	531.		0.51 ± 0.11	17.48 ± 1.88
U(VI)-Blanks ($NaClO_4$) pH 7		497.4	512.5	531.		0.40 ± 0.07	22.51 ± 1.27
UO_2^{2+} and hydrolytic species							
UO_2^{2+} (aq) pH 4		488	509.1	532.2		1.3 ± 0.1	8.0 ± 0.7
UO_2^{2+} (aq) pH 6		-	513.1	-		7.8 ± 0.1	24.1 ± 3.8
UO_2^{2+} (aq) pH 7		-	512.8	-		7.4 ± 0.3	23.5 ± 0.9
UO_2OH^+		497.3	518.4	541.3		32.8 ± 2.0	
$(UO_2)_2(OH)_2^{2+}$		498.3	519.7	543.4		9.5 ± 0.3	
$(UO_2)_3(OH)_5^+$		496	514	534		23 ± 3.0	
U(VI)-S. bentonitica pH 5.5							
2 h		496.20	518.1	542.1		1.31 ± 0.08	36.86 ± 1.74
24 h		494	517.1	539.6		1.05 ± 0.07	15.31 ± 1.34
48 h		495.9	518.1	542.1		0.59 ± 0.06	11.22 ± 1.06
U(VI)-S. bentonitica pH 7							
2 h		495.3	518.4	542.4		0.76 ± 0.04	10.73 ± 0.72
24 h		500.8	523	548.2		0.96 ± 0.05	6.69 ± 0.69
48 h		500.8	523.6	547.3		1.15 ± 0.04	9.36 ± 0.94
Organic phosphate complexes							
UO_2-fructose-6-phosphate		497.1	519	543.3		0.13 ± 0.05	
UO_2-AMP		497	519	542		-	
UO_2-LPS (R-O-PO_3-UO_2)		498.1	519.6	542.9		1.2 ± 0.4	
U(VI)-*R. mucilaginosa pH 7*		498	518	540		11.1 ± 0.3	
Organic carboxylate complexes							
Peptidoglycan-(R-COO)$_2$-UO_2	466	498.1	518	539	566	0.7 ± 0.1	
UO_2-acetate	462.9	494.6	514.3	535.9		-	
U(VI)-*S. acidocaldarius pH 6*		502.6	523.1	545.4		-	
Inorganic phosphate complexes							
U(VI)-*Pseudomonas fluorescens*		498	518	540		0.52 ± 0.06	
$UO_2(HPO_4)$aq		497	519	543		-	
Autunite		504	524.2	548		5.15 ± 0.28	
Meta-autunite		501.8	522.9	546.9		0.74 ± 0.1	

The luminescence emission maxima obtained at pH 5.5 (495, 518, 542 nm) could correspond to U(VI)-organic phosphate complexes comparing with those of reference compounds (Table 2). Specifically, phosphate groups from organic molecules such as phosphorylated nucleosides (Merroun et al., 2003a), carbohydrate phosphates (Koban et al., 2004), or lipopolysaccharides from the outer membrane of Gram-negative bacteria (Barkleit et al., 2008) have been reported to be involved in U(VI) complexation. In the same way, emission peaks obtained for the yeast *Rhodotorula mucilaginosa* in $NaClO_4$ (498.4, 517.7, 540 nm) indicated that mainly organic phosphate molecules are responsible for the complexation of U(VI) at the cell wall (Lopez-Fernandez et al., 2018). No significative differences were observed in the emission bands regarding the incubation time at this pH.

The luminescence emission maxima obtained for pH 7 after 2h incubating (495, 518, 542) were very similar to those obtained for pH 5.5, and slightly shifted to higher wavelength values (~5 nm) after 24 and 48h (500, 523, 548 nm) (Table 2). This slight shift in the luminescence band positions with increasing pH revealed a pH dependency of the U(VI) speciation. The emission bands after 2h can be attributed to the formation of organic phosphate complexes with U(VI) as discussed above. However, the luminescence peaks maxima observed after 24 and 48h may be associated to U(VI) inorganic phosphate minerals such as meta-autunite ($Ca(UO_2)_2(PO_4)_2 \cdot 8H_2O$) (501.8, 522.9, and 546.9 nm) (G. Geipel et al., 2000).

The effect of the pH on U(VI) speciation has been previously reported in other microorganisms. For instance, (Lütke et al., 2012) reported a small shift of 1.2 nm in U(VI)-loaded cells of *P. fluorescens* when increasing the pH from 4 to 7. Their results agree very well with the calculated U(VI) speciation in dependence on the pH, which showed a more relevant role of protonated phosphoryl and carboxylic groups in U(VI) binding in the acidic pH region, and a greater influence of deprotonated phosphoryl sites at neutral pH range.

Time resolved measurements indicated a biexponential luminescence decay for all samples, indicating two different coordination environments of U(VI). It can be concluded that two different uranyl species were formed with luminescence lifetimes around 0.5-1.3 and 11-36 µs for pH 5.5, and 0.7-1.2 µs and 6-11 µs for pH 7. It must be noted that U(VI) carboxyl complexes do not show luminescence at room temperature and it is assumed that only phosphoryl complexes can be detected with TRLFS under this conditions (Lütke et al., 2012). Anyway, we did not detect carboxyl signals in the

emission luminescence spectra of the samples. The short lifetimes found at both pHs have been previously attributed to deprotonated and protonated phosphoryl sites (R-O-PO_3-UO_2 and R-O-PO_3H-UO_2 complexes) from *P. fluorescens* (0.46 and 1.48 µs) and LPS molecules from the cell walls of *P. aeruginosa* (1.2 µs) (Barkleit et al., 2008; Lütke et al., 2012). However, inorganic uranyl phosphate minerals also show similar lifetime values ranging from 0.7 to 5.5 µs (G. Geipel et al., 2000). Specifically, the lifetime characteristic for meta-autunite (0.74 µs) is very close to the short lifetimes obtained for the U(VI)- *S. bentonitica* system (G. Geipel et al., 2000; Lopez-Fernandez et al., 2018). For the longer lifetimes not too many U(VI) complexes has been reported before. However, (Barkleit et al., 2008) attributed the lifetimes obtained at 8.3 and 13.3 µs to the formation of U(VI) complexes with phosphoryl groups from LPS (R-O-PO_3H-UO_2^+ and $(R\text{-}O\text{-}PO_3)_2$-$UO_2^{2-}$).

3.3.3. Cellular location of U(VI) precipitates by STEM/HAADF

Similar electron-dense precipitates were observed under non-growing conditions, mainly located at the cell surface and intracellularly at both 5.5 and 7 pH (Fig. 9 and 10). In case of pH 5.5, no precipitates were detected until 48 h, whereas a few precipitates were visible at 2 h of incubation in the cells at pH 7. EDX and elemental mapping analyses indicated the presence of U and P (Fig. 9e and 10d, f), suggesting the formation of U(VI)-phosphate minerals, in line with TRLFS results. Furthermore, extracellular precipitates were also observed distributed in the media, especially in samples at pH 7 at 48 h. Those accumulations were more abundant at pH 7, which also suggest a higher efficiency of endogenous phosphatase activity in *S. bentonitica* at pH 7 than 5.5.

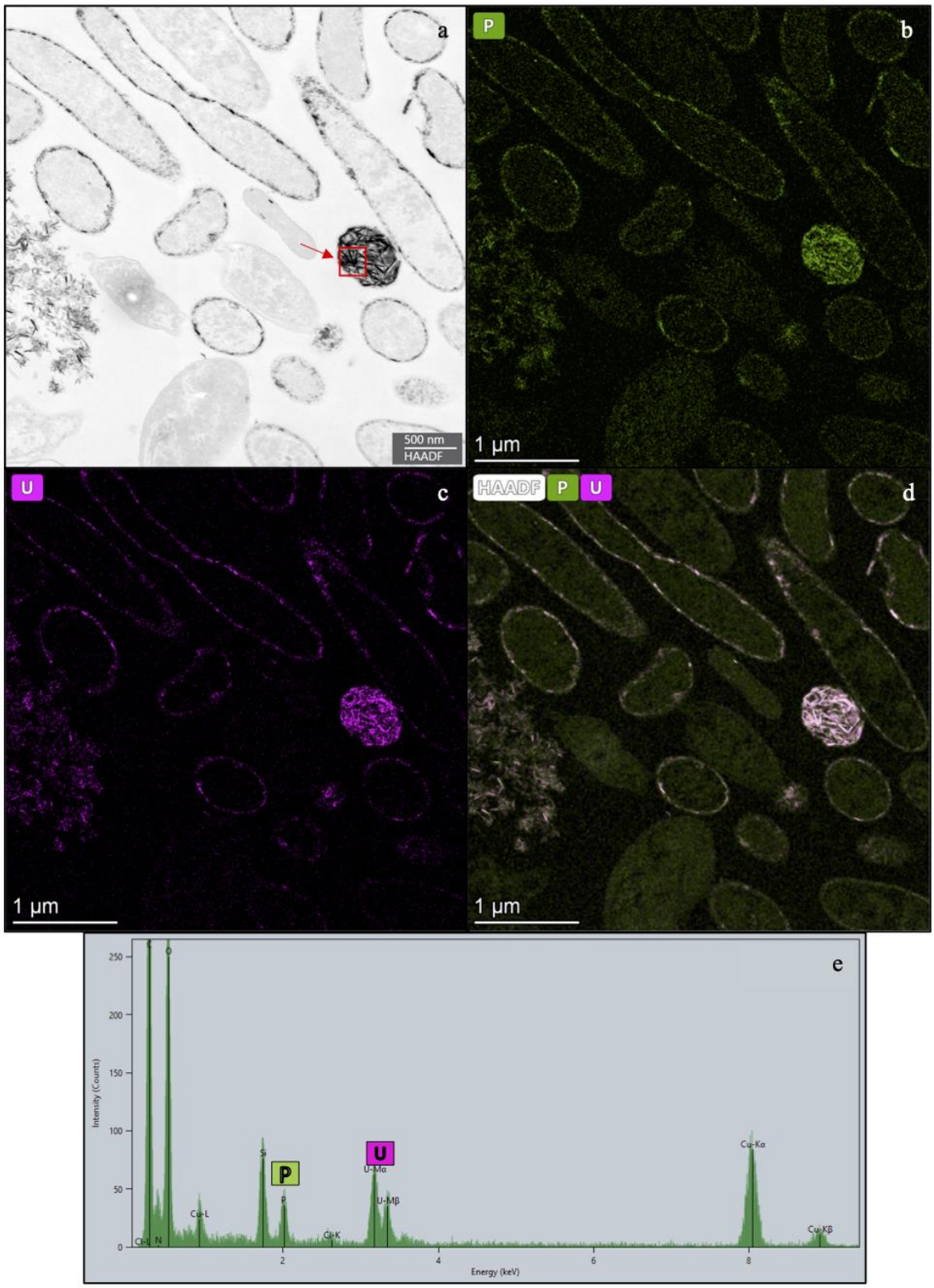

Fig. 9. STEM-HAADF micrographs of *S. bentonitica* under non-growing conditions after 24 h of incubation in MOPS at pH 7. Elemental mapping (b, c, d) and EDX (e) revealed the presence of U and P in their composition.

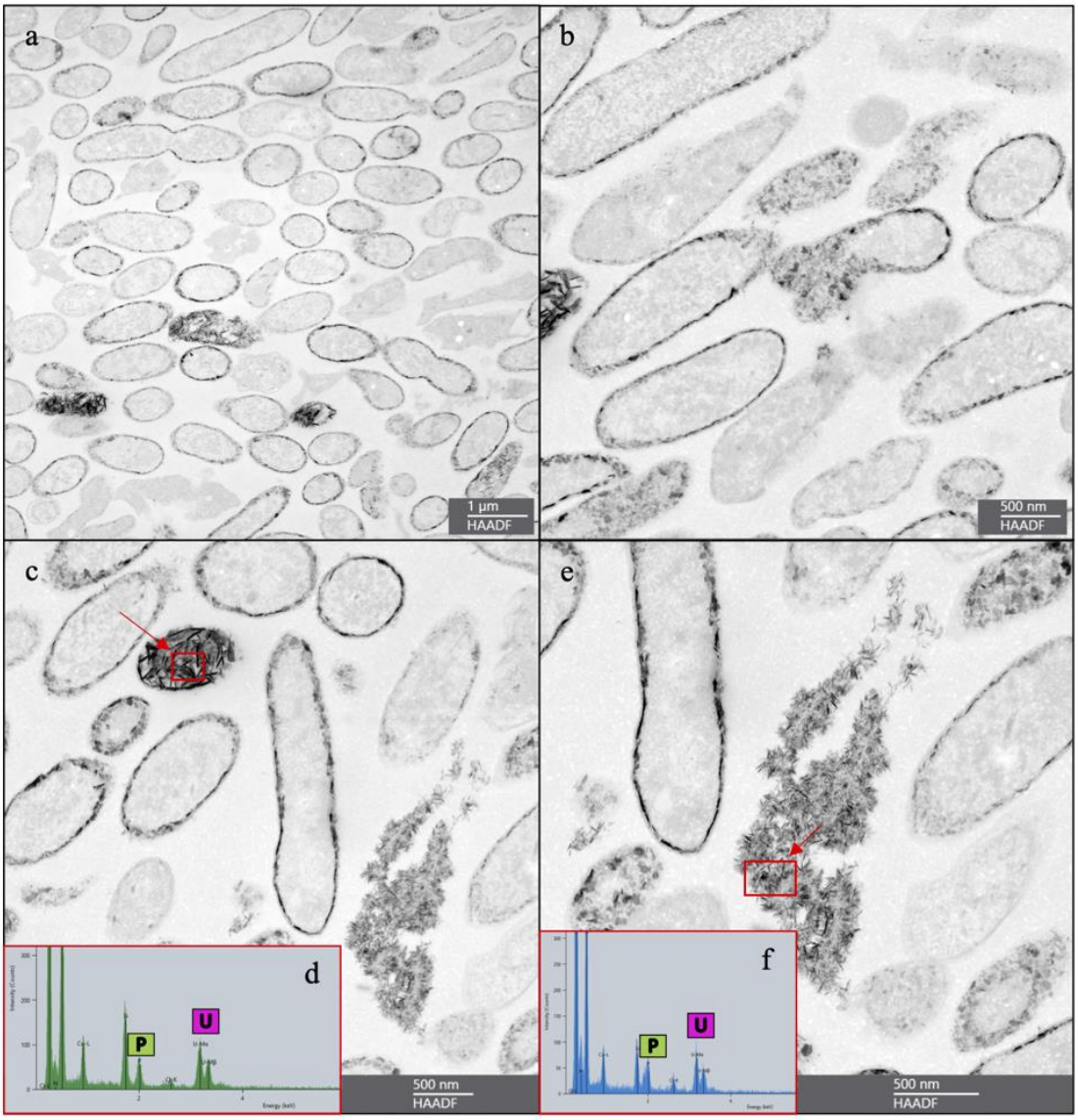

Fig. 10. Precipitates formed at pH 5.5 (a, b) and 7 (c, d) in MOPS after 48 h of incubation, and EDX analyses of intracellular (d) and extracellular (f) accumulates.

4. Discussion

The ability of microbes to precipitate U(VI) in form of U(VI)-phosphates for U bioremediation purposes has been well-documented (Choudhary and Sar, 2015; Merroun and Selenska-Pobell, 2008; Newsome et al., 2014; Sánchez-Castro et al., 2020). However, the impact of abiotic and biotic parameters in this process is still not fully explored. Therefore, optimization of the performance conditions needs to be done in order to improve the yielding of the bioremediation techniques (Song et al., 2019). Nonreductive biomineralization has been described as a tolerance mechanism employed

by microorganisms to cope with toxic U(VI), as it produces immobile U(VI) species, reducing its bioavailability (Singh et al., 2010; Tu et al., 2019b).

The present work describes the effect of growth conditions and pH in the U biomineralization in *S. bentonitica* BII-R7, combining analytic (ICP-MS), biochemical (phosphate activity quantification), microscopic (STEM/HAADF) and spectroscopic (TRLFS) techniques. This strain has shown a high tolerance to U(VI), being able to grow at similar concentrations than bacteria isolated from highly U contaminated sites, or even more (Chandwadkar et al., 2018; Sousa et al., 2013). It is the case of *Serratia* sp. strain OT II 7, isolated from subsurface soil of a U ore deposit in India, with a MIC of up to 4 mM against the 6 mM observed in BII-R7 (Chandwadkar et al., 2018; López-Fernández et al., 2014). The antibiotic and heavy metals resistance has been widely reported in this genus, making them an interesting target for bioremediation approaches (Lampis et al., 2017; Ryan et al., 2009; Shuona et al., 2017). In spite of that, the optimization of a specific culture media for metal tolerance studies in *Stenotrophomonas* genus has never been performed before. The key role of the phosphatase enzymes in the biomineralization process in this strain could be highlighted since the whole sequence genome indicated the presence of genes codifying for theses enzymes (Sánchez-Castro et al., 2017a). However, the application of biochemical and spectroscopic techniques is needed to quantify the phosphatase activity and to characterize the U precipitates formed. On the other hand, the study of the biomineralization in non-growing conditions shed light on the contribution of the physiological state of the cells in the process. Understanding the interactions between *S. bentonitica* and radionuclides is particularly of great interest for disposal of nuclear waste concept, since bentonites have been selected as artificial barriers for deep geological disposal of radioactive residues in Spain (Lopez-Fernandez et al., 2015; López-Fernández et al., 2014).

A time-dependent U(VI) removal by *S. bentonitica* was demonstrated, following the same tendency regardless the cell physiological state (growing and non-growing conditions). The U precipitation process was more efficient at pH 7, especially under growing conditions in TMM, taking only 24 h to remove up to 93% of U(VI) in solution, while it took two-fold this time to reach 96% of U(VI) removal by non-growing cells in MOPS supplemented with G2P. This high U(VI) removal percentage was maintained at the initial concentration of 250 μM (96% of soluble U(VI) removed during the first 24 h of incubation). The low abiotic precipitation detected at both conditions indicates the involvement of the bacterial metabolism, and the success in the optimization of culture

medium TMM. The U(VI) removal efficiencies reported here for *S. bentonitica* are high with regard to those described in previous studies performed at similar conditions. *Stenotrophomonas* sp. Br8 was able to precipitate nearly 90% of the soluble U(VI) after 48 h at an initial concentration of 100 μM, producing minerals of similar morphology and location (Sánchez-Castro et al., 2020). The amount of U(VI) precipitated was even less in *Rhodanobacter* A2-61, also isolated from U(VI)-rich environments, in which only 29% of the precipitation was attributed to cell metabolism (Sousa et al., 2013).

A combination of microscopic, spectroscopic and biochemical methods was applied to characterize the U solid phase removed by the cells and to identify the U-BII-R7 strain interaction mechanism. Measurements of the phosphatase activity in growing conditions suggest that 100 and 250 μM of U(VI) exert a possible induction of phosphatases at early times of incubation (1 h). These results fit very well with those obtained for U(VI) removal, indicating the involvement of these enzymes in BII-R7 to cope with U(VI) toxicity. By contrast, the levels of P_i released increased over time. During the first hours, most of the P_i produced would be used to precipitate U(VI); once soluble U(VI) has been almost completely removed, P_i would accumulate in the medium, and then it can be detected at longer incubation times despite the lack of phosphatase activity. Hence, the phosphatase activity at this incubation time could also be under the limit of detection of the method used in this study. Induction of bacterial phosphatase activity under U(VI) exposure has been previously reported. Zhang et al. (2018) suggested that the stress caused by the metal in *Bacillus cereus* 12-2 leads to the expression of phosphatases, and Sánchez-Castro et al. (2020) reported an induction of the phosphatase activity in *Stenotrophomonas* sp. Br8 which was dependent on the initial concentration. However, this last strain showed higher levels of activity compared to BII-R7 (Sánchez-Castro et al., 2020). In addition, while free P_i was detected in the control samples, they did not show any activity in this assay. Therefore, further studies are necessary in order to evaluate the factors that are inducing the expression of phosphatase activity in this strain.

STEM-HAADF analyses confirmed the higher U(VI) biomineralization efficiency under growing conditions demonstrated by the U(VI) removal efficiencies, since the precipitates observed were more abundant than those under non-growing conditions. Although some of them were found attached to the cell surface, the precipitates were mainly distributed in the extracellular media at both initial concentrations of U(VI). As at 48 h of incubation less precipitates were observed at a cell

wall level, the precipitation could occur first at a membrane level. Then, membrane-bound precipitates would be progressively released to the extracellular media. The faster removal of U(VI) under growing conditions at the same pH could explain the differences in the location of the precipitates, since more U(VI)-phosphate could be released at earlier incubation times in these conditions.

The biomineralization of U(VI) was also investigated under non-growing conditions as function of pH (5.5 and 7) and time incubation (2, 24 and 48 h) in presence of G2P as organic phosphate substrate.

TRLFS analysis showed that association of U(VI) species with the cells of BII-R7 is a pH dependent process. At pH 5.5, the fluorescence emission bands of U(VI) complexes formed by the cells at the three incubation times (2, 24 and 48 h) are similar to those of U-organic phosphate compounds (UO_2-fructose-6-phosphate (Koban et al., 2004); and UO_2-AMP (Merroun et al., 2003). These results indicate that the U is coordinated to organic phosphate groups mainly at the cell surface through a biosorption process. This is in line with microscopic analyses, which showed accumulates composed by U and P, mainly in the cell wall or accumulated intracellularly at 48 h of incubation. Since no accumulates were observed at earlier incubation times (2 and 24 h), it is suggested that U(VI)-P precipitation is a progressive process. The U(VI) would bind initially to phosphate groups at the surface, and the nucleation and precipitation would take place throughout the incubation time.

On the other hand, at pH 7 TRLFS studies demonstrated that the U species formed by the cells is a time dependent process. After 2h, U-organic phosphate species were identified as in the case of samples at pH 5.5. However, the U speciation associated to the cells after 24 and 48h is quite different to that at pH 5.5 and pH 7 (2h) since inorganic phosphate groups were involved in the coordination of U(VI). The fluorescence emissions bands of the U complexes formed at pH 7 (24h and 48h) are similar to those of U mineral phase references (meta-autunite) (Gerhard Geipel et al., 2000). These results indicate that a pH 7, two different U species (U-organic and U-inorganic phosphates) were involved in the interaction with this radionuclide as function of incubation time. Therefore, a two-stage process involving the biosorption and biomineralization mechanisms would take place in *S. bentonitica* cells to cope with the toxicity of U. The positive-charged U(VI) species in the medium would bind to the organic phosphate groups at the cell wall within the first minutes of metal exposure in a fast-passive biosorption process. This interaction would provide nucleation sites for biomineralization

to occur by interaction with P_i released by phosphatases. Similar biosorption process prior to precipitation has been reported in many bacterial strains, such as *B. cereus* 12-2 and *B. subtilis* ATCC-6633 (Banala et al., 2021; Song et al., 2019; J. Zhang et al., 2018).

The pH can influence the phosphatase activity and the charge of the functional groups present in the cell surface, explaining the differences detected at both pH in BII-R7 (Shukla et al., 2017; Yang et al., 2015; Zhang et al., 2018). Since a lower amount of U(VI) precipitation was observed at pH 5.5, it is possible that less functional groups were available for the radionuclide under these conditions, leading to less precipitation at the surface and extracellular level. On the other hand, this could not be the optimal pH neither for acid nor alkaline phosphatase activity, which could also impact the biomineralization efficiency. The influence of the pH on U(VI) biomineralization has been previously addressed, as it determines the chemical speciation of the radionuclide. Kulkarni et al. (2016) compared the biomineralization capability of *E. coli* and a recombinant strain of *Deinococcus radiodurans* expressing acid and alkaline phosphatases at pH 7 and 9. Their findings indicate that both strains eliminated higher amounts of U(VI) at neutral pH. On the other hand, U(VI) precipitation on *Serratia* sp. OT II 7 was more efficient at neutral and alkaline pH than pH 5. These authors also reported differences in the location of the precipitates as a function of pH, regardless the location of the phosphatases (Chandwadkar et al., 2018; Kulkarni et al., 2016). Although extracellular precipitates were more frequent at pH 7 after 48 h of incubation in *S. bentonitica*, no significant differences were found in the cellular location of the U(VI)-phosphate minerals among the pH tested. This could be due to the fact that the main chemical species of U(VI) were the same at pH 5.5 and 7.

5. Conclusions

The present work has shown the ability of the newly described bacterial species *S. bentonitica* to efficiently remove soluble U(VI) under growing and non-growing conditions, by forming U(VI)-phosphate precipitates. The higher yielding on the process was obtained at growing conditions, suggesting the key role of the physiological state of the cells. At these conditions, the induction of the phosphatase activity and the subsequent release of P_i led to the precipitation of U(VI)-phosphate minerals at the surface of the cell and the extracellular media. On the other hand, studies under non-growing conditions revealed the influence of the pH in the effectiveness of the biomineralization process. TRLFS and EXAFS analysis suggested the involvement of two metal interaction

mechanisms in the process for U(VI) removal at pH 7, mediated by the fast biosorption of the with the later biomineralization of U(VI). The product of the interactions described would be meta-autunite, a U(VI)-phosphate mineral, which is less toxic and highly stable for long-term U(VI) removal. Further biochemical studies would determine the role of the phosphatase activity in the biomineralization under non-growing conditions. These findings show that U(VI) tolerance in *S. bentonitica* is mediated by complex co-existing mechanisms highly influenced by environmental and biological factors, such as pH and the state of the cells. In conclusion, this study reveals the potential of *S. bentonitica* for the long-term removal of U(VI) in less bioavailable forms of U(VI)-phosphate minerals, allowing to consider it an interesting tool for bioremediation purposes in contaminated environments with U(VI).

6. Acknowledgements

This work has been supported by the grant FPU 15/04284 (Formación de Profesorado Universitario) from the Spanish Ministry (Ministerio de Educación, Cultura y Deporte) and from European projects MIND-661880 and CGL2014-59616-R. Part of this work was also cofinanced by the European Radioecology Alliance mobility grant awarded to MAR-F. The authors acknowledge the assistance of María del Mar Abad Ortega and Concepción Hernández Castillo (Centro de Instrumentación Científica, University of Granada, Spain) with microscopy measurements.

7. Supplementary material

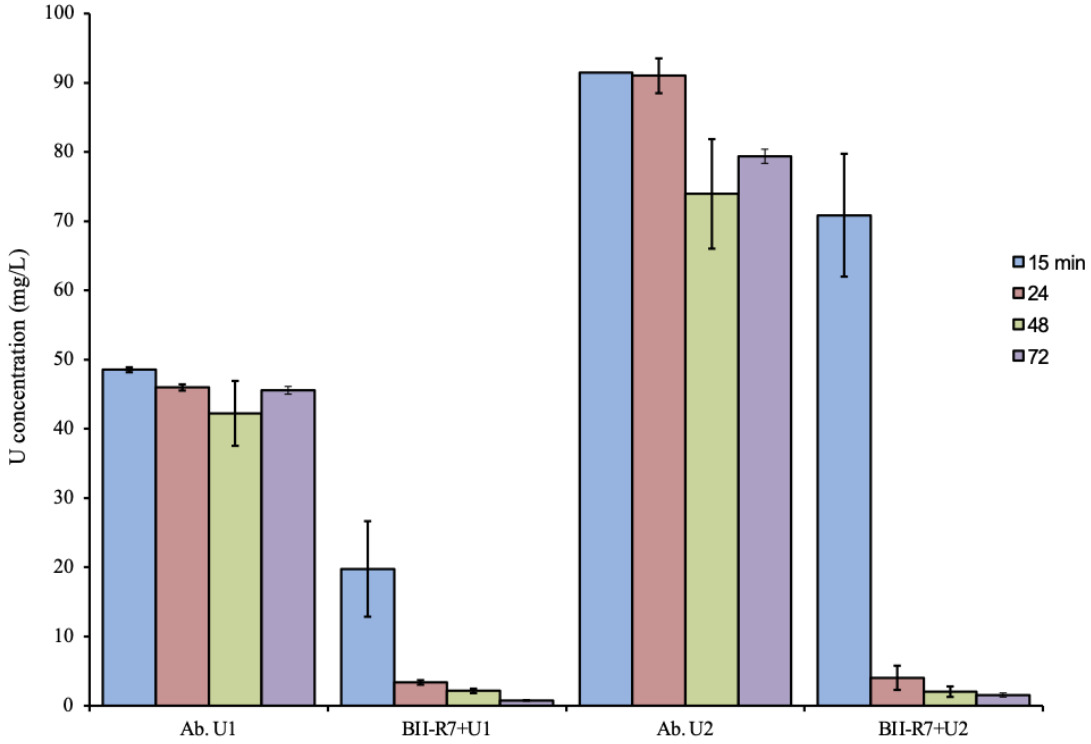

Figure S1. U(VI) concentration in the culture medium as mg/mL with Arsenazo III method at 100 (U1) and 250 (U2) µM. Abiotic controls (Ab. U1 and U2) were also performed.

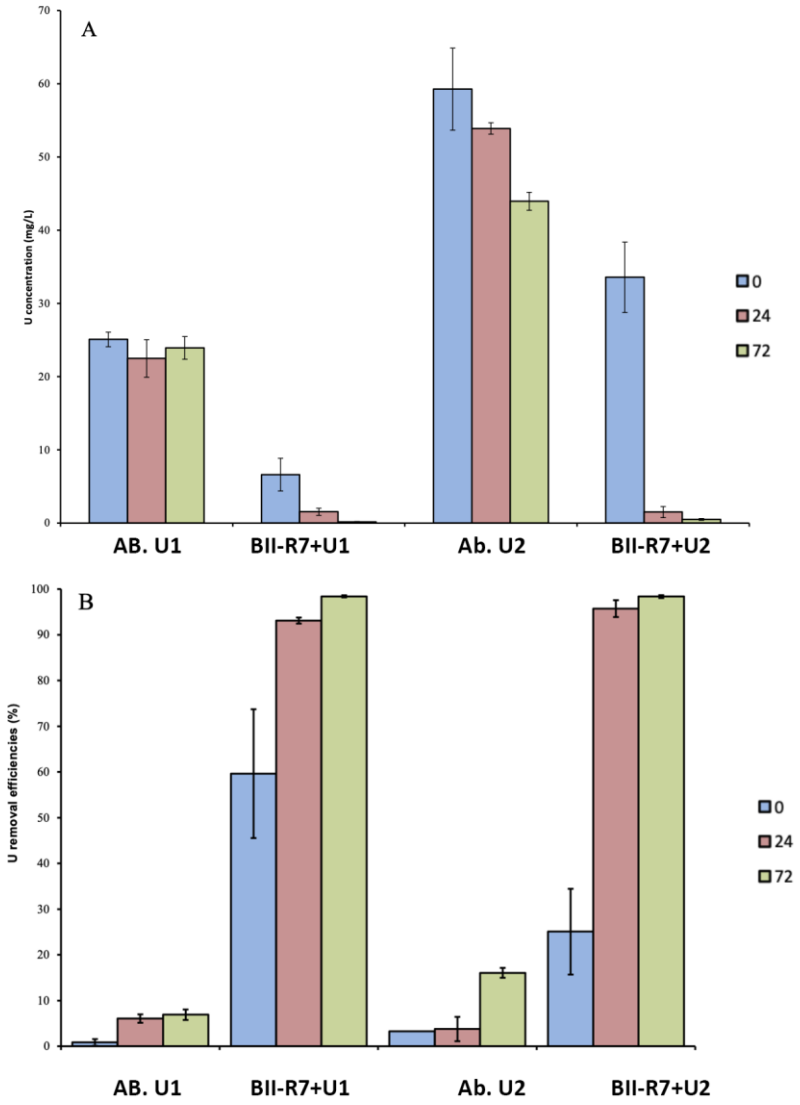

Figure S2. Residual concentration of U(VI) (a) (mg/L) and % of U(VI) removed (b) measured with ICP-MS method at 100 (U1) and 250 (U2) □M. Abiotic controls (Ab. U1 and U2) were also performed.

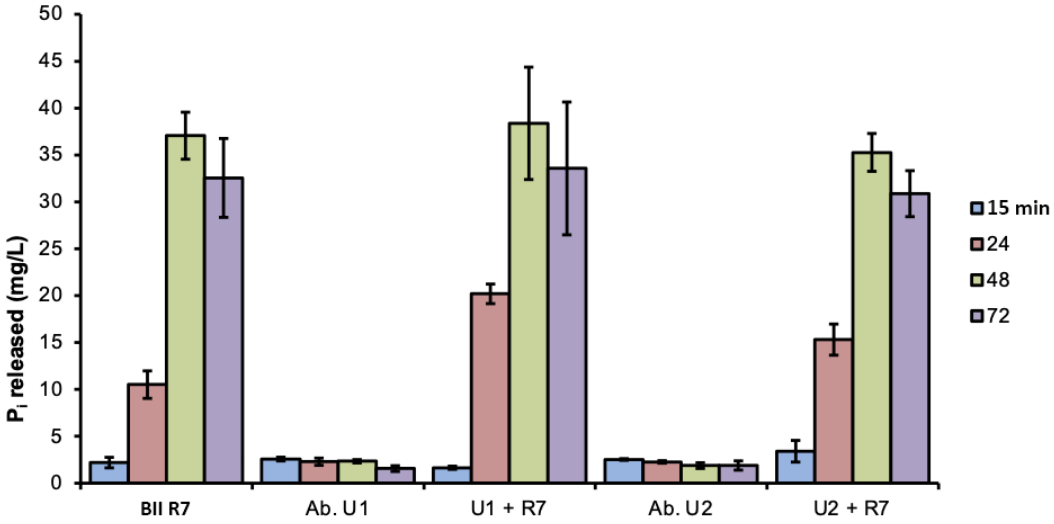

Figure S3: Amount of inorganic phosphate (P_i) released as mg/mL in cultures of *S. bentonitica* BII-R7

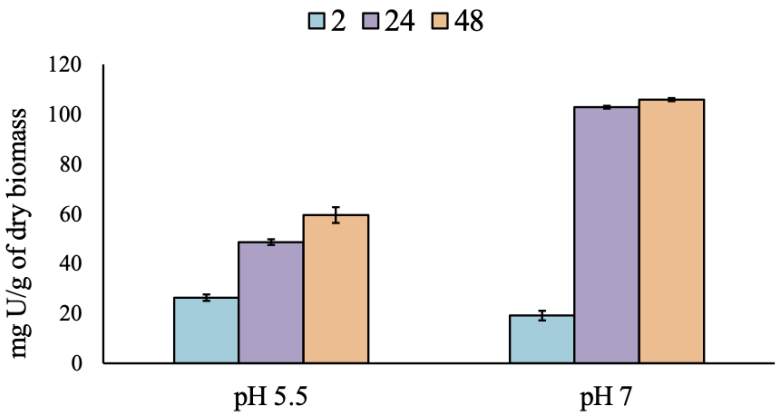

Figure S4.: Time dependence in the amount of U(VI) removed by *S. bentonitica* as mg of U/g dry biomass

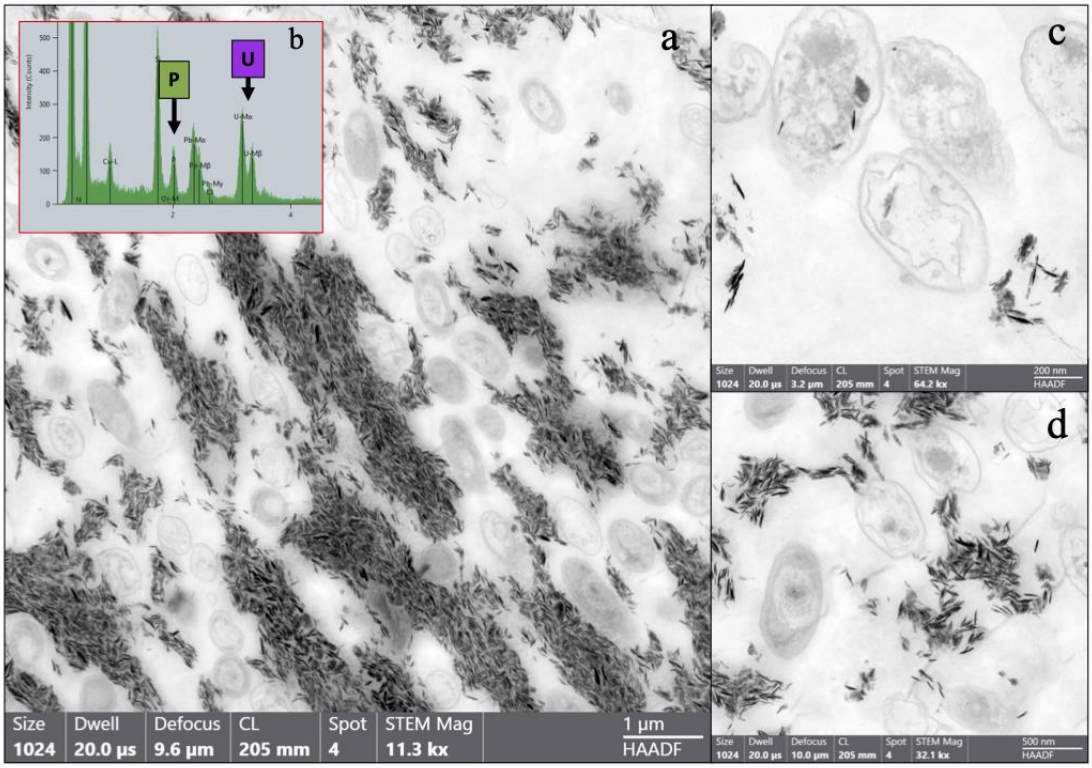

Figure S5. STEM/HAADF micrographs showing precipitates formed by *S. bentonitica* growing in TMM supplemented with 250 µM of (VI) at 48 h. EDX analyses suggest the formation of U(VI)-P complexes (b).

CHAPTER II

Multisystem combined uranium resistance mechanisms and bioremediation potential of Stenotrophomonas bentonitica BII-R7: Transcriptomics and microscopic study

María Pinel-Cabello[1*], Fadwa Jroundi[1], Margarita López-Fernández[2], Robert Geffers[3], Michael Jarek[3], Ruy Jauregui[4], Alexander Link[5], Ramiro Vílchez-Vargas[5], Mohamed L. Merroun[1]

[1]Department of Microbiology, University of Granada, Campus Fuentenueva s/n, 18071, Granada, Spain

[2]Institute of Resource Ecology, Helmholtz-Zentrum Dresden-Rossendorf, Bautzner Landstraße 400, 01328 Dresden, Germany

[3]Genome Analytics, Helmholtz Centre for Infection Research (HZI), 38124 Braunschweig, Germany

[4]AgResearch Grasslands Research Centre, Tennent drive, Palmerston North, New Zealand

[5]Department of Gastroenterology, Hepatology and Infectious Diseases, University of Magdeburg, Leipziger Str. 44.39120, Magdeburg, Germany

Journal of Hazardous Materials 403 (2021) 123858

Contents lists available at ScienceDirect

Journal of Hazardous Materials

journal homepage: www.elsevier.com/locate/jhazmat

Multisystem combined uranium resistance mechanisms and bioremediation potential of *Stenotrophomonas bentonitica* BII-R7: Transcriptomics and microscopic study

Pinel-Cabello M.[a,*], Jroundi F.[a], López-Fernández M.[b], Geffers R.[c], Jarek M.[c], Jauregui R.[d], Link A.[e], Vílchez-Vargas R.[e], Merroun M.L.[a]

Este capítulo ha sido publicado en la revista Journal of Hazardous Materials (doi.org/10.1016/j.jhazmat.2020.123): ***Pinel-Cabello M.,*** *Jroundi F., López-Fernández M., Geffers R., Jarek M., Jauregui R., Link A., Vílchez-Vargas R., Merroun M.L. 2021.Multysistem combined uranium resistance mechanisms and bioremediation potential of Stenotrophomonas bentonitica BII-R7: Transcriptomics and microscopic study. J Hazard Materials. 403, 123858.*

Abstract

The potential use of microorganisms in the bioremediation of U pollution has been extensively described. However, a lack of knowledge on molecular resistance mechanisms has become a challenge for the use of these technologies. We reported on the transcriptomic and microscopic response of *Stenotrophomonas bentonitica* BII-R7 exposed to 100 and 250 μM of U. Results showed that exposure to 100 μM displayed up-regulation of 185 and 148 genes during the lag and exponential phases, respectively, whereas 143 and 194 were down-regulated, out of 3786 genes (>1.5-fold change). Exposure to 250 μM of U showed up-regulation of 68 genes and down-regulation of 290 during the lag phase. Genes involved in cell wall and membrane protein synthesis, efflux systems and phosphatases were up-regulated under all conditions tested. Microscopic observations evidenced the formation of U-phosphate minerals at membrane and extracellular levels. Thus, a biphasic process is likely to occur: the increased cell wall would promote the biosorption of U to the cell surface and its precipitation as U-phosphate minerals enhanced by phosphatases. Transport systems would prevent U accumulation in the cytoplasm. These findings contribute to an understanding of how microbes cope with U toxicity, thus allowing for the development of efficient bioremediation strategies.

Keywords: microbial remediation, RNA-Seq, biosorption, biomineralization, uranium tolerance

1. Introduction

Uranium (U) is a naturally occurring radionuclide found as part of minerals such as uraninite (UO_2), pitchblende (U_3O_8), etc. (Selvakumar et al., 2018). Its concentration commonly ranges from 1 to 5 mg/kg in soil, and from 0.1 to 5 µg/L in water (Celik et al., 2018). Anthropogenic activities including U mining, milling and nuclear energy production have increased its concentration to hazardous levels, leading to the contamination of soils, sediments, and waters (Selvakumar et al., 2018). The high persistence of this radionuclide, along with its health and ecological toxicity, underline the need for effective technologies to remediate U pollution. Contamination with U has been associated with renal and liver damage, developmental and reproductive disorders, and DNA damage, being a human carcinogen when its concentration in water exceeds 50 mg/L (Wang et al., 2009; Xu et al., 2018). Conventional remediation approaches may depend on the features of each contaminated environment, and they are expensive, making them difficult to apply accurately. The fact that methods based on chemical and physical techniques can be hard to carry out *in situ* limits their large-scale use. Furthermore, secondary waste forms would be generated due to the employment of chemicals (Gavrilescu et al., 2009). Nowadays, the use of microorganisms as bioremediation agents is seen as an efficient and cost-effective strategy compared to the traditional methods. The benefits of this strategy include the use of native microorganisms from the contaminated site, the transformation in place of the contaminant into a less toxic form, and good environmental regeneration (Selvakumar et al., 2018; Wei et al., 2019). These emerging techniques rely on the use of highly U tolerant microorganisms belonging to bacteria, fungi, algae or yeast (Liang et al., 2016).

In the environment, U exists in many oxidation states —+3, +4, +5 and +6— depending on the geochemical conditions, which control the fate and migration of such radionuclides (Gavrilescu et al., 2009). Most reducing conditions lead to the rapid oxidation of U(III), while U(V) is disproportionate to U(IV) and U(VI), the latter two oxidation states being the most common in nature (Gavrilescu et al., 2009). Under anaerobic conditions, U(IV) precipitates as uraninite, a stable insoluble mineral; under oxidizing conditions, the main U(VI) species is uranyl ion (UO_2^{2+}), held to be the most toxic U species due to its solubility and mobility, in turn highly dependent upon pH. This ion may be absorbed by a mineral surface, precipitated as a phosphate mineral phase, or even form complexes with organic matter over a range of pH below circumneutral values.

In the case of alkaline environments, uranyl ions mostly form mobile aqueous complexes with carbonates in groundwaters, increasing U solubility (Beazley et al., 2007) .

The ability of a number of bacterial species to use U(VI) as an electron acceptor in anoxic conditions, with the subsequent reduction to an insoluble form of U(IV), has widely been reported —for example, in Fe(III)- and sulphate-reducing bacteria, thermophilic or acidotolerant bacteria (Lakaniemi et al., 2019; Newsome et al., 2014). Li et al. (2017) described this process in *Bacillus* sp. dwc-2, resulting in crystalline accumulations that probably correspond to uraninite phases. Other mineral phases in which U(IV) could precipitate include uramphite [$(NH_4)(UO_2)PO_4 \cdot 3H_2O$] or metaschoepite [$(UO_2)_8O_2(OH)_{12}] \cdot 10H_2O$, as observed for *Carboxydothermus ferrireducens* and *Shewanella putrefaciens* CN32 (Fredrickson et al., 2000; Slobodkin et al., 2006). Recent studies described the production of noncrystalline U(IV) species both abiotially and biotically, through different mechanisms (Boyanov et al., 2011; Latta et al., 2014), apparently favoured by EPS and biofilms (Bone et al., 2017). Loreggian et al. (2020) studied the stability of noncrystalline U(IV) species in biostimulated sediments under different geochemical conditions, as this form would be more prevalent in the environment. They found that the presence of FeS and reactive oxygen species could lead to a rapid oxidation of tetravalent U in oxic environments, compromising the long-term stability of this approach. The biomineralization of U, resulting in biogenic minerals of U(VI)-phosphate has been found to be a very efficient process of U sequestration over long periods of time (Sowmya et al., 2014; Tu et al., 2019b).

The biomineralization of U(VI) mediated by microorganisms has been well documented in recent years (Merroun and Selenska-Pobell, 2008). The interaction of the metal with different metabolites derived from microbial activity (e.g. phosphate) gives rise to the most insoluble form of the metal (Merroun and Selenska-Pobell, 2008). This process, firstly described for the *Citrobacter* genus, was thereafter confirmed in many other bacteria such as *Acinetobacter*, *Pseudomonas*, *Serratia*, *Sphingomonas* and *Bacillus*, as well as in fungi like *Aspergillus, Paecilomyces* or *Rhizopogon* species, and in yeasts (Fomina et al., 2007; Merroun et al., 2011; Tu et al., 2019). Bader et al. (2018) described U biomineralization in the Haloarchaea *Halobacteria noricense* DSM 15987. Phosphatase enzymes expressed by microorganisms are able to efficiently precipitate U(VI) in the presence of organic phosphate sources such as glycerol-2-phosphate (G2P), G3P, phytic acid, or fructose-1,6-bisphosphate. This leads to the formation of different

U(VI)-phosphate minerals —mainly autunite, although chernikovite and ankoleite have also been observed (Beazley et al., 2009; Salome et al., 2017).

Effective bioremediation based on U biomineralization requires an understanding of the mechanisms involved in the bacterial U precipitation, as well as of the response of microorganisms to this radionuclide toxicity. High throughput technologies (e.g. transcriptomic-based approaches) allow for retrieval of great quantities of data regarding biological, molecular and functional processes. The integral analysis of such valuable information sheds light on the response of the entire cellular system under specific conditions. Holmes *et al*. (2009) performed a transcriptomic analysis of *Geobacter uraniireducens* grown in contaminated sediments from an aquifer in Rifle (Colorado). They described a high expression of genes for energy metabolism, especially those implicated in electron transfer such as c-type cytochromes, and possibly involved in U(VI) reduction. Wang et al. (2019) compared the gene expression between a U(VI)-tolerant strain of *Bacillus atrophaeus* and a sensitive strain of the same species, to determine specific genes that could be involved in U(VI) tolerance. These authors showed the presence of two genes, *ytiB* and *ythA*, encoding for a carbonic anhydrase and a subunit I of cytochrome bd oxidase, respectively, that could have a negative effect on bioremediation of the radionuclide. In another study of U resistance, Dekker et al. (2016) investigated the proteomic response of *Acidithiobacillus ferrooxidans* exposed to 0.5 mM of U(VI). In view of the up-regulated proteins, the authors proposed protection from oxidative stress and U-binding to phosphate compounds as the main mechanisms underlying U tolerance in this bacterium.

The present work focuses on the transcriptional response to U toxicity of a new bacterial species, *Stenotrophomonas bentonitica* BII-R7, isolated from Spanish bentonite clay formations. Previous whole genome analysis of this strain revealed the presence of many genes that confer tolerance to heavy metals, including U and selenium (Se) (Sánchez-Castro et al., 2017a), and grow even in the presence of 6 mM of U (López-Fernández et al., 2014). Here, it is of particular interest to additionally highlight the presence of phosphatase enzymes, previously shown to take part in the biomineralization process of U(VI) to U(VI)-phosphate minerals (López-Fernández et al., 2014; López-Fernández et al., 2015; Sánchez-Castro et al., 2017a). Still, genetic and molecular mechanisms underlying this tolerance remain unknown. The aim of this study was therefore to determine the transcriptomic profile of *S. bentonitica* BII-R7 for the identification of pathways and genes involved in U stress response.

2. Materials and methods

2.1.Bacterial strain and growth conditions

The strain used in this study is a new bacterial species isolated in 2014 from Spanish bentonite formations at "El Cortijo de Archidona, Cabo de Gata" Natural Park (Almería, Spain) and described as *S. bentonitica* BII-R7 (López-Fernández et al., 2014; Sánchez-Castro et al., 2017b). The cells were grown aerobically in Luria-Bertani (LB) medium (tryptone 10 g/L, yeast extract 5 g/L, and NaCl 10 g/L, pH 7.0 ± 0.2) for 24 h at 28 ºC in a rotatory shaker at 180 rpm.

2.2. U removal by the cells of S. bentonitica BII-R7

To establish the % of U(VI) removal and the P_i released by the bacterium, a preinoculum was grown aerobically in liquid LB medium (at a concentration of 10%) at 28 ºC under shaking during 24 hours. Afterwards, the cells were harvested by centrifugation (for 10 min at 11,000 rpm), washed twice, and resuspended in NaCl 0.9% (w/v). Aliquots were cultivated in Tris Minimal Medium (TMM) modified from Choudhary and Sar (2011), at an initial Optical Density of 0.05 at 600 nm (OD_{600}) (Genesys 10S UV-Vis; Thermo scientific, MA, USA). TMM consisted of Tris-HCl, 6.06 g; NaCl, 4.68 g; KCl, 1.49 g; NH_4Cl, 1.07 g; Na_2SO_4, 0.43 g; $MgCl_2$, 0.2 g; $CaCl_2$, 0.03 g (pH 7.3-7.4); supplemented with D-(+)-Xylose, 105 mM, as carbon source instead of glucose; β-Glycerol phosphate disodium salt pentahydrate, 1.4 mM; sodium acetate, 15 mM; and tryptone, 0.02% (in 1 L of distilled water). A stock solution of $UO_2(NO_3)_2{\cdot}6H_2O$ was prepared at a concentration of 1 M in 0.1 M of $NaClO_4$. This stock solution was filter-sterilized using nitrocellulose filters of 0.22 μm, then stored at 4 ºC. For the treated cells, flasks containing TMM were inoculated with a 24 h-old culture of *S. bentonitica* and amended with U to final concentrations of 100 and 250 μM, respectively. Three biological replicates per treatment and sampling time were performed. In addition, heat-killed cells served as controls in order to verify active elimination of the metal by BII-R7. Cell samples corresponding to 0, 3.5, 18, 21 and 24 h of incubation were collected by centrifugation at 11,000 rpm during 5 min, and supernatants were stored at -20ºC for further analyses. U speciation in the medium was determined using the software Visual MINTEQ (version 3.1). Xylose and tryptone present in the medium were not considered in the calculations as these organic compounds are not included in the databases of the software.

Residual U(VI) present in the supernatants was measured using the Arsenazo III method, described by Jauberty et al. (2013). To this end, 250 µL of the sample were mixed in 1 mL of Arsenazo reagent and the absorbance was measured at 651 nm after 30-60 s. The concentration of free inorganic phosphate (P_i) was determined according to Murphy and Riley (1962), by measuring the absorbance at 850 nm after 30 min of the addition of the reagents.

2.3. Impact of uranium on S. bentonitica BII-R7 growth

To determine the effects of U on the growth rate of *S. bentonitica* BII-R7, the strain was grown in TMM liquid medium amended with 100 and 250 µM. Treatments without U were also carried out as controls. All were incubated at 28 ºC under shaking. Aliquots of 1 mL were taken every 3 h from all treatments in order to quantify the bacterial growth by measuring the OD_{600}.

2.4. HAADF-STEM/EDX analyses

Cells treated with 100 and 250 µM of U were harvested after 0, 7, 22, 48 and 72 h of incubation and prepared for microscopic analyses as described in Merroun et al. (2005). The cellular location of U precipitates was determined using high-angle annular dark field scanning transmission electron microscopy (HAADF-STEM, FEI TITAN G22 80-300) combined with energy dispersive X-ray (EDX) spectrometry analyses. Selected-area electron diffraction (SAED) allowed us to characterize the nature of minerals formed. TEM specimen holders were cleaned by plasma prior to STEM analysis to minimize contamination.

2.5. RNA extraction and sequencing

To perform transcriptomic analyses, cultures of *S. bentonitica* were prepared in TMM and treated with U under the conditions described above. Samples corresponding to lag and middle-exponential growth phases were harvested at different incubation times: 1 and 5 h of incubation for untreated cell samples, or 1 and 52 h for treatments with 100 and 250 µM of U. Cells were washed twice in NaCl 0.9% (w/v) and pellets were recovered by centrifuging at 5,000 x *g* for 15 min at 4 ºC. RNA extractions were carried out immediately.

Total RNA was extracted from each sample using the RNeasy Bacteria Mini kit (Qiagen, Germany) following the manufacturer's instructions. This extraction method included mechanical lysis of the cells using acid-washed glass beads (212-300 µm; Sigma-Aldrich) in FastPrep® FP120, at 6.5 ms^{-1} of speed for 40 s, done twice with an

interval of 5 min between cycles. Contaminating DNA was removed from the obtained total RNA using the TURBO DNA-free kit (Ambion, TX, USA), followed by a clean-up protocol with the RNeasy Bacteria Mini kit. Finally, the extracted RNA was eluted using nuclease-free water and EDTA (1 mM) added to each tube for preservation of the samples. Quantification of extracted RNA was determined by means of a Qubit 3.0 Fluorometer (Life Technology), and the quality was checked on 1.5 % (w/v) agarose electrophoresis gel in 1X TAE buffer.

Samples having an amount of total RNA below 50 ng/μL were concentrated to reach the adequate concentration by the ethanol precipitation method. Briefly, 4 vol. of absolute ethanol and 1 vol. of sodium acetate (3M, pH 5.2) were added to each sample, and the samples were incubated overnight at -20 ºC. Pellets were obtained by centrifuging at 16,000 x g for 30 min at 4 ºC, and resuspended in nuclease-free water and EDTA (1 mM). Samples were stored at -80 ºC until further analyses.

The quality and integrity of total RNA were checked using an Agilent Technologies 2100 Bioanalyzer (Agilent Technologies; Waldbronn, Germany). The RNA sequencing library was generated from 100 ng total RNA using RiboZerorRNA Removal Kit – Bacteria (Illumina) for rRNA depletion, followed by NEBNext® Ultra™ II Directional RNA Library Prep Kit (New England BioLabs), according to the manufacturer's protocols. The libraries were sequenced on Illumina NovaSeq 6000 using the NovaSeq 6000 S1 PE Reagent Kit (100 cycles) with an average of 24,073,898 reads per RNA sample (a maximum of 33,187,977 and a minimum of 15,829,801 reads).

2.6. Computational processing of the transcriptome samples

A reference for the program BBMap was made using the genes from *S. bentonitica* BII-R7 genome (obtained from GenBank/ENA/DDBJ database) and 191 genomic contigs. This reference was used to generate index files with the BBMap program version 37.90 (sourceforge.net/projects/bbmap/). Using this program, paired-end read files of 14 samples were mapped, producing SAM format files. The program samtools version 1.8 was then used to collect mappings with quality scores higher than or equal to 30. Generation of read counts per gene for each of the quality filtered SAM files was carried out by the mapcount program (https://github.com/mpcox/mapcount). Finally, a Ruby script served to compile the read counts of all samples into a single table with genes as rows and count values as columns.

2.7.Biostatistical analyses

Transcripts were obtained by annotating the genes with Rapid Annotation using the SEED-based method of Subsystem Technology (RAST, version 2.0). SSU and LSU subunits of rRNA were eliminated and mRNA raw data were normalized to transcript per million (tpm) in order to have comparable data. A cut-off was set at 500 tpm and all genes below this value were not considered for further analyses. Several genes with high levels of expression were annotated as hypothetical proteins, for which reason manual annotation was performed with BLAST (Basic Local Alignment Search Tool), and the closest bacterial phylogenetic sequences were selected with a minimal query cover level of 60%. Sequences were aligned in Seaview software (version 4.7) for the phylogenetic tree building.

RNA profiles of each sample were clustered using Past3 v. 3.18 according to the Bray-Curtis similarity index. Genes were grouped according to their function, and differential expression was represented in heatmaps using the gplots package with the heatmap.2 function of R software, and in stacked bars with Explicet version 2.10.5. In addition, an interaction network between genes was derived by calculating the Pearson correlation coefficient in R package reshape2; genes that passed a cut-off between -0.9 and 0.9 were represented in Cytoscape 3.6.0 using the Betweenness Centrality of each node.

Raw sequences were submitted to the European Nucleotide Archive (ENA) under the accession number PRJEB37934.

3. Results and discussion

3.1. Impact of U toxicity on S. bentonitica and quantification of U removal

The impact of U(VI), added as uranyl nitrate at concentrations of 100 and 250 µM, on the growth of *S. bentonitica* BII-R7 cells at different incubation times was determined. Significant differences between the untreated and U(VI)-treated samples were observed (Fig. 1). On the one hand, the untreated cells (control sample) exhibited the typical growth curve characterized by a short lag phase and the presence of exponential (0-16 h) and stationary phases (24-96 h). On the other hand, metal-treated cells showed a lag phase whose duration increased in tandem with the metal concentration, i.e. of about 48 h at 250 µM and up to 36 h when cells were exposed to the 100 µM U(VI) initial concentration. In addition, the longer lag phase observed at the 250 µM initial concentration clearly evidenced a higher metal toxicity than the lowest concentration tested. The substantial lag phase found in the present work is most likely

related to differential expressions of genes involved in U(VI) tolerance. Many authors have reported variable durations of the lag phase in cells of different bacterial populations treated with U(VI) (Park and Jiao, 2014). For instance, Newsome et al. (2015) observed a lag phase of up to 50 h when *Serratia* species isolated from Sellafield sediments grew in 1 mM of U(VI) under anaerobic conditions.

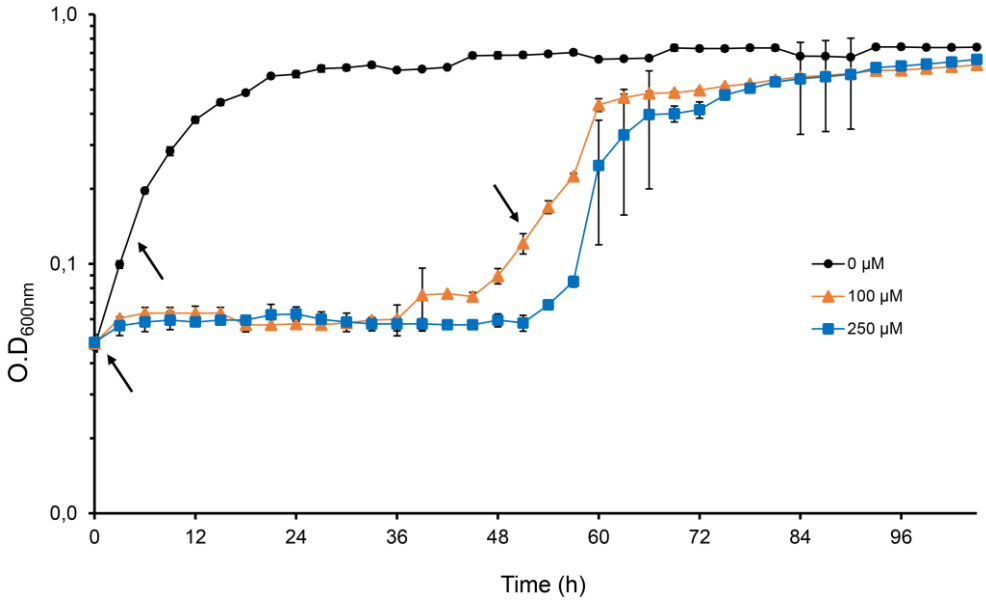

Fig. 1. Growth of Stenotrophomonas bentonitica BII-R7 in absence (control) and presence of 100 and 250 µM of uranyl nitrate.

It is well known that the toxicity of U depends on its oxidation state. While U(VI) is a soluble, mobile and toxic species, insoluble U(VI) species such as U(VI)-phosphate minerals are less toxic and stable (Gavrilescu et al., 2009). In general, the large lag phase exhibited by U-treated cells could be associated with removal of toxic U species from the medium. Therefore, the U removal rate exhibited by the *S. bentonitica* cells at different incubation times was investigated. For this purpose, the cells were grown in TMM amended with 100 and 250 µM of uranyl nitrate, and samples were collected at different incubation times: 0, 24, 48 and 72h. As the major part of U (93%-96%) was eliminated within the first hours (data not shown), the kinetic of U removal in 24 h of incubation was studied. The amount of the inorganic phosphate (P_i) released was also evaluated.

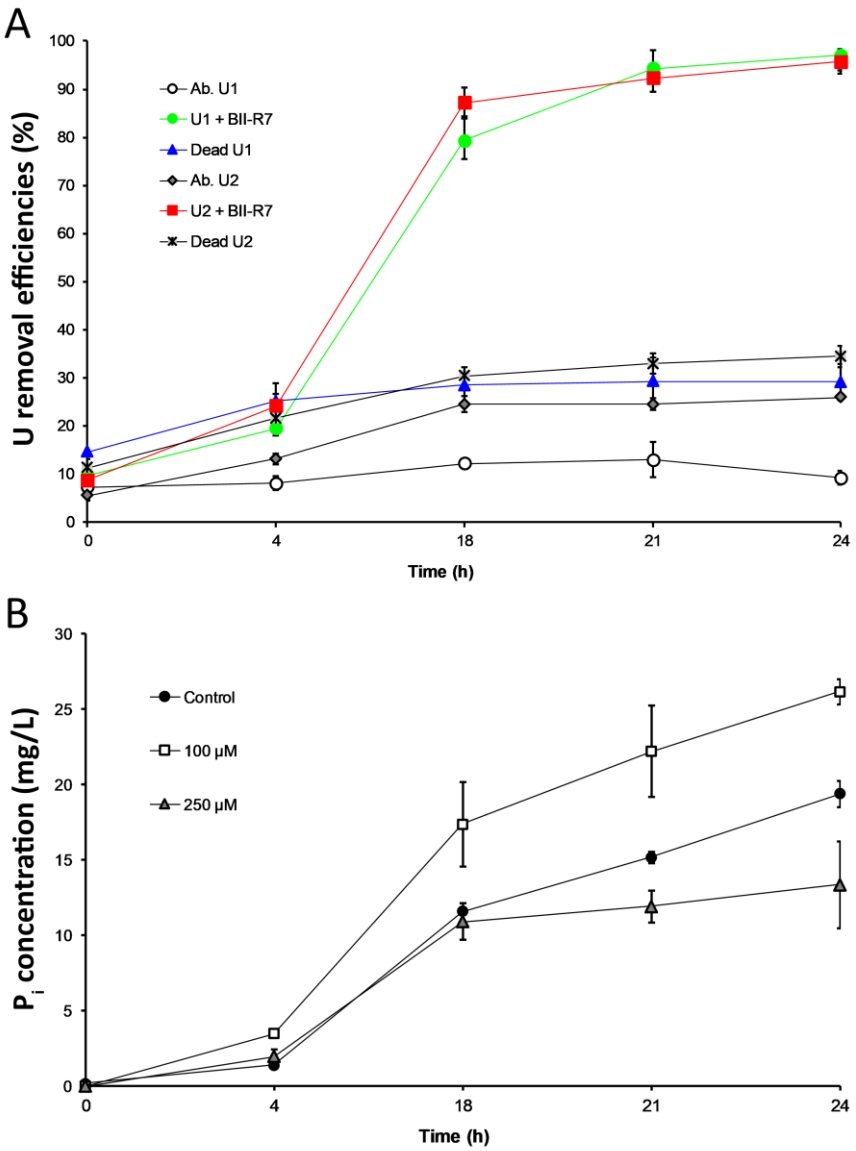

Fig.2. A. U concentration in the supernatant during the first 24 h of incubation in presence of 100 (U1) and 250 µM (U2) of U. Abiotic (Ab. U1 and Ab. U2) and heat-killed controls (Dead U1 and Dead U2) were performed under the same conditions. B. Concentratio in mg/L of the inorganic phosphate (Pi) released by S. bentonitica in presence of U.

The results indicated that 97% and 96% of U were removed after 24 h of incubation under 100 and 250 µM, respectively (Fig. 2A). A time-dependent increase in the concentration of P_i in the medium was also detected in all treatments, the highest values being obtained under 100 µM of U (Fig. 2B). Differences observed between abiotic controls could be explained by the different initial concentration. The major U species in the TMM (Table 1) are positively charged $(UO_2)_3(OH)_5^+$ and $(UO_2)_4(OH)_7^+$. U removal in the dead biomass is probably due to the sorption of the positively charged metal species to the negatively charged groups of the cell surface. In any case, these values were much lower than those observed with the active cells, suggesting that the U

removal is a metabolism-dependent process that probably involves P_i. This is in line with previous results from U removal assays performed with other bacteria. Chandwadkar et al. (2018) showed that *Serratia* sp. strain OT II 7 was able to eliminate up to 94% of 1 mM of uranyl acetate after 24 h of exposure, also with a progressive increase in P_i. Similar levels of U removal were observed in *phoN*-expressing *Deinococcus radiodurans* after 13 h of incubation (R. Xu et al., 2018).

Table 1. U speciation in the TMM and total concentration of each U species

% of total concentration		**Species name**
100 µM	250 µM	
0.383	0.201	UO_2OH^+
0.039	0.027	$(UO_2)_2(OH)_2^{+2}$
60.809	54.793	$(UO_2)_3(OH)_5^+$
37.205	43.945	$(UO_2)_4(OH)_7^+$
0.536	0.483	$(UO_2)_3(OH)_7^-$
0.031	0.028	$(UO_2)_3(OH)_4^{+2}$
0.151	0.079	$UO_2(OH)_3^-$
0.703	0.368	$UO_2(OH)_2$ (aq)
0.046	0.024	UO_2-$(Acetate)_3^-$
0.047	0.024	UO_2-$(Acetate)_2$ (aq)
0.039	0.02	UO_2-$Acetate^+$

The exponential growth phase occurred much later than when the concentration of U(VI) decreased. These results suggest that, after U removal, the cells still need some time to grow, most likely to recover from the damage caused by the radionuclide. The stationary phase was reached after 60 and 72 h of incubation, respectively under 100 and 250 µM of U. After this incubation time, however, the toxic effect of U(VI) at both studied concentrations was reduced and the cells reached a final cell density (expressed as OD_{600}) relatively similar to that of the untreated cells. Such findings indicated that, despite the low growth rate in presence of U (nearly 4-fold less than that of controls), *S. bentonitica* cells were probably able to develop detoxification strategies to cope with U(VI) toxicity and grow to nearly normal levels.

3.2.HAADF-STEM/EDX analyses

Analyses by STEM of *S. bentonitica* cells treated with 250 µM of U for 22 h (Fig. 3A) revealed that the cell wall may be the main precipitation site of this radionuclide. The amount of U precipitated increased at the longer incubation time, which appeared to be mainly distributed extracellularly as shown in Fig. 3B (48 h). Similar results were obtained when cells were treated with 100 µM of U, where the metal precipitated mostly in the medium surrounding the biomass after 52 h, as shown in Fig. 4. EDX spectra

revealed that the observed electro-dense precipitates were composed of U and P. Selected area electron diffraction (SAED) patterns showed the minerals obtained to be amorphous at both membrane and extracellular levels, although this could be due to the TEM high vacuum (Hu et al., 2005). Interestingly, no intracellular precipitation or accumulation in the treated cells was observed in the studied samples, in contrast with other bacteria (Zhang et al., 2018). The ability of strains of *Stenotrophomonas* genus to bioprecipitate U(VI) has been previously described. Merroun and Selenska-Pobell (2008) reported intracellular deposits of U in *S. maltophilia* JG-2. Furthermore, Islam and Sar (2016) studied the interactions with U of six bacterial species, which showed U precipitates on their surfaces. One of them —related to *Stenotrophomonas* genus (*Stenotrophomonas* sp. U18)— also produced such precipitates extracellularly.

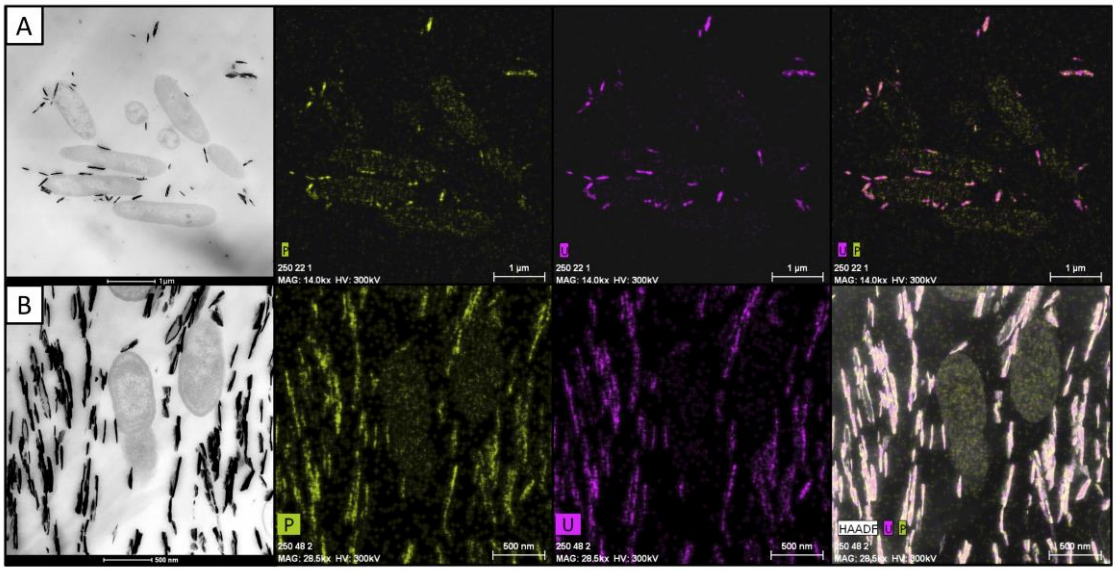

Fig. 3. HAADF-STEM micrographs of extracellular and membrane-associated precipitates formed by S. bentonitica after 22 (A) and 48 h (B) of incubation in 250 µM of U. Although RNA samples at these incubation times could not be sequenced, microscopic analysis showed precipitates identical to those formed under 100 µM.

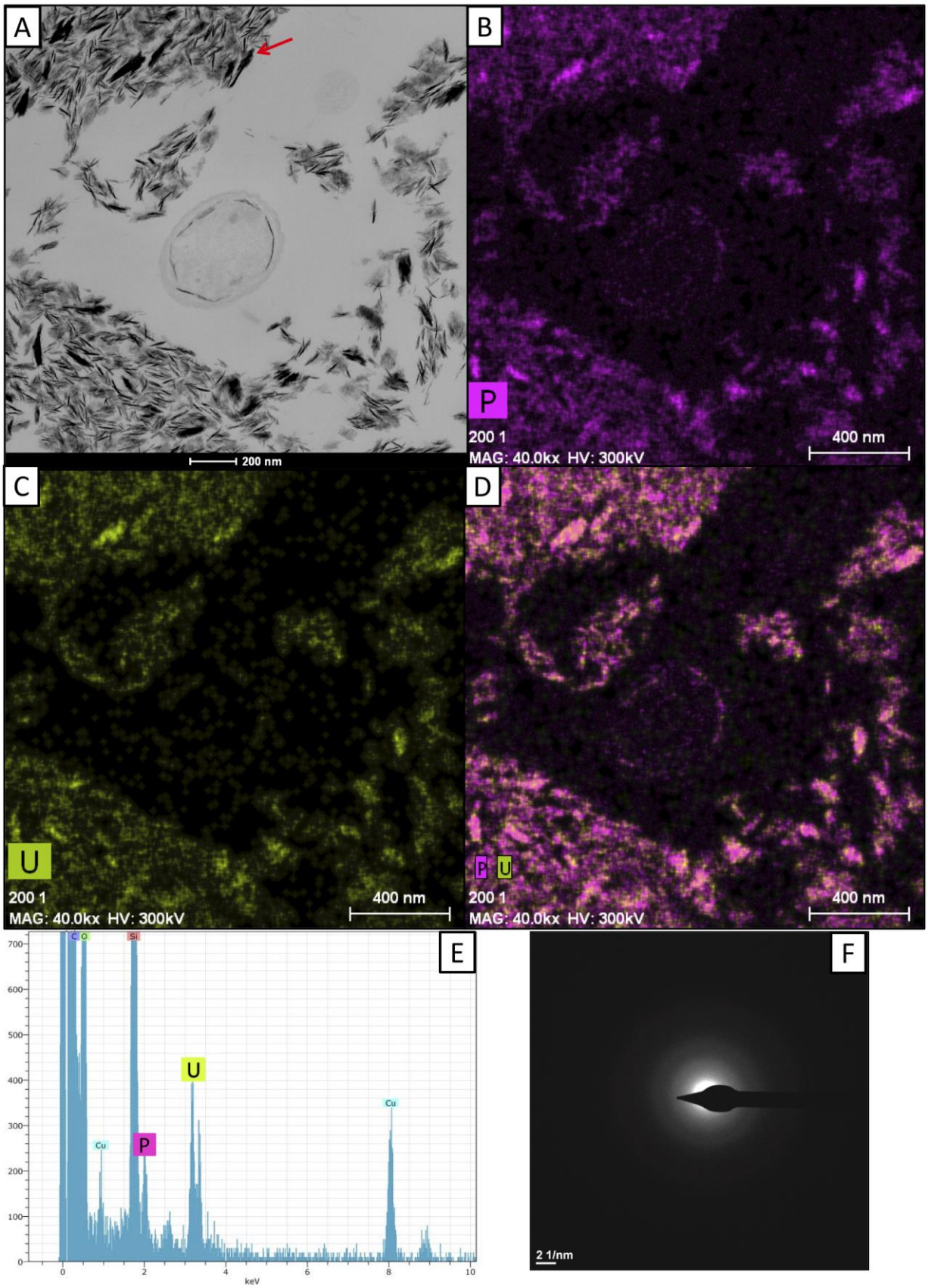

Fig.4. HAADF-STEM micrographs of S. bentonitica cells (A) and element-distribution maps (B, C and D) after 52 h of 100 µM of U exposure. E) EDX analysis showing the presence of U and P in the precipitates. F) SAED pattern of the precipitates.

3.3. Transcriptomic analysis

Transcriptomics studies were applied to investigate whether there are any relationships between the large lag phase of cells treated with U(VI) and differential expressions of genes involved in U(VI) tolerance. We focused on gene expression levels obtained during the lag phase (1 h of incubation; time 1) and exponential phase (5 h and 52 h of untreated and metal treated cells, respectively; time 2).

RNA libraries derived for U-treated and untreated cells were constructed for this purpose. Sequencing detected 4191 transcripts, which were aligned with the *S. bentonitica* genome sequence (NCBI Genebank accession number MKCZ00000000.1). On one hand, cells in the lag phase showed up-regulation of 185 genes and down-regulation of 143 under 100 μM of U, while exposure to 250 μM displayed 68 and 290 genes up- and down-regulated, respectively, out of the 3786 genes present in the genome. On the other hand, 148 genes were up-regulated during the exponential phase under 100 μM of U, while 194 were down-regulated. In view of the RNA profiles obtained, Fig. 5 shows the similarities among samples collected at different incubation times. After 1 h of cell incubation, corresponding to the lag phase (Fig. 1), untreated samples form a cluster clearly separate from those under U exposure, showing only 50% of similarity between Uranium and controls. In the exponential phase, controls and uranium did not group separately. These results are in agreement with the growth curves observed (Fig. 1), supporting the existence of a strong correlation between the gene expression and the sampling times (1 and 52 h).

After 1 h of incubation, significant changes in the gene expression were observed compared to the controls, probably helping the cells cope with the toxicity of U(VI) present in the solution. This similarity in the gene expression observed in the treated and untreated cells in the exponential growth phase (52 h) may be explained by the fact that the metabolic activity at that time was probably more related to simple growth activity than to U depletion or tolerance, which occur in the first hours of the lag phase in the treated cells (Fig. 2A). The high U(VI) removal rate (97%) would help the cells to adapt to metal exposure, resulting in their growth to almost the same level as that of the untreated cells. Consequently, we were interested in investigating the changes occurring in the lag phase, when the difference in gene expression between treated and untreated

cells was more than evident as a consequence of the presence of uranium in the medium and the metabolic cell activity to cope with such a toxic radionuclide.

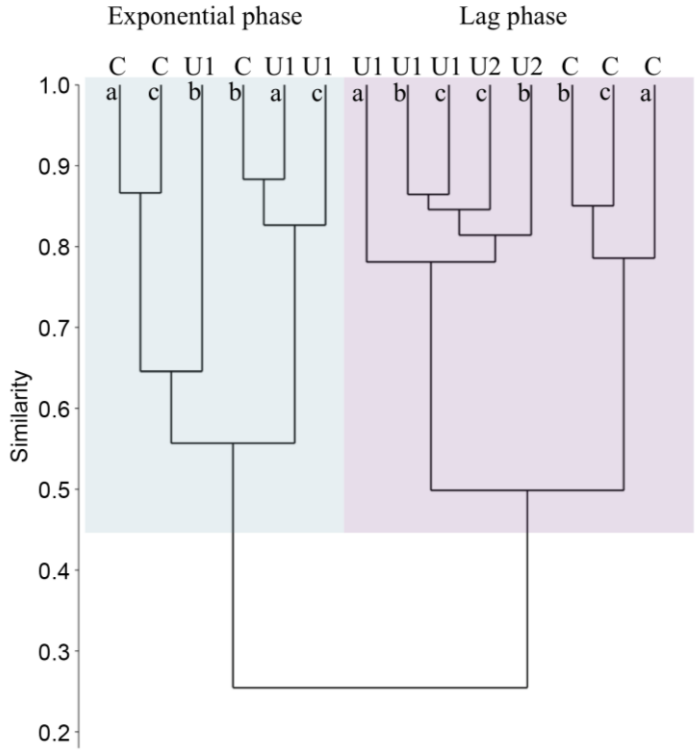

Fig.5. RNA profiles clustering according to similarity between replicates of each sample (a, b and c). Gene expression during lag phase was clearly different from that in exponential phase. Treated samples also grouped separately from the untreated samples during lag phase.

S. bentonitica BII-R7 developed a complex response to U(VI) exposure during lag phase, as shown in Fig. 6. (The complete correspondence of numbers and transcripts are indicated in supplementary table S1.) Metal stress caused gene expression similar to that seen in stationary or nutrient-starvation conditions (Hu et al., 2005). We observed down-regulation of genes involved in DNA synthesis and replication (*ribonucleotide reductase class I* and *dnaA*), suggesting important alterations in the cell cycle. Interestingly, expression of *ribonucleotide reductase class I* was negatively correlated with the expression of *phoU*, two *tonB-dependent receptors*, the *RND efflux system*, and *tail-specific protease*, among others. Given that *phoU* is a transcriptional regulator of genes of P metabolism, interactions with a high number of genes could be expected. The same occurred with *tonB-dependent receptors* and the *RND efflux system*. These transcripts form part of protein complexes involved in transport processes, and interactions with other members of the system and membrane proteins, also up-regulated, are essential. *Tail-specific protease* is implicated in the degradation of damaged proteins and the protection from thermal and other stresses.

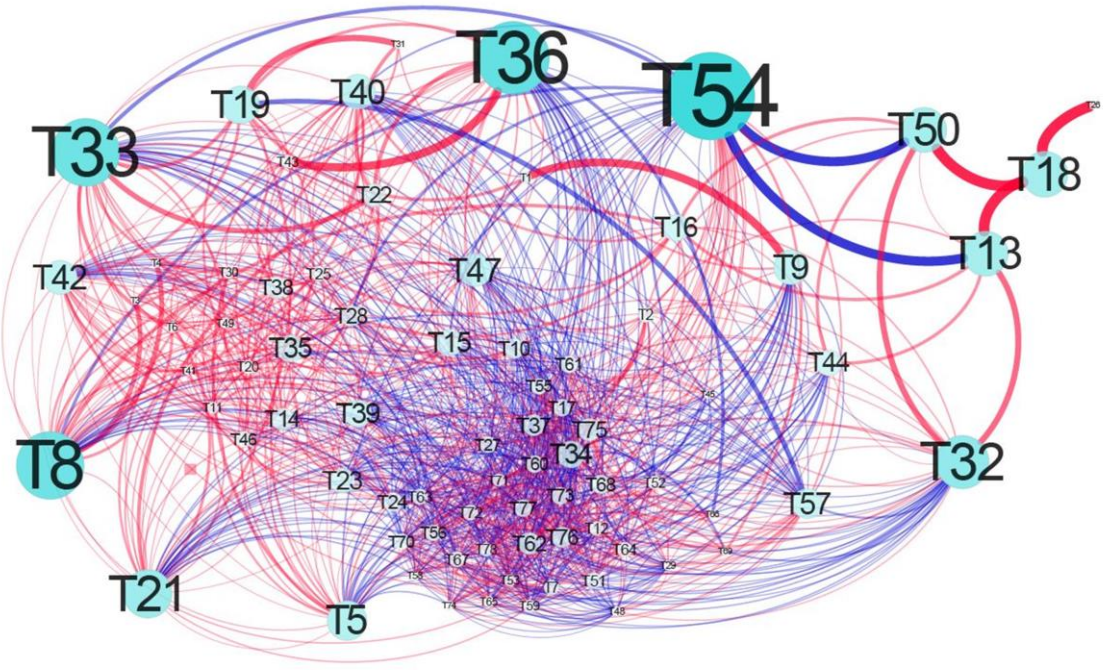

Fig. 6. Interaction network between gene transcripts during time 1. Positive and negative correlations are represented in red and blue lines, respectively. T54 *(ribonucleotide reductase class I)*, T50 *(phoU)*, T13, T18 *(tonB-dependent receptors)*, T8 *(RND efflux system)*, and T33 *(tail-specific protease)* expression showed interaction with a high number of transcripts at this incubation time. See supplementary table S1 for the complete nomenclature and the Pearson correlation coefficient of each transcript.

In addition, chemotaxis and cell motility genes (e.g. flagellar regulatory gene *fleQ*) and those related to cell adhesion, like pilus IV assembly proteins, were down-regulated in all U concentrations. Similar results were obtained for transcripts of aminoacids, carbon metabolism (e.g. *phenylalanine-4-hydroxylase*, *aminomethyl transferase*, *fumaratehydratase*), as well as of lipid metabolism (e.g. *malonyl-CoA transacylase*, *3-oxoacyl reductase*) and aerobic oxidative phosphorylation (e.g. *NADH-ubiquinone oxidoreductase*, *cytochrome O ubiquinol oxidase*, *succinate dehydrogenase*), especially under 250 µM, showing the higher toxicity of this metal concentration.

These results were in agreement with the effects reported in studies on mutants of *Caulobacter crescentus* exposed to U (Hu et al., 2005; Park and Jiao, 2014). Nevertheless, wild type cells of *S. bentonitica* were able to grow at almost the same level in all tested U concentrations, suggesting the presence of more efficient mechanisms against the toxic effects of this radionuclide. Yung et al. (2014) suggested that the changes in cell cycle were insufficient to produce significant differences in the growth rate, thus explaining the

observed growth recovery. Yet in the case of *S. bentonitica*, the lag phase extended about 35 h more, indicating that the down-regulation of cell cycle genes had a strong impact on the growth. We barely found expression of chaperones or oxidative stress enzymes. This was not surprising, since U seemed to cause less direct oxidative damage than metals such as cadmium or chromate (Hu et al., 2005). This might also be explained by the fact that U was unable to enter *S. bentonitica* cells.

After manual annotation (see section 2.7), more transcripts were identified as affected by uranium and potentially involved in its biomineralization. For instance, genes related to processes such as transport, cell wall and lipopolysaccharide biosynthesis, and phosphate metabolism (among others) were up-regulated.

3.3.1. *Transporters*

Figure 7 reflects the complex response of the transporters involved in cations, drugs and toxic compound transporters —such as resistance-nodulation-cell division (RND transporters) efflux system, ABC transporters (ATP-binding cassette) or the TonB-dependent receptors— that showed different expression levels in U-exposed cell cultures.

Genes pertaining to *RND transporters* were highly expressed in U treated cells, mainly in the early hours of the experiment (lag phase), with fold changes up to 9.8 and 6.7, respectively in 100 μM and 250 μM. Several studies have shown the ability of RND family proteins to prevent the toxicity of various heavy metals. Members of this family associate with membrane proteins or factors to form a protein complex that permits export of the substrate outside the cells. Among these RND transporters, CzcCBA complex was firstly described in *Ralstonia metallidurans* as conferring Co^{2+}, Zn^{2+}, Cd^{2+} and Ni^{2+} resistance (Nies, 2003). Moreover, Orellana et al. (2014) reported a higher abundance of this protein complex in *Geobacter sulfurreducens* proteome in presence of 100 μM of uranyl acetate, highlighting its role in U tolerance. *S. bentonitica* showed up-regulation of two genes encoding for CzcA/CusA and one for CzcD (1.6-, 1.62- and 2.2-fold changes, respectively) in the exponential phase under 100 μM of U. However, none of these genes were detected during the lag phase.

Transcripts encoding SmeE and SmeD were up-regulated (Fig. 7), but the associated protein of the complex, SmeF was not detected. Similar results were observed for AcrA and AcrB, and MdtA, B and C. The function of these systems in antibiotic resistance has been demonstrated (Hayashi et al., 2015; Nies, 2003). Still, no information regarding their involvement in heavy metal tolerance is known.

In accordance with previous studies involving several heavy metals, including U (Yung et al., 2015), genes belonging to ABC transport systems were also positively regulated in this study, mainly during lag phase, varying in a range from 6 to 9-fold changes for 100 μM, and from 5 to 6-fold changes for 250 μM. Among them, the subunit CcmA was up-regulated, which along with CcmB and C, is involved in cytochrome c assembly (Feissner et al., 2006). Nevertheless, no transcripts were found for CcmB nor C. ABC transporters allow for the transport of drugs and toxic compounds across the membrane (Marquez, 2005). Although up-regulation of ABC transporters has been previously observed in presence of U (Choudhary et al., 2012), there is no evidence of this system´s implication in U detoxification, and the substrate translocated is still unknown (Verissimo and Daldal, 2014).

Another class of transporters whose expression was modulated under U stress were the TonB-dependent receptors. Different TonB-dependent receptors were up-regulated during the lag phase, especially under 100 μM of U (Fig. 7). It is an outer membrane receptor that interacts with TonB protein to couple the energy needed for high specificity translocation across the outer membrane of different substrates (e.g. iron siderophores or cobalamins) (Chimento et al., 2003). Several studies reported a higher abundance of these transporters in the presence of heavy metals, suggesting an important role in heavy metal resistance (Hu et al., 2005; Yung et al., 2014). Hu et al. (2005) furthermore observed this phenomenon when cells of *C. crescentus* were exposed to U, Cd and Cr, particularly in the latter. But the up-regulation of TonB-dependent protein may be also unrelated to transport processes. The receptor could bind to heavy metals to carry out signaling processes that give environmental information to the cells.

Other transcripts involved in the specific transport of metals were detected. A Ni^{2+}/Co^{2+} efflux regulator RcnB was 4.5-fold up-regulated during the lag phase, but down-regulated in the exponential phase. Furthermore, a $Mg^{2+}/Co^{2+}/Ni^{2+}$ transporter MgtE showed the opposite behavior, being down-regulated in the lag phase, but it was 1.9-fold higher than in the untreated cells during the exponential phase.

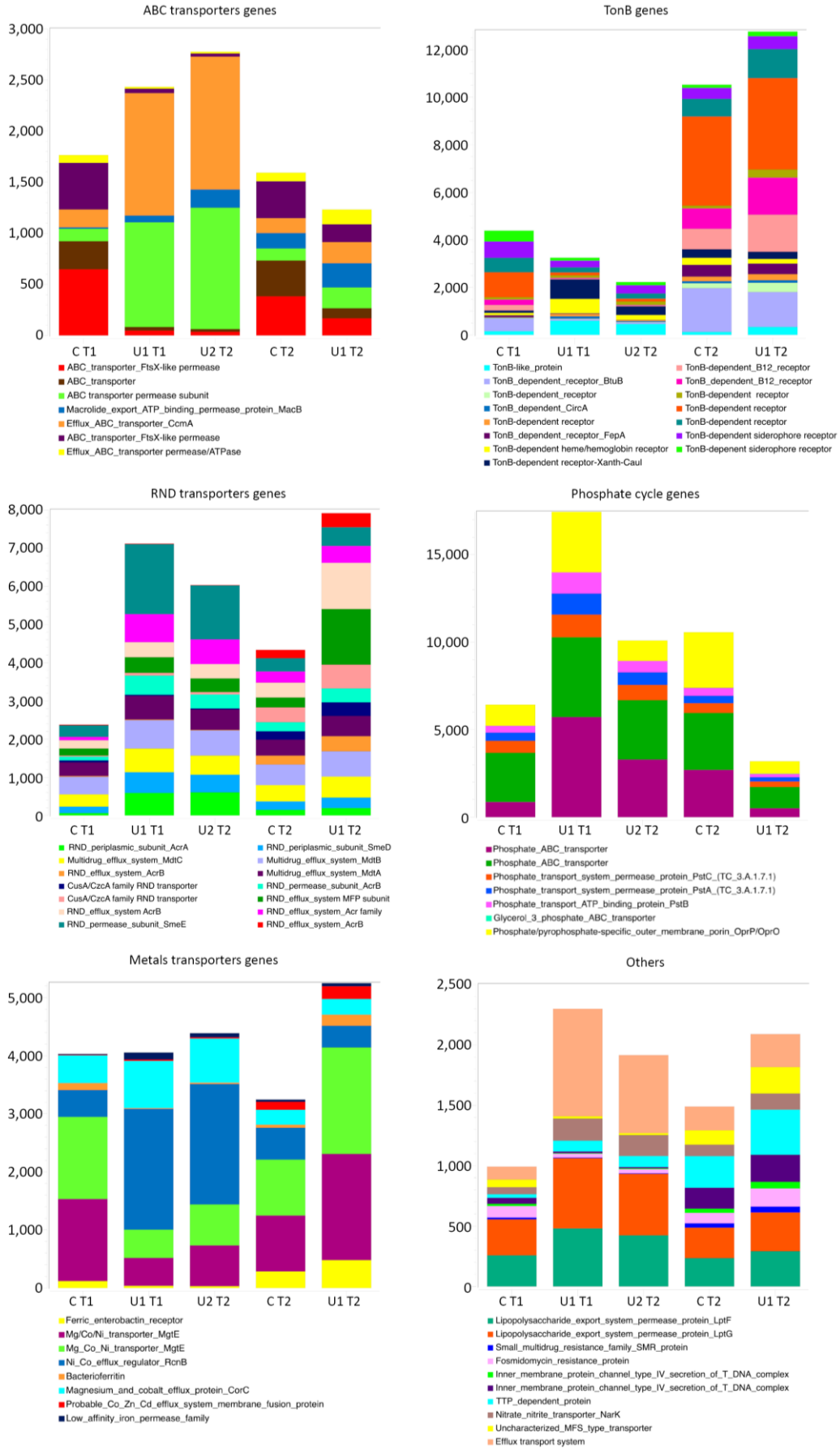

Fig.7. Distribution of transcripts encoding different transporters in absence (C) and in presence of 100 (U1) and 250 µM (U2) of uranyl nitrate, during the lag (T1) and exponential (T2) phases.

While the role of some of these genes in the transport of cations such as Co^{2+}, Zn^{2+} or Na^{2+} to maintain metal homeostasis of the cells has been extensively described (Fath and Kolter, 1993; Nies, 2003), no information exists about the involvement of these systems in U transport. U intracellular accumulation can cause damage to proteins and DNA due to its affinity to thiol or carboxyl groups. Given the lack of any known biological function of this radionuclide, bacteria would have to use transporters that serve to maintain metal cation homeostasis, to export U from the cells (Choudhary et al., 2012; Orellana et al., 2014). The up-regulation of transporters implicated in the efflux of different substrates, i.e. antibiotic export, could be related to other processes triggered by U toxicity such as the envelope stress response. Hence, these genes could play an important structural role associated with the cell envelope stability, as was demonstrated for the SmeIJK system in *S. maltophilia* (Huang et al., 2014).

In contrast with previous results, certain transcripts of transporter proteins—ABC transporters, TonB-dependent receptors, or Mg, Co and Ni transporters— were down-regulated in all sampled metal concentrations and times, probably due to membrane perturbation caused by metal stress (Yung et al., 2014).

It is also worth noting that expression levels of genes implicated in phosphate transport in the untreated cells during lag phase are similar to those obtained for the U-treated cells at time 2, and vice versa. These results could be explained by the effect of U on the cell metabolism. On the one hand, there is no growth during the lag phase of treated samples, but the up-regulation of phosphate transporters suggests the use of phosphate for U removal through its precipitation as U phosphates (Fig. 2A). On the other hand, untreated cells increased P uptake to face the requirements for growth during the exponential phase, whereas this uptake decreased in U-treated cells, as most of the U had already been removed. Furthermore, the treated cells required less P to grow, since the growth rate is lower in these samples, which explains the higher expression of these genes in untreated cells despite being in the same growth phase.

3.3.2. *Cell wall and lipopolysaccharide biosynthesis*

Exposure to U changed the expression of genes encoding cell wall and membrane proteins, which play a key role in maintaining membrane integrity and in cell envelope synthesis. These changes were dependent on the incubation time and the concentration of the metal, the main changes being observed after 1 h of incubation (lag phase) at 100 µM of U. A high number of transcripts belonging to CreD protein and GTB-type superfamily glycosyltransferase (GT), followed by the proteins OmpA, LolA, an ArnT GT, and a lipid-A disaccharide synthase, were observed in U treated samples after 1 h of incubation (Fig. 8). Some genes involved in biofilm formation, such as *degQ* (Wang et al., 2015), were also up-regulated during the lag phase (4.5- and 3.4-fold change under 100 and 250 µM, respectively).

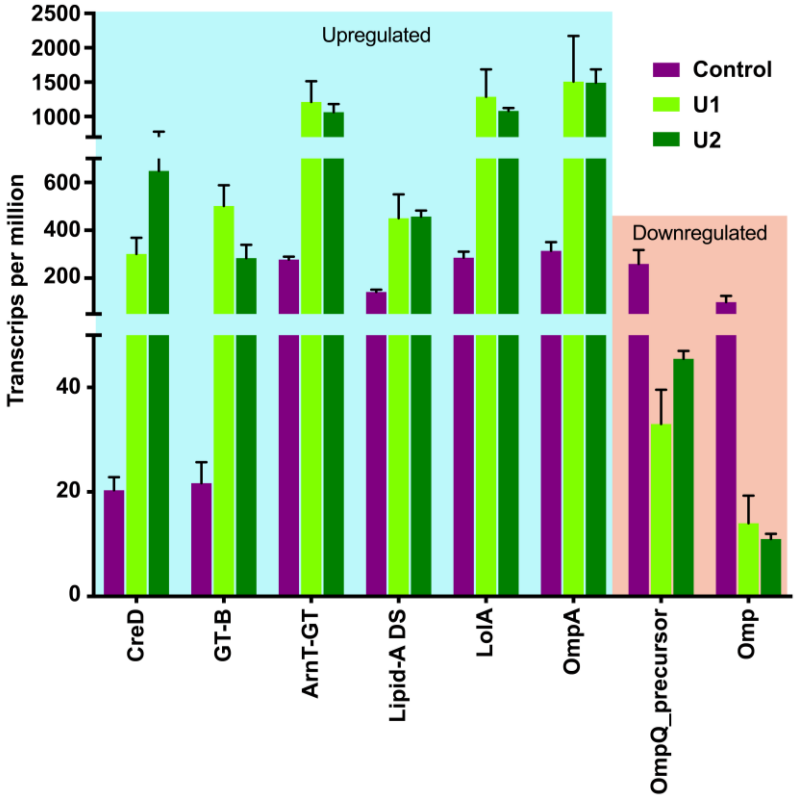

Fig.8. Genes encoding membrane proteins, enzymes and proteins taking part in cell wall structure biosynthesis that changed their expression under U exposure during lag phase. Expression levels are shown as transcript per million (TPM).

It is noteworthy that *creD* encoding an inner membrane protein was highly induced (21-fold) in the presence of 250 µM of U. Huang et al. (2015) investigated the possible functions of CreD in *S. maltophilia*. Mutants lacking this protein showed altered outer membrane permeability, suggesting it is key for cell envelope homeostasis and integrity. They also proved that CreD protein increased in the case of high bacterial density, probably to address inner membrane expansion. As up-regulation of CreD in *S. bentonitica* was observed during the lag phase, this supports a possible key role in U

tolerance by decreasing the permeability of the cell envelope, preventing the metal from reaching the cytoplasm.

Furthermore, genes also located in the *cre* locus (Fig. S4) have been previously related to the phosphate metabolism. In P_i starvation conditions, *creC* can act as a response regulator of the CreBC two-component system involved in phosphorylation of PhoR, required for the expression of the alkaline phosphatase PhoA (Cariss et al., 2008). It has been demonstrated that CreBC strongly induces *creD* expression in *E. coli* DH5α (Avison et al., 2001). Notwithstanding, Huang et al. (2015) showed that CreBC regulated negatively the activity of *creD*.

Up-regulation levels of 23- and 4-fold, respectively, of a glycosyltransferase B superfamily (GT-B) and ArnT belonging to the GT-C superfamily were observed in 100 μM, and to a lesser extent under 250 μM of U treatment (13- and 2.5-fold). Another type of GT from family 19, the Lipid A disaccharide synthase (LpxB), was found 3-fold higher after 1 h of 100 μM of U exposure, as compared to untreated cells. Bacterial GT consists of inner membrane enzymes known to be involved in several biosynthetic processes. Up-regulated GT participates in lipopolysaccharide (LPS) biosynthesis by adding sugar residues at different levels to the LPS structure. The GTB-type is closely related to the GT1 family, whose members take part in LPS biosynthesis by adding activated nucleotide sugar to the core oligosaccharide (Luke et al., 2010; Schmid et al., 2016). In turn, ArnT is characterized by the addition of 4-amino-4-*deoxy*-L-arabinose (L-Ara4N) residues to the lipid A of LPS (Tavares-Carreón et al., 2015). LpxB, located in the cytoplasmic membrane, takes part in the synthesis of the intermediary molecule lipid A disaccharide, a precursor necessary for the lipid A formation of LPS (Metzger and Raetz, 2009).

The LPS of Gram-negative bacteria is known to protect the cells from antimicrobial compounds by avoiding their diffusion, and GT activity could lead to modifications in the oligosaccharide structure that provides resistance to these compounds, as occurs with the addition of L-Ara4N residues to lipid A of LPS, and polymixin resistance (Rosenfeld and Shai, 2006; Tavares-Carreón et al., 2015). Therefore, it can be surmised that the up-regulation of these GT enzymes would physically block U entrance. The L-Ara4N modifications observed could also result in changes in the global structure of the LPS to promote a more specific response to the presence of the metal. The two processes might act together to conform an efficient mechanism for U tolerance.

A periplasmic protein encoded by the gene *lolA* was also up-regulated at both U concentrations tested after 1 h of incubation (5-fold and 2.5-fold). LolA is a chaperone belonging to the Lol system, which comprises five proteins: LolA, B, C, D and E. The proteins LolCDE of this system form an inner membrane ABC transporter, which interacts with the periplasmic protein LolA to transfer lipoproteins such as Pal. Then, LolA associates with LolB in order to anchor the lipoprotein at the outer membrane (Murahari et al., 2013). Similar results were found for *G. sulfurreducens*, whose proteome in presence of U likewise showed an up-regulation of LolB, as well as other outer membrane lipoproteins (Orellana et al., 2014). The slight up-regulation of the rest of the Lol complex (B, C, D and E) indicates that the cells were actively involved in biogenesis of the outer membrane under U stress.

Up-regulation of *ompA* was observed when *S. bentonitica* grew with 100 and 250 µM of U (5- and 3-fold changes, respectively). OmpA is a two-domain outer membrane porin highly expressed in Gram-negative bacteria and tightly regulated by environmental changes (Smith et al., 2007). This protein has been linked to cell survival under environmental stress, and the maintenance of cell shape and membrane integrity (Sonntag et al., 1978; Wang, 2002). The fact that a TonB-dependent receptor related to OmpA was down-regulated under 250 µM of U could be explained by the higher toxicity under this concentration. The up-regulation of this protein suggests that an increase of the surface of the outer membrane may occur, hindering intracellular U accumulation by BII-R7 cells (Nilsson et al., 1984). Because such a response has been described with other heavy metals like Cr in *C. crescentus* (Hu et al., 2005), it might be a general response to various heavy metal stresses.

In contrast to OmpA, the expression of a phosphate-selective porin belonging to the Phosphate-selective porin O/P family, *oprP*, decreased when cells reached the middle-exponential phase (52 h) under 100 µM of U. This outer membrane protein exhibits a high affinity for polyphosphate anions (Modi et al., 2015). Dekker et al. (2016) obtained similar results with a porin of the same family, Omp40, when *A. ferrooxidans* were exposed to 0.5 mM of U(VI). These authors suggested that the protein´s down-regulation could be a means of impeding the passage of the radionuclide-phosphate complex through the membrane, given the affinity of phosphate ions to the metal.

The results of our study suggest that U exposure could have an effect on the σ^E regulon. Up-regulation of RNA polymerase σ factors E (*rpoE*) was also observed after 1 h, especially under 100 µM of U. Envelope stress caused by metal sorption to the surface

activates σ^E, which explains the up-regulation of genes involved in the rearrangement of LPS and membrane composition (Mitchell and Silhavy, 2019). However, σ^E also triggers the synthesis of *micA*, a small RNA that inhibits the expression of *ompA* (Brooks and Buchanan, 2008; Smith et al., 2007). The up-regulation of *ompA* observed is therefore explained by the presence of the inner membrane protein RseA (3.45- and 2.32-fold change under 100 and 250 μM, respectively) that represses σ^E function (Mitchell and Silhavy, 2019).

The cell wall is the first barrier that bacteria can use to protect themselves from toxic compounds, including heavy metals. Indeed, microbial biomass shows high affinity to U. Metal cation complexation on the surface of bacteria has also been widely described in the context of biosorption.

Since a bacterial surface has a number of charged functional groups within its layers, it makes direct contact with the environment and affords centers for metal cation binding by means of electrostatic and Van der Waals interactions with carboxyl, phosphate, hydroxyl and amine groups. The presence of a metal could affect the distribution of these ligands, increasing cell wall and LPS structures, and explaining the up-regulation of these genes in *S. bentonitica* (Merroun and Selenska-Pobell, 2008; J. Zhang et al., 2018). This is known as the fast metabolism-independent mechanism. It occurs during the first minutes of metal exposure (Celik et al., 2018; Yang et al., 2015b), and has been described for many other bacteria when in contact with U. According to Gerber et al. (2016), this chelation process takes place in *Acidovorax facilis* within the first 8 h of incubation with U at pH 5, followed by a slower process of U accumulation in the cytoplasm; fast U adsorption was also observed in *Microbacterium oleivorans* A9 incubated at different temperatures and concentrations of the metal (Theodorakopoulos et al., 2015).

Several studies depict the bacterial surface as a dynamic structure able to vary even in a single cell in response to the surrounding environment, determining the distribution of ligands and proteins within it (Khalid et al., 2008). A presence of heavy metals in the growing medium could give rise to an overexpression of genes related to cell wall and lipopolysaccharide synthesis, thus explaining the gene up-regulation seen for *S. bentonitica* in our study (Merroun and Selenska-Pobell, 2008; J. Zhang et al., 2018).

3.3.3. *Phosphate metabolism and U biomineralization*

The transcriptomic analyses performed detected an up-regulation of phosphatase in U treated cells after 1 h of incubation (lag phase), suggesting how important this type of enzyme may be for coping with metal stress. Despite the fact that 43 genes encoding phosphatases were detected, only four of them showed high induction when cells of BII-R7 were exposed to both 100 and 250 μM of U. Remarkably, one acid and one alkaline phosphatase were found about 7-fold higher than in the untreated cells under 100 μM of U in lag phase (Fig. 9). This finding suggests that U enhanced the native phosphatase activity, supported by the increase in P_i observed in the supernatant (Fig. 2B). In addition, the wide range of phosphatases identified in *S. bentonitica* cells could condition its adaptation to the low-P environment of bentonite formations where this strain was isolated, through a variety of organic P sources (Skouri-Panet et al., 2018).

Within the sampling time 2 (52 h), four types of phosphatase showed significant changes in their expression levels. Alkaline and acid phosphatases were also up-regulated, yet to a lesser extent than after 1 h of incubation. The other two proteins —an inositol-1-monophosphatase and inorganic pyrophosphatase— were down-regulated when cells were exposed to U. Bacterial phosphatases, both acid and alkaline, are assumed to play a major role in U biomineralization, leading to the formation of U-phosphate mineral phases when using organic phosphate as P_i source, reducing U availability and toxicity in the environment (Chandwadkar et al., 2018).

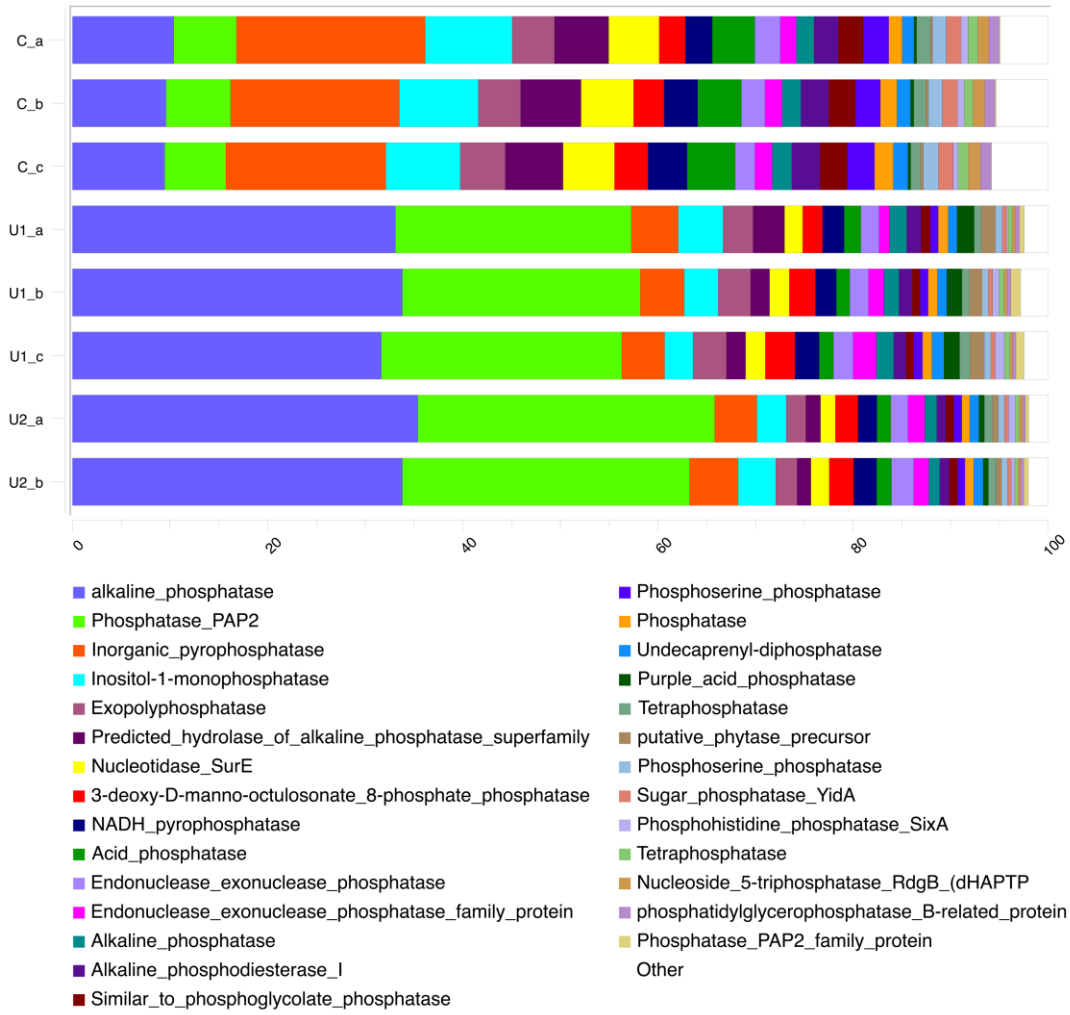

Fig. 9. Differential expression of genes with phosphatase activity in S. bentonitica, in presence (U1, U2) and absence (C) of uranium. Transcripts shown correspond to lag phase (1 h of incubation).

The alkaline phosphatase up-regulated in *S. bentonitica* BII-R7 is related to an inner membrane phosphoethanolamine transferase (with 100% similarity) similar to OpgE from *E. coli* (E-value 6.05e-99). This enzyme catalyzes the substitution of constitutive glucose from osmoregulated periplasmic glucans (OPGs) by phosphoethanolamine residues (Bontemps-Gallo et al., 2013). Modifications of OPGs with phosphoglycerol, succinyl and/or phosphoethanolamine confer an anionic character to the molecule (Bontemps-Gallo et al., 2017). Thus, the addition of phosphoethanolamine to OPGs could promote the biosorption process previously mentioned by providing U binding sites (see section 3.3.2).

Further studies have highlighted the importance of diverse alkaline phosphatases in U(VI) biomineralization. Yung and Jiao (2014) proposed a U(VI)-biomineralization mechanism in *C. crecentus* NA1000 mediated by the naturally-expressed periplasmic PhoY. This non-specific ALP-like superfamily phosphatase produced extracellular

precipitates of meta-autunite [$(NH_4)(UO_2)(PO_4)\cdot 3H_2O$] —the uranyl phosphate species of U(VI)— by releasing P_i to the medium from G2P. Similar results are described for PhoK from *Sphingomonas* sp. BSAR-1 when up-regulated in *E. coli* and *D. radiodurans* (Kulkarni et al., 2013; Nilgiriwala et al., 2008). Thus, this enzyme may enhance U resistance via two processes: biosorption of U to the surface through increasing LPS production; and additional promotion of the biomineralization process once U is linked to the membrane.

The acid phosphatase found in the present study belongs to the membrane-associated type 2 phosphatidic acid phosphatase (PAP2) superfamily. Appukuttan et al. (2011) investigated the role of *phoN* —a periplasmic nonspecific acid phosphatase also included in the PAP2 superfamily— in U biomineralization by means of a *phoN*-expressing *D. radiodurans* strain; they showed that lyophilized cells could achieve 100% precipitation in the presence of 10 mM of uranyl nitrate after 13 days, whereas complete depletion of higher concentrations of U (15 and 20 mM) was reached after 17 days. Scanning Electron Microscopy revealed that the precipitated U was mainly associated with the cell membranes, without signs of extracellular precipitation. In the study by Xu et al. (2018), the same recombinant bacterium, when exposed to 1 mM of uranyl acetate, was able to precipitate up to 95% of uranium after 13 h.

In light of the microscopic results obtained in this study (see section 3.2), the interaction of U with the cells of BII-R7 signals a biphasic process. At first, a fast process mediated by biosorption of U to the cell surface through phosphate-containing molecules (including proteins) is enhanced by the up-regulation of membrane proteins described above. This rapid process lays out a nucleation site for precipitation of the metal (Merroun and Selenska-Pobell, 2008), which is conditioned by phosphatase activity in the second phase. The U-phosphate minerals formed would be released from the cells to the extracellular medium. Several studies evoke this two-phase precipitation model as a very likely phenomenon in bacteria possessing the ability to precipitate U (Chandwadkar et al., 2018; Liang et al., 2016).

Furthermore, the cellular location of U phosphates apparently depends mostly on the aqueous U species predominant under specific conditions, rather than on the enzyme location. Kulkarni et al. (2016) investigated U precipitation in terms of acid (*phoN*) and alkaline (*phoK)* phosphatases, expressing the enzymes from *Salmonella enterica* serovar Typhimurium in *E. coli* and *D. radiodurans*. They affirmed that carbonate-deficient conditions triggered mainly cell-bound bioprecipitation, while carbonate-abundant

conditions led to an extracellular location of precipitates; phosphatase activity yielded chernikovite [$H_2(UO_2)_2(PO_4)_2 \cdot 8H_2O$] at pH 6.8. Differential locations of U precipitates were also described for *Serratia* sp. strain OT II 7 cells after incubation at pH 5, 7 and 9 (Chandwadkar et al., 2018). Neutral and alkaline conditions resulted in the precipitation of calcium uranyl phosphate hydrate [$Ca(UO_2)_2(PO_4)_2 \cdot 6H2O$], mainly distributed in the extracellular medium. However, at pH 5, uranyl phosphate hydrate [$HPUO_6 \cdot 4H_2O$] as well as calcium uranyl phosphate hydrate were observed, mostly as intracellular accumulations. These results suggest that the location of U precipitates is determined by the pH of the culture medium, which in turn conditioned the metal speciation, the type of phosphatase enzyme (acid or alkaline) exhibiting more activity, and the binding capacity of the functional groups of the cell wall.

A 3-fold induced polyphosphate kinase (*ppk*) was detected in presence of 100 µM after 1 h of incubation. The immobilization of U and other metals in polyphosphate granules —a mechanism conferring tolerance— has been widely reported (Acharya and Apte, 2013; Hu et al., 2005; Sivaswamy et al., 2011). In a study by Suzuki and Banfield (2004), *Arthrobacter ilicis* increased the amount of polyphosphate granules when it was exposed to U, pointing to a significant role of polyphosphates in the immobilization of uranyl ions to avoid cellular damage. EDX analysis of the polyphosphates generated by BII-R7 revealed, however, that U did not accumulate in these granules (data not shown). The expression of this enzyme might therefore be induced in response to the presence of G2P in the culture medium, stored as a source of P by synthesizing polyphosphates to be later used for U precipitation (Gallois et al., 2018). An absence of *ppk* expression during the exponential growth phase may owe to depletion of P_i used earlier in U biomineralization.

In this study, transcripts of genes involved in specific P uptake and metabolism (such as pho regulon genes) were also identified. Expression of genes of the *pstSCAB* system, *phoB* and *phoU*, changed especially after 1 h of incubation (lag phase). PhoB and PhoU are transcriptional regulators that respectively control, positively and negatively, the transcription of phosphate regulon genes. PhoB accumulation has been linked to phosphate starvation conditions, activating transcription of *pstSCAB* to allow the high-affinity import of P_i inside the cell (Chen et al., 2015; Santos-Beneit, 2015). Given the G2P-rich conditions in the culture medium, in this study *phoU* exhibited 4-fold induction in the presence of 100 µM of U. The *phoB* (1.86-fold change) and *pst* system (1.9-, 2.57-

and 3.11-fold changes respectively for PstC, A, and B) was also up-regulated, albeit to a lesser extent.

These findings suggest that both PstSCAB and PhoB may increase during the first minutes of incubation in order to transcribe the phosphatases that release P_i from G2P. Part of the released P_i could be used not only to address cellular requirements, but also to synthesize polyphosphate granules via PPK activity (as described above); then, PhoU would intervene to stop P_i import, thereby impeding the possibly toxic effects of an excess of this compound (Santos-Beneit, 2015). The demonstrated lack of these processes at concentration 250 µM and in the middle-exponential growth phase could be attributed, respectively, to the toxic effects of the metal and the adaptation of the cells to the conditions of exposure. Meanwhile, part of P_i would have interacted with uranyl to form uranyl-phosphate minerals.

3.3.4. *Iron transport and metabolism*

Some previous studies related U exposure to an increase in proteins governing iron uptake and metabolism (Gallois et al., 2018; Orellana et al., 2014). Analysis of the expression regulation of genes involved in iron metabolism in our samples was therefore deemed necessary. Three ferrichrome-iron receptors located in the outer membrane (involved in the import of Fe^{3+}-siderophore complexes into the periplasmic space) were detected in the samples treated with 100 µM U for 1 h. The most abundant one, with 2.3-fold change, shared similarity with the Fiu domain sequence; the other two belonged to CirA superfamily receptors, which exhibited changes 2.27- and 1.75-fold higher than in control samples.

Fiu and CirA proteins are outer membrane transporters that import Fe^{3+} attached to catecholate siderophores by interacting with TonB and inner membrane proteins. These interactions provide energy for transport (Andrews et al., 2003; Grinter and Lithgow, 2019). Once inside the cell, proteins such as bacterioferritin-associated ferredoxin (up-regulated 1.85-fold) can reduce Fe^{3+}, then release it from the ferrichrome under iron restriction conditions. Furthermore, a gene belonging to a *feoB* superfamily protein was slightly up-regulated in our study (1.43-fold change). The function of this protein, located in the cytoplasmic membrane, is Fe^{2+} uptake, usually under anaerobic conditions, where the stability of this ion is higher (Andrews et al., 2003).

Transcripts of genes encoding the cytosolic proteins NufA and SufB were also found in higher proportions only at 1 h of 100 µM of uranyl exposure, with fold changes

ranging between 1.62 and 1.66. These genes are induced under oxidative stress to help form [Fe-S] clusters and act as chaperones to repair damaged [Fe-S] proteins as well. SufB is part of the SufABC complex, which is regulated by the Fur protein, which controls the transcription of many genes, including those involved in divalent metal ion uptake (Andrews et al., 2003; Troxell and Hassan, 2013). In presence of Fe^{2+}, the Fur-Fe^{2+} complex binds to DNA to prevent transcription of Fe^{3+}, and the same process has been observed for Mg^{2+} or Co^{2+}. According to the results obtained here, *fur* gene was down-regulated (-1.26- and -1.98-fold changes under 100 and 250 μM, respectively). Orellana et al. (2014) reported, in contrast, that Fur protein was more abundant under U exposure in *G. Sulfurreducens*.

Although these genes were not detected at 52 h of incubation, a ferric enterobactin receptor was up-regulated (1.68-fold) through the same mechanism as described for Fiu and CirA to obtain the enterobactin siderophore.

Gallois et al. (2018) expounded an induction of proteins involved in the iron metabolism of the proteome of *M. oleivorans* A9 strain when exposed to 10 μM of uranyl nitrate at pH 5. This bacteria demonstrated its ability to form intracellular U(VI) phosphate accumulations when exposed to 50 μM of uranyl nitrate; U tended to be uptaken via proteins involved in the iron transport (Gallois et al., 2018). As some siderophores showed high affinity to U, the above authors proposed that iron uptake systems could influence the intracellular accumulation of U, as put forth in studies demonstrating the ability of this strain to form intracellular accumulations containing U (Theodorakopoulos et al., 2015). The microscopic analyses undertaken here showed that BII-R7 is not able to bioaccumulate U, yet the variation in the location of the minerals could be due to the influence of the pH, as previously suggested in this study. Still, all the mentioned genes were induced under iron-starvation conditions. Their slight up-regulation might be explained by the lack of Fe sources in the used culture medium, but also as an indirect effect of U exposure. The increase in the P_i induced by the metal would lead to the formation of Fe-P complexes, thereby reducing the availability of Fe for the cells.

4. Conclusions

This study describes the response of the novel bacterial strain *Stenotrophomonas bentonitica* BII-R7 in the presence of U. U removal experiments demonstrate its effectiveness in eliminating 98% of the U present in the medium after 26 h of incubation

at 100 μM of U; and 96% when exposed to 250 μM. Analysis of gene expression during U exposure revealed a high up-regulation of genes involved in cell wall biosynthesis, transport of toxic compounds, and acid and alkaline phosphatases. Cell wall proteins such as CreD and OmpA —crucial for maintaining membrane integrity— may block the entrance of U inside the cells when up-regulated. According to microscopic observations, soluble uranyl ions would bind to functional groups of the cell wall of *S. bentonitica*, where they precipitate to form U-phosphate minerals due to the phosphatase activity of PAP2 or ALP-like phosphatases. Meanwhile, transport systems (e.g. RND transporters) would prevent U accumulation inside the cells by means of active efflux of the metal. Altogether, the results of this work provide quality information about the behaviour of this bacterium at the molecular level, which is of high relevance for understanding how bacteria cope with radionuclides, and for designing effective bioremediation strategies.

5. Acknowledgements

This work was supported by the grants FPU 15/04284 ("*Formación de Profesorado Universitario*") and EST 17/00739 ("*Ayudas a la movilidad para estancias breves y traslados temporales*") obtained by the first author, from the Spanish Ministry (*Ministerio de Educación, Cultura y Deporte*), and from the European projects MIND-661880 and CGL2014-59616-R. Alexander Link and Ramiro Vílchez-Vargas are supported by the grants from the European Regional Development Fund of the European Commission. The authors are grateful to Concepción Hernández-Castillo and María del Mar Abad Ortega for their assistance at Microscopy services (*Centro de Instrumentación Científica*, University of Granada), to Maren Scharfe for technical support at sequencing services (Genome Analytics, Helmholtz Centre for Infectious Diseases) and to Jean Sanders for English revision of the manuscript.

6. Supplementary material

Figure S1. Phylogenetic tree based on amino-acid sequence similarities of *S. bentonitica* PAP2 phosphatase with other bacteria.

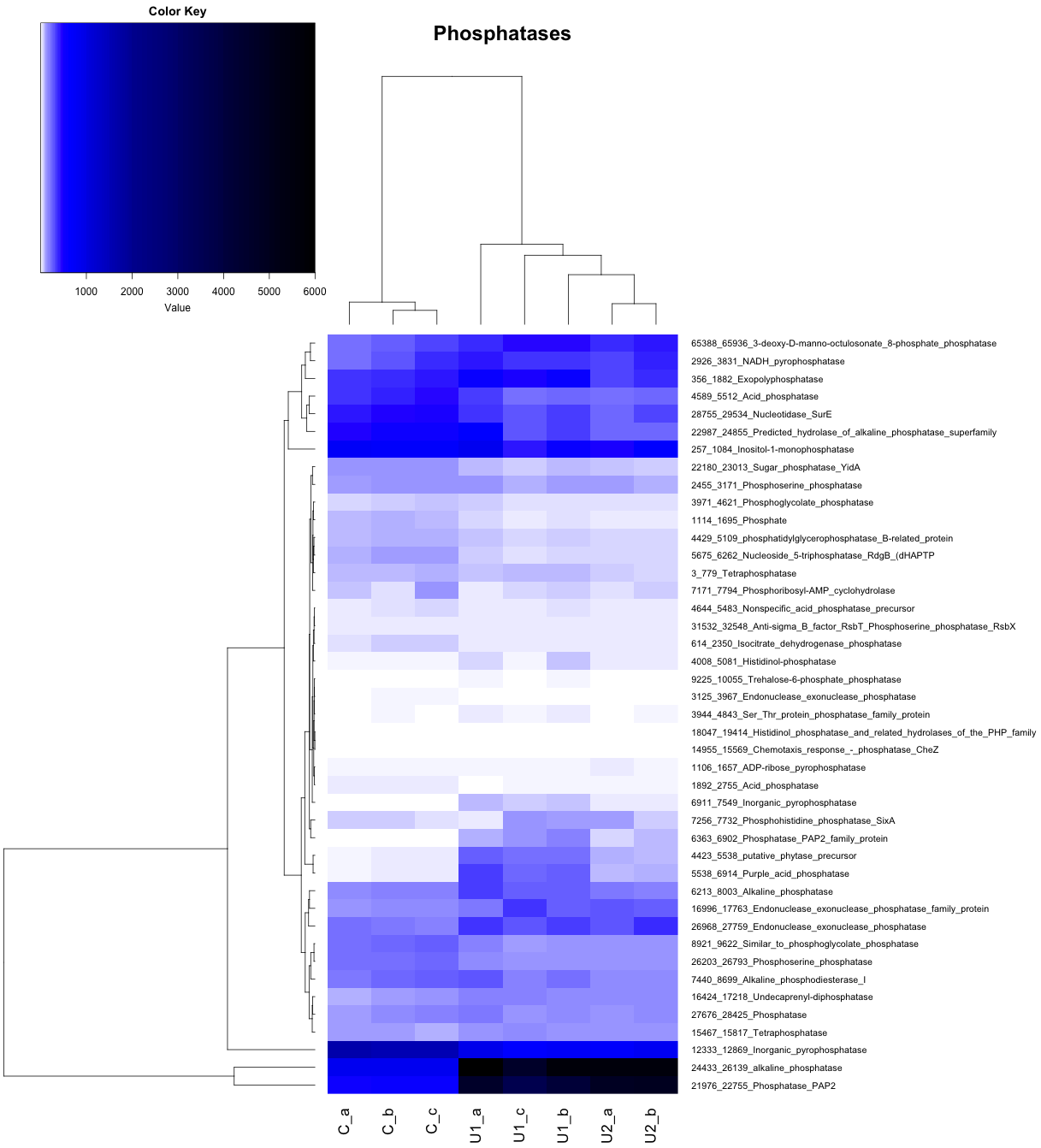

Figure S2. Heatmap of differential expression of genes with phosphatase activity in *S. bentonitica*, in presence (U1, U2) and absence (C) of uranium. Transcripts shown correspond to lag phase (1 h of incubation).

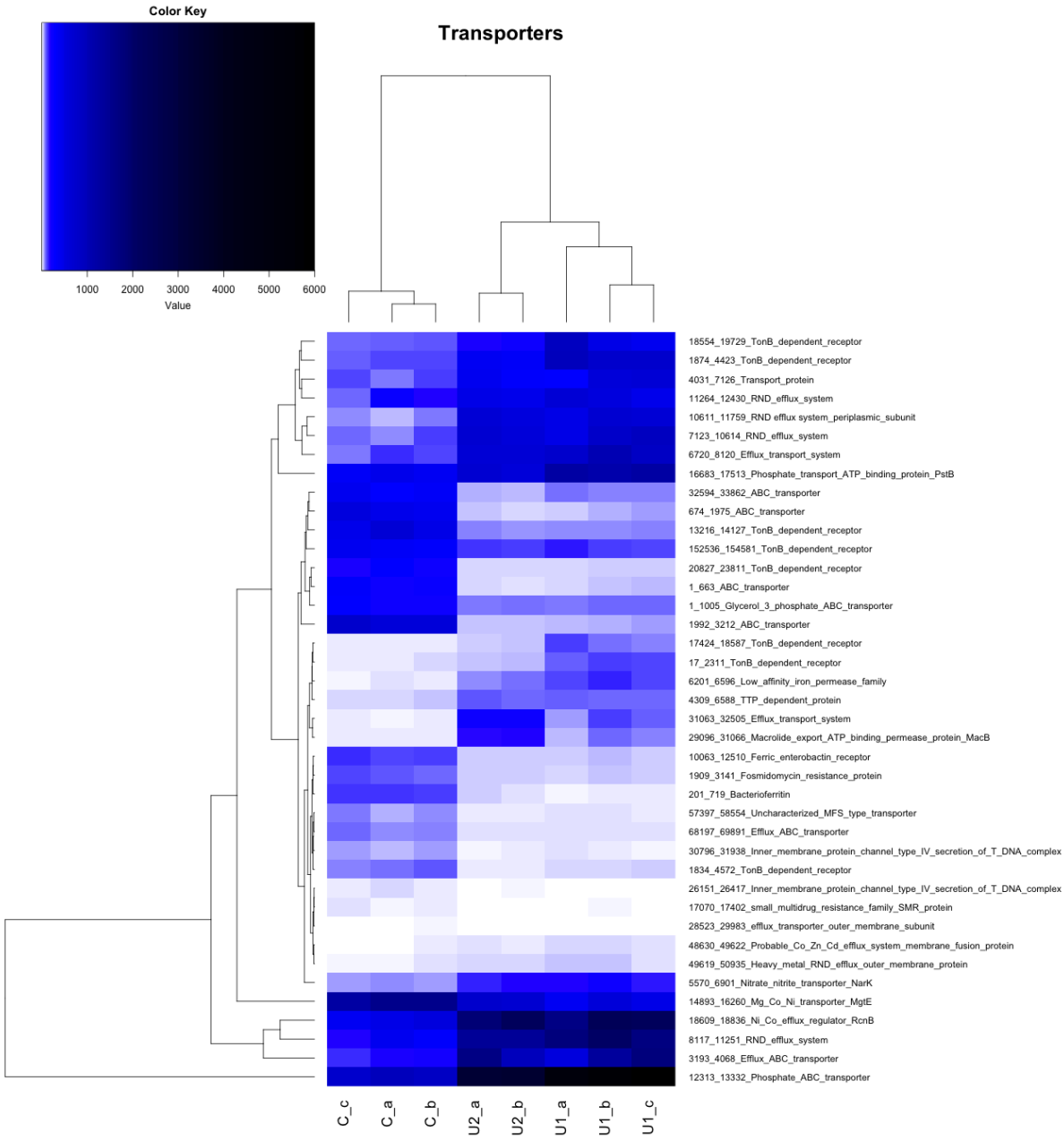

Figure S3. Heatmap of different transporter expression during time 1 in presence of 100 and 250 μM of U (U1 and U2, respectively).

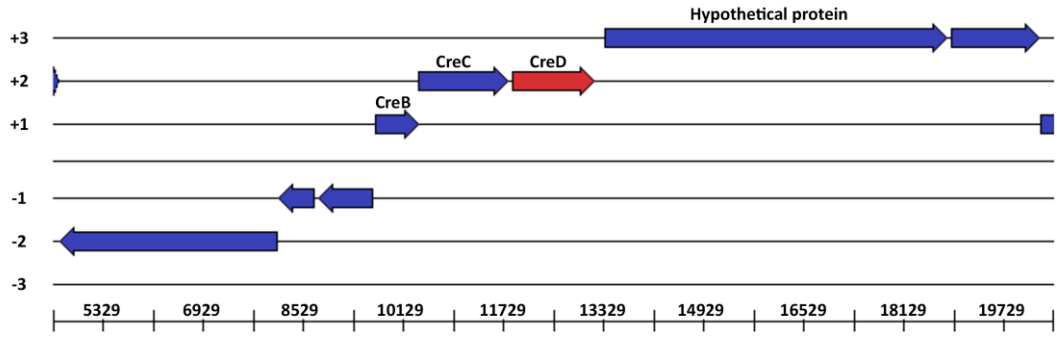

Figure S4. Genomic organization of the *creD* locus in *S. bentonitica.*

Table S1. Nomenclature of transcripts represented in Fig. 6.

1074035788_MKCZ01000083.1_11870_13189 Inner_membrane_protein_CreD	T1
1074037323_MKCZ01000026.1_5246_6382 Glycosyltransferase	T2
1074035103_MKCZ01000142.1_651_1238 hypothetical_protein	T3
1074035103_MKCZ01000142.1_1251_2138 hypothetical_protein	T4
1074035492_MKCZ01000101.1_10611_11759 Probable_Co/Zn/Cd_efflux_system_membrane_fusion_protein	T5
1074035103_MKCZ01000142.1_2165_3196 hypothetical_protein	T6
1074036975_MKCZ01000036.1_21976_22755 hypothetical_protein	T7
1074035492_MKCZ01000101.1_7123_10614 RND_efflux_system	T8
1074035383_MKCZ01000110.1_7925_8338 hypothetical_protein	T9
1074035543_MKCZ01000097.1_6720_8120 Efflux_transport_system	T10
1074035103_MKCZ01000142.1_3193_4068 Efflux_ABC_transporter	T11
1074036777_MKCZ01000042.1_24433_26139 Putative_inner_membrane_protein	T12
1074038434_MKCZ01000003.1_1874_4423 TonB-dependent_receptor	T13
1074035103_MKCZ01000142.1_4065_4427 Transcriptional_regulator	T14
1074035103_MKCZ01000142.1_4430_4681 hypothetical_protein	T15
1074036714_MKCZ01000044.1_12313_13332 Phosphate_ABC_transporter	T16
1074035543_MKCZ01000097.1_8117_11251 RND_efflux_system	T17
1074036234_MKCZ01000061.1_18554_19729 TonB-dependent_receptor	T18
1074035295_MKCZ01000118.1_10071_10940 3-ketoacyl-CoA_thiolase_[fadN-fadA-fadE_operon]_(EC_2.3.1.16)	T19
1074038434_MKCZ01000003.1_11779_12474 Outer_membrane_porin	T20
1074036975_MKCZ01000036.1_5504_7027 Serine_protease_precursor_MucD/AlgY_associated_with_sigma_factor_RpoE	T21
1074037728_MKCZ01000016.1_52452_52748 3-ketoacyl-CoA_thiolase_[fadN-fadA-fadE_operon]_(EC_2.3.1.16)	T22
1074036276_MKCZ01000059.1_10220_10714 Peptidoglycan-associated_outer_membrane_lipoprotein	T23
1074037081_MKCZ01000033.1_18609_18836 hypothetical_protein	T24
1074035492_MKCZ01000101.1_4031_7126 Transport_protein	T25
1074038120_MKCZ01000008.1_13279_13803 RNA_polymerase_ECF-type_sigma_factor	T26
1074037081_MKCZ01000033.1_18351_18524 FIG01209995:_hypothetical_protein	T27
1074036807_MKCZ01000041.1_27075_27713 Outer_membrane_lipoprotein_carrier_protein_LolA	T28
1074036975_MKCZ01000036.1_20154_21866 Polymyxin_resistance_protein_ArnT	T29
1074036042_MKCZ01000069.1_2328_2798 hypothetical_protein	T30
1074037728_MKCZ01000016.1_50047_52419 3-hydroxyacyl-CoA_dehydrogenase_[fadN-fadA-fadE_operon]_(EC_1.1.1.35)_/_Enoyl-CoA_hydratase_[fadN-fadA-fadE_operon]_(EC_4.2.1.17)	T31

1074037512_MKCZ01000021.1_38195_39889 Aerotolerance_protein_BatD	T32
1074035801_MKCZ01000082.1_13345_15522 tail-specific_protease	T33
1074036777_MKCZ01000042.1_26241_27404 Response_regulator	T34
1074038268_MKCZ01000005.1_61698_62381 hypothetical_protein	T35
1074036975_MKCZ01000036.1_22791_24767 Dipeptidyl_carboxypeptidase	T36
1074036975_MKCZ01000036.1_7895_8515 RNA_polymerase_sigma_factor_RpoE	T37
1074036276_MKCZ01000059.1_6760_7584 hypothetical_protein	T38
1074036975_MKCZ01000036.1_7092_7898 Sigma_factor_RpoE_negative_regulatory_protein_RseA	T39
1074038268_MKCZ01000005.1_24701_25297 hypothetical_protein	T40
1074036777_MKCZ01000042.1_23716_24147 CBS_domain_protein	T41
1074036234_MKCZ01000061.1_117_989 Protease_HtpX	T42
1074035543_MKCZ01000097.1_13307_14683 ATP-dependent_hsl_protease_ATP-binding_subunit_HslU	T43
1074037512_MKCZ01000021.1_36441_38198 Aerotolerance_protein_BatB_/_Aerotolerance_protein_BatC	T44
1074038561_MKCZ01000002.1_125248_125826 TonB-like_protein	T45
1074035010_MKCZ01000156.1_3792_4682 hypothetical_protein	T46
1074038268_MKCZ01000005.1_60898_61695 hypothetical_protein	T47
1074035411_MKCZ01000107.1_1802_2146 hypothetical_protein	T48
1074037904_MKCZ01000012.1_41430_41654 UptF_protein	T49
1074036714_MKCZ01000044.1_17573_18277 Phosphate_transport_system_regulatory_protein_PhoU	T50
1074035892_MKCZ01000077.1_9915_13139 Proline_dehydrogenase_(EC_1.5.5.2)_/_Delta-1-pyrroline-5-carboxylate_dehydrogenase_(EC_1.2.1.88)	T51
1074037775_MKCZ01000015.1_14893_16260 Mg/Co/Ni_transporter_MgtE	T52
1074038007_MKCZ01000010.1_51283_52425 Type_IV_fimbrial_biogenesis_protein_PilW	T53
1074038356_MKCZ01000004.1_62703_65075 Ribonucleotide_reductase_of_class_Ia_(aerobic)	T54
1074035340_MKCZ01000114.1_3802_5289 Flagellar_regulatory_protein_FleQ	T55
1074035943_MKCZ01000074.1_20000_20353 twitching_motility_protein_PilG	T56
1074038007_MKCZ01000010.1_50283_50798 Type_IV_fimbrial_biogenesis_protein_FimT	T57
1074035943_MKCZ01000074.1_10510_16914 PilL_protein	T58
1074038063_MKCZ01000009.1_46787_49642 Serine_protease	T59
1074035503_MKCZ01000100.1_9872_10768 Phenylalanine-4-hydroxylase_(EC_1.14.16.1)	T60
1074035170_MKCZ01000132.1_3915_6974 OmpA-related_protein	T61
1074036622_MKCZ01000047.1_11188_13572 Ribonucleotide_reductase_of_class_Ia_(aerobic)	T62
1074037244_MKCZ01000028.1_10134_11267 Uncharacterized_protein_with_LysM_domain	T63

1074036181_MKCZ01000063.1_3800_4504 hypothetical_protein	T64
1074037904_MKCZ01000012.1_43372_44499 Type_IV_pilus_assembly_ATPase_component_PilU	T65
1074038007_MKCZ01000010.1_45410_48622 Oar_protein	T66
1074035943_MKCZ01000074.1_17009_19045 pilus_biogenesis_protein	T67
1074036622_MKCZ01000047.1_13708_14727 Ribonucleotide_reductase_of_class_Ia_(aerobic)	T68
1074036357_MKCZ01000056.1_1339_2925 Cytochrome_d_ubiquinol_oxidase_subunit_I_(EC_1.10.3.-)	T69
1074038561_MKCZ01000002.1_69913_72105 hypothetical_protein	T70
1074037512_MKCZ01000021.1_146_1471 Xaa-Pro_dipeptidase_PepQ_(EC_3.4.13.9)	T71
1074037512_MKCZ01000021.1_27780_28838 Type_IV_pilus_biogenesis_protein_PilM	T72
1074037512_MKCZ01000021.1_30899_32878 Type_IV_pilus_biogenesis_protein_PilQ	T73
1074035084_MKCZ01000145.1_3703_5046 Histidine_kinase/response_regulator_hybrid_protein	T74
1074035480_MKCZ01000102.1_13216_14127 TonB-dependent_receptor	T75
1074034901_MKCZ01000183.1_2_1855 TonB-dependent_receptor	T76
1074035084_MKCZ01000145.1_674_1975 ABC_transporter	T77
1074035084_MKCZ01000145.1_1992_3212 ABC_transporter	T78

Table S1. Pearson correlation values of network in Fig. 6.

Var1	Var2	value
T19	T1	0,9054807
T22	T1	0,92420439
T31	T1	0,95540207
T9	T1	0,91955428
T12	T10	0,91876692
T15	T10	0,94429225
T16	T10	0,96183174
T17	T10	0,99495268
T23	T10	0,91454264
T24	T10	0,94800532
T25	T10	0,91044179
T27	T10	0,94630945
T28	T10	0,90749686
T32	T10	0,96308412
T33	T10	0,90051702
T34	T10	0,95970398
T37	T10	0,95441927
T39	T10	0,94349605
T40	T10	0,93989518
T44	T10	0,92304221
T45	T10	0,95826679
T47	T10	0,94995813
T52	T10	-0,9257474
T54	T10	-0,9690676
T55	T10	-0,9238799
T56	T10	-0,9047434
T57	T10	-0,9123273
T58	T10	-0,9205719
T60	T10	-0,936266
T61	T10	-0,9386127
T62	T10	-0,9267045
T63	T10	-0,9320811
T65	T10	-0,9036975
T67	T10	-0,9212733
T70	T10	-0,9441704
T71	T10	-0,926288
T72	T10	-0,9262171
T73	T10	-0,9268736
T75	T10	-0,912814
T76	T10	-0,9047175
T77	T10	-0,9315755
T78	T10	-0,929396
T14	T11	0,97623939
T15	T11	0,90670127
T20	T11	0,98451457
T21	T11	0,94049488
T23	T11	0,90966459
T25	T11	0,92809602
T28	T11	0,91407215
T30	T11	0,96883379
T33	T11	0,93789213
T35	T11	0,96993332
T38	T11	0,97996975
T39	T11	0,90963435
T40	T11	0,90562353
T41	T11	0,92758877
T42	T11	0,92114421
T46	T11	0,97193437
T49	T11	0,96705385
T15	T12	0,90131188
T17	T12	0,94567303
T21	T12	0,90185099
T24	T12	0,9189019
T27	T12	0,93993663
T29	T12	0,96877185
T32	T12	0,95688954
T33	T12	0,90653122
T34	T12	0,97787153
T36	T12	0,93419457
T37	T12	0,97941605
T39	T12	0,94461059
T44	T12	0,9383221
T45	T12	0,93837891
T47	T12	0,93211162
T48	T12	0,97892047
T51	T12	-0,9552769
T52	T12	-0,9437017
T53	T12	-0,9754051
T54	T12	-0,9390029
T55	T12	-0,9829781
T56	T12	-0,9624995
T57	T12	-0,968258
T58	T12	-0,9466594
T59	T12	-0,9869466
T60	T12	-0,974102
T61	T12	-0,9665347
T62	T12	-0,962493
T63	T12	-0,9504499
T64	T12	-0,9946218
T65	T12	-0,962995
T67	T12	-0,9716699
T68	T12	-0,9543644
T70	T12	-0,9505744
T71	T12	-0,972169
T72	T12	-0,9830789
T73	T12	-0,9836489
T74	T12	-0,9332524
T75	T12	-0,9635877
T76	T12	-0,958996
T77	T12	-0,9807894
T78	T12	-0,9674106
T16	T13	0,93946468
T18	T13	0,94590951
T32	T13	0,9328538
T44	T13	0,95038604
T50	T13	0,99081622
T54	T13	-0,9117828
T15	T14	0,97098598
T19	T14	0,91675009
T20	T14	0,96619257
T21	T14	0,97772373
T23	T14	0,96368717
T24	T14	0,94069527
T25	T14	0,9233041
T28	T14	0,92731026
T30	T14	0,96837143
T33	T14	0,97318133
T35	T14	0,97799806
T36	T14	0,95227136
T38	T14	0,97258151
T39	T14	0,96317833
T40	T14	0,94068951

T41	T14	0,91243885
T42	T14	0,96694529
T46	T14	0,97784791
T47	T14	0,92718011
T49	T14	0,96962025
T56	T14	-0,9150707
T57	T14	-0,9211053
T63	T14	-0,9340671
T67	T14	-0,914049
T70	T14	-0,9212937
T72	T14	-0,9070928
T17	T15	0,93592419
T20	T15	0,92318909
T21	T15	0,9666902
T23	T15	0,99100106
T24	T15	0,99341565
T25	T15	0,91996852
T27	T15	0,97101711
T28	T15	0,94416281
T33	T15	0,96637091
T34	T15	0,93588943
T35	T15	0,9470283
T36	T15	0,94303621
T37	T15	0,96183384
T38	T15	0,91303429
T39	T15	0,97572478
T40	T15	0,96949097
T42	T15	0,980918
T46	T15	0,95968279
T47	T15	0,97066052
T49	T15	0,93407964
T53	T15	-0,9223571
T54	T15	-0,913224
T55	T15	-0,918056
T56	T15	-0,9438963
T57	T15	-0,9532419
T58	T15	-0,9376946
T59	T15	-0,9046448
T60	T15	-0,9381529
T61	T15	-0,9511795
T62	T15	-0,9300273
T63	T15	-0,9606121
T65	T15	-0,9043625

T67	T15	-0,9490385
T68	T15	-0,9014481
T70	T15	-0,9631212
T71	T15	-0,9343354
T72	T15	-0,9499566
T73	T15	-0,9404668
T75	T15	-0,9292986
T76	T15	-0,9176226
T77	T15	-0,9438084
T78	T15	-0,9398538
T17	T16	0,95498435
T25	T16	0,9088247
T28	T16	0,91967978
T32	T16	0,94459533
T34	T16	0,90776218
T40	T16	0,93075491
T44	T16	0,91440682
T47	T16	0,92509996
T50	T16	0,9583584
T52	T16	-0,9242053
T54	T16	-0,9613135
T23	T17	0,90576958
T24	T17	0,94446454
T27	T17	0,94962652
T29	T17	0,92271838
T32	T17	0,97553597
T33	T17	0,90522051
T34	T17	0,97318333
T37	T17	0,96906311
T39	T17	0,94931129
T40	T17	0,93036092
T44	T17	0,9431779
T45	T17	0,96809659
T47	T17	0,95348381
T52	T17	-0,9368107
T53	T17	-0,9160609
T54	T17	-0,9810383
T55	T17	-0,9522177
T56	T17	-0,928941
T57	T17	-0,9325774
T58	T17	-0,9441376
T59	T17	-0,9288321
T60	T17	-0,9577541

T61	T17	-0,9557654
T62	T17	-0,9357109
T63	T17	-0,9496671
T64	T17	-0,922445
T65	T17	-0,9363377
T67	T17	-0,9440736
T70	T17	-0,9559422
T71	T17	-0,9518793
T72	T17	-0,9462857
T73	T17	-0,9510918
T74	T17	-0,9241747
T75	T17	-0,9216992
T76	T17	-0,9147332
T77	T17	-0,9538853
T78	T17	-0,9534983
T26	T18	0,98053664
T50	T18	0,90950217
T21	T19	0,94013214
T22	T19	0,99679589
T30	T19	0,90386807
T31	T19	0,9780075
T33	T19	0,92460755
T35	T19	0,92986734
T36	T19	0,94226222
T38	T19	0,94592453
T42	T19	0,91038935
T43	T19	0,94541343
T57	T19	-0,9026383
T10	T2	0,98124798
T13	T2	0,9029546
T16	T2	0,96149436
T17	T2	0,97132173
T24	T2	0,90337896
T27	T2	0,91819288
T32	T2	0,95218928
T34	T2	0,90748848
T37	T2	0,90931369
T44	T2	0,93342051
T45	T2	0,95533059
T47	T2	0,90258027
T50	T2	0,91678005
T52	T2	-0,9083949
T54	T2	-0,9466148

T21	T20	0,95293282
T23	T20	0,94133725
T25	T20	0,94897986
T28	T20	0,96554369
T30	T20	0,91888854
T33	T20	0,95563921
T35	T20	0,98480185
T36	T20	0,90144853
T38	T20	0,97852194
T39	T20	0,9246562
T40	T20	0,95241269
T41	T20	0,95282221
T42	T20	0,95239343
T46	T20	0,98790609
T47	T20	0,91498666
T49	T20	0,95778144
T22	T21	0,92227543
T23	T21	0,96857665
T24	T21	0,95319149
T27	T21	0,92239834
T28	T21	0,93696797
T30	T21	0,91366117
T33	T21	0,9987776
T34	T21	0,93898824
T35	T21	0,97492762
T36	T21	0,98801413
T37	T21	0,94489185
T38	T21	0,96759193
T39	T21	0,98740015
T40	T21	0,95820145
T42	T21	0,98461905
T46	T21	0,96365713
T47	T21	0,96672342
T49	T21	0,90997616
T53	T21	-0,9492769
T55	T21	-0,9274286
T56	T21	-0,9674888
T57	T21	-0,9735018
T58	T21	-0,9362944
T59	T21	-0,9262877
T60	T21	-0,9417914
T61	T21	-0,9477109
T62	T21	-0,9227953
T63	T21	-0,9686097
T65	T21	-0,9204443
T67	T21	-0,96024
T68	T21	-0,9136327
T70	T21	-0,9534318
T71	T21	-0,9372708
T72	T21	-0,9594063
T73	T21	-0,9504747
T75	T21	-0,9372446
T76	T21	-0,9261935
T77	T21	-0,949719
T78	T21	-0,9445438
T31	T22	0,98679249
T33	T22	0,9052993
T35	T22	0,90275215
T36	T22	0,93323603
T38	T22	0,91972682
T43	T22	0,93466692
T24	T23	0,98878742
T25	T23	0,91687697
T27	T23	0,96495311
T28	T23	0,96504667
T33	T23	0,96865428
T34	T23	0,90759184
T35	T23	0,96758811
T36	T23	0,93329397
T37	T23	0,94717706
T38	T23	0,93030456
T39	T23	0,96294662
T40	T23	0,98057401
T41	T23	0,91868312
T42	T23	0,99406483
T46	T23	0,96550949
T47	T23	0,97464449
T49	T23	0,93815245
T53	T23	-0,9132944
T55	T23	-0,9055503
T56	T23	-0,9371985
T57	T23	-0,9477745
T58	T23	-0,9247265
T60	T23	-0,9294775
T61	T23	-0,940184
T62	T23	-0,9233311
T63	T23	-0,9500088
T67	T23	-0,9351984
T70	T23	-0,9485867
T71	T23	-0,920414
T72	T23	-0,9365529
T73	T23	-0,9258315
T75	T23	-0,9163104
T76	T23	-0,9037115
T77	T23	-0,9300459
T78	T23	-0,9263356
T27	T24	0,99122233
T28	T24	0,93938022
T33	T24	0,95464423
T34	T24	0,9390461
T35	T24	0,92498458
T36	T24	0,93201739
T37	T24	0,97664857
T39	T24	0,96804075
T40	T24	0,96876956
T42	T24	0,9772388
T46	T24	0,93518773
T47	T24	0,979365
T51	T24	-0,9026793
T53	T24	-0,9344759
T54	T24	-0,9332044
T55	T24	-0,9365796
T56	T24	-0,9511539
T57	T24	-0,9603954
T58	T24	-0,9447133
T59	T24	-0,9208056
T60	T24	-0,9523288
T61	T24	-0,9663747
T62	T24	-0,951057
T63	T24	-0,9617718
T65	T24	-0,914596
T67	T24	-0,9550564
T68	T24	-0,9187947
T70	T24	-0,9710439
T71	T24	-0,9496585
T72	T24	-0,9588238
T73	T24	-0,9526626
T74	T24	-0,9053602
T75	T24	-0,940398

T76	T24	-0,9312773
T77	T24	-0,9576936
T78	T24	-0,9519016
T28	T25	0,96260237
T35	T25	0,9070529
T40	T25	0,95050962
T41	T25	0,96902881
T42	T25	0,90426529
T46	T25	0,97095124
T47	T25	0,90245143
T49	T25	0,93385254
T28	T27	0,90838598
T29	T27	0,90367024
T32	T27	0,92061208
T33	T27	0,92576384
T34	T27	0,939409
T36	T27	0,91025661
T37	T27	0,98460491
T39	T27	0,94876879
T40	T27	0,9469847
T42	T27	0,95169586
T47	T27	0,97245433
T51	T27	-0,9170002
T52	T27	-0,9115103
T53	T27	-0,9409002
T54	T27	-0,9441171
T55	T27	-0,951066
T56	T27	-0,9481162
T57	T27	-0,9581557
T58	T27	-0,9435742
T59	T27	-0,9355976
T60	T27	-0,9608892
T61	T27	-0,9706338
T62	T27	-0,9651935
T63	T27	-0,9520269
T64	T27	-0,9177431
T65	T27	-0,9209881
T67	T27	-0,9540516
T68	T27	-0,9314565
T70	T27	-0,9662112
T71	T27	-0,9570942
T72	T27	-0,9625683
T73	T27	-0,958906

T74	T27	-0,9103999
T75	T27	-0,9461571
T76	T27	-0,9390024
T77	T27	-0,9640596
T78	T27	-0,9551724
T33	T28	0,94755934
T35	T28	0,95154231
T38	T28	0,91388681
T39	T28	0,93438441
T40	T28	0,99301315
T41	T28	0,95091485
T42	T28	0,96437245
T46	T28	0,97685847
T47	T28	0,96495475
T49	T28	0,91395697
T54	T28	-0,9062207
T63	T28	-0,9045976
T70	T28	-0,9056537
T32	T29	0,95801971
T34	T29	0,92607515
T37	T29	0,93481464
T44	T29	0,97501162
T45	T29	0,95083899
T48	T29	0,97968579
T51	T29	-0,9138778
T52	T29	-0,9283765
T53	T29	-0,909579
T54	T29	-0,924207
T55	T29	-0,943446
T59	T29	-0,9385416
T60	T29	-0,9265452
T61	T29	-0,9171489
T62	T29	-0,9286109
T64	T29	-0,974891
T65	T29	-0,9089836
T67	T29	-0,9022959
T68	T29	-0,9105951
T71	T29	-0,923652
T72	T29	-0,9202202
T73	T29	-0,9281078
T75	T29	-0,909631
T76	T29	-0,9100241
T77	T29	-0,9284771

T78	T29	-0,9128503
T11	T3	0,95610728
T20	T3	0,96008927
T25	T3	0,95614484
T28	T3	0,91203476
T35	T3	0,90416145
T38	T3	0,90096038
T4	T3	0,982231
T41	T3	0,95881827
T46	T3	0,94072943
T49	T3	0,93187085
T6	T3	0,94839912
T8	T3	0,9226504
T33	T30	0,90099987
T35	T30	0,92933896
T38	T30	0,95008478
T43	T30	0,90358288
T46	T30	0,91743098
T49	T30	0,95125716
T43	T31	0,94883108
T34	T32	0,97384735
T37	T32	0,95159143
T39	T32	0,92114685
T44	T32	0,98738134
T45	T32	0,96835395
T47	T32	0,93393775
T48	T32	0,93317917
T50	T32	0,91853802
T51	T32	-0,9368182
T52	T32	-0,97213
T53	T32	-0,9031809
T54	T32	-0,9790806
T55	T32	-0,9441239
T56	T32	-0,904927
T57	T32	-0,9137427
T59	T32	-0,9257698
T60	T32	-0,9403382
T61	T32	-0,9437356
T62	T32	-0,9578667
T63	T32	-0,9072914
T64	T32	-0,9508058
T65	T32	-0,9070585
T67	T32	-0,9146803

T68	T32	-0,9380423
T69	T32	-0,9250725
T70	T32	-0,9310159
T71	T32	-0,9314599
T72	T32	-0,9323135
T73	T32	-0,9375685
T75	T32	-0,9452927
T76	T32	-0,9452495
T77	T32	-0,9429209
T78	T32	-0,9281374
T34	T33	0,94722734
T35	T33	0,97155679
T36	T33	0,98469397
T37	T33	0,94960752
T38	T33	0,96177586
T39	T33	0,99059293
T40	T33	0,96734534
T42	T33	0,98424934
T46	T33	0,96717512
T47	T33	0,9748385
T49	T33	0,90410796
T51	T33	-0,9024087
T53	T33	-0,9497571
T54	T33	-0,9092936
T55	T33	-0,9340121
T56	T33	-0,9687819
T57	T33	-0,9750445
T58	T33	-0,9391024
T59	T33	-0,9297705
T60	T33	-0,9484772
T61	T33	-0,9526143
T62	T33	-0,9304451
T63	T33	-0,9712638
T65	T33	-0,9245099
T67	T33	-0,961711
T68	T33	-0,9191112
T70	T33	-0,9570285
T71	T33	-0,941479
T72	T33	-0,9618198
T73	T33	-0,9539924
T74	T33	-0,903784
T75	T33	-0,941955
T76	T33	-0,9311848

T77	T33	-0,9537819
T78	T33	-0,9487299
T36	T34	0,953134
T37	T34	0,97871837
T39	T34	0,97947105
T40	T34	0,92559349
T42	T34	0,91476189
T44	T34	0,93332622
T45	T34	0,94238235
T47	T34	0,96232373
T48	T34	0,93128832
T51	T34	-0,9538029
T52	T34	-0,9529941
T53	T34	-0,9571192
T54	T34	-0,9684551
T55	T34	-0,969997
T56	T34	-0,9633352
T57	T34	-0,9681325
T58	T34	-0,9441882
T59	T34	-0,9631748
T60	T34	-0,9681678
T61	T34	-0,9765173
T62	T34	-0,9661123
T63	T34	-0,9639905
T64	T34	-0,9626906
T65	T34	-0,9516159
T67	T34	-0,9685606
T68	T34	-0,9558572
T69	T34	-0,9116853
T70	T34	-0,9730731
T71	T34	-0,9688437
T72	T34	-0,9765916
T73	T34	-0,9784111
T74	T34	-0,9237455
T75	T34	-0,9719395
T76	T34	-0,9690152
T77	T34	-0,9802902
T78	T34	-0,9695379
T36	T35	0,9342162
T38	T35	0,99070718
T39	T35	0,93880662
T40	T35	0,95052938
T41	T35	0,92798584

T42	T35	0,97923114
T46	T35	0,97694456
T47	T35	0,92897066
T49	T35	0,9599022
T56	T35	-0,9029682
T57	T35	-0,9101805
T63	T35	-0,9136764
T37	T36	0,9483703
T38	T36	0,93552782
T39	T36	0,98246783
T40	T36	0,91687684
T42	T36	0,95631827
T43	T36	0,90015782
T46	T36	0,92064877
T47	T36	0,94635124
T51	T36	-0,9261915
T53	T36	-0,9669294
T55	T36	-0,9395936
T56	T36	-0,9744367
T57	T36	-0,9790163
T58	T36	-0,9341402
T59	T36	-0,9489587
T60	T36	-0,9433941
T61	T36	-0,9524668
T62	T36	-0,930041
T63	T36	-0,9644279
T64	T36	-0,9100632
T65	T36	-0,9336014
T66	T36	-0,9053264
T67	T36	-0,968255
T68	T36	-0,9341677
T70	T36	-0,9535639
T71	T36	-0,9467211
T72	T36	-0,9704501
T73	T36	-0,9634387
T74	T36	-0,904876
T75	T36	-0,953231
T76	T36	-0,9458358
T77	T36	-0,9611535
T78	T36	-0,9508805
T39	T37	0,97512344
T40	T37	0,94137211
T42	T37	0,94498218

T44	T37	0,91538877
T45	T37	0,92219776
T47	T37	0,97904782
T48	T37	0,94125892
T51	T37	-0,939859
T52	T37	-0,9393946
T53	T37	-0,9786994
T54	T37	-0,9658325
T55	T37	-0,9872964
T56	T37	-0,9817372
T57	T37	-0,9867562
T58	T37	-0,9736793
T59	T37	-0,9786407
T60	T37	-0,9893132
T61	T37	-0,9906598
T62	T37	-0,9742854
T63	T37	-0,9814191
T64	T37	-0,9584393
T65	T37	-0,9679777
T67	T37	-0,9871282
T68	T37	-0,9499471
T70	T37	-0,9833938
T71	T37	-0,988003
T72	T37	-0,9919138
T73	T37	-0,9923533
T74	T37	-0,9515105
T75	T37	-0,9656674
T76	T37	-0,9590649
T77	T37	-0,9934755
T78	T37	-0,9868549
T39	T38	0,92298847
T40	T38	0,91199187
T42	T38	0,95160406
T43	T38	0,92807725
T46	T38	0,95933703
T49	T38	0,94466068
T40	T39	0,96442412
T42	T39	0,97107123
T46	T39	0,95301653
T47	T39	0,98134614
T51	T39	-0,9279545
T52	T39	-0,9191244
T53	T39	-0,9616878
T54	T39	-0,9430362
T55	T39	-0,9574169
T56	T39	-0,9773615
T57	T39	-0,9828114
T58	T39	-0,9565552
T59	T39	-0,951079
T60	T39	-0,9669132
T61	T39	-0,974077
T62	T39	-0,9523587
T63	T39	-0,9828914
T64	T39	-0,9157505
T65	T39	-0,9467312
T67	T39	-0,9773965
T68	T39	-0,9385008
T70	T39	-0,9783103
T71	T39	-0,9643407
T72	T39	-0,9790545
T73	T39	-0,9746867
T74	T39	-0,9252214
T75	T39	-0,9615501
T76	T39	-0,9531008
T77	T39	-0,975396
T78	T39	-0,9694904
T11	T4	0,98343755
T14	T4	0,92305897
T20	T4	0,96617694
T25	T4	0,91878216
T30	T4	0,929529
T35	T4	0,92422758
T38	T4	0,94192096
T41	T4	0,91920961
T46	T4	0,93907199
T49	T4	0,93436015
T6	T4	0,98825618
T8	T4	0,91626931
T41	T40	0,92478655
T42	T40	0,97906295
T46	T40	0,97461997
T47	T40	0,98783868
T49	T40	0,90680345
T52	T40	-0,9098926
T54	T40	-0,9375879
T55	T40	-0,9094326
T56	T40	-0,9257331
T57	T40	-0,938051
T58	T40	-0,9119999
T60	T40	-0,9342625
T61	T40	-0,9373864
T62	T40	-0,9343801
T63	T40	-0,9419939
T67	T40	-0,9223448
T68	T40	-0,9014387
T70	T40	-0,9414851
T71	T40	-0,9138247
T72	T40	-0,9284128
T73	T40	-0,9200988
T75	T40	-0,9225473
T76	T40	-0,9108617
T77	T40	-0,9255892
T78	T40	-0,9207411
T42	T41	0,90297395
T46	T41	0,95672593
T49	T41	0,96564033
T46	T42	0,96999404
T47	T42	0,97760744
T49	T42	0,92648613
T53	T42	-0,9264944
T55	T42	-0,9110901
T56	T42	-0,9477141
T57	T42	-0,9589941
T58	T42	-0,9199552
T59	T42	-0,9011087
T60	T42	-0,9324011
T61	T42	-0,9434089
T62	T42	-0,932899
T63	T42	-0,9516145
T67	T42	-0,9402078
T68	T42	-0,9124143
T70	T42	-0,9483304
T71	T42	-0,9225906
T72	T42	-0,9444735
T73	T42	-0,9326898
T75	T42	-0,9328004
T76	T42	-0,92147
T77	T42	-0,9361684
T78	T42	-0,9283973

T45	T44	0,96036662
T48	T44	0,94021468
T50	T44	0,92284517
T51	T44	-0,9084027
T52	T44	-0,9585843
T54	T44	-0,951938
T55	T44	-0,9191189
T59	T44	-0,900989
T60	T44	-0,9092077
T61	T44	-0,9019972
T62	T44	-0,9285069
T64	T44	-0,9415726
T68	T44	-0,9071041
T73	T44	-0,9007184
T75	T44	-0,9065301
T76	T44	-0,9077965
T77	T44	-0,905072
T52	T45	-0,9083434
T54	T45	-0,9317003
T55	T45	-0,9055804
T60	T45	-0,9001345
T61	T45	-0,9000675
T64	T45	-0,9366384
T73	T45	-0,9015063
T77	T45	-0,9037119
T47	T46	0,94544368
T49	T46	0,9604137
T63	T46	-0,9071025
T70	T46	-0,9049184
T51	T47	-0,925875
T52	T47	-0,9436973
T53	T47	-0,9499468
T54	T47	-0,9652153
T55	T47	-0,9594531
T56	T47	-0,9656466
T57	T47	-0,9752146
T58	T47	-0,9476392
T59	T47	-0,9424036
T60	T47	-0,9729091
T61	T47	-0,9756727
T62	T47	-0,9712396
T63	T47	-0,9700771
T64	T47	-0,9021887
T65	T47	-0,9315061
T67	T47	-0,9629095
T68	T47	-0,9447305
T70	T47	-0,9716115
T71	T47	-0,9599264
T72	T47	-0,9703949
T73	T47	-0,9663674
T74	T47	-0,9145968
T75	T47	-0,9604354
T76	T47	-0,9520312
T77	T47	-0,9703929
T78	T47	-0,9627681
T51	T48	-0,9344328
T52	T48	-0,9260914
T53	T48	-0,9508021
T54	T48	-0,9113924
T55	T48	-0,9632447
T56	T48	-0,9268331
T57	T48	-0,9304867
T58	T48	-0,9019176
T59	T48	-0,9690259
T60	T48	-0,943056
T61	T48	-0,9344616
T62	T48	-0,9399269
T64	T48	-0,9816739
T65	T48	-0,9330791
T67	T48	-0,9297467
T68	T48	-0,9352831
T70	T48	-0,9036121
T71	T48	-0,9438466
T72	T48	-0,9453658
T73	T48	-0,9525082
T74	T48	-0,902561
T75	T48	-0,930978
T76	T48	-0,9319069
T77	T48	-0,950739
T78	T48	-0,9338008
T10	T5	0,94409465
T11	T5	0,9145948
T12	T5	0,9364047
T14	T5	0,97180347
T15	T5	0,98191977
T17	T5	0,94401059
T20	T5	0,91811205
T21	T5	0,98063216
T23	T5	0,96143415
T24	T5	0,96889486
T25	T5	0,90408968
T27	T5	0,94586148
T28	T5	0,92139411
T30	T5	0,90376112
T32	T5	0,90970046
T33	T5	0,98140851
T34	T5	0,97325675
T35	T5	0,93373331
T36	T5	0,97759376
T37	T5	0,96656473
T38	T5	0,91808194
T39	T5	0,99522652
T40	T5	0,95358118
T42	T5	0,96558797
T46	T5	0,95467428
T47	T5	0,96756536
T51	T5	-0,9265658
T52	T5	-0,9033553
T53	T5	-0,944828
T54	T5	-0,9233434
T55	T5	-0,9372645
T56	T5	-0,9607046
T57	T5	-0,968982
T58	T5	-0,9405076
T59	T5	-0,933131
T60	T5	-0,9493613
T61	T5	-0,9609519
T62	T5	-0,9439438
T63	T5	-0,9696078
T64	T5	-0,9108828
T65	T5	-0,9264629
T67	T5	-0,9648035
T68	T5	-0,9328557
T7	T5	0,93849947
T70	T5	-0,9701479
T71	T5	-0,9473442
T72	T5	-0,9687969
T73	T5	-0,9604354
T74	T5	-0,9023979

T75	T5	-0,9583252
T76	T5	-0,9492102
T77	T5	-0,9613684
T78	T5	-0,9527543
T8	T5	0,97122358
T54	T50	-0,904366
T52	T51	0,95365775
T53	T51	0,91949527
T54	T51	0,90243534
T55	T51	0,91866216
T56	T51	0,90948898
T57	T51	0,93075643
T59	T51	0,92468513
T60	T51	0,91723489
T61	T51	0,93315789
T62	T51	0,98421624
T64	T51	0,9630555
T66	T51	0,96028423
T67	T51	0,90859223
T68	T51	0,99753367
T69	T51	0,92935196
T70	T51	0,91704715
T71	T51	0,90581181
T72	T51	0,94290476
T73	T51	0,93107518
T75	T51	0,99386409
T76	T51	0,99430905
T77	T51	0,93578369
T78	T51	0,90005763
T53	T52	0,90745688
T54	T52	0,94410317
T55	T52	0,93689868
T57	T52	0,92196733
T59	T52	0,92759151
T60	T52	0,94627087
T61	T52	0,91725017
T62	T52	0,97052152
T64	T52	0,94078853
T67	T52	0,90655628
T68	T52	0,95885474
T71	T52	0,90397279
T72	T52	0,93793815
T73	T52	0,92600144

T75	T52	0,96006972
T76	T52	0,94990256
T77	T52	0,92508459
T78	T52	0,90109152
T54	T53	0,92181439
T55	T53	0,99021782
T56	T53	0,99437158
T57	T53	0,99434989
T58	T53	0,97761659
T59	T53	0,99554373
T60	T53	0,98584111
T61	T53	0,97361827
T62	T53	0,94316391
T63	T53	0,98153537
T64	T53	0,95293074
T65	T53	0,98449439
T67	T53	0,99416468
T68	T53	0,93019036
T70	T53	0,96022123
T71	T53	0,98638792
T72	T53	0,99302705
T73	T53	0,9941947
T74	T53	0,96561661
T75	T53	0,9446389
T76	T53	0,93612365
T77	T53	0,98889946
T78	T53	0,98542262
T55	T54	0,95892474
T56	T54	0,93809281
T57	T54	0,93707143
T58	T54	0,9349061
T59	T54	0,93133313
T60	T54	0,95638848
T61	T54	0,97161192
T62	T54	0,94998812
T63	T54	0,94554037
T64	T54	0,91392532
T65	T54	0,93433647
T67	T54	0,93928494
T68	T54	0,916004
T69	T54	0,91211009
T70	T54	0,96516801
T71	T54	0,96125336

T72	T54	0,94122661
T73	T54	0,95489894
T74	T54	0,92456972
T75	T54	0,92939293
T76	T54	0,93053207
T77	T54	0,96312353
T78	T54	0,96112986
T56	T55	0,98639209
T57	T55	0,98620926
T58	T55	0,98155675
T59	T55	0,99540666
T60	T55	0,99541608
T61	T55	0,97972668
T62	T55	0,95282167
T63	T55	0,98044527
T64	T55	0,96087959
T65	T55	0,98920499
T67	T55	0,99018756
T68	T55	0,92969129
T70	T55	0,96429599
T71	T55	0,99200799
T72	T55	0,99017719
T73	T55	0,99539819
T74	T55	0,9733072
T75	T55	0,94355703
T76	T55	0,93588896
T77	T55	0,99189756
T78	T55	0,99034938
T57	T56	0,9964757
T58	T56	0,98451338
T59	T56	0,98475269
T60	T56	0,98381097
T61	T56	0,98480319
T62	T56	0,9413284
T63	T56	0,99351157
T64	T56	0,93234503
T65	T56	0,98443465
T67	T56	0,99670039
T68	T56	0,9235822
T70	T56	0,97867652
T71	T56	0,99212721
T72	T56	0,99000046
T73	T56	0,99485464

T74	T56	0,97189793
T75	T56	0,94222639
T76	T56	0,93580406
T77	T56	0,99295881
T78	T56	0,99362061
T58	T57	0,97717325
T59	T57	0,98631678
T60	T57	0,98893706
T61	T57	0,98212557
T62	T57	0,95882899
T63	T57	0,98956647
T64	T57	0,94245378
T65	T57	0,97527816
T67	T57	0,99526312
T68	T57	0,94368791
T70	T57	0,97374871
T71	T57	0,98522058
T72	T57	0,9964966
T73	T57	0,99425213
T74	T57	0,9557948
T75	T57	0,96020668
T76	T57	0,95087695
T77	T57	0,99139811
T78	T57	0,9863006
T59	T58	0,97329328
T60	T58	0,98249773
T61	T58	0,96584494
T62	T58	0,90326897
T63	T58	0,99315841
T64	T58	0,90915749
T65	T58	0,9926906
T67	T58	0,99100576
T70	T58	0,96239433
T71	T58	0,98646895
T72	T58	0,97507964
T73	T58	0,98237557
T74	T58	0,99229993
T77	T58	0,97696699
T78	T58	0,98935875
T60	T59	0,98934454
T61	T59	0,96805226
T62	T59	0,94622378
T63	T59	0,97262566
T64	T59	0,96963065
T65	T59	0,98621963
T67	T59	0,98896928
T68	T59	0,93224626
T70	T59	0,95032189
T71	T59	0,98389192
T72	T59	0,99143657
T73	T59	0,99285759
T74	T59	0,96410314
T75	T59	0,94467032
T76	T59	0,93563095
T77	T59	0,9863513
T78	T59	0,98150466
T11	T6	0,99326386
T14	T6	0,95032144
T20	T6	0,97119161
T21	T6	0,91629435
T30	T6	0,96048175
T33	T6	0,91257382
T35	T6	0,95229825
T38	T6	0,97573466
T43	T6	0,91590616
T46	T6	0,94453066
T49	T6	0,93913911
T8	T6	0,9200717
T61	T60	0,97388735
T62	T60	0,95677742
T63	T60	0,98392477
T64	T60	0,94937241
T65	T60	0,98187058
T67	T60	0,99000222
T68	T60	0,93017986
T70	T60	0,96014112
T71	T60	0,98385027
T72	T60	0,99279213
T73	T60	0,9911001
T74	T60	0,96452178
T75	T60	0,94670165
T76	T60	0,93385827
T77	T60	0,98608153
T78	T60	0,98394718
T62	T61	0,96649702
T63	T61	0,97946724
T64	T61	0,94182544
T65	T61	0,96360364
T67	T61	0,98106438
T68	T61	0,94565581
T70	T61	0,99606985
T71	T61	0,99215042
T72	T61	0,9797657
T73	T61	0,98966911
T74	T61	0,95209234
T75	T61	0,95979561
T76	T61	0,96118912
T77	T61	0,99590471
T78	T61	0,99133746
T63	T62	0,92790478
T64	T62	0,95647828
T65	T62	0,90383806
T66	T62	0,91537026
T67	T62	0,94065757
T68	T62	0,99182785
T69	T62	0,93060609
T70	T62	0,95154147
T71	T62	0,94326533
T72	T62	0,96626721
T73	T62	0,95871787
T75	T62	0,99324475
T76	T62	0,99066719
T77	T62	0,96429197
T78	T62	0,93913332
T64	T63	0,91413862
T65	T63	0,98462234
T67	T63	0,99538392
T68	T63	0,90045354
T70	T63	0,97947908
T71	T63	0,98829749
T72	T63	0,98437776
T73	T63	0,98856569
T74	T63	0,977528
T75	T63	0,9263806
T76	T63	0,91647999
T77	T63	0,98601325
T78	T63	0,99239486
T65	T64	0,9322457
T66	T64	0,91213244

T67	T64	0,94344455
T68	T64	0,95664772
T70	T64	0,92170085
T71	T64	0,94443417
T72	T64	0,96322545
T73	T64	0,96089173
T75	T64	0,96020332
T76	T64	0,95713106
T77	T64	0,95805142
T78	T64	0,93708701
T67	T65	0,9897325
T70	T65	0,95425701
T71	T65	0,98856475
T72	T65	0,97589553
T73	T65	0,98642326
T74	T65	0,99349942
T77	T65	0,97985481
T78	T65	0,98954084
T68	T66	0,95288534
T75	T66	0,94374975
T76	T66	0,94399512
T68	T67	0,9197806
T70	T67	0,97524565
T71	T67	0,99216823
T72	T67	0,99439582
T73	T67	0,99652146
T74	T67	0,97627471
T75	T67	0,94101329
T76	T67	0,93138555
T77	T67	0,99235781
T78	T67	0,9935951
T69	T68	0,93101616
T70	T68	0,92926246
T71	T68	0,91822136
T72	T68	0,95148786
T73	T68	0,94081866
T75	T68	0,99680142
T76	T68	0,99666311
T77	T68	0,94616466
T78	T68	0,91319727
T75	T69	0,92995411
T76	T69	0,9451998
T12	T7	0,98839602
T15	T7	0,90622088
T17	T7	0,90444868
T21	T7	0,92537013
T24	T7	0,92080642
T27	T7	0,93521114
T29	T7	0,93237286
T32	T7	0,9102171
T33	T7	0,92398312
T34	T7	0,95838337
T36	T7	0,95958759
T37	T7	0,97223551
T39	T7	0,94658023
T42	T7	0,90135414
T47	T7	0,92762941
T48	T7	0,96770724
T51	T7	-0,9520173
T52	T7	-0,9124575
T53	T7	-0,9883165
T54	T7	-0,9031822
T55	T7	-0,9758341
T56	T7	-0,9739933
T57	T7	-0,9794461
T58	T7	-0,945829
T59	T7	-0,9883867
T60	T7	-0,9674815
T61	T7	-0,9632002
T62	T7	-0,9544975
T63	T7	-0,9534363
T64	T7	-0,9805243
T65	T7	-0,9595585
T66	T7	-0,9276372
T67	T7	-0,9768999
T68	T7	-0,9539077
T70	T7	-0,9475643
T71	T7	-0,9693971
T72	T7	-0,9864168
T73	T7	-0,9836615
T74	T7	-0,9294312
T75	T7	-0,9624436
T76	T7	-0,9570386
T77	T7	-0,979473
T78	T7	-0,9650393
T9	T7	0,97964904
T71	T70	0,98527261
T72	T70	0,96946728
T73	T70	0,9804258
T74	T70	0,94652621
T75	T70	0,94851566
T76	T70	0,95066212
T77	T70	0,9881962
T78	T70	0,98650556
T72	T71	0,98403035
T73	T71	0,99587412
T74	T71	0,98122681
T75	T71	0,93580769
T76	T71	0,93333108
T77	T71	0,99678212
T78	T71	0,99940677
T73	T72	0,99560508
T74	T72	0,95238866
T75	T72	0,96723742
T76	T72	0,95682072
T77	T72	0,9915954
T78	T72	0,98377542
T74	T73	0,9696808
T75	T73	0,95675038
T76	T73	0,95107717
T77	T73	0,99847437
T78	T73	0,99522737
T77	T74	0,96454751
T78	T74	0,9831213
T76	T75	0,99750745
T77	T75	0,96085049
T78	T75	0,93291673
T77	T76	0,95836319
T78	T76	0,92949639
T78	T77	0,99579357
T10	T8	0,93680049
T11	T8	0,95507098
T14	T8	0,97426629
T15	T8	0,97182144
T16	T8	0,90692971
T17	T8	0,92092142
T20	T8	0,97245897
T21	T8	0,96452334
T23	T8	0,96770058

T24	T8	0,95233826
T25	T8	0,97568249
T27	T8	0,91315205
T28	T8	0,97681542
T30	T8	0,90187247
T33	T8	0,97061611
T34	T8	0,92677481
T35	T8	0,95917642
T36	T8	0,92811691
T37	T8	0,91791592
T38	T8	0,93750326
T39	T8	0,97050401
T40	T8	0,98241899
T41	T8	0,94045057
T42	T8	0,96709831
T46	T8	0,99340775
T47	T8	0,96258268
T49	T8	0,94467084
T54	T8	-0,9102339

T56	T8	-0,9091385
T57	T8	-0,9188053
T60	T8	-0,9022588
T61	T8	-0,9183946
T62	T8	-0,9020523
T63	T8	-0,932713
T67	T8	-0,9080415
T70	T8	-0,9355986
T72	T8	-0,909346
T73	T8	-0,9004719
T75	T8	-0,9076614
T77	T8	-0,9060489
T78	T8	-0,902554
T12	T9	0,95085866
T36	T9	0,92125626
T37	T9	0,91031281
T48	T9	0,95764048
T51	T9	-0,910731
T53	T9	-0,9610533

T55	T9	-0,9335529
T56	T9	-0,9338323
T57	T9	-0,9357358
T59	T9	-0,960023
T60	T9	-0,9141205
T61	T9	-0,9069638
T64	T9	-0,9503242
T65	T9	-0,9210523
T66	T9	-0,9270548
T67	T9	-0,9306405
T68	T9	-0,9105109
T71	T9	-0,9227814
T72	T9	-0,9399565
T73	T9	-0,9394837
T75	T9	-0,9107275
T76	T9	-0,9081729
T77	T9	-0,9321247
T78	T9	-0,9152197

Table S2 Genes that showed the most significative changes in their expression in the lag phase in presence of U, and their fold changes values

100 µM	Fold change
1074037323_MKCZ01000026.1_5246-6382 Glycosyltransferase	22,99
1074035492_MKCZ01000101.1_10611-11759 RND efflux system periplasmic subunit	9,77
1074035103_MKCZ01000142.1_2165-3196 ABC transporter permease subunit	8,40
1074035543_MKCZ01000097.1_6720-8120 Efflux transport system	8,30
1074035492_MKCZ01000101.1_7123-10614 RND efflux system Acr family	8,19
1074038434_MKCZ01000003.1_1874-4423 TonB-dependent receptor-Xanth-Caul	8,03
1074036975_MKCZ01000036.1_21976-22755 Phosphatase PAP2 family protein	7,34
1074035103_MKCZ01000142.1_3193-4068 ABC transporter ATP-binding protein CcmA	6,83
1074036714_MKCZ01000044.1_12313-13332 Phosphate ABC transporter PstS	6,61
1074036234_MKCZ01000061.1_18554-19729 TonB-dependent heme/hemoglobin receptor	6,54
1074036777_MKCZ01000042.1_24433-26139 Phosphoethanolamine transferase	6,50
1074038120_MKCZ01000008.1_13279-13803 RNA polymerase ECF-type sigma factor	6,14
1074035543_MKCZ01000097.1_8117 11251 RND efflux system SmeE	6,03
1074035103_MKCZ01000142.1_4065-4427 Transcriptional regulator	5,55
1074035492_MKCZ01000101.1_4031-7126 RND permease subunit AcrB	4,99
1074038434_MKCZ01000003.1_11779-12474 OmpA	4,80
1074036276_MKCZ01000059.1_10220-10714 Peptidoglycan-associated outer membrane lipoprotein	4,61
1074036975_MKCZ01000036.1_5504-7027 DegQ family periplasmic serine endoprotease	4,54
1074036807_MKCZ01000041.1_27075-27713 Outer membrane lipoprotein carrier protein LolA	4,50
1074037081_MKCZ01000033.1_18609-18836 Integral membrane protein	4,50
1074036975_MKCZ01000036.1_20154-21866 Polymyxin resistance protein ArnT	4,36
1074036777_MKCZ01000042.1_26241-27404 Response regulator	3,84
1074035295_MKCZ01000118.1_10071-10940 3-ketoacyl-CoA thiolase [fadN-fadA-fadE operon] (EC 2.3.1.16)	3,83

1074036714_MKCZ01000044.1_17573-18277 Phosphate transport system regulatory protein PhoU	3,82
1074037728_MKCZ01000016.1_52452-52748 3-ketoacyl-CoA thiolase [fadN-fadA-fadE operon] (EC 2.3.1.16)	3,66
1074035801_MKCZ01000082.1_13345-15522 tail-specific protease	3,64
1074038561_MKCZ01000002.1_125248-125826 TonB-like protein	3,64
1074036975_MKCZ01000036.1_7895-8515 RNA polymerase sigma factor RpoE	3,59
1074036975_MKCZ01000036.1_7092-7898 Sigma factor RpoE negative regulatory protein RseA	3,46
1074036975_MKCZ01000036.1_22791-24767 Dipeptidyl carboxypeptidase	3,37
1074036234_MKCZ01000061.1_117-989 Protease HtpX	3,32
1074035010_MKCZ01000156.1_3792-4682 Ligand-binding protein SH3	3,29
1074035411_MKCZ01000107.1_1802-2146 Lipid-A-disaccharide synthase	3,17
1074035185_MKCZ01000130.1_3-1616 Polyphosphate kinase (EC 2.7.4.1)	3,17
1074035543_MKCZ01000097.1_11264-12430 RND efflux system SmeD	3,16
1074036975_MKCZ01000036.1_18047-19333 Two-component system sensor histidine kinase	3,13
1074036714_MKCZ01000044.1_16683-17513 Phosphate transport ATP-binding protein PstB (TC 3.A.1.7.1)	3,11
1074038721_MKCZ01000001.1_123655-123933 Membrane protein	3,03
1074035411_MKCZ01000107.1_2146-2868 Dolichol-phosphate mannosyltransferase	3,01
1074035340_MKCZ01000114.1_3802-5289 Flagellar regulatory protein FleQ	-2,60
1074038063_MKCZ01000009.1_46787-49642 Serine protease	-2,62
1074035943_MKCZ01000074.1_10510-16914 PilL protein	-2,65
1074036357_MKCZ01000056.1_169-1323 Cytochrome d ubiquinol oxidase subunit II (EC 1.10.3.-)	-2,66
1074038561_MKCZ01000002.1_65805-66437 hypothetical protein	-2,72
1074037244_MKCZ01000028.1_10134-11267 Uncharacterized protein with LysM domain	-2,84
1074035170_MKCZ01000132.1_3915-6974 TonB-dependent receptor	-2,84
1074035503_MKCZ01000100.1_9872-10768 Phenylalanine-4-hydroxylase (EC 1.14.16.1)	-2,86
1074037904_MKCZ01000012.1_43372-44499 Type IV pilus assembly ATPase component PilU	-2,89
1074036181_MKCZ01000063.1_3800-4504 hypothetical protein	-2,91
1074037775_MKCZ01000015.1_14893-16260 Mg/Co/Ni transporter MgtE	-2,92
1074035943_MKCZ01000074.1_17009-19045 pilus biogenesis protein	-2,93
1074036622_MKCZ01000047.1_11188-13572 Ribonucleotide reductase of class Ia (aerobic)	-2,99

1074036622_MKCZ01000047.1_13708-14727 Ribonucleotide reductase of class Ia (aerobic)	-3,15
1074038356_MKCZ01000004.1_62703-65075 Ribonucleotide reductase of class Ia (aerobic)	-3,23
1074038561_MKCZ01000002.1_69913-72105 TonB-depenent receptor	-3,50
1074037512_MKCZ01000021.1_146-1471 Xaa-Pro dipeptidase PepQ (EC 3.4.13.9)	-4,12
1074037512_MKCZ01000021.1_27780-28838 Type IV pilus biogenesis protein PilM	-4,60
1074036357_MKCZ01000056.1_1339-2925 Cytochrome d ubiquinol oxidase subunit I (EC 1.10.3.-)	-4,70
1074037512_MKCZ01000021.1_30899-32878 Type IV pilus biogenesis protein PilQ	-4,98
1074035084_MKCZ01000145.1_3703-5046 Histidine kinase/response regulator hybrid protein	-5,49
1074035480_MKCZ01000102.1_13216-14127 TonB-dependent receptor BtuB	-7,79
1074034901_MKCZ01000183.1_2-1855 TonB-dependent receptor	-8,91
1074035084_MKCZ01000145.1_674-1975 ABC transporter FtsX-like permease	-10,70
1074035084_MKCZ01000145.1_1992-3212 ABC transporter FtsX-like permease	-13,28

250 µM	Fold change
1074035788_MKCZ01000083.1_11870-13189 Inner membrane protein CreD	21,11
1074037323_MKCZ01000026.1_5246-6382 Glycosyltransferase	12,97
1074035492_MKCZ01000101.1_10611-11759 RND efflux system periplasmic subunit	6,68
1074035103_MKCZ01000142.1_2165-3196 ABC transporter permease subunit	6,50
1074036975_MKCZ01000036.1_21976-22755 Phosphatase PAP2 family protein	5,78
1074035103_MKCZ01000142.1_3193-4068 Efflux ABC transporter CcmA	4,94
1074035492_MKCZ01000101.1_7123-10614 RND efflux system Acr family	4,81
1074036777_MKCZ01000042.1_24433-26139 Phosphethanolamine transferase	4,39
1074037728_MKCZ01000016.1_52452-52748 3-ketoacyl-CoA thiolase [fadN-fadA-fadE operon] (EC 2.3.1.16)	4,17
1074035295_MKCZ01000118.1_10071-10940 3-ketoacyl-CoA thiolase [fadN-fadA-fadE operon] (EC 2.3.1.16)	4,15
1074035103_MKCZ01000142.1_4065-4427 Transcriptional regulator	4,14
1074035543_MKCZ01000097.1_6720-8120 Efflux transport system outer membrane subunit TolC	4,01
1074037728_MKCZ01000016.1_50047-52419 3-hydroxyacyl-CoA dehydrogenase [fadN-fadA-fadE operon] (EC 1.1.1.35) / Enoyl-CoA hydratase [fadN-fadA-fadE operon] (EC 4.2.1.17)	3,65
1074036975_MKCZ01000036.1_5504-7027 Serine protease precursor MucD/AlgY associated with sigma factor RpoE	3,40
1074036276_MKCZ01000059.1_10220-10714 Peptidoglycan-associated outer membrane lipoprotein	3,18
1074038434_MKCZ01000003.1_11779-12474 OmpA	3,17
1074035543_MKCZ01000097.1_8117-11251 RND efflux system SmeE	3,10
1074037904_MKCZ01000012.1_13788-14843 dTDP-glucose 4	-2,51
1074035425_MKCZ01000106.1_3240-5609 Transcription accessory protein (S1 RNA-binding domain)	-2,52
1074037210_MKCZ01000029.1_7604-8083 FKBP-type peptidyl-prolyl cis-trans isomerase SlyD (EC 5.2.1.8)	-2,52
1074035618_MKCZ01000092.1_3914-4699 Succinate dehydrogenase iron-sulfur protein (EC 1.3.5.1)	-2,53
1074037585_MKCZ01000019.1_35826-37055 Acetylornithine aminotransferase (EC 2.6.1.11) @ N-succinyl-L	-2,54
1074036303_MKCZ01000058.1_8930-9820 3-hydroxyisobutyrate dehydrogenase (EC 1.1.1.31)	-2,54

1074037631_MKCZ01000018.1_18235-19356 Probable low-affinity inorganic phosphate transporter	-2,54
1074036303_MKCZ01000058.1_7758-8933 3-hydroxyisobutyryl-CoA hydrolase (EC 3.1.2.4)	-2,54
1074036839_MKCZ01000040.1_2235-3497 3-oxoacyl-[acyl-carrier-protein] synthase	-2,56
1074036412_MKCZ01000054.1_9835-10476 Cytochrome O ubiquinol oxidase subunit III (EC 1.10.3.-)	-2,58
1074035819_MKCZ01000081.1_5287-6561 Alanine transaminase (EC 2.6.1.2)	-2,60
1074036412_MKCZ01000054.1_10473-12476 Cytochrome O ubiquinol oxidase subunit I (EC 1.10.3.-)	-2,64
1074037549_MKCZ01000020.1_25246-26829 IMP cyclohydrolase (EC 3.5.4.10) / Phosphoribosylaminoimidazolecarboxamide formyltransferase (EC 2.1.2.3)	-2,66
1074035327_MKCZ01000115.1_3506-5812 Thymidine phosphorylase (EC 2.4.2.4)	-2,66
1074037631_MKCZ01000018.1_17595-18221 Phosphate transport regulator (distant homolog of PhoU)	-2,67
1074035618_MKCZ01000092.1_2054-3844 Succinate dehydrogenase flavoprotein subunit (EC 1.3.5.1)	-2,67
1074037687_MKCZ01000017.1_32570-34813 NADH-ubiquinone oxidoreductase chain G (EC 1.6.5.3)	-2,69
1074038169_MKCZ01000007.1_39381-41546 Sensory/regulatory protein rpfC (EC 2.7.3.-)	-2,72
1074036839_MKCZ01000040.1_3994-4737 3-oxoacyl-[acyl-carrier protein] reductase (EC 1.1.1.100)	-2,72
1074035590_MKCZ01000094.1_13836-15938 ATP-dependent helicase DinG/Rad3	-2,72
1074037210_MKCZ01000029.1_14715-16832 Metallopeptidase	-2,73
1074035618_MKCZ01000092.1_1017-1190 hypothetical protein	-2,73
1074035238_MKCZ01000124.1_8515-8658 hypothetical protein	-2,74
1074037585_MKCZ01000019.1_17730-20657 Iron siderophore receptor protein	-2,74
1074036016_MKCZ01000070.1_20106-20969 ATP synthase gamma chain (EC 3.6.3.14)	-2,76
1074036107_MKCZ01000066.1_16465-17550 Inner membrane protein YrbG	-2,76
1074036016_MKCZ01000070.1_16164-16958 ATP synthase F0 sector subunit a (EC 3.6.3.14)	-2,76

1074035943_MKCZ01000074.1_1293-2405 Aminomethyltransferase (glycine cleavage system T protein) (EC 2.1.2.10)	-2,77
1074035411_MKCZ01000107.1_4848-5645 Chromosome (plasmid) partitioning protein ParA	-2,77
1074036493_MKCZ01000051.1_21974-22549 hypothetical protein	-2,77
1074038561_MKCZ01000002.1_132652-133380 Histidine utilization repressor	-2,78
1074038561_MKCZ01000002.1_35104-36324 Uncharacterized MFS-type transporter	-2,81
1074035771_MKCZ01000084.1_16394-16954 Single-stranded DNA-binding protein	-2,86
1074036276_MKCZ01000059.1_10802-11011 Cold shock protein of CSP family	-2,87
1074037775_MKCZ01000015.1_25848-28214 dipeptidyl-peptidase	-2,88
1074036839_MKCZ01000040.1_4763-5707 Malonyl CoA-acyl carrier protein transacylase (EC 2.3.1.39)	-2,90
1074035503_MKCZ01000100.1_5545-7812 TonB-dependent receptor	-2,92
1074036085_MKCZ01000067.1_3730-5916 Zinc-regulated outer membrane receptor	-2,93
1074035729_MKCZ01000086.1_16121-17434 D-amino acid dehydrogenase (EC 1.4.99.6)	-2,95
1074036652_MKCZ01000046.1_23249-25285 Translation elongation factor G	-2,96
1074038561_MKCZ01000002.1_170777-173491 DNA gyrase subunit A (EC 5.99.1.3)	-2,97
1074038356_MKCZ01000004.1_62703-65075 Ribonucleotide reductase of class Ia (aerobic)	-2,98
1074036016_MKCZ01000070.1_17022-17324 ATP synthase F0 sector subunit c (EC 3.6.3.14)	-2,99
1074037687_MKCZ01000017.1_28554-29303 NADH-ubiquinone oxidoreductase chain C (EC 1.6.5.3)	-2,99
1074037775_MKCZ01000015.1_14893-16260 Mg/Co/Ni transporter MgtE	-3,01
1074036412_MKCZ01000054.1_12479-13519 Cytochrome O ubiquinol oxidase subunit II (EC 1.10.3.-)	-3,01
1074035480_MKCZ01000102.1_3936-5540 Peptide chain release factor 3	-3,02
1074037210_MKCZ01000029.1_37862-38965 Chorismate synthase (EC 4.2.3.5)	-3,02
1074036276_MKCZ01000059.1_13766-15283 Fumarate hydratase class I	-3,03
1074035618_MKCZ01000092.1_1247-1639 Succinate dehydrogenase cytochrome b-556 subunit	-3,03
1074037819_MKCZ01000014.1_9178-9561 twitching motility protein PilH	-3,03

1074035892_MKCZ01000077.1_6964-8307 Long-chain fatty acid transport protein	-3,04
1074037585_MKCZ01000019.1_12333-12869 Inorganic pyrophosphatase (EC 3.6.1.1)	-3,04
1074035749_MKCZ01000085.1_561-1859 nucleoside transporter	-3,04
1074037687_MKCZ01000017.1_29300-30607 NADH-ubiquinone oxidoreductase chain D (EC 1.6.5.3)	-3,05
1074038268_MKCZ01000005.1_59095-60150 Phosphoribosylformylglycinamidine cyclo-ligase (EC 6.3.3.1)	-3,06
1074037687_MKCZ01000017.1_31233-32573 NADH-ubiquinone oxidoreductase chain F (EC 1.6.5.3)	-3,09
1074035892_MKCZ01000077.1_19417-20619 Heme A synthase	-3,09
1074037687_MKCZ01000017.1_27967-28521 NADH-ubiquinone oxidoreductase chain B (EC 1.6.5.3)	-3,10
1074038063_MKCZ01000009.1_45611-46708 Branched-chain amino acid dehydrogenase [deaminating] (EC 1.4.1.9)(EC 1.4.1.23)	-3,11
1074037040_MKCZ01000034.1_27381-28574 hypothetical protein	-3,12
1074036747_MKCZ01000043.1_10746-12080 Chromosomal replication initiator protein DnaA	-3,13
1074037395_MKCZ01000024.1_25868-27127 Type IV fimbrial assembly protein PilC	-3,17
1074037549_MKCZ01000020.1_22802-24088 Phosphoribosylamine--glycine ligase (EC 6.3.4.13)	-3,18
1074037687_MKCZ01000017.1_27572-27976 NADH ubiquinone oxidoreductase chain A (EC 1.6.5.3)	-3,18
1074036878_MKCZ01000039.1_462-4160 Indolepyruvate ferredoxin oxidoreductase	-3,18
1074035119_MKCZ01000140.1_50-1684 NAD synthetase (EC 6.3.1.5) / Glutamine amidotransferase chain of NAD synthetase	-3,23
1074037687_MKCZ01000017.1_22987-24855 Predicted hydrolase of alkaline phosphatase superfamily	-3,24
1074035943_MKCZ01000074.1_831-1226 Glycine cleavage system H protein	-3,28
1074037687_MKCZ01000017.1_19538-20905 Phosphoglucosamine mutase (EC 5.4.2.10)	-3,35
1074035103_MKCZ01000142.1_134-559 FIG01112600: hypothetical protein	-3,38
1074036357_MKCZ01000056.1_1339-2925 Cytochrome d ubiquinol oxidase subunit I (EC 1.10.3.-)	-3,41
1074036559_MKCZ01000049.1_19731-20744 Biotin synthase (EC 2.8.1.6)	-3,47
1074037687_MKCZ01000017.1_30702-31229 NADH-ubiquinone oxidoreductase chain E (EC 1.6.5.3)	-3,58

1074038721_MKCZ01000001.1_68915-69412 Stress response diiron-containing protein YciF	-3,70
1074036559_MKCZ01000049.1_18439-19650 8-amino-7-oxononanoate synthase (EC 2.3.1.47)	-3,71
1074035892_MKCZ01000077.1_9915-13139 Proline dehydrogenase (EC 1.5.5.2) / Delta-1-pyrroline-5-carboxylate dehydrogenase (EC 1.2.1.88)	-3,74
1074035340_MKCZ01000114.1_3802-5289 Flagellar regulatory protein FleQ	-3,86
1074037323_MKCZ01000026.1_24850-25938 Outer membrane protein	-3,87
1074036622_MKCZ01000047.1_11188-13572 Ribonucleotide reductase of class Ia (aerobic)	-4,00
1074038007_MKCZ01000010.1_50795-51271 Type IV fimbrial biogenesis protein PilV	-4,04
1074038007_MKCZ01000010.1_52428-52952 Type IV fimbrial biogenesis protein PilX	-4,08
1074035503_MKCZ01000100.1_9872-10768 Phenylalanine-4-hydroxylase (EC 1.14.16.1)	-4,09
1074035170_MKCZ01000132.1_3915_6974 TonB-dependent receptor	-4,17
1074035943_MKCZ01000074.1_10510-16914 PilL protein	-4,23
1074038007_MKCZ01000010.1_52964-56728 Type_IV_fimbrial_biogenesis_protein_PilY1	-4,31
1074038007_MKCZ01000010.1_51283-52425 Type_IV_fimbrial_biogenesis_protein_PilW	-4,45
1074038007_MKCZ01000010.1_50283-50798 Type_IV_fimbrial_biogenesis_protein_FimT	-4,48
1074035943_MKCZ01000074.1_20000-20353 Twitching_motility_protein_PilG	-4,50
1074038063_MKCZ01000009.1_46787-49642 Serine_protease	-4,59
1074037244_MKCZ01000028.1_10134-11267 Uncharacterized_protein_with_LysM_domain	-4,61
1074037904_MKCZ01000012.1_43372-44499 Type_IV_pilus_assembly_ATPase_component_PilU	-4,71
1074036622_MKCZ01000047.1_13708-14727 Ribonucleotide_reductase_of_class_Ia_(aerobic)	-4,85
1074038561_MKCZ01000002.1_69913-72105 TonB-dependent siderophore receptor	-5,07
1074035943_MKCZ01000074.1_17009-19045 Pilus_biogenesis_protein	-5,34
1074037512_MKCZ01000021.1_146-1471 Xaa-Pro_dipeptidase_PepQ_(EC_3.4.13.9)	-6,64
1074038007_MKCZ01000010.1_45410-48622 Oar_protein	-9,06

1074037512_MKCZ01000021.1_30899-32878 Type_IV_pilus_biogenesis_protein_PilQ	-9,30
1074037512_MKCZ01000021.1_27780-28838 Type_IV_pilus_biogenesis_protein_PilM	-9,46
1074035084_MKCZ01000145.1_3703-5046 Histidine_kinase/response_regulator_hybrid_protein	-9,57
1074035480_MKCZ01000102.1_13216-14127 TonB-dependent_receptor BtuB	-12,52
1074034901_MKCZ01000183.1_2-1855 TonB-dependent_receptor	-13,74
1074035084_MKCZ01000145.1_674-1975 ABC transporter FtsX-like permease	-22,29
1074035084_MKCZ01000145.1_1992-3212 ABC transporter FtsX-like permease	-25,51

Table S2. Genes that showed the most significative changes in their expression in the exponential phase in presence of U, and their fold changes values

100 µM	Fold change
1074035875_MKCZ01000078.1_18024-18998 Ketol-acid reductoisomerase (NADP(+)) (EC 1.1.1.86)	11,21
1074035194_MKCZ01000129.1_4818-5261 Mar Transcriptional regulator	7,40
1074035875_MKCZ01000078.1_16251-17987 Acetolactate synthase large subunit (EC 2.2.1.6)	6,24
1074036777_MKCZ01000042.1_24433-26139 Phosphoethanolamine transferase	5,86
1074036975_MKCZ01000036.1_21976-22755 Phosphatase PAP2 family protein	5,82
1074035875_MKCZ01000078.1_4750-5880 RND efflux system MFP subunit	5,61
1074036777_MKCZ01000042.1_23716-24147 CBS domain protein	5,06
1074037118_MKCZ01000032.1_6287-8809 Aspartokinase (EC 2.7.2.4)/Homoserine dehydrogenase (EC 1.1.1.3)	4,36
1074036652_MKCZ01000046.1_18996-19994 Cyclic pyranopterin monophosphate synthase accessory protein/Molybdopterin adenylyltransferase (EC 2.7.7.75)	4,28
1074036652_MKCZ01000046.1_20002-20982 Cyclic pyranopterin phosphate synthase (MoaA) (EC 4.1.99.18)	3,91
1074035875_MKCZ01000078.1_3953-4624 TetR/AcrR family transcriptional regulator	3,83
1074036652_MKCZ01000046.1_17740-18999 Molybdopterin molybdenumtransferase (EC 2.10.1.1)	3,47
1074035875_MKCZ01000078.1_5884-9048 RND efflux system AcrB	3,10
1074036384_MKCZ01000055.1_25315-25971 TonB-dependent receptor	3,03
1074036714_MKCZ01000044.1_16683-17513 Phosphate transport ATP-binding protein PstB (TC 3.A.1.7.1)	-2,45
1074036839_MKCZ01000040.1_4763-5707 Malonyl CoA-acyl carrier protein transacylase (EC 2.3.1.39)	-2,46
1074036681_MKCZ01000045.1_30447-30665 Translation initiation factor 1	-2,47
1074037512_MKCZ01000021.1_15943-17220 Citrate synthase (si) (EC 2.3.3.1)	-2,47
1074035209_MKCZ01000127.1_7040-8041 NAD-dependent glyceraldehyde-3-phosphate dehydrogenase (EC 1.2.1.12)	-2,48
1074035943_MKCZ01000074.1_1293-2405 Aminomethyltransferase (glycine cleavage system T protein) (EC 2.1.2.10)	-2,48
1074035666_MKCZ01000089.1_1-849 Fructose-bisphosphate aldolase class I (EC 4.1.2.13)	-2,50
1074036933_MKCZ01000037.1_5069-5659 Anthranilate synthase	-2,59
1074035503_MKCZ01000100.1_9872-10768 Phenylalanine-4-hydroxylase (EC 1.14.16.1)	-2,60
1074035228_MKCZ01000125.1_6192-6761 Translation elongation factor P	-2,61
1074036714_MKCZ01000044.1_13632-14723 Phosphate ABC transporter PtsS	-2,69
1074037512_MKCZ01000021.1_9130-9429 DNA-directed RNA polymerase omega subunit (EC 2.7.7.6)	-2,73
1074037473_MKCZ01000022.1_9701-10768 Branched-chain alpha-keto acid dehydrogenase	-2,75

1074035185_MKCZ01000130.1_6389-7396 Isocitrate dehydrogenase [NAD] (EC 1.1.1.41)	-2,78
1074035119_MKCZ01000140.1_3183-4352 Succinyl-CoA ligase [ADP-forming] beta chain (EC 6.2.1.5)	-2,84
1074035289_MKCZ01000119.1_6327-7493 Phosphate/pyrophosphate-specific outer membrane porin OprP/OprO	-2,90
1074037687_MKCZ01000017.1_26908-27351 Protein translocase membrane subunit SecG	-2,94
1074037585_MKCZ01000019.1_12333-12869 Inorganic pyrophosphatase (EC 3.6.1.1)	-3,11
1074037473_MKCZ01000022.1_17348-18463 4-hydroxyphenylpyruvate dioxygenase (EC 1.13.11.27)	-3,34
1074036136_MKCZ01000065.1_6918-7364 Transamidase GatB domain protein	-3,43
1074036777_MKCZ01000042.1_32594-33862 ABC transporter	-3,50
1074035156_MKCZ01000134.1_3564-4523 Uncharacterized ABC transporter ATP-binding protein YadG	-3,56
1074037473_MKCZ01000022.1_10761-11891 Branched-chain alpha-keto acid dehydrogenase	-3,88
1074035289_MKCZ01000119.1_4717-6066 C4-dicarboxylate transport protein	-4,23
1074037819_MKCZ01000014.1_24808-25965 2-methylcitrate synthase (EC 2.3.3.5)	-4,26
1074036839_MKCZ01000040.1_3601-3840 Acyl carrier protein	-4,39
1074036652_MKCZ01000046.1_23249-25285 Translation elongation factor G	-4,41
1074037819_MKCZ01000014.1_25994-26884 Methylisocitrate lyase (EC 4.1.3.30)	-4,43
1074036714_MKCZ01000044.1_7762-8973 Phosphate/pyrophosphate-specific outer membrane porin OprP/OprO	-4,46
1074036652_MKCZ01000046.1_25286-25528 hypothetical protein	-4,64
1074035185_MKCZ01000130.1_2968-3657 Phosphate regulon transcriptional regulatory protein PhoB (SphR)	-4,66
1074037585_MKCZ01000019.1_37814-38260 electron transfer protein azurin I	-4,83
1074036714_MKCZ01000044.1_12313-13332 Phosphate ABC transporter	-5,27

CHAPTER III

Delineation of cellular stages and identification of key proteins for reduction and biotransformation of Se(IV) in *Stenotrophomonas bentonitica* BII-R7

María Pinel-Cabello [1*], Virginie Chapon [2], Miguel A. Ruiz-Fresneda[3], Beatrice Alpha-Bazin[4], Catherine Berthomieu[2], Jean Armengaud[4], Mohamed L. Merroun[1]

[1]*Department of Microbiology, University of Granada, Campus Fuentenueva s/n, 18071, Granada, Spain*

[2]*CEA, CNRS, Aix-Marseille Université, BIAM, IPM, 13108 Saint-Paul-lez-Durance, France*

[3]*Department of Crystallography and Structural Biology, Institute of Physical-Chemistry "Rocasolano" (IQFR), CSIC, 28006 Madrid, Spain*

[4]*Université Paris-Saclay, CEA, INRAE, Département Médicaments et Technologies pour la Santé (DMTS), SPI, 30200 Bagnols sur Cèze, France*

This chapter has been submitted to the Journal of Hazardous Materials (under revision)

Abstract

The wide use of selenium (Se) in technological applications (*e.g.*, solar cells or electronic devices) has led to an increase of this metalloid in the environment until toxic concentrations. The newly described bacterial strain *Stenotrophomonas bentonitica* BII-R7 has shown the ability to reduce mobile Se(IV) to Se(0)-nanoparticles (Se(0)NPs) and Se volatile species. Amorphous Se-nanospheres were reported to aggregate to form crystalline nanostructures which turned into trigonal selenium. In order to elucidate the molecular mechanisms underlying the biotransformation of Se(IV) into less toxic forms, differential shotgun proteomics was performed with cells grown in presence of sodium selenite for three different time-points. From 1,922, proteins previously described for their involvement in Se(IV) reduction and stabilization of the Se(0)NPs, such as glutathione reductase, were evidenced. Abundance of proteins with transport function, like RND systems, possibly facilitating its uptake, and proteins able to cope with oxidative stress (*e.g.* catalase/peroxidase HPI) also increased in presence of Se(IV). Microscopy analyses (STEM-HAADF) confirmed the biotransformation process from amorphous nanospheres to trigonal Se over time. These results highlight the potential of *S. bentonitica* in reducing the bioavailability of Se, which is of high relevance for the development of bioremediation strategies and the eco-friendly synthesis of biotechnological nanomaterials.

Key words: Selenium, Stenotrophomonas, nanoparticles, proteomics, microscopy

1. Introduction

Selenium (Se) is an essential element for Life required in trace amounts, selenoproteins being crucial components of a large number of biological processes such as immunity and fertility. Se is widely used in electronic, glass, metallurgy, chemical or pharmaceutic industry (Nancharaiah and Lens, 2015; Srivastava and Mukhopadhyay, 2015). However, it has shown to be extremely toxic when exceeding the concentration required for Life (Elahian et al., 2017; Zhang et al., 2019). Anthropogenic activities such as mining, have led to mobilization of Se, reaching hazardous levels in water and soils that might end in the food chain (Etteieb et al., 2020; Zhang et al., 2019). It is naturally found at low concentration in the environment at different oxidation states, selenate [Se(VI)] and selenite [Se(IV)] being the most soluble and toxic species mainly found under oxidizing conditions, while elemental Se [Se(0)] and selenide [Se(-II)] are the common redox state present in anoxic environments (Schilling et al., 2020; Winkel et al., 2015). These last Se species are less water-soluble than Se(VI) and Se(IV), reducing thus their bioavailability (Ruiz Fresneda et al., 2018).

Se oxyanions have been shown to be very susceptible to changes in redox state (Schilling et al., 2020). Microorganisms play a key role in the biogeochemical cycle of this element, as they can determine its fate and mobility by changing its chemical speciation. Se(IV) reduction has been described in bacteria from different genera, such as *Pseudomonas, Rhodococcus* or *Bacillus* (Fischer et al., 2020; Hunter, 2014; Presentato et al., 2018; Wells et al., 2019), and even fungal species like *Streptomyces* (Tan et al., 2016). In the recent years, many gram-positive and gram-negative bacteria have been described for their ability to reduce Se(IV) to immobile and less toxic Se(0), via assimilatory or dissimilatory metabolisms or detoxification process (Nancharaiah and Lens, 2015). Se can be also volatilized in methylated forms (Ruiz-Fresneda et al., 2020). Some of these microorganisms, like *Acinetobacter* sp. SW 30, *Stenotrophomonas maltophilia* SeITE02, *Bacillus subtillis* or *Thauera selenatis,* are able to form intracellular and/or extracellular spherical red-colored Se(0) nanoparticles (SeNPs) (Debieux et al., 2011; Lampis et al., 2017; Wadhwani et al., 2018; Wang et al., 2010) with different physicochemical properties (size, morphology, crystallinity, etc) (Ruiz Fresneda et al., 2018, 2019). The presence of an organic coating upon biogenic SeNPs (BioSeNPs) of proteins and polymeric substances, can also affects their colloidal stability, their interactions with metal ions and mobility (Fischer et al., 2020).

Microbial SeNPs are usually amorphous (a-Se), but the formation of monoclinic and trigonal phases (*m*-Se and *t*-Se, respectively) has been also reported. Srivastava and Mukhopadhyay (2015) described the synthesis of hexagonal-shape *t*-Se nanorods in *Ralstonia eutropha* in contact with 1.5 mM of sodium selenite in mesophilic conditions (30 ºC). *t*-Se nanostructures were also produced anaerobically in a thermophilic (55 ºC) bioreactor inoculated with anaerobic granular sludge, while the BioSeNPs produced in a mesophilic (30 ºC) bioreactor were spherical, suggesting the influence of temperature on the process (Dessì et al., 2016). Biotechnological synthesis of SeNPs mediated by microorganisms is gaining momentum given the wide range of biotechnological applications in different fields such as cancer therapy or bioremediation of Se-contaminated environments (Gómez-Gómez et al., 2019), especially nanorods, due to their high settling efficiency and low colloidal stability (Jain et al., 2017a). Although many studies have suggested different pathways leading to Se(IV) reduction and formation of Se volatile species, little is known about the specific bacterial mechanisms for those events.

Next-generation proteomics is a proven tool that provides valuable information about cellular processes occurring under different conditions (Armengaud, 2016). While differential proteomics based on label-free methodology is robust (Gouveia et al., 2020), only few studies have applied this technique to elucidate the biochemical pathways and proteins involved in Se(IV) response in bacteria. Hunter (2014) identified several enzymes that showed Se(IV) reductase activity from cell-free extracts of *Pseudomonas seleniipraecipitans,* like glutathione reductase, aspartate-semialdehyde dehydrogenase or isopropylmalate dehydrogenase. Similar studies were carried out in *S. maltophilia* SeIT02 (Lampis et al., 2017), only focussing in the proteins possibly involved in the reduction process. Previous works have also identified the proteins that compose the organic layer covering the SeNPs. Gonzalez-Gil et al. (2016) used proteomics to identify the proteins attached to SeNPs produced by a microbial community of an anaerobic granular sludge from a reactor of a treating brewery wastewater. Their results showed high amount of outer membrane porins and the elongation factor Tu. A similar strategy was developed by Fischer et al. (2020) in NPs synthetised by *B. safensis* JG-B5T, detecting a great variety of proteins from different metabolic pathways, with glutathione reductase, thioredoxin reductase, NAD(P)/FAD-dependent oxidoreductases among others. Nevertheless, the approach carried out in the above mentioned studies does not provide clues about the entire cellular processes that could contribute not only to bioreduction of

the metalloid and formation of Se(0) and Se volatile species, but also to cope with Se(IV) toxicity and the biotransformation of amorphous Se(0) into crystalline Se nanostructures.

The present work focuses on the proteomic and microscopic analysis of Se(IV) bioreduction to Se(0) and SeNPs formation in *Stenotrophomonas bentonitica* BII-R7, a new bacterial strain isolated from Spanish bentonites from Almería (Spain), selected material for their use as artificial barrier in the future Spanish repository of nuclear wastes. The transcriptomic response to uranium (U) in this biofilm-forming strain has been recently reported (Pinel-Cabello et al., 2021). This strain showed tolerance to high concentrations of Se(VI) and Se(IV), being able to reduce Se oxyanions and produce BioSeNPs under aerobic, anaerobic and alkaline-conditions. a-Se nanospheres synthetized formed *t*-Se nanostructures by aggregation upon extracellular flagella-like structures (Ruiz-Fresneda et al., 2018, 2019). Furthermore, it is also capable to further transform Se(0) to Se volatile species (Ruiz-Fresneda et al., 2018, 2019, 2020). This work provided a better understanding on the molecular basis of the interactions of *S. bentonitica*, which include reduction of Se(IV) to Se(0) and formation of Se volatile species, allowing us to develop a cellular model that links the mechanisms that act synergistically to lead to Se(IV) tolerance. The results obtained would help to design bioremediation technology of Se(IV) contaminated environments. Furthermore, the knowledge of these mechanisms enables the optimization of the process for the use of biotechnological synthesis of BioSeNPs in nanotechnology.

2. Material and methods

2.1.Bacterial growth and culture

Cells of *S. bentonitica* were grown aerobically in Lysogeny broth medium (tryptone 10 g L^{-1}, yeast extract 5 g L^{-1} and NaCl 10 g L^{-1}, pH 7.0 ± 0.2) at 28ºC under shaking at 150 rpm. After 24h, cells were washed twice in NaCl 0.9% and flask containing LB with and without 2 mM of sodium selenite (Na_2SeO_3) were inoculated at an initial OD_{600} of 0.2, and incubated at 28ºC in a rotatory shaker at 180 rpm. Control treatments without selenite (biotic) and without bacteria (abiotic) were also incubated in the same conditions. All treatments were performed in three biological replicates.

Sodium selenite powder (Sigma-Aldrich) was added to Milli Q water and sterilized by filtration using 0.22 μm filters to prepare a 1M stock solution.

2.2.Sample preparation for proteomics

Bacteria were cultured with and without 2 mM sodium selenite as previously described. Aliquots (circa 2-3 mg of wet biomass) were collected at lag, mid-exponential and stationary growth phases (15 min, 14 and 40 h for untreated samples, and 24, 72 and 144 h for treatments with Se(IV)). For each time point and condition, three biological replicates were performed, resulting in a total of 18 samples. Samples were centrifuged at maximum speed for 10 min. After discarding the supernatants, the pellets were immediately fixed in liquid nitrogen and stored at -20ºC until analysis.

2.3.Protein extraction and in-gel proteolysis

Frozen bacterial pellets were dissolved into SDS-PAGE loading buffer (100 µL per 1.7 mg of cell pellet for non-treated samples and 100 µL per 3.4 mg of cell pellet for Se-treated samples, wet weight), supplemented with β-mercaptoethanol. Cell lysis was carried out as described in Hayoun et al. (2019). Briefly, samples were incubated for 5 min at 99ºC and sonicated for 5 min in a VWR ultrasonic cleaner. Cells were subjected to bead-beating lysis with Precellys Evolution instrument at 10,000 rpm for 10 cycles of 30 s, with an interval of 30 s between cycles. Centrifugation at 16,000 x *g* for 1 min and incubation of the samples at 99ºC for 5 min was performed before SDS-PAGE. To evaluate the yield of protein extraction, NuPAGE 4-12% Bis-Tris (Invitrogen) gel was loaded with 20 µL of each sample for 4 min migration in denaturing conditions at 200 V using MES/SDS (Invitrogen) running buffer. Results of short migration were visualized by staining with ready-to-use Coomassie SimplyBlue SafeStain (Thermo Fisher Scientific).

Excision of the whole proteome as a single polyacrylamide band was performed for each sample. Each band was deposited in a 96 well-plate for achieving homogeneous trypsin proteolysis. Polyacrylamide bands were washed with MilliQ water after a dehydration step with CH_3CN:NH_4HCO_3 50 mM (1:1 v:v) and CH_3CN 100% was added. Afterwards, bands were dried for 5 min under vacuum and rehydrated with 25 mM of dithiothreitol in 100 mM of NH_4HCO_3 and incubated at 56ºC for 10 min, followed by treatment with 100 mM NH_4HCO_3 with 55 mM iodoacetamide during 10 min in the dark at room temperature. The gel bands were dried with vacuum and rehydrated for proteolysis with 20 µL of 50 mM NH_4HCO_3 supplemented with trypsin gold with 0.01% ProteaseMAX (Promega) according to the protocol described in Hartmann et al. (2014).

2.4.Analysis by Nanoscale liquid chromatography coupled to tandem mass spectrometry (NanoLC-MS/MS)

The 18 resulting peptide pools were identified using a UltiMate 3000 nano LC system (Dionex) coupled to a Q-Exactive HF tandem mass spectrometer (Thermo Fisher Scientific) operated in similar conditions as those previously described (Klein et al., 2016). A volume of 4 μL of the total peptide mixture (50 μL) were first loaded and desalted on-line in a precolumn PepMap 100 C18 (5 μm bead size, 100 Å pore size, 300 μm i.d. x 5 mm, Thermo Fisher Scientific), and were then resolved onto a reverse phase Acclaim PepMap 100 C18 column (3 μm porosity, 100 Å, 75 μm i.d. x 500 mm, Thermo Fisher Scientific) injected at a flow rate of 0.2 μL/min with 90 min gradient (4–25% B from 3 to 78 min, and 25–40% B from 78 to 93 min) with mobile phases A (0.1% HCOOH/100% H_2O) and B (0.1% HCOOH/80%CH_3CN/20%H_2O). The mass spectrometer was operated in Top20 data-dependent acquisition method according to Klein et al. (2016). A scan cycle with a full scan of peptide ions was established using the ultra-high-field Orbitrap analyser followed by selection of a precursor, its high energy collisional dissociation and MS/MS scan for the 20 most abundant precursor ions. Full scan mass spectra were obtained at a resolution of 60,000 from *m/z* 350 to 1800, with an Automatic Gain Control Target set at 3×10^6 ions. Resolution of MS/MS scan was 15,000 when the AGG target reached 1×10^5 ions with a intensity threshold of 83,000. Only potential charge states of 2+ and 3+ were selected for ion dissociation, and the selection was performed with a dynamic exclusion of 10 s.

2.5.Mass Spectrometry data interpretation

The recorded MS/MS spectra were searched for peptide assignment against a database comprising the 3,796 annotated proteins from *S. bentonitica* BII-R7 (UniProt database proteome ID UP000175905)(Sánchez-Castro et al., 2017a). Peak lists were generated using MASCOT DAEMON software version 2.5.1 (Matrix Science). Search parameters were set with trypsin as proteolytic enzyme and a maximum of 2 missed cleavages, 5 ppm mass tolerance for the precursor and 0.02 Da mass tolerance for the MS/MS signals, fixed modifications for carbamidomethylation of cysteine residues, and glutamine and asparagine deamidation and methionine oxidation as variable modifications. Mascot results were parsed using the IRMa software version 1.31.1c (Dupierris et al., 2009). Peptide-to-spectra matches were assigned with a *p* value of 0.05, and proteins were validated with the detection of at least two different peptide sequences.

Comparative analysis of protein abundances based on total spectral counts were performed by calculating using Excel formula (Microsoft) the T-Fold and T-test *p*-values

previously developed for the PatternLab software (Carvalho et al., 2008), and following standard normalization. The proteins were classified according to their T-Fold and *p*-values. For this work, only proteins with T-Fold ≥ 1.5 or ≤ -1.5 and with a *p*-value ≤ 0.05 (Blue class) were retained. The estimated detection of the spectral counts and their abundances were visualized by grouping them into a hierarchical cluster tree using R package pvclust (n=2000 bootstrap) using war.D method and spearman distance, in order to establish the similarity or dissimilarity between the samples. Pearson correlation coefficient was calculated in R package reshape2. Proteins that passed a cut-off of -0.9 and 0.9 were used to build an interaction network in Cytoscape v. 3.8.2 using the Betweenness Centrality of each node.

The mass spectrometry proteomics data have been deposited to the ProteomeXchange Consortium via the PRIDE (Perez-Riverol et al., 2019) partner repository with the dataset identifier PXD023459 and project DOI 10.6019/ PXD023459. [The reviewers may access this private dataset using reviewer_pxd023459@ebi.ac.uk as Username and hn9u20tf as Password].

2.6. High-angle annular dark field scanning transmission electron microscopy (HAADF-STEM) and energy dispersive X-ray (EDX) spectrometry analyses

In order to determine the cellular localization and to characterize the physicochemical properties (size, morphology and structure) of the Se nanoparticles produced by the cells as consequence of Se(IV) reduction, samples for microscopic analyses were harvested at the different growth phases. Aliquots of 1 mL of Se(IV)-treated samples were centrifuged at 11,000 rpm for 10 min at room temperature after 24, 72 and 144 h of incubation. Samples were fixed in 0.1 M cacodylate buffer (pH 7.2) with 2.5 % glutaraldehyde during 24 h at 4ºC. Cells were washed with the same cacodylate buffer and stored at 4ºC until sample preparation as described in Merroun et al. (2005). Samples were analysed using HAADF-STEM FEI TITAN G2 80-300 with energy dispersive X-ray (EDX) spectrometer. TEM specimen holders were cleaned with plasma prior to analyses in order to avoid contamination.

3. Results

3.1. Growth of S. bentonitica in presence of Se(IV)

The strain BII-R7 was able to grow in all conditions, with or without 2 mM Se(IV). Se(IV) reduction by *S. bentonitica* was revealed by the red-coloured culture after 24h incubation as shown in Fig. 1. This colour turned more intense at higher incubation times, indicating an increase in the amount of reduced Se with time. The Se(IV) reduction process is mediated by *S. bentonitica*, as no colour change was observed in the abiotic controls. Previous studies showed that when BII-R7 cells grew in presence of 2 mM Se(IV), there was an extended lag phase of 48 h, the stationary growth phase was reached at around 100 h and all the Se(IV) was reduced to Se(0) at around 144 h of incubation (Ruiz-Fresneda et al., 2018 and Fig. S1). Sampling times (24, 72 and 144 h) for proteomics were established according to these results, so as to identify the specific mechanisms of Se(IV) reduction occurring in each growth phase.

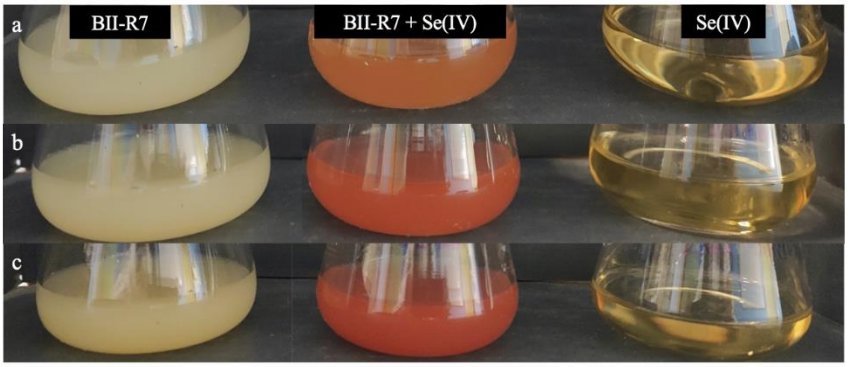

Fig. 1. Colour change of cultures of BII-R7 amended with 2 mM of Se(IV) at 24 (a), 48 (b) and 72 h (c) of incubation. No changes were detected in biotic and abiotic control cultures.

3.2. General overview of shotgun proteomics

The nanoLC-MS/MS analysis of the 18 samples yielded 1,151,245 MS/MS recorded spectra, of which 682,785 could be assigned to peptide sequences of *S. bentonitica* BII-R7 proteome with a *p*-value 0.05. The high assignment rate (60%) indicates the good quality of the MS/MS spectra. These spectra were assigned to 12,150 unique peptide sequences, which resulted in 1,922 proteins certified by at least two different peptides matches. Thus, the whole experimental dataset corresponds to 50% of the predicted proteome of the strain. 385 additional proteins were detected with only one peptide but were not considered for further analysis. The samples were analysed by hierarchical clustering in order to determine the similarity of the protein profiles between them. According to the results showed in Fig. S2, Se(IV)-treated and untreated samples grouped in two different clusters, which in turn were divided in three subgroups

corresponding to each growth phase. The uniformity between replicated samples indicates the high reproducibility of the experimental procedure. Fig. S3 shows the Venn diagrams comparing the proteins pools obtained for the untreated and Se(IV)-treated samples at each growth phase, revealing that the majority of proteins found were present in the three growth phases (around 86% of the proteome), regardless of the treatment. Furthermore, similar results were observed when Se(IV)-treated and non-treated cells were compared, showing that only around 10% of the detected proteins were specifically different between treatments at each growth phase, although the total proteins detected in Se-treated samples was lower than that in the untreated samples. This comparison also revealed that the proteins detected in lag, exponential and stationary phases corresponded to 14.1, 23.8 and 26.3 % of the total proteome, respectively.

Considering the proteins classified in the Blue class (proteins identified with a fold change ≥ 1.5 or ≤ -1.5 and p-value ≤ 0.05), a total of 828 proteins were detected with statistically differential abundances in Se(IV)-treated and non-treated samples: 271 in lag, 458 in exponential and 505 in stationary phase, as indicated in Figure 2. On one hand, 511 proteins are specifically differentially abundant for a particular growth phase. Among these, 82, 181 and 248 proteins corresponded to lag, exponential and stationary phases, respectively. On the other hand, the comparison of these proteins at the three growth phases showed that 89 proteins were found in common, among which 38 were statistically more abundant in Se-treated samples and 43 proteins were more abundant in non-treated samples (Fig. 2). A network based on the positive and negative correlations between these common proteins (represented as P1 to P89) was built, as shown in Fig. 3, highlighting the complex response triggered by Se(IV). The correspondence between the numbers on the figure and the proteins is indicated in supplementary table S1. Among the proteins that established the higher number of interactions there were 2 hypothetical proteins (P72, P81), a sulfurtransferase (P15), the chemotaxis protein CheW (P52), a FMN-dependent NADH-azoreductase (P12), a glutathione peroxidase (P54) or a diguanylate cyclase (P74). Among them, only sulfurtransferase and FMN-dependent NADH-azoreductase were more abundant in Se-treated cells, especially during stationary phase (6- and 14.7-fold change respectively). It is also worth to notice that FMN-dependent NADH-azoreductase correlates positively with many enzymes implicated in oxidative stress, such as catalase/peroxidase HPI, which also showed high abundance during stationary phase. The rest of the mentioned proteins were found less abundant in treated than in untreated cells, showing their lowest fold-changes during the exponential growth: -3-, -7.5-fold

change for hypothetical proteins P72 and P81, -5-fold change for diguanylate cyclase, and -2.3- and -4.5-fold changes for CheW and glutathione peroxidase, respectively.

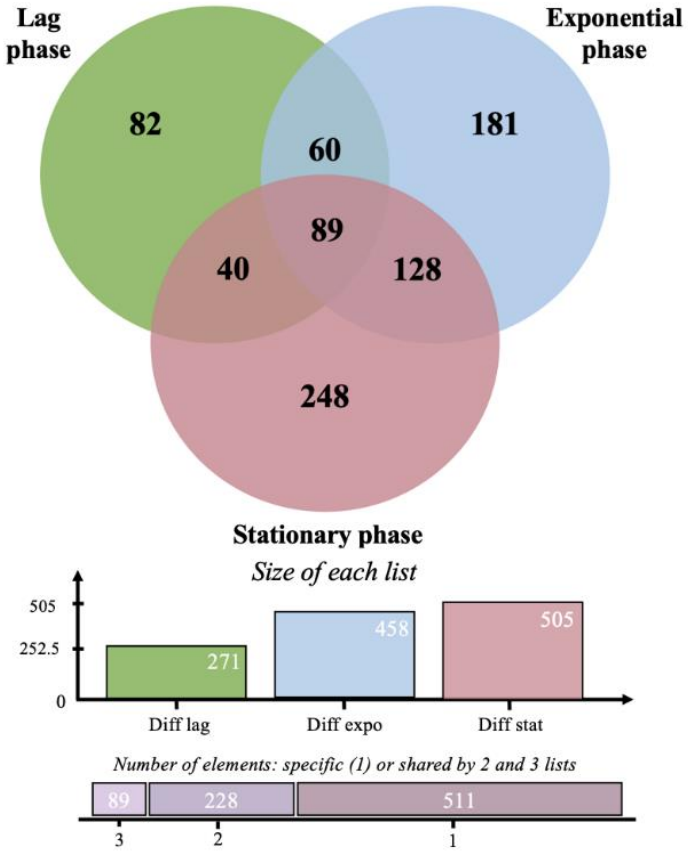

Fig.2. Venn diagram comparing the proteins of Blue class at lag (green), exponential (blue) and stationary (red) growth phases.

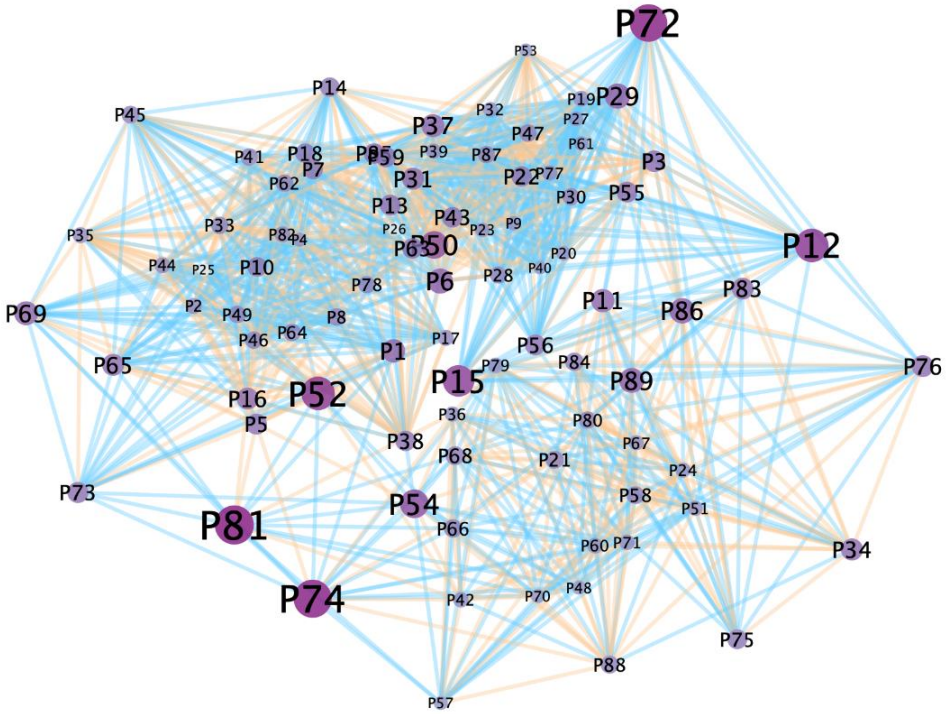

Fig. 3. Network of positive (blue) and negative (red) interactions between Blue class proteins found in all growth phases tested. The size of the nodes is proportional to the number of interactions of each protein.

3.3. Proteome response over time in S. bentonitica during Se(IV) stress

The 828 proteins found significantly affected by the presence of Se(IV) were involved in a variety of metabolic pathways, and were gathered in 6 groups according to their predicted function: oxidoreductases, transporters, actors of stress response, transcriptional regulators, general metabolism and motility. However, 96 out of these 828 proteins were classified as hypothetical proteins due to the lack of their functional characterization. Although the 89 common proteins with significant changes detected in all growth phases were grouped in these 6 categories, the abundance of some proteins is specifically modulated at a given incubation time, according to the physiological needs and the rate of Se(IV) reduction in each growth phase.

Around 24 % of common proteins were annotated as proteins with oxidoreductase activity (Table 1) from different metabolic processes. They appeared throughout the entire experiment, but their fold-changes showed high fluctuation between the different growth phases. It is noteworthy that the highest number of oxidoreductases was identified in the stationary phase, and the majority of them were more abundant than in the other growth phases. Remarkably, these proteins were mainly more abundant in Se-treated than in untreated samples. The most modulated oxidoreductase, FabG, a NAD/NADP-dependent oxidoreductase 3-oxoacyl-ACP reductase belonging to the short-chain dehydrogenase/reductase (SDR) family, was found during the lag phase with a fold change of 76.5. In the second place, there is a dioxygenase, with 27.3-fold change in the lag phase. Both FabG and dioxygenase followed the same tendency, decreasing their fold changes gradually in the exponential and stationary phases (14.1 and 11.7-fold changes for FabG; 15.3 and 12.7-fold changes for dioxygenase, respectively). In addition, the subunit F of an alkyl hydroperoxide reductase was the protein with the most significant fold change observed with this activity when the strain reached the stationary growth. The subunit C of the alkyl hydroperoxide reductase was also found more abundant than in untreated samples, but to a lesser extent (Table 1). This oxidoreductase, associated with cell protection against oxidative stress by detoxifying peroxides, showed an opposite behaviour than the two enzymes mentioned above, being up-regulated according to time, especially between the exponential and stationary phase for the subunit F (from 6.5 to 33.4-fold change). Furthermore, ArsH and ArsC, two reductases involved in arsenic resistance with NADPH-dependent FMN reductase and arsenate reductase activity respectively, were up-regulated in presence of Se(IV) in the lag (4.3 and 2.4-fold changes, respectively) and stationary phases (10 and 7.8-fold changes, respectively). Nevertheless,

no significant changes were found during the exponential growth phase for these proteins with regard to the unexposed cells. It is also worth noting the increase of enzymes involved in glutathione metabolism such as glutamate—cysteine ligase or glutathione synthase in Se(IV)-treated cells, both related to the synthesis of glutathione (*e.g.* glutathione-disulfide reductase) (Table 1). The glutamate—cysteine ligase fold change increased over time, while the glutathione synthase was more modulated by Se in the lag phase than in the subsequent growth phases. Similar behaviour was observed for other enzymes like a SDR family aklaviketone reductase, malate:quinone oxidoreductase or glutaredoxin 3 (GrxC family), but the fold-change of this last protein slightly decreased in the stationary phase (from 1.9 to 1.5). On the contrary, some proteins in this category were down-modulated, especially the subunit alpha of a ribonucleoside-diphosphate reductase, which exhibited a drastic reduction of its abundance from –4.1 to -33.7-fold change, from lag to stationary phases, respectively. Furthermore, a cyclic pyranopterin phosphate synthase involved in the synthesis of the Mo cofactor (MoCF), needed for the activity of oxidoreductases in carbon, nitrogen and sulphur metabolism, was the protein with the lowest fold-change in the lag phase, and decreased even more during the exponential growth (from -12.3 to -17.7-fold change, respectively). Two coproporphyrinogen III oxidase HemN, involved in biosynthesis of heme groups, were also down-regulated in all sampling times (-6.5, -4.5 and -12.3 and -6.5, -8.7 and -1.0-fold changes for lag, exponential and stationary phases, respectively).

Table 1. Differentially abundant proteins with oxidoreductase activity present in all growth phases.

Protein description	TFold (Se-treated vs non-treated samples)		
	Lag phase	Exponential phase	Stationary phase
Short-chain dehydrogenase	76.50	14.10	11.69
Dioxygenase	27.33	15.33	12.67
NADPH:quinone reductase	10.00	6.00	2.00
NAD(P)H dehydrogenase	10.00	8.00	6.67
FMN-dependent NADH-azoreductase	6.67	4.67	14.67
3-beta hydroxysteroid dehydrogenase	6.64	5.43	3.14
Malonic semialdehyde reductase	4.97	3.51	2.56
Luciferase-like monooxygenases	3.08	6.71	9.13
Alkene reductase	2.96	5.56	12.40
Glutathione synthase	2.13	1.70	1.76
Oxidoreductase	1.98	2.05	2.87
Alkyl hydroperoxide reductase subunit F	1.84	6.51	33.38
Oxidoreductase	1.83	2.42	4.50
Alkyl hydroperoxide reductase subunit C	1.76	2.39	3.90
Glutathione-disulfide reductase	1.73	2.09	1.54
Alkene reductase	1.72	2.62	2.69
Fe-S cluster assembly ATPase SufC	1.71	1.81	1.72
Fe-S cluster assembly protein SufD	1.69	2.38	3.58
Thioredoxin-disulfide reductase	1.53	2.11	1.68
Aldehyde dehydrogenase iron-sulfur subunit	-1.62	-4.42	-1.75
FAD-dependent monooxygenase	-1.74	-2.03	-11.33
Glutathione peroxidase	-1.75	-4.50	-2.27
Molybdopterin dehydrogenase	-1.95	-5.22	-2.22
Oxidoreductase	-2.00	-4.50	-1.89
Molybdopterin converting factor subunit 2 protein	-2.00	-2.60	-4.67
Twin-arginine translocation pathway signal	-2.67	-8.75	-3.00
GMC family oxidoreductase	-3.05	-5.70	-2.14
Coproporphyrinogen III oxidase	-6.50	-4.50	-12.33

Among the 89 proteins shared in the three growth phases, nine are involved in stress response in Se(IV)-treated cells. Here are included proteins implicated in DNA modification and repair, chaperones, cold-shock and heat-shock proteins and enzymes that provide protection against reactive oxygen species (ROS). These proteins are either found at equal levels in all growth phases or up-regulated as the bacteria grew. One of them, a catalase/peroxidase HPI showed a remarkable up-regulation over the time, especially from exponential (20.5-fold change) to stationary phase (257-fold change). This protein was not only the most abundant in this growth phase, but also in the entire experiment. The stress response seemed to increase throughout the experiment, being more important during the stationary phase, as more proteins related to this process have positive fold changes at this sampling time. During the lag phase, the stress response was represented mostly by proteins involved in DNA repair (*e.g.,* RadA, recombinase RmuC, RecA), a few enzymes protecting the cells from oxidative stress (*e.g.,* catalase/peroxidase HPI, organic hydroperoxide resistance), and the ATP-dependent chaperone ClpB. Then, at the exponential and stationary phases and in addition to the latter proteins, the number of modulated chaperones increased, such as DnaK, HtpG and GroEL. The majority were common to both phases, increasing in the stationary phase (2.4, 1.8 and 2.3-fold changes in the stationary phase for DnaK, HtpG and GroEL, respectively), included ClpB (from 1.8 to 3.5-fold change).

The same number of proteins were annotated as transcriptional regulators or part of two-component systems. Among them, a transcriptional regulator of the LysR family, which act as activator or repressor of genes of the carbon/nitrogen metabolism, decreased its fold-change over time (from 2.2 in lag phase to 1.7-fold change in stationary phase). A heavy metal-responsive transcriptional regulator was also found up-regulated only in the stationary phase (3-fold change). Two YhaK family proteins, previously related to biofilm formation in *E. coli* (Hancock et al., 2010) were also up-regulated in Se(IV)-treated samples, in particular one of them during the exponential phase (25-fold change). In line with this, an UDP-N-acetylenolpyruvoylglucosamine reductase (MurB) involved in the initial steps of peptidoglycan biosynthesis, and the monofunctional biosynthetic peptidoglycan transglycosylase (MtgA), acting at final stages of the same process, were found up-regulated at the stationary and lag phases, respectively (3.8 and 1.5-fold change). The RelE protein from the toxin/antitoxin system RelE/RelB, was up-regulated during lag (2-fold change) and exponential phase (3.3-fold change).

Around 9% of the common proteins of the Blue class had a predicted transporter function, such as TonB-dependent or metal transporters, with RND type efflux systems being the most significantly up-regulated in lag and exponential phases. Although these proteins were more important during the first hours of the experiment (lag phase) in terms of fold-change, the number of predicted transporters was higher in the following hours, especially during the exponential phase. At 24 h of Se(IV) exposure, the permease subunit of a AcrB multidrug efflux RND transporter was found 81-fold more abundant than in untreated samples. Although the fold change decreased in the following sampling time, it still appeared at high levels during the rest of the experiment (39 and 49-fold changes during exponential and stationary phases, respectively). Similar results were observed for another RND transporter lipoprotein from NodT family, which had almost the same fold-change in the lag and exponential phase (43 and 46-fold-change) and decreased its fold change nearly to half once *S. bentonitica* started the stationary growth (21-fold change). On one hand, a probable CircA TonB-dependent receptor or the permease subunit SmeE from an RND system were specifically produced at the exponential growth. On the other hand, specific transporters from the stationary phase encompassed an AcrB subunit from a multidrug pump or a copper-transporting ATPase. Other proteins involved in transport of different compounds, such as protein-export SecD or sodium:dicarboxylate symporter, also showed positive fold changes (1.7-fold change at the stationary phase). However, nitrogen and iron uptake systems were negatively affected by Se(IV). A transcriptional regulator from the Fis family similar to NtrX of *Azorhizobium caulinodans*, which activates nitrogen assimilation, was down-regulated in all phases (Levicán et al., 2008). The transcriptional regulators for iron uptake Fur (-2.3 and -2.7-fold change in lag and exponential phase respectively) and FecR (-1.9 in lag phase and -3.2-fold change in stationary phase) had also negative fold changes (Passmore et al., 2020; Troxell and Hassan, 2013).

Analysis of the specific changes during the lag phase showed the ubiquity of many proteins belonging to ribosomal subunits. These proteins were up-regulated at this growth phase (ranging from 6.3 to 1.5-fold change), whereas very few were detected in the following hours, being all in lower amount than in untreated samples. Proteome in the lag phase suggest that cells were metabolically less active than in the other phases. Proteins of the general metabolism such as the subunit 3 of gluconate 2-dehydrogenase family protein (–8.8-fold change in the exponential phase), were found mainly minor than in non-treated samples in all growth phases. However, Se(IV) treated cells in the exponential

and stationary phase showed higher abundance of proteins such as cell division proteins (*e.g.*, FtsX, FtsZ or FtsK), elongation factors, DNA polymerases and helicases (*e.g.*, DEAD/DEAH box helicase), or aminoacid, carbohydrate and lipid metabolism (*e.g.*, sugar hydrolase), compared to lag phase. Some of these proteins were present in all growth phases, most of them down-regulated compared to non-treated samples. Lastly, very few proteins related to motility processes, like PilT or CheW, were found in the Blue class, and they were all less abundant than in the non-treated samples.

3.4. Microscopic characterization of Se(IV) bioreduction using HAADF-STEM and EDX

In order to characterize the Se(IV) bioreduction process at nano and molecular scale (cellular localization and structural properties of the produced Se(0)NPs), STEM/HAADF analysis was conducted. Micrographs of samples at 24 h (lag phase) showed the presence of a few electron-dense Se-containing nanospheres inside the cells (Fig. 4). The SAED pattern clearly indicated their amorphous nature (Fig. 4c). After 72 h (exponential phase), a higher number of both intra and extracellular Se-nanospheres were observed, with also an increased size ranging from 120 to 350 nm (Fig. 5). Finally, only a few nanospheres, mainly present in the extracellular space, were found after 144 h of incubation (stationary phase). Interestingly, at this time/phase we could observe that some of them presented damaged or lysed cells nearby (Fig.6).

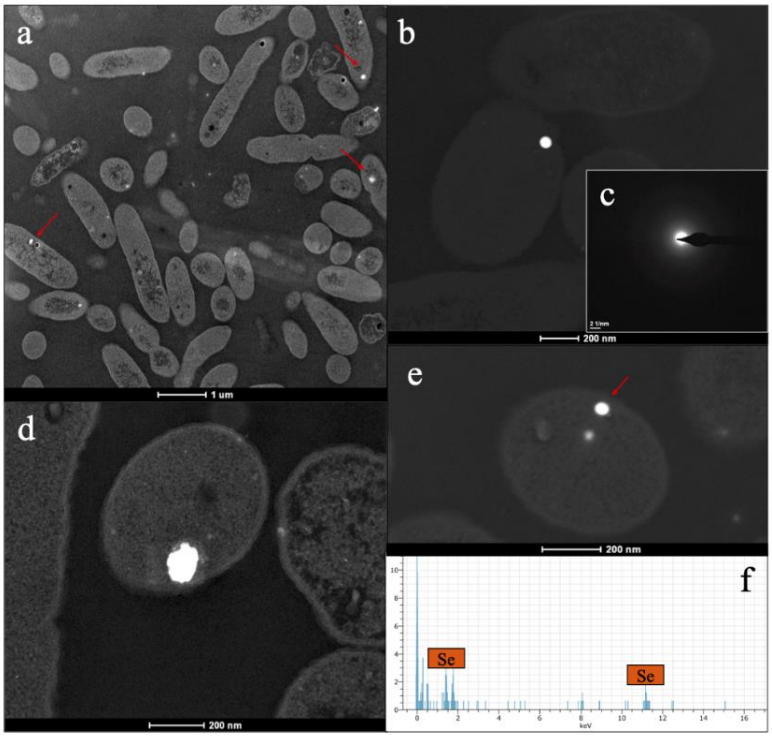

Fig. 4. HAADF-STEM micrographs of amosphous nanospheres formed by *Stenotrophomonas bentonitica* BII-R7 at 24 hours of incubation (a, b, d, e). EDX analysis (f) of a nanosphere (e) showed Se in its composition.

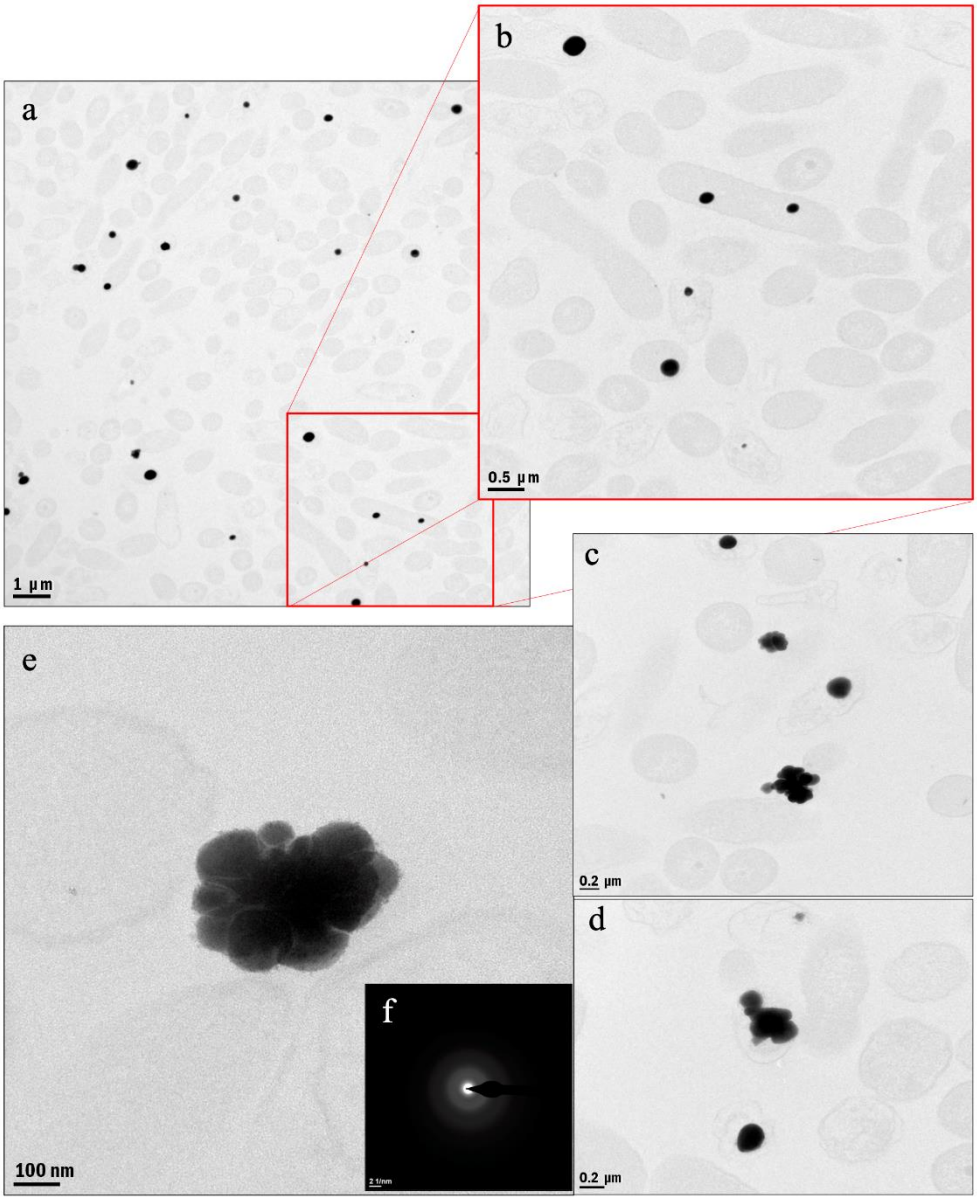

Fig. 5. Micrographs of SeNPs (a, b) and irregular structures (e, c, d) formed after 72 h of incubation. SAED patterns showed its amorphous nature (e).

Samples incubated for 72 and 144 h are characterized mainly by the presence large Se nanostructures in the extracellular space, which also contained S in their structure as indicated the EDX analysis (Fig. 8c). Irregular Se nanostructures were observed at these sampling times (Fig. 5c, d, e), which seemed to be formed by aggregation of Se-nanospheres. Irregular aggregations found at 144 h differ from those observed in 72 h with the presence of small gaps in their structure (Fig. 6c). Patterns obtained from SAED analysis showed the amorphous nature of the nanostructures (Fig. 5f). However, crystalline structures such as nanowires were also found at both incubation times (Fig. 7a, d and 8). HRTEM analyses along with the FFT of the nanowires formed after 72 h

indicated two lattice spacings of 0.2 and 0.32 nm, which would correspond to different planes (1 2 5; -2 4 1; etc.) and (1 1 3) of *m*-Se, respectively (Fig. 7b and c). Lattice spacings measured in samples collected at 144 h were 0.3, 0.37 and 0.49 nm, which could correspond to different planes of both *m*-Se and *t*-Se (Fig. 7e and f). Specifically, the d-spacing of 0.3 nm could correspond to planes (1 0 1) of *t*-Se and (2 2 1) of *m*-Se. The d-spacing of 0.37 nm clearly correspond to the plane (1 0 0) of *t*-Se. Finally, the lattice spacing of 0.49 nm is close to that found at 0.45 nm, which could be related to the plane (0 2 0) of *m*-Se. These results evidenced the presence of two different crystal structures (monoclinic and trigonal) in the biosynthesized nanowires, and confirmed the structure transformation hypothesis suggested by Ruiz-Fresneda et al. (2018, 2019, 2020) in previous studies.

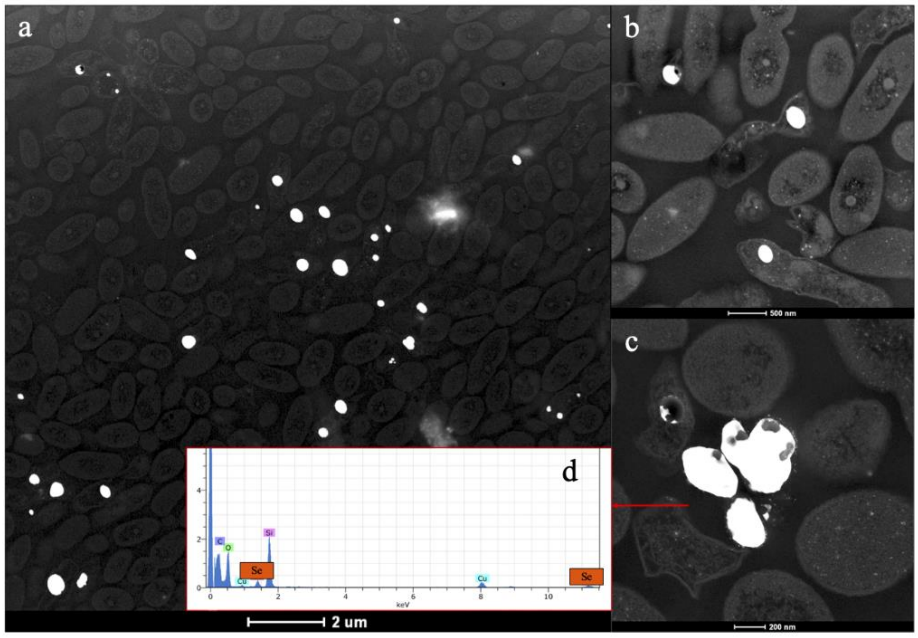

Fig. 6. Se nanospheres (a, b) and irregular aggregation (c) from samples of BII-R7 after 144 h of incubation in presence of 2 mM of Se(IV). EDX analysis showed the presence of Se in the irregular aggregations (d).

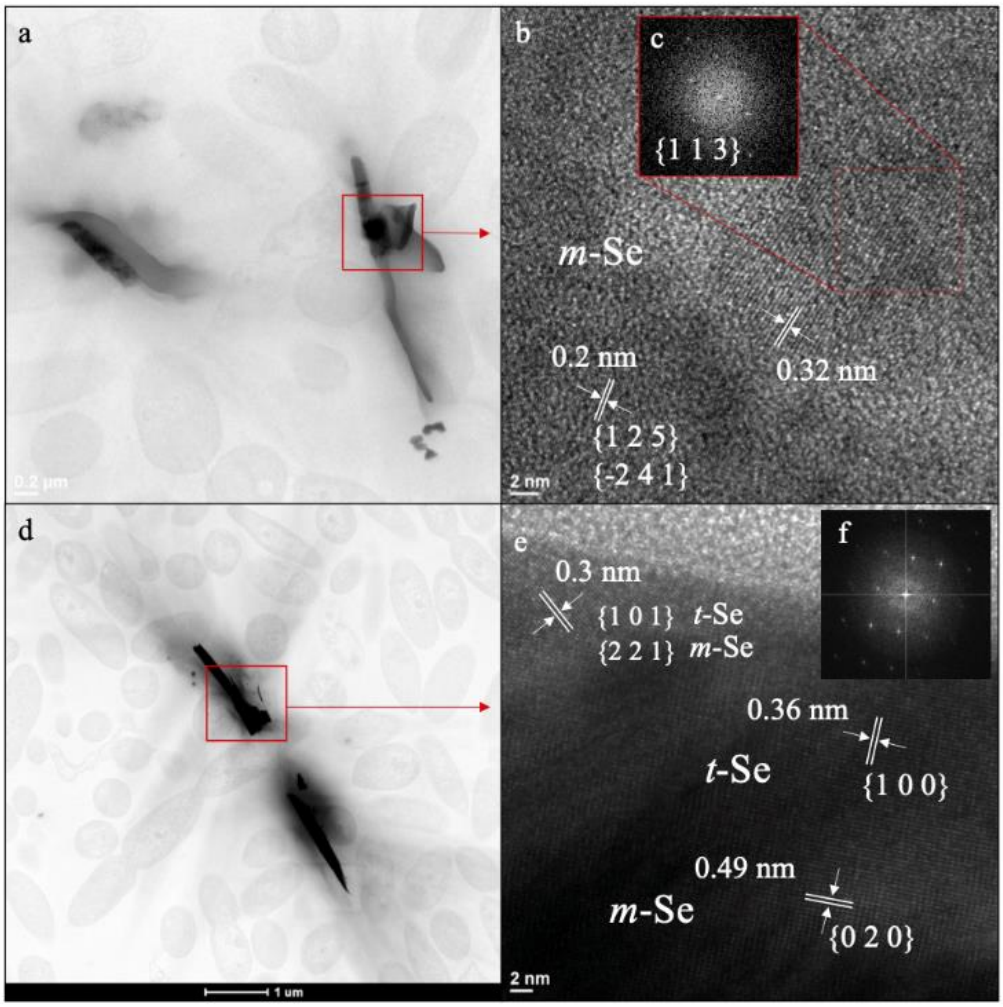

Fig. 7. Cells of *S. bentonitica* with Se nanowires micrographs and HRTEM with FTT analysis from 72 h (a, b and c) and 144 h of incubation (d, e and f).

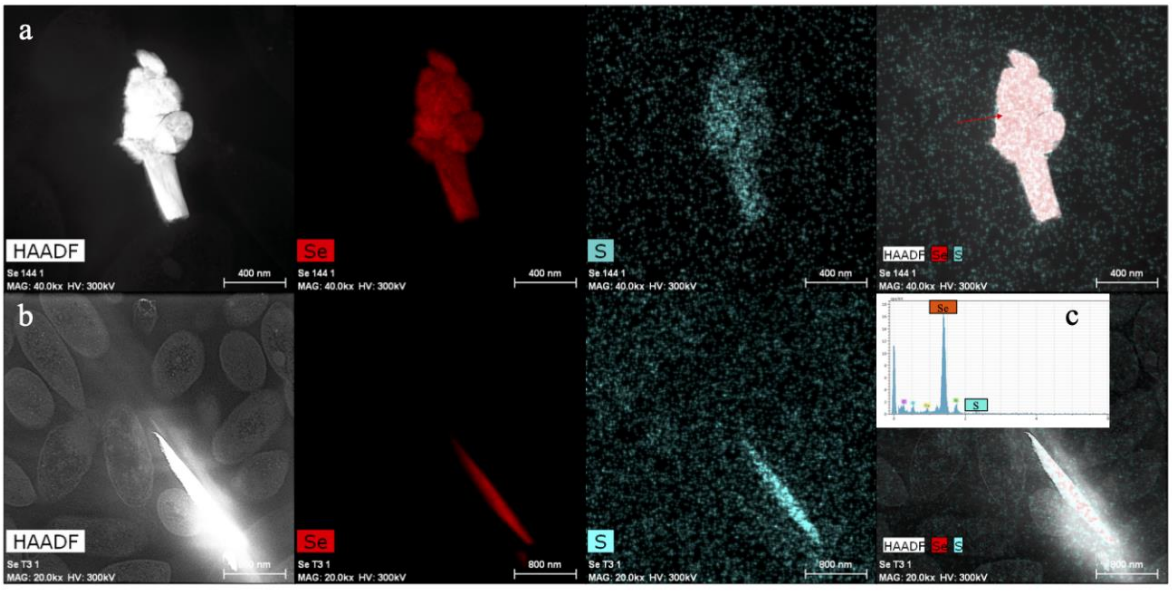

Fig. 8. Elemental mapping of crystalline aggregation and nanowire observed at 144 h of incubation. Both nanostructures are mainly composed of Se and S.

Elemental mapping of both irregular and crystalline nanostructures observed at 72 and 144 h of incubation showed S in their structure, in contrast to nanospheres at 24 h, where no S was detected probably due to their small size (Fig. 9). These results suggest that S-rich molecules (*e.g.*, GSH) are involved in the biochemical pathways of Se reduction.

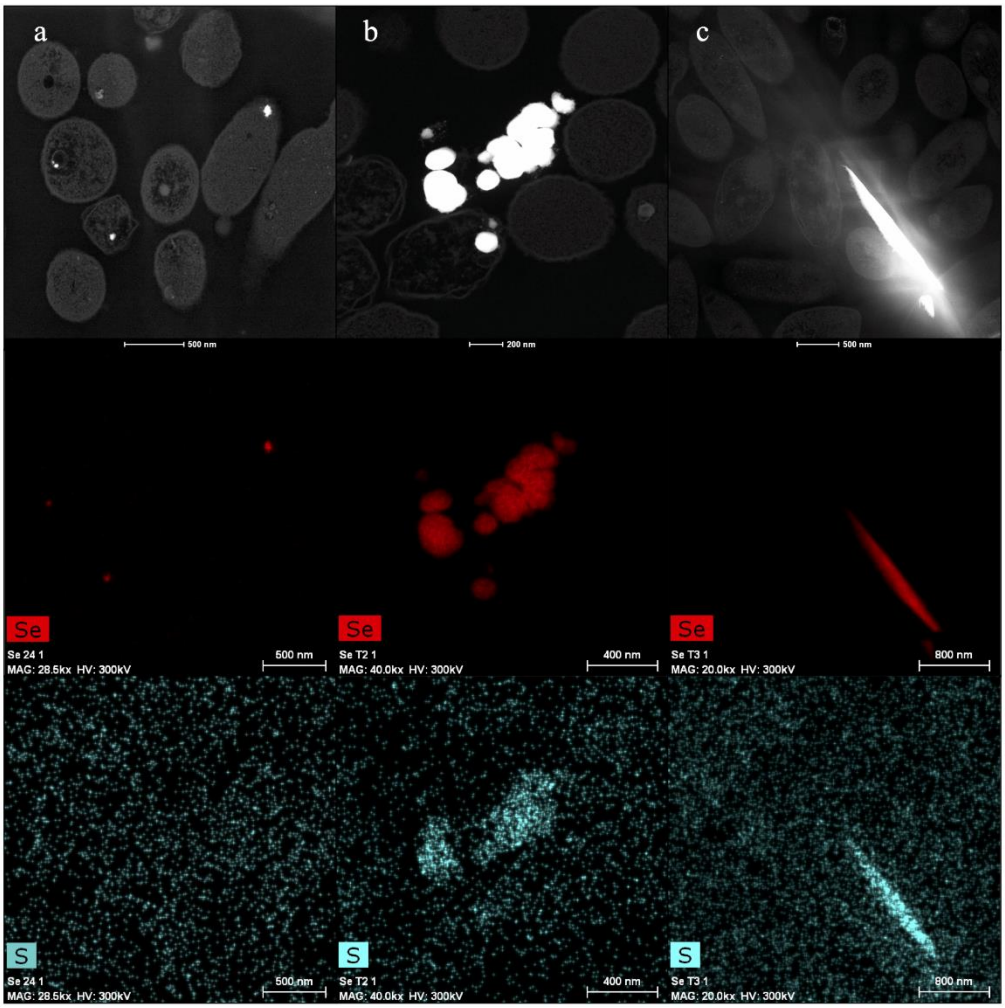

Fig. 9. Biotransformation process from a-nanospheres (a, 24 h), to an intermediate stage of amorphous aggregations (b, 72 h), which eventually turn into crystalline structures (c, 144 h).

4. Discussion

4.1. General overview of proteomics data

The comparison of the proteome detected between treatments showed that the majority of proteins were less abundant in the Se(IV)-treated samples than in the controls, especially during exponential and stationary phases. These results are in line with the effect of Se(IV) observed in *S. bentonitica* growth by Ruiz-Fresneda et al. (2018). The authors observed that BII-R7 growth was highly affected by the presence of the metalloid, with an extended lag phase and a lower final cell density as compared to the non-treated

samples (Ruiz-Fresneda et al., 2018). The lower percentage of proteins detected during the lag phase in Se-treated samples than in the untreated samples is consistent with what was previously observed, and the negative effect of Se(IV) in the bacterial growth is supported by the up-regulation of the RelE protein from RelE/RelB toxin-antitoxin system, promoting growth arrest in this phase (Kolodkin-Gal et al., 2009). However, total proteins for lag phase was slightly higher regarding exponential phase in Se(IV)-treated samples. Despite the lack of growth in this phase, the cells are metabolically active to cope with the toxicity of the oxyanion, reducing the amount of soluble Se(IV) in order to be able to grow, which could explain the higher number of proteins in lag phase for Se(IV) treated samples. According to Ruiz-Fresneda et al., (2020), the lag phase showed the same length regardless the initial concentration of Se(IV), which suggest that the growth is not recovered when certain amount of Se(IV) is reduced, but rather when the cells adapts to the damage caused by the toxic oxyanion.

4.2. Proteins involved in Se(IV) transport into the cells

In the present study, microscopic analysis of Se(IV)-treated cells of *S. bentonitica* showed intracellular Se(IV) reduction to Se(0) and subsequent formation of intracellular Se(0) nanospheres. It is well known that Se(IV) bioreduction to Se(0) as a detoxification mechanism takes places mainly in the cytoplasm, mediated by reduced biomolecules such as thiols (Antonioli et al., 2007; Nancharaiah and Lens, 2015), but bioreduction in the periplasmic space, whether via thiol groups exported to periplasm via ABC-type transporter (Pittman et al., 2005) or periplasmic enzymes (Gonzalez-Gil et al., 2016) is also likely to occur. However, there is very few information in the literature about how Se(IV) could reach the cytoplasm. Proteome analysis of *S. bentonitica* suggests involvement of outer membrane transporters like RND lipoprotein NodT, TonB-dependent transporters, metal transporters or porins. RND lipoprotein NodT was described for its role as a transporter for small molecules such as antibiotics and toxic compounds across the two cell envelopes operating with a primary ABC-transporter (ATPase subunit), also up-regulated in all growth phases, and a membrane fusion protein (MFP) (Ibrahim et al., 2012). The second family of outer membrane proteins with probable Se(IV) uptake function was the TonB-dependent receptor CircA (3.08 and 3.29 fold-changes in lag and exponential phase). However, the energy transducer TonB protein that interacts with the TonB-dependent receptor to perform the transport across the outer membrane (Noinaj et al., 2010) was down-regulated at all incubation time tested,

suggesting a different role, like signalling environmental information. Other metal cation transporters such as dicarboxylate/amino acid:cation symporter or magnesium transporter MgtE (found 4 and 1.6 fold higher in lag phase, respectively) were also detected. A phosphate selective porin OprP was up-regulated in lag and exponential phase (1.8 and 2.1-fold changes, respectively). According to this, Gonzalez-Gil et al. (2016) proposed that Se(IV) could reach the periplasm through outer membrane porins, and the porin-like protein ExtI along with ExtH has been recently related with Se(IV) uptake in *Geobacter sulfurreducens* (Jahan et al., 2019), suggesting a possible role of OprP in Se(IV) transport. The higher abundance of proteins from other transport systems like AcrAB, SmeE or CcmA, widely known to provide antibiotic resistance (Hayashi et al., 2015; Marquez, 2005), could play a role in maintaining the cell envelope integrity which could be disturbed by the presence of the oxyanion (Huang et al., 2014). Other proteins like lipocalin Bcl during the lag phase, or the down-regulation of the cell shape determination bactofilin CcmA, also suggest envelope stress (Campanacci et al., 2006; Taylor et al., 2020). This hypothesis is supported by the microscopy observations, where detachment of plasma membrane from cell wall can be observed in some cells, as reported by Poirier et al. (2016) in *Pseudomonas fluorescens* BA35SM1 when exposed to CdSe NPs. Exposure of *S. bentonitica* to U triggered a similar response. Transcripts of AcrAB, SmeED and TonB-dependent receptor were also up-regulated as a consequence of the interaction of the radionuclide with the cell. However, OprP transcripts were found down-regulated, probably to avoid the entrance of U inside the cells (Pinel-Cabello et al., 2021).

Previous studies reported that nitrate uptake systems could be involved in transport of selenite in *S. maltophilia* SeITE02, as inhibitors of this transport system resulted in a diminished Se(IV) uptake (Antonioli et al., 2007). However, it is also likely that down-regulation of Fis, Fur and FecR transcriptional regulators prevent the entrance of oxyanions, preventing cellular damage.

4.3. Proteins implicated in bioreduction of Se(IV) and formation of Se(0) NPs and Se volatiles species

It has been previously demonstrated the ability of *S. bentonitica* to reduce Se(IV) and form NPs of elemental selenium intracellularly during the first 24 h and extracellularly later (72-144 h) (Ruiz-Fresneda et al., 2018). Proteobacteria possess abundant thiol-containing compounds (Fischer et al., 2020), and several studies have described the contribution of glutathione (GSH), glutaredoxin or thioredoxin (THX) in

Se(IV) bioreduction (Khoei et al., 2017; Nancharaiah and Lens, 2015). Abundance of enzymes such as glutathione synthase, glutathione-disulfide reductase or thioredoxin-disulfide reductase, was modulated in Se(IV)-treated BII-R7 cells, suggesting their role in the reduction of this metalloid. Therefore, Se(IV) could interact quickly in the first place with the reduced thiols present in the cytoplasm. As they are consumed, the above-mentioned enzymes would be up-modulated in order to maintain the pool of reduced thiols. Antonioli et al. (2007) studied the role of GSH in *S. maltophilia* SeITE02 exposed to 0.2 mM Se(IV). They concluded that GSH plays a key role at the early steps of cell response to oxyanions (lag and exponential phases) and highlighted the importance of the glutathione reductase (GR) in keeping the pool of reduced GSH. This is in line with our results, which also show differences between growth phases in *S. bentonitica*. During lag phase, the cell uses the existent pool of reduced GSH and glutaredoxin for Se(IV) bioreduction, and starts the synthesis of new GSH molecules from glutamate, cysteine and/or glycine via the glutamate—cysteine ligase and glutathione synthase (GS) (1.5 and 2.1-fold change respectively). At the exponential phase, the strain simultaneously replenishes the GSH used via glutathione-disulfide reductase (2.1-fold change). It is also worth to mention the up-regulation of enzymes that produce NADPH, cofactor needed for the reduction of oxidised glutathione (GSSG), such as 6-phosphogluconate dehydrogenase (1.6 and 1.5-fold change in exponential and stationary growth phases) from the pentose phosphate pathway, during exponential and stationary phases. Down-regulation of other enzymes of the pentose phosphate pathway, like glucose dehydrogenase (-1.8 and -2.0-fold change in exponential and stationary phases, respectively), support the role of 6-phosphogluconate dehydrogenase in glutathione metabolism. The thioredoxin-disulfide reductase showed a similar behaviour than glutathione-disulfide reductase, suggesting that thioredoxin is also implicated in the Se(IV) bioreduction.

Other mechanisms for selenite reduction are likely to occur simultaneously. Enzymes such as 3-oxoacyl-ACP reductase (FabG), dioxygenase, or NADPH:quinone reductase, were highly induced during the lag phase (76.5, 27.3 and 10-fold change, respectively). FabG from the wide family of short chain dehydrogenases involved in fatty acid biosynthesis (Filip'echeva et al., 2018), was previously detected in *Pseudomonas moraviensis* subsp. stanleyae, showing Se(IV) reductase activity in presence of NADPH (Ni et al., 2015). Filip'echeva et al. (2018) also demonstrated the importance of FabG activity in both polar and lateral flagella assembly in *Azospirillum brasilense* Sp245.

However, systems for flagella assembly were down-detected in the case of *S. bentonitica.* Similarly, NAD(P)H reductases have been previously related to Se(IV) reduction in some bacteria, like *Burkholderia fungorum* strain 95 (Khoei et al., 2017). Proteins from old yellow enzyme (OYE) family involved in the reduction of activated alkenes, such as alkene reductase, showed a progressive increase of the fold-change over time (3-, 5.6- and 12-fold change in lag, exponential and stationary phase respectively). Hunter (2014) described the possible implication of a flavin oxidoreductase of this family, that uses NADH as cofactor in reduction of selenite to Se(0) and protection against oxidative stress in *Rhizobium selenitireducens.*

Furthermore, some proteins may also play a role in the formation and stabilization of SeNPs, controlling their size. It is the case of alcohol dehydrogenase, which has been previously found attached to SeNPs produced by *Escherichia coli* (Dobias et al., 2011), and also found in *S. maltophilia* SeITE02 (Lampis et al., 2017) and *P. seleniipraecipitans* in presence of Se(IV) (Hunter, 2014). Up-regulation of proteins for Fe-S cluster assembly were also identified in the present study, such as some members of the Suf system. Fischer et al. (2020) reported different proteins of this system attached at the surface of SeNPs produced by *Bacillus safensis* JG-B5T, suggesting their role in reduction and stabilization of the NPs. However, a possible implication of Fe-S cluster assembly proteins in oxidative stress response has been previously suggested (Poirier et al., 2016), such as SufC in *Lactobacillus reuteri* CRL 1101 (Gómez-Gómez et al., 2019). Ni et al. (2015) also proposed glutathione reductase as one of the main enzymes involved in nanoparticles formation in *P. moraviensis*, and suggested a probable function in stabilization and size control of the nanospheres. The hypothesis of bioreduction and stabilization of SeNPs mediated by thiol groups in *S. bentonitica* is supported by the accumulation of S in Se nanostructures, suggesting that GSH, apart from acting in Se(IV) bioreduction, could be implicated in biotransformation process of Se nanospheres to different nanostructures.

Furthermore, Khoei et al. (2017) also observed changes in the enzymatic mechanisms for Se(IV) reduction between growth phases in two strains of *B. fungorum*, and even in the cellular fractions where it takes place. Even though the majority of the positively modulated oxidoreductases are cytoplasmic, some periplasmic enzymes suggest that bioreduction can also occur in this cellular compartment, showing variations in the cellular fractions depending on sampling time in *S. bentonitica* as well. Bioreduction of Se(IV) in the periplasm has been previously demonstrated in other

bacteria, such as *Shewanella oneidensis* MR-1 via fumarate reductase (D.-B. Li et al., 2014).

These findings suggest that reduction in *S. bentonitica* takes place by different mechanisms that act synergistically throughout the entire incubation time. Ruiz-Fresneda et al. (2018) studied the reduction rate in this strain under the same conditions. The authors reported that 15% of the sodium selenite added to the culture medium was reduced after 24 h of incubation. The rate increased until 60% at 72 h, corresponding to the exponential growth phase, and recently demonstrated that 100% is reached after 120 h (Ruiz-Fresneda et al., 2020). The extended reductase activity observed could be due to the fact that Se(IV) bioreduction in *S. bentonitica* is not limited to Se(0)NPs formation. Recent studies have demonstrated the further reduction of Se(0) to volatile methylated forms including dimethyl diselenide (DMDSe) and dimethyl selenyl disulphide (DMSeDS) by means of a gas chromatography-mass spectrometry (GC-MS) system (Ruiz-Fresneda et al., 2020). Formation of volatile species of Se have been observed in other bacteria (Eswayah et al., 2019; Kessi, 2006), and even fungi (Eswayah et al., 2016). Several mechanisms have been proposed, which involve reduction and methylation reactions, and intermediaries like dimethyl selenone (Harrison et al., 1984) or methyl selenol (Eswayah et al., 2019) have been detected. Kessi (2006) reported that inhibition of glutathione synthesis in *Rhodospirillum rubrum* and *Rhodobacter capsulatus* resulted in a reduced formation of methylated Se, suggesting of thiol groups are also involved in reduction of Se oxyanion to selenide. It is the case of thioredoxin reductase, that catalyses two steps of the selenocompound metabolism: the transformation of selenite to hydrogen selenide and methyl selenic acid to methyl selenol. This enzyme is up-regulated in all growth phases in *S. bentonitica* possibly taking part in the formation of the volatile reduced forms of Se. Methyltransferases are probably involved in the transfer of methyl groups, such as thiopurine methyltransferase from *P. syringae* that uses S-adenosylmethionine (SAM) as methyl group donor (Ranjard et al., 2002). Thus, methyltransferases methylate hydrogen selenide to produce methyl selenol, which would also receive a methyl group from methyltransferases to form dimethyl-selenide. Methyltransferases were up-regulated at all incubation times in BII-R7, being some of them SAM-dependent such as class I rRNA methyltransferase in the stationary phase (2-fold change). These findings, along with the high abundance of thiol-metabolism enzymes (*e.g.*, glutathione-disulfide reductase, glutamate—cysteine ligase), suggest that thiols and methyltransferases are likely to be the pathway of Se-methylated products in

S. bentonitica. Biomethylated selenium is less toxic than other species of the metalloid, and provides an efficient mechanism for a long-term elimination of Se oxyanions in soil and water (Eswayah et al., 2016).

4.4.Proteins involved in ROS and stress protection

As a consequence of the high reductase activity to face Se(IV) toxicity, an increase of the oxidative stress would occur in the cells (Gómez-Gómez et al., 2019). This explains the increase of proteins involved in ROS and stress protection, such as catalases, DNA repair proteins, chaperones or proteases. It is the case of thiol:disulfide interchange protein DsbG, a disulfide isomerase that corrects non-native disulfide bonds and prevent aggregation of misfolded proteins, and also shows chaperone activity (Collet and Bardwell, 2002). The up-regulation of DsbG in lag phase (1.7-fold change) regarding non-exposed samples could indicate an increase of the protein damage in the periplasm as a consequence of the entrance of the oxyanion. However, the homologue DsbC was down-regulated in lag and exponential phases (-2.6 and -1.9-fold changes), as well as DsbA in exponential and stationary phases (-2.9 and -3.7-fold changes, respectively) (Nakamoto and Bardwell, 2004). Deletion of DsbA has been related to reduced motility, as it seems to be important for the structure of flagellar proteins (Collet and Bardwell, 2002), which could explain the down-regulation of proteins of type IV pilus assembly system or even flagellin (-16-fold change in exponential phase). It is important to highlight the great induction of the catalase/peroxidase HPI observed at 144 h (257-fold change), which has shown increased effectiveness under high doses of H_2O_2 (Poirier et al., 2016). The catalase HPII was also detected in the stationary phase, but in a lesser extent (2-fold change). The high over production of this enzyme when the Se(IV) reduction is complete, suggest the possible involvement of this protein in another process. Further studies are needed in order to elucidate the role of the catalase HPI in this growth phase. Proteins with oxidoreductase activity could also have a role in mitigate oxidative stress, such as luciferase-like monooxygenase, alkyl hydroperoxide reductase subunit F or subunit C (Poirier et al., 2016). ArsC, which reduces arsenate in presence of THX, GSH or glutaredoxin, and ArsH, both present in *ars* operon (Yang and Rosen, 2016), were also more abundant. Although conferring resistance to trivalent organoarsenicals has been recently described to be the physiological role of the ArsH (Yang and Rosen, 2016), studies have demonstrated that ArsH could act protecting from oxidative stress damage (Hervás et al., 2012; Vorontsov et al., 2007). The fold changes of these enzymes

progressively increased throughout the experiment, as well as the oxidative stress in the cells due to the reduction, which support this hypothesis.

4.5.Biotransformation of amorphous (a)-Se to trigonal (t) Se nanostructures

Production of a-Se nanospheres, with their subsequent biotransformation to crystalline Se nanostructures by *S. bentonitica* has been confirmed in this work by HAADF-STEM analyses. STEM micrographs showed the presence of a-Se nanospheres in all incubation times tested. These nanospheres were intracellular at earlier incubation times, appearing progressively in the extracellular media when increasing the incubation time, in line with previous observations by Ruiz-Fresneda et al. (2018) in the same strain. The ability to reduce Se(IV) to Se(0) have been described in many phylogenetically diverse microorganisms (Nancharaia and Lens, 2015). Wang et al. (2018) reported the biosynthesis of extracellular SeNPs in *Proteus mirabilis* YC801, while the NPs were intracellular in *P. moraviensis subsp.* stanleyae (Ni et al., 2015). *S. oneidensis* MR-1 also produced intracellular SeNPs under anaerobic conditions (D.-B. Li et al., 2014). In case of *S. bentonitica,* a-Se nanospheres are formed intracellularly, and afterwards are released to the extracellular space. Several mechanisms have been suggested to explain how these NPs are exported outside the cell (Debieux et al., 2011; Nancharaiah and Lens, 2015). Some authors proposed the formation of vesicles as a stress response in order to release the SeNPs (McBroom and Kuehn, 2007), cellular lysis or via specific transport such as Selenium factor A (SefA) described in *Thauera selenatis* (Debieux et al., 2011). Since lysed cells were found nearby some extracellular nanospheres and no vesicles were observed in the STEM micrographs, cellular lysis is probably the mechanism explaining the release of SeNPs in BII-R7. This hypothesis is supported by the higher induction of the toxin RelE during the exponential phase (3.3-fold change).

Once outside the cells, a-Se nanospheres undergo a transformation process leading to the formation of trigonal Se with different size and morphologies (polygons, nanowires, etc.). Amorphous and polygonal and needle-shape crystalline aggregations were found after 72 h of incubation, being the crystalline structures more frequent at 144 h. The amorphous aggregations presented irregular shape, suggesting an intermediate form before their transformation to *m*-Se nanostructures observed and lately to *t*-Se (Ruiz-Fresneda et al., 2020). These results are consistent with those obtained previously, where a-Se nanospheres formed at 24 h, started to coalesce and aggregate between 48-72 h of incubation, to form crystalline *t*-Se nanostructures at 144 h (Ruiz-Fresneda et al., 2018,

2019, 2020). In these studies, *m*-Se was suggested as a possible crystalline structure of the SeNPs produced by *S. bentonitica*, based on the results obtained with HAADF-STEM, XAS and Raman spectroscopy. However, the presence of *m*-Se in such nanostructures is demonstrated here for the first time, confirming the transformation process from *a*-Se to *m*-Se, and finally to *t*-Se, which is the most thermodynamically stable form of Se.

It has been proposed that SeNPs would act as seeds in a nucleation mechanism, allowing to increase the size following a process similar to Ostwald ripening (Lampis et al., 2017; Nancharaiah and Lens, 2015). In *S. bentonitica*, a-Se nanospheres seemed to coalesce along an axis, indicating the possible implication of flagella-like proteins as a template for aggregation (Ruiz-Fresneda et al., 2018), although some of these proteins were in lower amount than in control samples, like flagellin. Other authors have described the importance of organic capping compounds associated with the nanospheres in this process (Bao et al., 2016; Debieux et al., 2011; D. Xu et al., 2018). It is known that SeNPs synthesized by *S. bentonitica* are covered by an organic layer composed mainly by amine-rich proteins (Ruiz-Fresneda et al., 2020). Fischer et al. (2020) identified the proteins coating SeNPs formed by *B. safensis* JG-B5T. Many of them correspond with those detected in BII-R7, such as thioredoxin-disulfide reductase, glutathione reductase, SufC, D and B, or NADH-dependent alcohol dehydrogenase. These findings suggest that, after Se(IV) reduction, these enzymes could bind to SeNPs to stabilize them and to allow the aggregation to form the nanostructures, explaining the accumulation of S in the nanostructures by the adhesion of GSH or Suf system proteins, among others. Nevertheless, given that all the proteins found were intracellular, it is also possible that these proteins adhere to the NPs during cellular lysis (Fischer et al., 2020). Further studies should be performed to determine the role of specific proteins in the biotransformation process of a-Se nanospheres to *t*-Se.

4.6. Cellular mechanism of Se(IV) detoxification in S. bentonitica

Next-generation label-free shotgun proteomics along with microscopic observations carried out in the present work shed light on the molecular basis that enable the development of a cellular model of biotransformation of Se(IV) in *S. bentonitica* (Fig. 10). When BII-R7 is exposed to Se(IV), cells need to adapt to the toxicity caused by the metalloid in order to be able to grow. This occurs during the 48 h lag phase in Se(IV)-treated samples. The process begins with Se(IV) uptake, possibly mediated by proteins like RND systems, porins or other metal transporters across the envelopes. Meanwhile,

the oxyanion could also bind to the extracellular polysaccharide and membranes, causing envelope disruption. This would lead to activation of mechanisms that readjust envelope organization to maintain membrane homeostasis (lipocalin Blc, SmeE, AcraAB or CcmA) (Campanacci et al., 2006; Huang et al., 2014). Once inside the cell, Se(IV) would interacts with proteins, causing damage in their structure, which induce the activity of chaperones or proteases to avoid accumulation of misfolded proteins. The strain would use enzymes with oxidoreductase activity from different pathways to reduce Se(IV) to Se(0), with the subsequent production of SeNPs. Proteins from thiol metabolism, especially GSH synthesis (glutathione-disulfide reductase, glutamate—cysteine ligase, glutathione synthase, etc.) (Nancharaiah and Lens, 2015), 3-oxoacyl-ACP reductase FabG from fatty acid synthesis (Ni et al., 2015), or NAD(P)H-reductases are some of the proposed cytoplasmic enzymes (Khoei et al., 2017), although bioreduction could also occur in the periplasm mediated by quinones and flavin oxidoreductases (Gonzalez-Gil et al., 2016). After 48 h, all these mechanisms allowed the strain to cope with Se(IV) toxicity, and the exponential phase of growth begins. Bioreduction would also lead to the formation of volatile DMDSe and DMSeDS (Ruiz-Fresneda et al., 2020) by the activity of thioredoxin reductase and methyltransferases (Eswayah et al., 2016). Meanwhile, intracellular nanospheres would increase their size by an Ostwald ripening-like process as more Se(IV) is reduced (Lampis et al., 2017; Nancharaiah and Lens, 2015). As a result of the reduction, the oxidative stress would increase and ROS species would be generated, inducing proteins for DNA repair (DnaA, RadA, recombinases RmuC and RecA, etc.), chaperones (*e.g.,* ClpB), and catalases, such as catalase/peroxidase HPI, among others (Poirier et al., 2016). The damage produced by the levels of stress and the metalloid itself, in addition to the higher size of SeNPs, would induce proteins related to cell death as toxin RelE (Kolodkin-Gal et al., 2009), leading to the release of the nanosphere to the extracellular media. During the cellular lysis, different proteins would attach to the surface of SeNPs, forming the coating material observed (Fischer et al., 2020). This organic layer would trigger the coalescence of the a-nanospheres until the formation of aggregations of different sizes and forms. By the time that the strain reached the stationary phase after 100 h of incubation, all the Se(IV) was reduced, and amorphous and irregular aggregations would continue to coalescence, producing crystalline structures of *m*-Se over the incubation time, which eventually transformed in *t*-Se.

These findings indicate that *S. bentonitica* is able to efficiently remove toxic Se(IV) into a stable immobile form, reducing its bioavailability, and providing a starting

point to prioritize specific targets for further analysis. The label-free shotgun proteomic approach carried out in the present work provides high amounts of quality information data not only about proteins and enzymes implicated in the Se(IV) reduction process, but also the probable metabolic pathways that act against Se(IV) toxicity, giving a full overview of the response of *S. bentonitica* cells exposed to the oxyanion. Understanding the behaviour of the enzymes and biomolecules implicated in this process is of high importance not only for the development of bioremediation strategies, but also for the eco-friendly and cost-effective synthesis of nanomaterials for important technological applications, such as in electronic and biomedical industries.

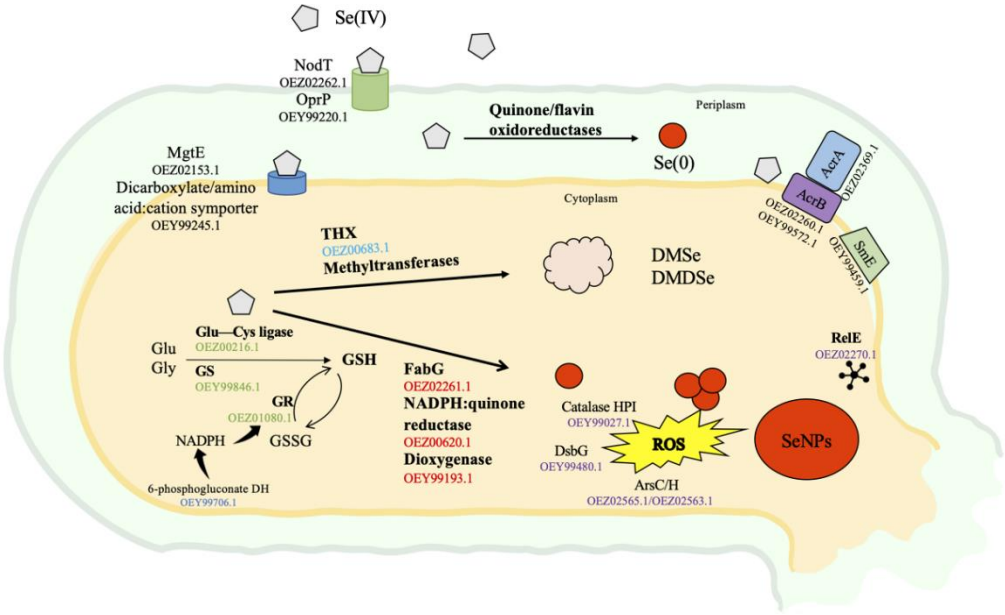

Fig. 10. Cellular mechanism of Se(IV) tolerance in *S. bentonitica* BII-R7. Se(IV) would be transported inside the cell, where it can be reduced until the formation of SeNPs or to volatile species (DMSe and DMDSe). The SeNPs would grow in the cytoplasm until their

5. Acknowledgements

This work was supported by the grants obtained by the first author FPU 15/04284 ("Formación de Profesorado Universitario") and EST 18/00610 ("Ayudas a la movilidad para estancias breves y traslados temporales") from Spanish Ministry (Ministerio de Educación, Cultura y Deporte), and grants CGL2014-59616-R; RTI2018.101548.B.I00 obtained by the last author. The authors are grateful to Concepción Hernández-Castillo and María del Mar Abad Ortega for their assistance at Microscopy services at the University of Granada ("Centro de Instrumentación Científica").

6. Supplementary material

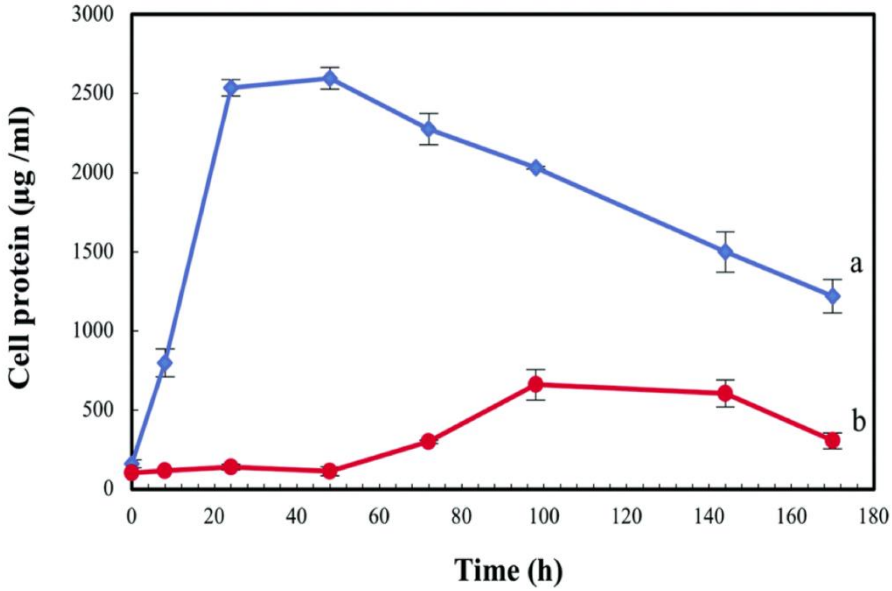

Figure S1 Growth curve of *S. bentonitica* in absence (blue line) and in presence of 2 mM of Se(IV) (red line). Image obtained from Ruiz-Fresneda et al. (2018).

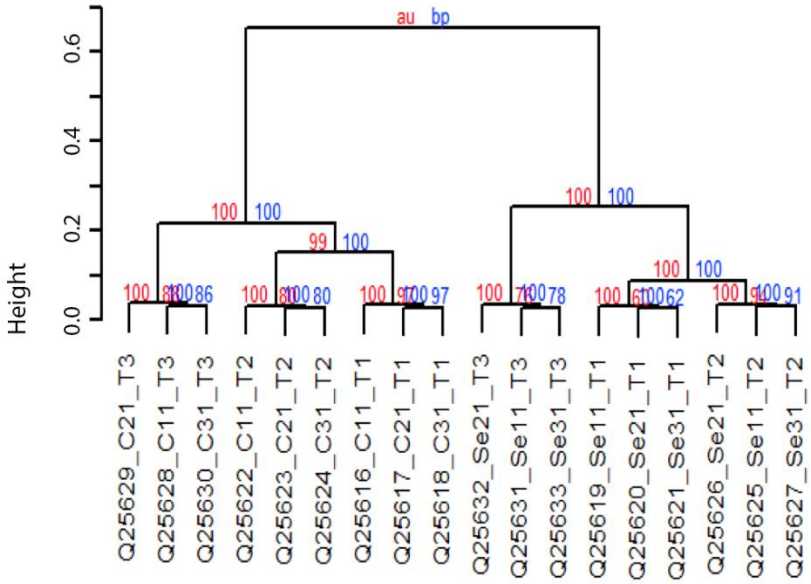

Figure S2. Hierarchical clustering of the samples according to the similarity of their proteomic profiles. Control and Se-treated samples were grouped separately, forming 3 subgroups each corresponding to the different growth phases. Boosstrap probability (bp) and approximately unbiased (au) values for each branch are also represented.

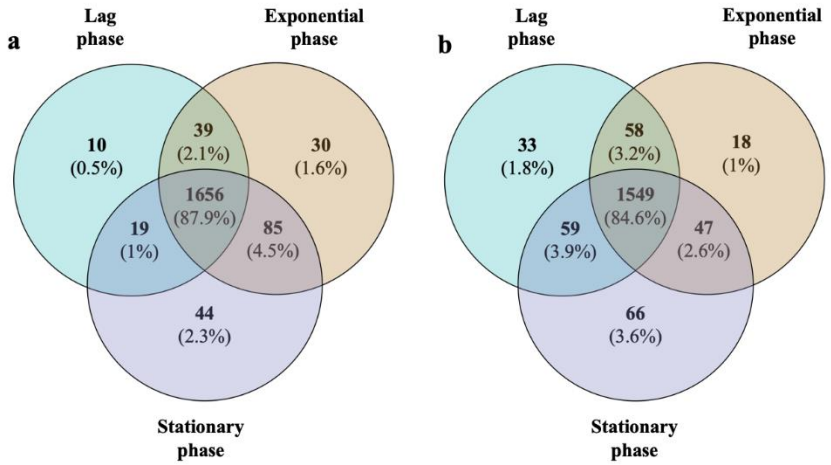

Figure S3. Venn diagrams comparing the growth-phase proteomes for non-treated (a) and Se-treated (b) samples. Around 86% of the proteins were common to the three growth phases in both conditions.

CHAPTER IV

Mechanisms for selenate resistance and formation of *t*-Se nanostructures in *S. bentonitica* BII-R7

María Pinel Cabello[1], María Victoria Fernández Cantos[1], Robert Geffers[2], Michael Jarek[2], Ruy Jauregui[3], Alexander Link[4], Mohamed L. Merroun[1]

[1]Department of Microbiology, University of Granada, Granada, Spain

[2]Genome Analytics, Helmholtz Centre for Infection Research (HZI), 38124 Braunschweig, Germany

[3]AgResearch Grasslands Research Centre, Tennent drive, Palmerston North, New Zealand

[4]Department of Gastroenterology, Hepatology and Infectious Diseases, University of Magdeburg, Leipziger Str. 44.39120, Magdeburg, Germany

Abstract

The rapid industrialization of the last decades has led to the appearance of toxic concentrations of highly mobile species of selenium (Se) in the environment. While the reduction of Se(IV) to nanoparticles of Se(0) (SeNPs) by bacterial strains has been widely reported, reduction of the most oxidized Se species, Se(VI), is limited to a few microorganisms. In this study, the bacterial strain *Stenotrophomonas bentonitica* BII-R7 showed its ability grow even a high concentrations of Se(VI), and to reduce it to less toxic Se(0). Transcriptomic approaches were applied on this strain in order to determine the specific mechanisms activated to cope with the toxicity of the metalloid. The results revealed that the metabolic response was highly different depending on the initial concentration of Se(VI): while genetic expression was highly induced under 50 mM of Se(VI), most of the transcripts detected under 200 mM were down-regulated. The transcriptome also showed that the resistance in BII-R7 is based on reduction of Se(VI), mainly through molybdenum-dependent enzymes such as respiratory nitrate reductase, the mitigation of oxidative stress by the activity of antioxidant enzymes such as glutathione peroxidase or glutathione S-transferase. On the other hand, microscopic analyses demonstrated the formation of nanotubes of monoclinic (*m*-Se) and trigonal Se (*t*-Se) for the first time, suggesting a biotransformation process that leads to long-term stable forms of Se(0). Hence, these results highlight the potential of *S. bentonitica* to remove Se(VI) from contaminated environments, and provides specific gene targets for further studies that allow to increase its effectiveness as bioremediation agent.

Key words: Selenium, bioremediation, *Stenotrophomonas*, transcriptomics, microscopy

1. Introduction

Selenium (Se) is a metalloid widely studied in the recent years due to the health benefits and multiple technological applications that offers (Nancharaiah and Lens, 2015; Ojeda et al., 2020). Industrial applications of this element include supplementation for cancer prevention and therapy (H. Tan et al., 2018), or their use in nanotechnology for electronical devices, among others benefits (Tan et al., 2016). Although Se is a micronutrient with important biological functions, the range between necessary and toxic concentration is very narrow, with detrimental effects in human health above 400 μg per day (Duntas and Benvenga, 2015; Nancharaiah and Lens, 2015). The damage caused by the excessive exposition to Se is not limited to human, affecting severely to wildlife in soil and aquatic ecosystems, with deformities, reproduction failure or mortality death among the frequent consequences (Chapman et al., 2010; Tan et al., 2016). Environmental sources of Se include natural processes like leaching and weathering of seleniferous rocks, but the major contribution to pollution comes from human activity such as metal refinery, mining, agricultural drainage or power generation (Shi et al., 2020b; Z. Zhang et al., 2018). Se can be found as selenate (SeO_4^{2-}), selenite (SeO_3^{2-}), elemental selenium (Se^0) and selenide (Se^{2-}) (Ojeda et al. 2020; Shi et al., 2020). SeO_4^{2-} and $SeO_3^{2-}$are the most toxic oxidation states of this element, given their high water-solubility and toxicity even at low concentrations (Zhang et al., 2018). Conventional physicochemical methods for SeO_4^{2-} remediation such as ion exchange, reverse osmosis or zerovalent iron treatment are expensive and produce high amounts of undesirable secondary residues (Sasaki et al., 2008; Tan et al., 2016). For this reason, it is necessary to design cleaner and cost-effective techniques for Se remediation.

The influence of naturally occurring microorganisms in the chemical speciation of these elements has increased the interest of their use as bioremediation agents, as microbial activity can reduce the solubility and bioavailability of organic and inorganic contaminants like heavy metals or metalloids (Yang et al., 2015b). Microbial activity impacts the geochemical cycle of Se via reduction, oxidation, methylation and demethylation reactions (Che et al., 2019). Se reduction in microorganisms can occur as a consequence of either dissimilatory metabolism, by using it as terminal electron acceptor, or as detoxification mechanism under aerobic and anaerobic conditions, to remove the harmful Se(VI) and Se(IV) oxyanions by producing Se(0) nanoparticles or methylated species of Se(II-) (Lopez-Fernandez et al., 2020; Nancharaiah and Lens, 2015). Many taxonomically diverse microbial species have been reported for Se(IV)

reduction in different environments, identifying several enzymes that take part in the process, such as thiol containing enzymes, fumarate reductase or NADP(H) dehydrogenases (Hunter, 2014; Song et al., 2017; Y. Tan et al., 2018). However, only few microorganisms are able to reduce Se(VI) to Se(0), in contrast with microbial reduction of Se(IV). A periplasmic selenate reductase (Ser) was described in *Thauera selenatis* as part of the electron transport chain, reducing the oxyanion in anaerobic respiration (Krafft et al., 2000; Schröder et al., 1997). In the same way, Kuroda et al. (2011) also identified a membrane-bound respiratory selenate reductase encoded by *srdBCA* in *Bacillus selenatarsenatis* SF-1. Se(VI) reduction has been also described in aerobic conditions, like *Enterobacter cloacae* SLD1a1 via membrane enzymes, *Pseudomonas stutzeri* NT-I or *Comamonas testosteroni* S44, and even in fungal strains such as *Aspergillus clavatus* (Ridley et al., 2006; Y. Tan et al., 2018; Urík et al., 2016).

Transcriptomics have been previously used to study differential gene expression in bacteria exposed to metals, such as Cr, Cd, U (Hu et al., 2005; Pinel-Cabello et al., 2021, chapter II; Zhang et al., 2014) or even sodium selenite (Yang et al., 2021). However, omics-based techniques have been barely applied in selenate reduction, which results in a lack of knowledge about the cellular response to Se(VI) exposure and the specific mechanisms involved in this process. Furthermore, most of the previous investigations of bacterial tolerance to Se(VI) have been performed under low concentrations (<50 mM) and are focused only on specific genes, rather than the general response of the cell. The transcriptional response of the anaerobe *Desulfuribacillus stibiiarsenatis* MLFW-2 in presence of different terminal electron acceptors, including 5 mM of Se(VI) (Abin and Hollibaugh, 2018). Debieux et al. (2011) identified the secreted proteins to the extracellular media by *T. selenatis* when was exposed to 10 mM of Se(VI). Similarly, proteomics approaches were used to study the effect of high concentrations of Se(VI) in *Herbaspirillum* sp. WT00C, and detected changes not only in the protein profile, but also in the growth and morphology of the cells (Chen et al., 2020).

Stenotrophomonas bentonitica BII-R7 is a Gram-negative bacterium isolated from bentonites from south-east of Spain, which showed high levels of tolerance to different heavy metals (Lopez-Fernandez et al., 2020; Ruiz-Fresneda et al., 2020; Sánchez-Castro et al., 2017b). Recent transcriptomic analyses performed in this strain enable to elucidate the mechanisms carried out by the cells when grew in presence of U(VI) (Pinel-Cabello et al., 2021). A cellular model for Se(IV) reduction to Se(0) nanoparticles (Se(0)NPs) and the biotransformation to different nanostructures has been

proposed by using label-free proteomics, highlighting the role of thiol groups (*e.g.* glutathione), oxidoreductases (*e.g.* NAD(P)H-reductases) and proteins with antioxidant activity (*e.g.* catalase/peroxidase HPI) in the detoxification mechanism of this Se oxyanion (Chapter III). BII-R7 is also able to grow even at 200 mM of Se(VI), reducing it to Se(0). However, the processes underlying Se(VI) tolerance in this strain remain still unknown. The present work is focused on shed light on the mechanisms of Se(VI) resistance in *S. bentonitica* growing under 50 and 200 mM of Se(VI) in aerobic conditions. The combined use of transcriptomics and microscopic techniques allowed the identification of genes potentially implicated in Se(VI) resistance and reduction, providing specific molecular targets for further studies, as well as the characterization of the products yielded by the reduction process. The results obtained here provide a better understanding of bacterial Se(VI) reduction and resistance, which is of high relevance for the design of effective bioremediation techniques. Furthermore, valuable reduced products generated during the process can be used for many industrial applications, reducing the environmental impact of the synthesis of nanomaterials.

2. Materials and methods

2.1.Bacterial strain and culture conditions

The bacterium used in this work has been isolated by our research group from Spanish bentonite formation in Cabo de Gata Nature Park (Almería, Spain), described as *S. bentonitica* BII-R7 (López-Fernández et al., 2014; Sánchez-Castro et al., 2017b). The cells were grown aerobically in liquid Luria Bertani (LB) broth medium (tryptone 10 g L-1, yeast extract 5g L-1 and NaCl 10 g L-1, pH 7.0 ± 0.2) at 28ºC under shaking at 180 rpm.

2.2. Bacterial reduction of Se(VI) and effect on S. bentonitica growth

Cell suspension from 24 h-old culture of *S. bentonitica* in LB liquid medium was used to inoculate LB liquid medium amended with sodium selenate (Na_2SeO_4), at an initial optical density (OD_{600}) of 0.1. A stock solution of the metalloid was prepared at a concentration of 1M. For this purpose, Na_2SeO_4 (Sigma-Aldrich) was dissolved in distilled water, and sterilized by filtration using 0.22 µm syringe filters. Appropriate amount of selenate was then added to the culture medium to obtain a final concentration of 50 and 200 mM. The cultures were incubated at 28ºC under shaking at 180 rpm. Biotic and abiotic controls were also incubated under the same conditions. The effect of the presence of the metalloid on growing cells was addressed by correlating the increase in

the cell growth with the total protein content. To that end, cells were grown aerobically as described in LB liquid medium supplemented with 50 and 200 mM of Se(VI) as described in section 2.1. Bacterial cultures without Se(VI) were used as controls. Samples were collected by centrifugation at 9000 rpm for 10 min at different intervals, and washed with NaCl (0.9 %). The resultant pellets were resuspended in extraction buffer (SDS 99%, Na_2HPO_4, Triton X-100 and β-Mercaptoethanol 99%) and stored for 24 h at -20ºC. Cells were then sonicated (Vibra cell™) with 30% amplitude and 7 cycles of 15 sec with an interval of 10 sec between cycles, followed by centrifugation at 9000 rpm for 20 min at 4ºC. Total protein content in bacterial cells extracts was measured using Bradford reagent (Bradford, 1976), and BSA was used as standard.

2.3.Sample preparation for transcriptomics analysis

Cultures of *S. bentonitica* were grown as described in the section 2.2. Samples were collected at different incubation times, corresponding to lag, early, middle and late exponential growth phases. No lag phase was observed in the growth of *S. bentonitica* for untreated cells. For this reason, sampling time for lag and early exponential phases were the same in these samples. Samples were harvested by centrifuging at 5,000 x *g* for 15 min at 4ºC. The supernatant was discarded and the pellet was resuspended in phenol 5% in absolute ethanol before its storage at -80ºC.

Extraction of total RNA was carried out using the RNeasy Bacteria Mini kit (Qiagen, Germany) with mechanical lysis of the cells using Fast-Prep®-24 (MP) and adding acid-washed glass beads (212-300 µm; Sigma-Aldrich). Total RNA was treated with TURBO DNA-free kit (Ambion, TX, USA) in order to eliminate possible contaminating DNA in the samples, followed by a clean-up protocol from RNeasy Bacteria Mini kit according to manufacturer's instructions. Total RNA obtained was finally eluted using nuclease-free water and 1 mM of EDTA was added to each tube for preservation of the samples. The amount of RNA extracted was measured in Qubit 3.0 Fluorometer (Life Technology). The quality of each sample was checked on 1.5% (w/v) agarose electrophoresis gel in 1X TAE buffer.

2.4.Sequencing and processing of transcriptome data

Quality and integrity of total RNA was controlled on 5200 Fragment Analyzer System (Agilent Technologies). The RNA sequencing library was generated from 500 ng total RNA using Ribo-off rRNA Depletion Kit (Bacteria) (VazymeBioTechCo.Ltd.) for rRNA depletion followed by NEBNext® Ultra™ II Directional RNA Library Prep Kit

(New England BioLabs) according to manufacturer's protocols. The libraries were treatedwith Illumina Free Adapter Blocking and were sequenced on Illumina NovaSeq 6000 using NovaSeq 6000 S1 PE Reagent Kit (100 cycles) with an average of 20 $x10^6$ reads per RNA sample.

2.5.Biostatistical analysis of transcriptomics data

Processed data were treated as described in Pinel-Cabello et al., (2021) for their analysis. Briefly, a reference of the genome of *S. bentonitica* was used to generate index files, and paired-end read files of the 33 samples were mapped using BBMap program version 37.90 (sourceforge.net/ projects/bbmap/), producing SAM format files. Mappings were collected in samtools (v. 1.8) with quality scores ≥ 30. The mapcount program (https://github.com/mpcox/mapcount) was used to generate read counts per gene for each of the SAM files. A total of 247 millions of read counts were obtained. Each sample produced an average of 75 millions of reads of 51 nucleotides of length.

Previous annotation was performed with SEED-based method of Subsystem Technology (RAST, version 2.0), and transcripts were normalized to transcript per million (tpm). Subunits LSU and SSU of rRNA were removed and genes with less than 500 tpm were not considered for further analyses. Annotation of hypothetical proteins were verified using the Basic Local Alignment Search Tool (BLAST). Preliminary comparison of RNA profiles of the 33 samples was carried out by Past 4.02 using Bray-Curtis similarity index. One-way ANOVA ($p<0.05$) with Bonferroni correction was used to determine the differences in genetic expression between the treatments in GraphPad Prism 9 software.

2.6.Characterization of Se(VI) reduction products by electron microscopy

2.6.1. *STEM-HAADF/EDX analysis*

High-angle Annular Dark Field Scanning-transmission Electron Microscopy (HAADF-STEM) coupled with energy dispersive X-ray (EDX) spectrometer was used to determine the location, size and morphology of reduced Se(0). Selected-area electron diffraction (SAED) and high resolution TEM combined with fast Fourier transform (FFT) enabled the structural characterization of Se nanostructures.

To that end, samples treated with 200 mM of Se(VI) of 24 and 48 h of incubation were harvested and prepared according to Merroun et al. (2005), and then analysed in

HAADF-STEM FEI TITAN G2 80-300. TEM specimen holders were cleaned by plasma prior to analysis in order to minimize sample contamination.

2.6.2. *Environmental Scanning Electron Microscopy*

Characterization of products of Se(VI) reduction was performed using Environmental Scanning Electron Microscopy (ESEM) equipped with secondary (ETD) and circular backscatter electron detectors (CBS). Cells of *S. bentonitica* growing in 200 mM Na_2SeO_4 were taken at 24 and 48 h of incubation by centrifugation (11,000 rpm for 5 min at 4ºC) and washed twice with 0.9% NaCl. Cells were fixed for 24 h at 4ºC in 2.5% glutaraldehyde in 0.1M cacodylate buffer (pH 7.2), and washed three times in the same buffer. The pellets were then fixed in 1% osmium tetroxide solution (OsO_4) in cacodylate buffer and dehydrated in graded ethanol solutions and the critical point method. Samples were finally coated with carbon and analysed in ESEM microscope (FEI QUEMSCAN 650F) with an X-ray microanalysis system Dual EDS XFlash Bruker with XFlash 6/30 detector.

3. Results

3.1. Effect of Se(VI) in the growth of S. bentonitica

S. bentonitica BII-R7 was able to grow at both 50 and 200 mM of Se(VI) concentrations, although the presence of the metalloid affected the growth of the strain. The presence of Se(VI) triggered an extension of the lag phase compared to control samples, where no lag phase was observed (Fig. 1). Prolongation of the lag phase was concentration-dependent, lasting 8 h in presence of 50 mM and even 24 h in cells exposed to 200 mM. Exponential growth lasted until 48 and 72 h of incubation for 50 and 200 mM of Se(VI), respectively.

Cultures amended with 200 mM of Se(VI) adopted a reddish color around 24 h of incubation with BII-R7, indicating that Se(VI) reduction to Se(0) took place (Fig. 2). No change of color was observed either in cells treated with 50 mM nor untreated samples and abiotic controls, which reveals that the process is carried out actively by *S. bentonitica* cells in response to high concentrations of Se(VI).

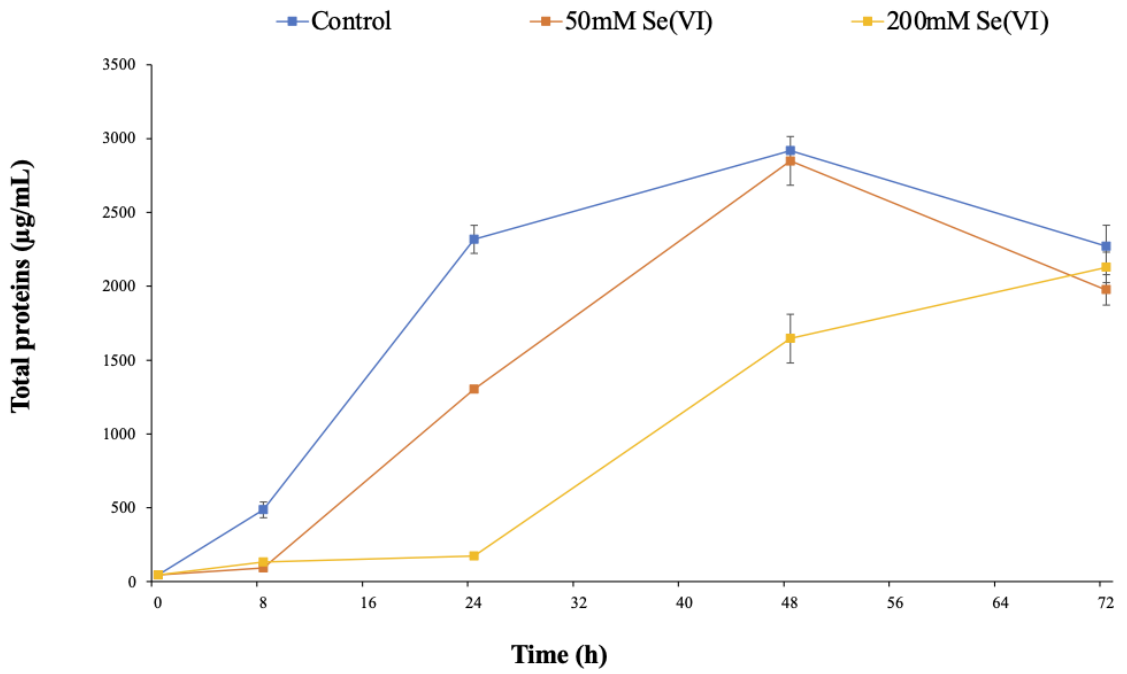

Fig. 1. Effect on the growth of *S. bentonitica* BII-R7 in presence of an initial concentration of 50 and 200 mM of Se(VI). The growth was determined by measuring total proteins in each sampling time to avoid posible interferences of the reduced Se products.

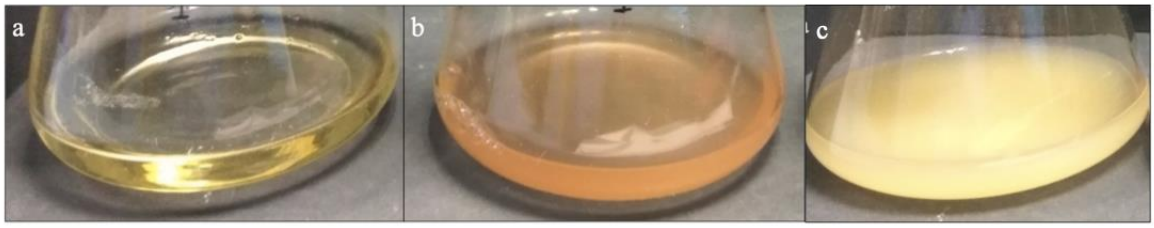

Fig. 2. Change of colour of the cultures of *S. bentonitica* BII-R7 amended with 200 mM (b). The coloration of the abiotic control (a), as well as the non-treated cells (c) remained unchanged throughout the incubation time.

3.2. General overview of transcriptome data

Transcriptomic analysis was performed to determine the differential gene expression between Se(VI)-treated and non-treated cells, and to identify the genes potentially involved in Se(VI) reduction and resistance. For this purpose, RNA libraries were constructed. The analysis yielded a total of 247 millions of read counts, with 247,500 millions of sequenced nucleotides. Each sample produced an average of 75 millions of reads of 51 nucleotides of length. The 4191 transcripts detected were aligned with the genome sequence of *S. bentonitica* (NCBI Genebank accession number MKCZ00000000.1). Samples of all treatments and collection times were grouped according to the similarity of their RNA profiles, so as to compare the cellular response under the different conditions tested. As it is shown in Fig. 3, samples treated with 200 mM of Se(VI) were grouped together in a cluster completely separated from both non-

treated samples and those exposed to 50 mM of Se(VI). These results indicate that the cells behave entirely different when grow in presence of elevated concentrations of the metalloid, in contrast with lower concentrations where the RNA profiles were more similar to untreated samples. Furthermore, replicates of 50 mM of Se(VI) and untreated cells paired according to the growth phase, except for samples corresponding to 50 mM of Se(VI) at early exponential phase, which clustered with those belonging to middle-exponential phase.

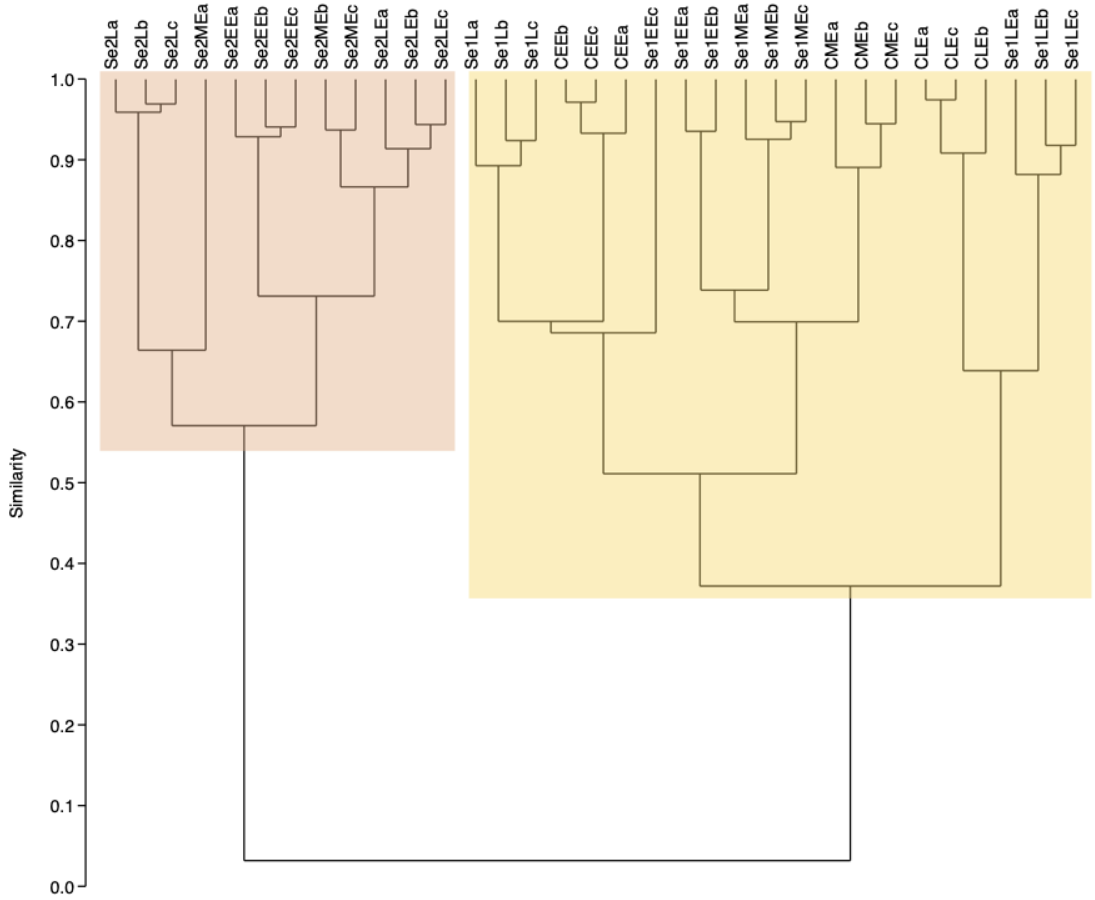

Fig. 3. Clustering of the samples according to the Bray-Curtis similarity index. Replicates of samples treated with 50 mM of Se(VI) (Se1) were grouped grouped with the untreated samples (C) (yellow squeare), while samples treated with 200 mM (Se2) were sepparated regardless the growth phase (lag (L), early (EE), middle (ME) and late (LE) exponential phases).

As it was expected, the number of down-regulated transcripts increased with higher concentrations of Se(VI) (Fig. 4) Furthermore, no significant up-regulation of gene expression was observed under 200 mM, as a consequence of the toxicity caused by the high concentration of the metalloid. Interestingly, many genes showed a high up-regulation when BII-R7 grew at 50 mM of Se(VI), even though no change of colour was observed in this culture during the experiment. In these conditions, the highest fold changes were found at lag phase, while the level of induction decreased progressively

during early and middle exponential phase (Fig. 4A). On the contrary, the number of up-regulated transcripts showed a gradual increase throughout the exponential phase. When the cells reached the late exponential phase, a sharp drop of gene expression was observed, diminishing both fold change and number of induced genes at this stage.

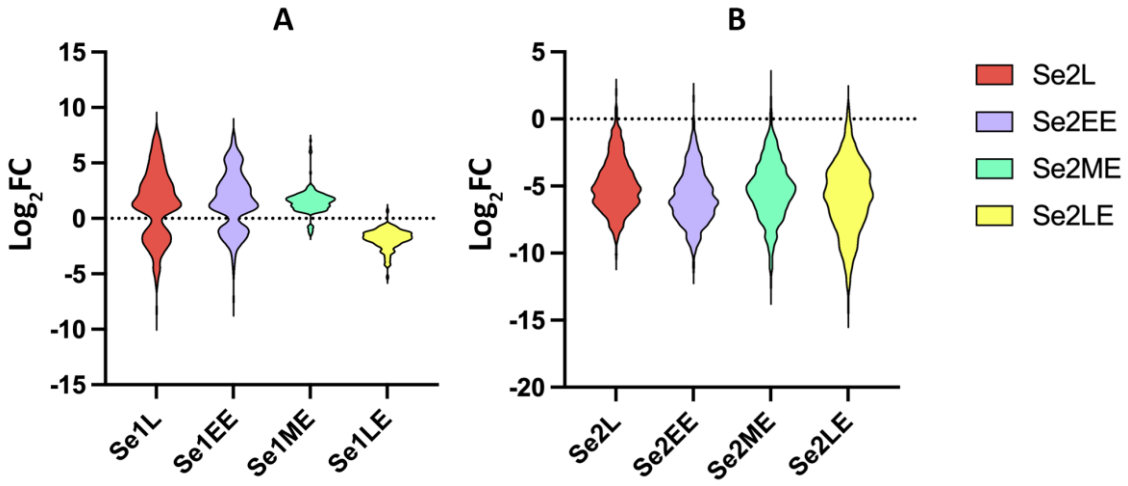

Fig. 4. Transcript modulation at lag (L), early (EE), middle (ME) and late (LE) exponential phases when *S. bentonitica* cells were exposed to 50 mM (a) and 200 mM of Se(VI) (b).

3.3. Specific response of S. bentonitica to Se(VI) over time

The presence of Se(VI) in the culture media led to a complex biological response with the differential expression of genes from very diverse metabolic pathways, which suggest that the oxyanion may affects many physiological processes. The expression of genes involved in motility, transport function, oxidative stress, carbon and lipid metabolism, and DNA/RNA processing, among others, were modulated during the growth of the strain at both Se(VI) concentrations tested. Furthermore, modulation of the expression of these genes between the different growth phases indicates the implication of multiple enzymatic mechanisms for Se(VI) detoxification, depending on the physiological state of the cells and/or the different stages of the process.

During the lag phase of cells treated with 50 mM of Se(VI), it is worth to mention the high induction of a short-chain dehydrogenase family enzymes. The most induced was an hypothetical protein and the NADPH-dependent aklaviketone reductase (220-fold change), followed by an another NAD(P)H-dependent oxidoreductase (151-fold change). A 3-oxoacyl-ACP reductase FabG from the same family was also detected, but to a lesser extent (16-fold change). In addition, oxidoreductases from other families were represented during this phase, such as FMN-dependent NADH-azoreductase (48-fold change), two xanthine dehydrogenase family proteins (52- and 27-fold change for

molybdopterin-binding and M subunits), malonic semialdehyde reductase or alkene reductase (11- and 6-fold change, respectively), among others. Several efflux systems were also up-regulated in this phase. Within the last group, different RND efflux systems like permease and periplasmic adaptor subunits (150-fold change and 76-fold change) and lipoprotein from NodT family (133-fold change), TonB-dependent receptor (probable vitamin B12 transporter BtuB, 64-fold change) or ABC transporters (24-fold change) were identified. It is interesting to mention the induction of genes from the *ars* operon for arsenic detoxification. Transcripts of arsenic resistance protein ArsH, arsenical efflux pump ArsB were detected, both up-regulated 4-fold, as well as arsenate reductases ArsC (with 4-, 5- and 6-fold changes) that use glutaredoxin and thioredoxin.

However, when cells started the exponential phase, the most induced transcripts were annotated as different subunits of the respiratory nitrate reductase (180-, 154- and 152-fold change for beta, gamma and alpha subunits, respectively; 129-fold change for molybdenum cofactor assembly chaperone). Furthermore, two nitrate/nitrite transporters NarK were also up-regulated, with 77- and 18-fold changes each. Other up-regulated genes encoded for enzymes with oxidoreductase activity and cytochromes were also detected in this growth phase, such as cytochrome d ubiquinol oxidase subunits I and II (50- and 64-fold changes respectively) or two oxygen-independent coproporphyrinogen III oxidases (60- and 21-fold changes), and even some of them were also found during lag phase, like xanthine dehydrogenases (79- and 36-fold changes for molybdopterin-binding and M subunits). Genes of enzymes for molybdenum cofactor synthesis MoeA (58-fold change), MoaE (56-fold change) and MoaC/B (31-fold change) were also induced, probably to support the activity of some of the mentioned reductases. Interestingly, there was an increase of the number of vitamin B12 TonB-dependent receptors BtuB up-regulated. During the middle-exponential phase, genes of valine degradation metabolism showed the highest fold changes regarding the untreated samples. These genes were a methylmalonate-semialdehyde dehydrogenase, two enoyl-CoA hydratase and a 3-hydroxyisobutyrate dehydrogenase (129-, 86-, 66- and 64-fold change, respectively). A potassium-transporting ATPase ATP-binding subunit KdpB followed these genes with 17-fold change. Iron ABC transporters (5- and 3.4-fold changes), a ferric enterobactin TonB-dependent receptor (2-fold-change), and Sec system for protein translocation were some other up-regulated genes with transport function at this sampling time.

Regarding the thiol metabolism, transcripts of glutathione S-transferase were up-regulated, especially at the lag phase (6.7-fold change), decreasing in the early and middle-exponential phase (1.8- and 2.2-fold changes, respectively), as well as glutathione peroxidase, with a slight up-regulation during the lag phase (1.5-fold change). Glutaredoxins from Grx4 were induced throughout the incubation time (3-fold change for lag and early exponential phase; 2.1- and 3.6-fold changes at middle-exponential phase), while one from Grx3 family was significantly up-regulated 2.9-fold during the lag phase. In addition, a Trx1 family thioredoxin was also induced at lag and middle-exponential phases (2.6- and 1.8-fold changes, respectively). It is interesting to notice the differential induction of the glutathione/L-cysteine ABC exporter CydD during the exponential growth, particularly at the beginning (7- and 3-fold changes for early and middle-exponential growth).

Furthermore, the expression level of genes related to modifications at the membrane level, oxidative stress and motility increased significantly. Within the first group are included outer membrane proteins such as OmpW, especially at the middle of the exponential growth (47.6-fold change) or lipocalin Blc, which maintained similar levels during lag and early exponential phases (45.4 and 42.2-fold changes). A ferritin-like diiron-containing protein expressed under stress conditions (97.3-fold change at lag phase), the catalase KatE or the universal stress protein UpsA (especially at the early exponential growth, with 113.2- and 46.2-fold changes for KatE and UpsA respectively) are some of the modulated genes in response to stress. Lastly, transcripts related to proteins involved in motility processes were also detected, such as chemotaxis or twitching motility proteins. In particular, the expression levels of genes encoding for two flagellin FliC and two genes encoding for chemotaxis proteins highlighted during the lag phase, due to their high induction with regard the control samples (163- and 118-fold for FliC, and 129.8 and 99.6-fold in case of chemotaxis proteins).

On the other hand, at the end of the exponential phase, there was almost no significant differences between the gene expression of untreated cells and those treated with 50 mM of Se(VI), and only a transcript of a cold shock protein of CSP family showed a slight up-regulation (1.6-fold change).

In contrast with the results observed at 50 mM of Se(VI), where a great amount of genes were positively modulated, the increase of the concentration of Se(VI) to 200 mM triggered the opposite response. All the detected transcripts were negatively modulated when cells were exposed to a high concentration of Se(VI). In addition, it was

observed that the expression levels decreased at higher incubation times. Interestingly, down-regulated genes at lag and early exponential phase were mainly the same, although the transcripts detected were lower in the last sampling time. Those genes belonged to many diverse metabolic pathways, and several proteases were found within the transcripts with lower fold changes. A C4-dicarboxylate transporter was the most down-regulated gene with -1229.2 and 2523.6-fold changes at lag and early exponential phases, followed by two metallopeptidases (-1082.8 and -550.7-fold in lag phase, and -2180.6 and -995.6-fold at the beginning of the exponential phase each one). However, at the middle-exponential phase, the transcripts strongly down-regulated were mainly different from those observed in previous phases. Thus, the most down-regulated genes were the ferritin-like domain-containing proteins YciF and YciE (-6823.6- and -3919-fold changes respectively), a PAS-containing domain S-box protein (-4508.8-fold down-regulated), and a SDR family oxidoreductase (-2490-fold change), among others. Finally, in the late exponential phase, a hypothetical protein and a putative lipoprotein showed the highest down-regulation, with -19121.2- and -16339.9-fold changes. They were followed by a lytic transglycosilase-like domain-containing protein and NAD(P)/FAD-dependent oxidoreductase, being -9284.2 and -6575.1-fold down-regulated compared to non-treated cells, respectively.

3.4.Characterization of Se(VI) reduction products by electron microscopy

3.4.1. *Environmental Scanning Electron Microscopy (ESEM)*

Cells of *S. bentonitica* exposed to 200 mM of Se(VI) for 24 and 48 h were analysed by environmental scanning electron microscopy to characterize the morphology, size and structure of reduced Se(VI) nanoparticles and their location in the cells. Electrodense accumulations were observed mostly intracellularly, but also embedded in the matrix of flagella-like structures (Fig. 5 b and c). The shape of the structures seemed to be mainly nanowires. Apparently, some spherical nanostructures were also observed, although it is not clear if they correspond to the axial view of the nanowires (Fig. 5 c). Interestingly, this analysis also showed that the number of the nanostructures decreased over incubation time, finding more nanostructures at 24 h than 48 h of incubation. Energy dispersive X-ray revealed the presence of Se in the composition of the nanostructures (Fig. 5 f), confirming the reduction of the oxyanion.

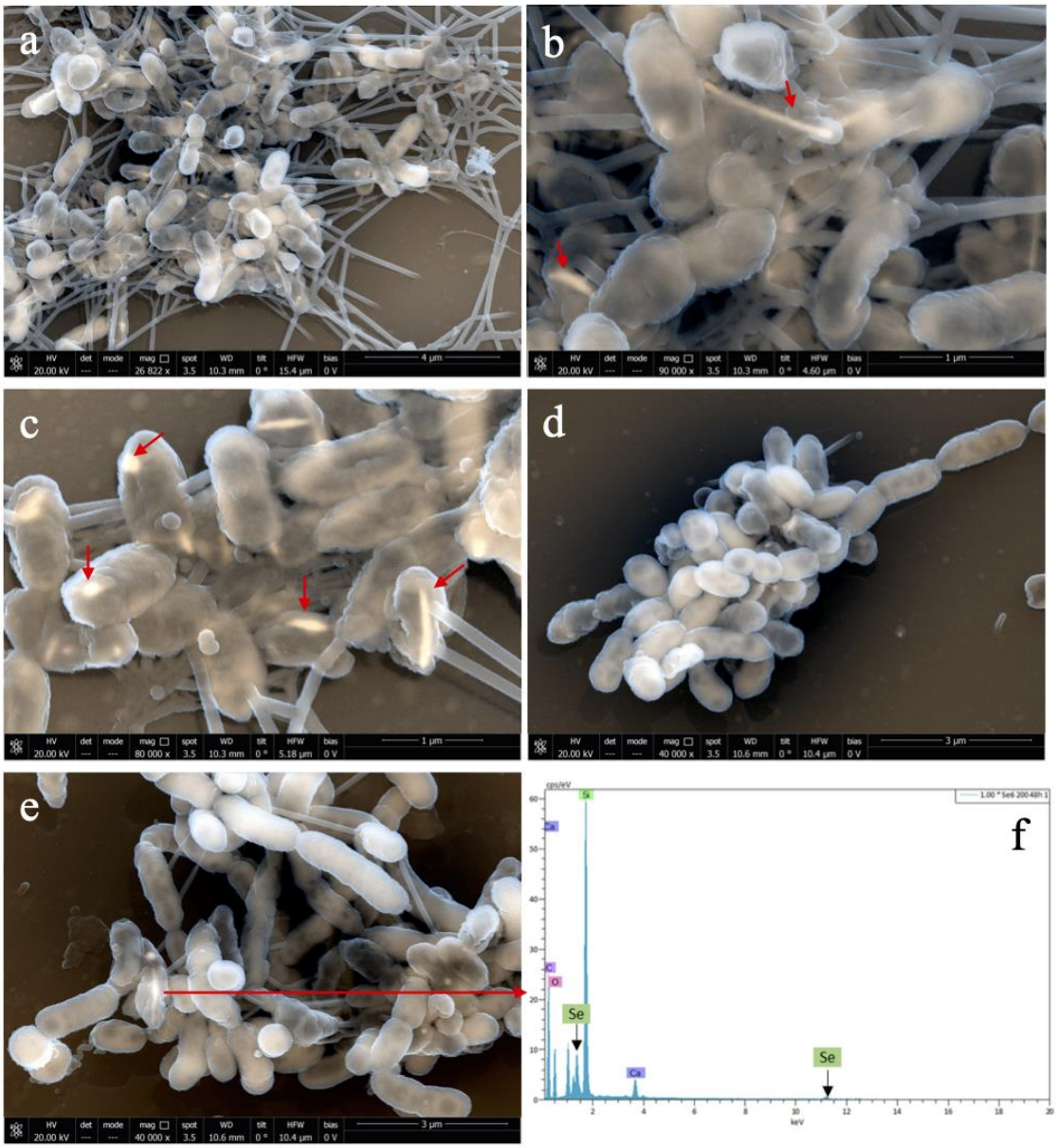

Fig. 5. ESEM images of *S. bentonitica* cells in presence of 200 mM of Se(VI) after 24 (a, b, c) and 48 h of incubation (d and e). EDX analysis show that the nanostructures were composed by Se (f).

3.4.2. *STEM-HAADF/EDX analysis*

Analysis of STEM-HAADF of the nanostructures formed after 24 and 48 h of incubation with 200 mM of Se(VI) enabled the further characterization of the nanostructures, and confirmed the location and the shape of the nanowires previously observed by ESEM. Similarly, intracellular nanowires were found, as well as some irregular nanostructures in a lesser extent (Fig. 6, 7), decreasing the number of nanostructures detected throughout the incubation time. Again, EDX showed Se as the main composition of the structures, however, a small peak corresponding to S was also detected (Fig. 6 E). This is in line with the results of elemental mapping, where

accumulation of S in the nanostructures was also observed (Fig. 6 C, D). Nevertheless, no significant S was detected in nanostructures after 48 h of incubation (Fig.7 D).

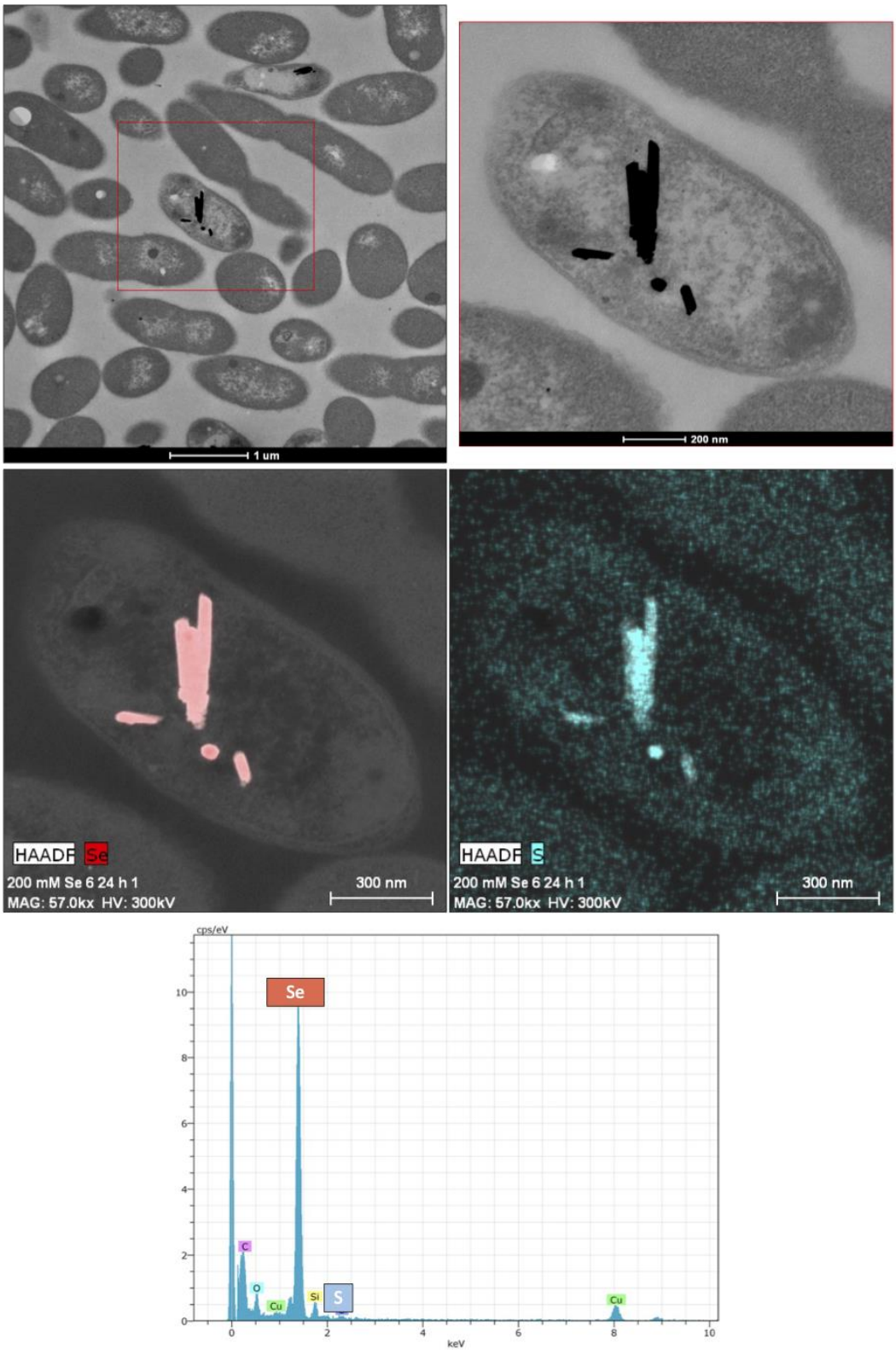

Fig. 6. Intracellular nanostructures of Se and S (a, b), as revealed by elemental mapping and EDX (c, d and e).

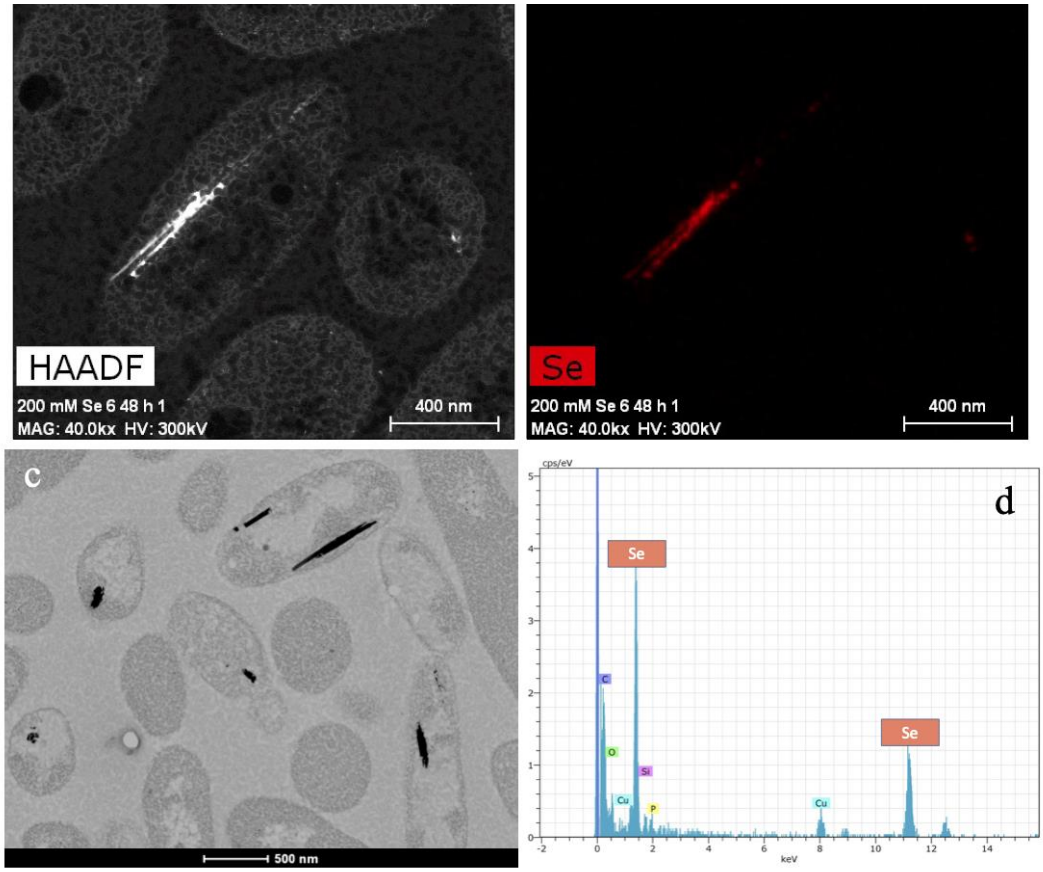

Fig. 7. Se nanostructures formed after 48 h in cells of BII-R7 exposed to 200 mM of Se(VI) (a and c). Elemental mapping (b) and EDX confirmed the presence of Se (d).

In order to further identify the structure of the crystals formed, SAED analyses, along with HRSTEM and FFT were applied. SAED patterns revealed the crystalline nature of both nanowires and nanoparticles observed (Fig. 8, 9). No amorphous accumulations were found at any incubation time. After 24 h, lattice spacings that could correspond to both monoclinical (*m*-Se) and trigonal (*t*-Se) phases of Se were identified. Three d-spacings of 0.29, 0.37 and 0.48 nm were obtained by SAED (Fig. 8 B and C). The lattice spacing of 0.29 nm is very close to that of the plane (1 0 1) of *t*-Se found at 0.3 nm. The d-spacing of 0.37 nm undoubtedly correspond to (1 0 0) plane of *t*-Se, while 0.48 nm could correspond to plane (0 2 0) of *m*-Se at 0.45 nm. On the other hand, HRSTEM and FTT revealed the lattice spacings 0.3 and 0.38 nm (Fig. 8 D, E, F, G). In case of 0.3 nm, this measure corresponds again to plane (1 0 1) of *t*-Se, and 0.38 nm fits with the plane (2 1 1) of *m*-Se. Nevertheless, this last spacing is close to the 0.37 nm previously obtained by SAED pattern, and therefore could also correspond to plane (1 0 0) of *t*-Se. Similar d-spacings were detected in samples after 48 h of incubation (Fig. 9), suggesting that the nanostructures remained unchanged between sampling times.

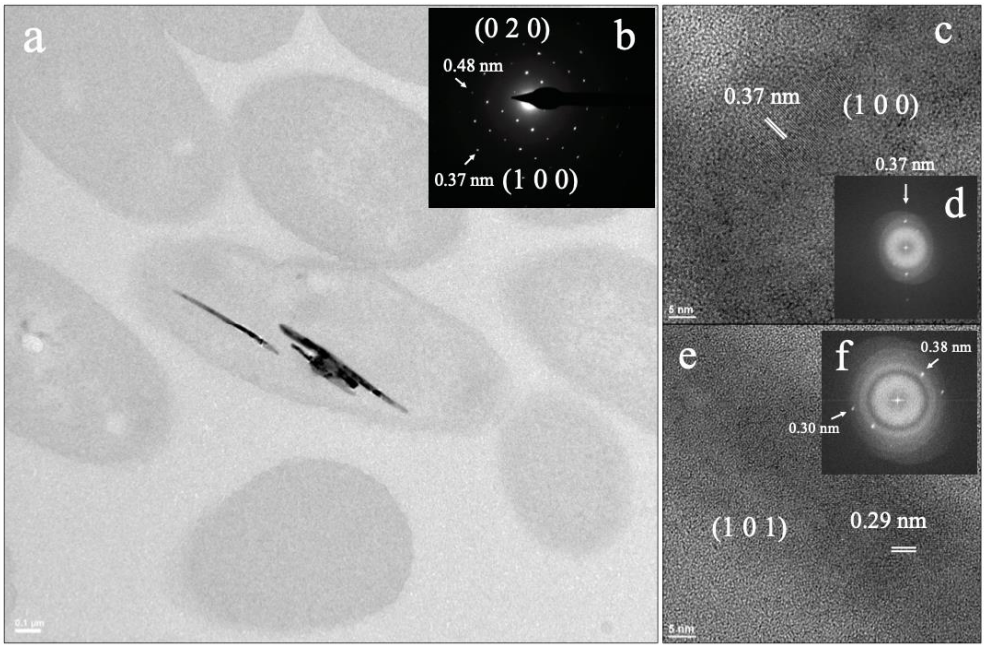

Fig. 8. Micrographs of *S. bentonitica* cells (a), SAED (b) and HRTEM with FTT analysis (c, d, e and f) of the intracellular nanotubes detected at 24 h of incubation in 200 mM of Se(VI).

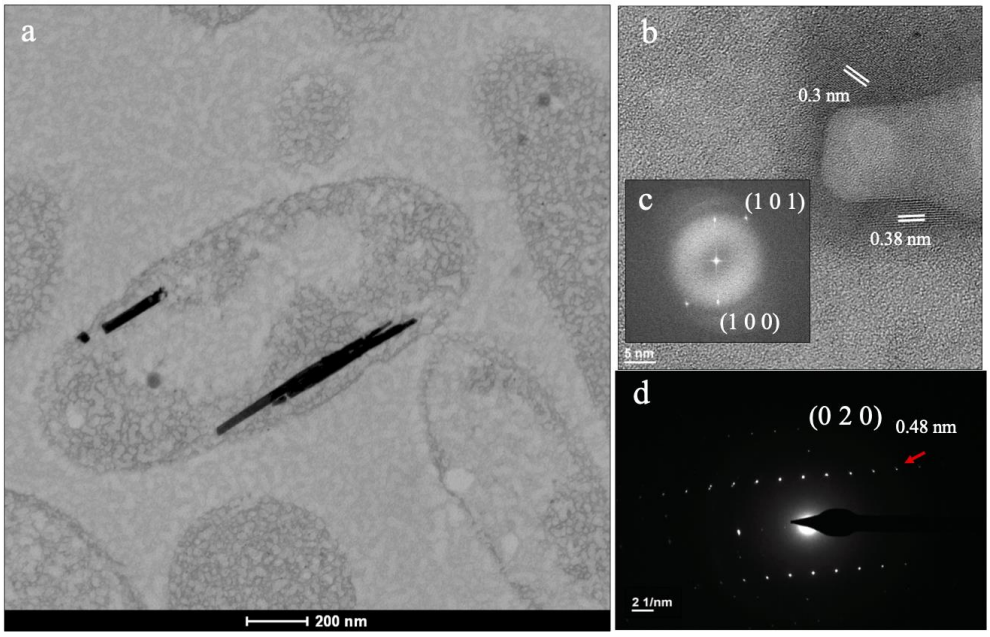

Fig. 9. Nanotubes found after 48 h of incubation of –BII-R7 with 200 mM of Se(VI) (a) and lattice spacings corresponding to *m*-Se and *t*-Se calculated by SAED pattern (e) and HRTEM with FFT (b and c).

4. Discussion

Bacterial reduction of Se oxyanions offers an attractive strategy for bioremediation of contaminated environments as well as the green synthesis of valuable Se(0) nanostructures with wide biotechnological uses. Although bacterial Se(IV)

reduction and formation of Se(0) nanospheres have been well documented (Nancharaiah and Lens, 2015; Ruiz Fresneda et al., 2018; Ruiz-Fresneda et al., 2020, 2019b), only a few microorganisms have been described to be able to reduce toxic Se(VI) to Se(0), and the specific mechanisms controlling the process have been barely explored. This work reveals the molecular systems potentially used by *S. bentonitica* BII-R7 to cope with Se(VI) toxicity, and the characterization of the nanostructures formed during the process, through a multidisciplinary approach that combines microscopic and transcriptomics analyses.

The first sign of the reduction of Se(VI) was the change in the coloration of the culture media, which acquired a reddish colour in treatments amended with 200 mM. Unlike Se(IV), only a few bacterial species have been reported to efficiently reduce Se(VI) to immobile Se(0). Since the presence of specific selenate reductases were described in *T. selenatis* and *Sulfurospirillum barnesii*, most studies of biochemical characterization of Se(VI) reduction focused in these two bacterial strains (Watts et al., 2003). Furthermore, these studies are limited to anaerobic conditions, and little is known about the mechanisms activated for Se(VI) in presence of oxygen.

Exposure of the bacterial strain to 50 and 200 mM of Se(VI) led to a lag phase that extended 8 and 24 h respectively compared to the control samples, which reflects the high toxicity exercised by this oxyanion. The longer duration of the lag phase could be explained by the fact that the cells require more time to adapt to increased Se(VI) concentrations in order to be able to grow. In addition, the up-regulation of the toxin RelE during lag and early exponential phase, which has been related to growth arrest, support the elongation of the lag phase observed (Kolodkin-Gal et al., 2009). This toxin was also detected under 2 mM of Se(IV) in this strain, with the same effect on bacterial growth (Chapter III). A prolongated lag phase has been also observed in other Se(VI)-resistant bacteria. *Herbaspirillum* sp. WT00C increased the length of the lag phase when grew at different concentrations of Se(VI), lasting 12 h when initial concentration was 200 mM (Cheng et al., 2019). However, the growth in this strain was determined by monitoring the optical density, which could result in an overestimation of the bacterial growth as a consequence of the formation of red-coloured Se(0)NPs.

On one hand, the addition of 50 mM in cultures of BII-R7 triggered the modulation of many genes from diverse metabolic pathways, showing some of them a high induction under these conditions. On the other hand, although cultures of the strain amended with 200 mM of Se(VI) acquired a reddish coloration that evinced the reduction

to Se(0), all the modulated genes showed a decreased expression with regard to non-treated cells. Even though the first sampling time at both concentrations corresponded to the lag phase, it is possible that the genetic mechanisms activated by the 200 mM of Se(VI) were induced during the first hours of incubation.

The transcriptome in presence of 50 mM of Se(VI) suggest that the oxyanion affected the membrane integrity, evidenced by the up-regulation of membrane proteins and extracellular structures, signalling systems or *rpoE* (Mitchell and Silhavy, 2019). However, this response is not limited to Se(VI). This strain also developed envelope stress when was exposed to 2 mM of Se(IV), and even when grew in presence of U(VI), which suggest that might be a general reaction to the interaction of toxic metal ions with the cell wall (Chapter III; Pinel-Cabello et al., 2021, Chapter II). Cheng et al. (2019) also reported alteration of the cell surface of *Herbaspirillum* sp. WT00C growing in presence of Se(VI), finding up-regulation of similar proteins. The disruption of the membrane can also affect other cellular processes such as nutrient transport, which in turn could also explain the extended lag phase (Kieliszek et al., 2019).

Transcriptomics results suggest that reduction took place inside the cells, which require the previous uptake of Se(VI) anions inside the cell (Fig. 10a). Despite the fact that Se is essential for Life, no specific transporters have been found for this element, and therefore Se(VI) uptake occurs via transporters for structurally related compounds such as Mo or S (Rosen and Liu, 2009; Tugarova and Kamnev, 2017). The high induction of the outer membrane factor lipoprotein from NodT family, involved in transport of different compounds such as heavy metal cations (Ibrahim et al., 2012), suggest its role in Se(VI) transport. Furthermore, this lipoprotein was also observed in presence of Se(IV) (Chapter III), which reinforce this hypothesis. Since a competition between nitrate and selenium uptake has been previously suggested in *S. maltophilia* SeITE02 (Antonioli et al., 2007), the nitrate/nitrite transporter NarK detected during the early exponential phase could be involved in the Se(VI) uptake. It is worth to notice that, on the contrary of NodT, this transporter was not detected when BII-R7 was exposed to Se(IV) (Chapter III). The thiol reductant ABC exporter CydD, previously related to glutathione transport from the cytoplasm to the periplasm (Pittman et al., 2005), could also be involved in Se(VI) or Se(IV) transport. However, it is possible that this transporter is indeed induced to meet the demand of reduced thiol groups in the periplasm, or to support the cytochrome *bd*-type terminal oxidase assembly (Pittman et al., 2005).

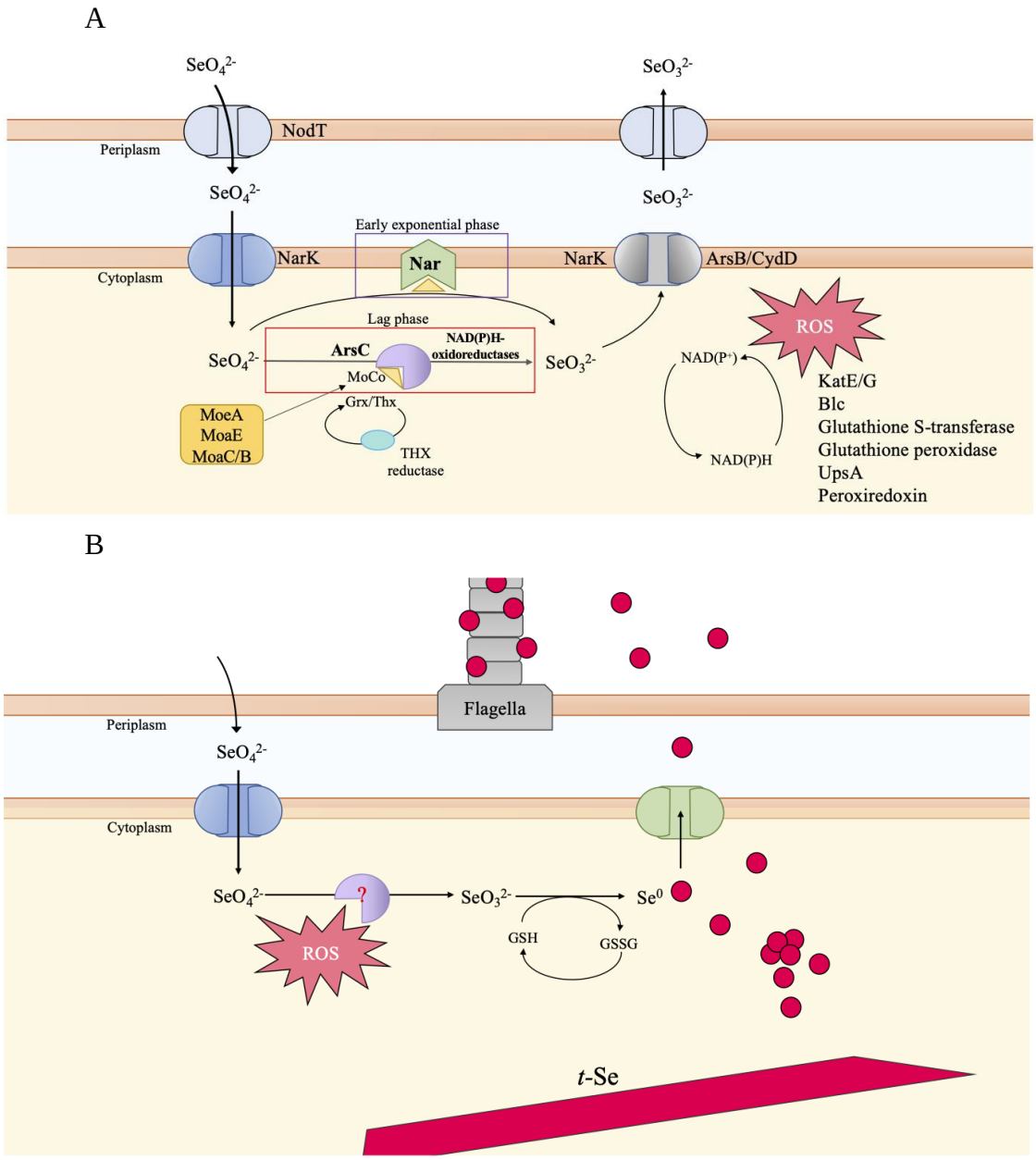

Fig. 10. Cellular mechanism for Se(VI) resistance in *S. bentonitica* during lag and early exponential phase in presence of 50 mM (a) and 200 mM of Se(VI) (b). Although the specific process is still unknown, *S. bentonitica* reduces Se(VI) to Se(0) to form intracelular nanotubes of t-Se. Furthermore, Se(0) also aggregates in the matrix of flagella-like proteins, yielding the same nanostructures.

The response of the cells to 50 mM of Se(VI) varied considerably from one sampling time to another (Fig.10a). Several oxidoreductases were highly induced during the lag phase. Some of them, such as 3-oxoacyl-ACP reductase FabG or NAD(P)-dependent oxidoreductases were also detected when *S. bentonica* grew in presence of Se(IV), and it has been related to Se(IV) reduction in other bacteria (Chapter III)(Khoei et al., 2017; Ni et al., 2015). However, the implication of FabG in the assembly and functioning of flagellar system has been demonstrated in *Azospirillum brasilense* Sp245 (Khoei et al., 2017; Ni et al., 2015). Hence, this enzyme could also be related to the up-

regulation of flagellin subunits of the flagella in BII-R7. Interestingly, transcripts from the *ars* operon ArsH, ArsB and ArsC for arsenic resistance were also up-regulated during the lag phase. Selenium and arsenic in microorganisms share similar mechanisms of toxicity (J. et al., 2002). The *ars* operon is induced in response to arsenate (As(V)) in the medium. This mechanism comprises the reduction of As(V) to arsenite (As(III)) by arsenate reductases C, and the subsequent efflux of the latest one outside the cell mediated by ArsB (J. et al., 2002; Yang et al., 2012). Given its role in resistance to toxic compounds, NodT lipoprotein could also be involved in the efflux of the metalloid. Hence, these results suggest that Se(VI) in *S. bentonitica* could be reduced in the cytoplasm by the arsenate reductase ArsC, taking the electrons from the thioredoxin and glutaredoxin. Once reduced, the arsenical efflux pump ArsB and NodT would extrude the more toxic Se(IV) outside the cell. Parallelly, the NADPH-dependent FMN oxidoreductase ArsH would prevent from the damage of the oxidative stress generated by the interactions of the oxyanions with biomolecules and the reduction itself (Hervás et al., 2012; Vorontsov et al., 2007). Furthermore, part of the Se(IV) could be reduced by the pool of reduced glutathione and/or incorporated for its use as co-factor for some enzymatic activity such as in xanthine dehydrogenase (Eswayah et al., 2016; Staicu and Barton, 2017). The high up-regulation of other oxidoreductases at this phase, could be to replenish the NADH and NADPH to support the activity of enzymes that protect the cells from oxidative stress, such as glutathione S-transferase and glutathione peroxidase (Cheng et al., 2019).

Nevertheless, when the early exponential growth was initiated, the cells switched the mechanism to cope with the toxicity of this oxyanion. The gene cluster encoding for the respiratory nitrate reductase system (*narH, narI, narG* and *narJ),* with putative Se(VI) and Se(IV) reductase activity (Che et al., 2019), was highly up-regulated in this growth phase. Nitrate reductases have been previously related to Se(IV) reduction in many bacterial species; however, the connection between these enzymes and Se(VI) reduction is less known (Tugarova and Kamnev, 2017). Sabaty et al. (2001) reported the use selenate and tellurite as electron acceptors by the membrane-bound and periplasmic nitrate reductase of *Ralstonia eutropha, Paracoccus denitrificans* and *Paracoccus pantotrophus*. These results suggest that Se(VI) might cause a switch from detoxification to the respiratory metabolism in *S. bentonitica* to reduce the metalloid, using it as final electron acceptor. Hence, the strain would use the oxyanion to provide energy to the cells by generating a proton-motive force, supporting the growth of the bacterium. However,

synthesis of membrane-bound nitrate reductase is inhibited by oxygen, while nitrate reduction in aerobic conditions is mediated by the periplasmic nitrate reductase (Rajta et al., 2020; Tugarova and Kamnev, 2017). As many enzymes with selenate reductase activity previously described are variants of nitrate reductases (Sabaty et al., 2001; Shi et al., 2020a), it is possible that these nitrate reductase were induced by Se(VI). Further investigations should be carried out in order to reveal the involvement of nitrate respiration in Se(VI) reduction process. The nitrate/nitrite transporter NarK previously described is also an antiporter that couples nitrate uptake with nitrite extrusion, which prevents the accumulation of the last in the periplasm (Zheng et al., 2013). Therefore, similar to ArsB and NodT, NarK could release the Se(IV) outside the cells. In fact, the efflux of Se(IV) by ArsB and NarK would explain the lack of change of colour of the culture, as the rate of Se(IV) reduction would be low. It is also worth to mention that both arsenate and nitrate reductases use Mo as a cofactor, as it has been seen in other selenate reductases (Shi et al., 2020a).

At the middle exponential growth, whilst the oxidoreductase activity appeared to decrease, enzyme activities associated with valine catabolism seemed to increase in presence of Se(VI). Some of these enzymes were also up-regulated in *Herbaspirillum* sp. WT00C cells exposed to Se(VI), such as methylmalonate-semialdehyde dehydrogenase or 3-hydroxybutirate dehydrogenase, which were related to the production of NADPH to support the antioxidant activity (Cheng et al., 2019). As a consequence of the reduction activity and the interaction of the metalloid with biomolecules, the levels of oxidative stress would increase over time, which explains the induction of metabolic pathways to maintain the activity of enzymes with antioxidant function.

In case of 200 mM of Se(VI), the strong decrease in the gene expression reflects the toxicity provoked by such amount of the metalloid. In contrast with 50 mM, the Se(VI) reduction would produce large quantities of toxic Se(IV), that could accumulate in the cell and the culture medium. As Se(IV) can alter the structure of proteins, causing several damage in the metabolism due to structural similarity to S (J. et al., 2002; Tugarova and Kamnev, 2017), *S. bentonitica* would have to reduce it until the less toxic Se(0) in order to survive, which would explain the red-coloured culture. Although no significant up-regulated genes were found in this treatment, the reduction of Se(VI) and Se(IV) could be performed by enzymes found at similar levels in the untreated samples and/or the pool of the reduced thiols, respectively. The reduction of Se oxyanions was also revealed by electron microscopy. Irregular nanostructures and nanotubes of *m*-Se

and *t*-Se located intracellularly and embedded in the matrix of flagella-like structures were observed at 24 and 48 h of incubation, which confirms the further reduction of Se(IV) to Se(0)(Fig. 10b). Apart from Se, these nanostructures were also composed by S, suggesting the implication of thiol groups in the reduction or coalescence of Se(0). The absence of Se nanospheres indicates that the nanostructures are formed by a different process than those synthetised from Se(IV) reduction. In presence of Se(IV), *S. bentonitica* produce different extracellular Se nanostructures from the coalescence of SeNPs, which are released from the cytoplasm by cell lysis. These nanostructures were also composed of *m*- and *t*-Se, but were visible at the extracellular media as of 72 h of incubation (Chapter III). In contrast with that, when BII-R7 grew in 200 mM of Se(VI), Se(0) nanostructures were found intracellularly only at 24 h of incubation, which along with the absence of Se nanospheres, indicates that the synthesis and aggregation is faster than with Se(IV). More studies are needed at shorter incubation times to determine if the synthesis of SeNPs takes place under these conditions. Furthermore, the decrease of the amount of the nanostructures at higher incubation times suggest the occurrence of other processes simultaneously, like reoxidation or production of volatile species by methylation, as it has been observed in this strain in presence of 100 mM of Se(VI) (data not shown). Similarly to what was observed with Se(IV), the nanotubes were composed with S in addition to Se, which suggest the possible implication of thiol-containing molecules in the stabilization and aggregation of the nanostructures, probably bound to the nanostructures during reduction process (Chapter III)(Fischer et al., 2020). Reduction of Se(VI) to Se(0) has been previously described in some bacteria. *Comamonas testosteroni* S44 exposed to Se(VI) produced intracellular SeNPs in aerobic conditions (Y. Tan et al., 2018). Soda et al. (2018) also reported the formation of intracellular and extracellular SeNPs in a halotolerant *Shewanella* strain, and *Stenotrophomonas maltophilia* produced high amounts of nanospheres located in the cell surface and the extracellular media in presence of Se(VI) (Dungan et al., 2003). However, the synthesis of intracellular Se nanotubes has not been previously described, being observed in *S. bentonitica* for the first time. In addition, BII-R7 was able to transform the Se(VI) to *t*-Se, the most stable allotrope of the metalloid, which is of high relevance for Se(VI) bioremediation strategies (Jain et al., 2017b). The results obtained here showed that this strain could be a powerful tool both as bioremediation agent and eco-friendly synthesis of valuable Se nanostructures.

5. Conclusions

In the present study, transcriptomics analysis shed light on the specific mechanism for Se(VI) resistance in *S. bentonitica* BII-R7 under aerobic conditions. The presence of Se(VI) caused a concentration-dependent inhibition of the cell growth, with a lag phase of up to 24 h in case of 200 mM of Se(VI). On the one hand, the transcriptome revealed that different detoxification mechanisms were activated between growth phases in cells exposed to 50 mM of Se(VI), where several oxidoreductases, as well as arsenic resistance *ars* operon were induced in the lag phase, while respiratory nitrate reductase genes were highly up-regulated during early exponential phase. These systems could reduce Se(VI) to Se(IV), with the extrusion of the last oxyanion to the culture medium via transporters ArsB and NarK, respectively. On the other hand, the mechanism observed in cells growing with 200 mM of Se(VI) consisted in the complete reduction to Se(0), forming intracellular nanostructures of *t*-Se, mainly in the form of nanotubes, which have been described here for the first time in bacteria. Altogether, the results obtained in this work showed that *S. bentonitica* drives a variety of efficient mechanisms for selenium biotransformations. Furthermore, key genes as specific targets for further investigations are proposed, which would lead to the design of cost-effective techniques for bioremediation purposes, with the additional production valuable nanomaterials for industrial uses.

6. Acknowledgements

This works was supported by the grant FPU 15/04284 (Formación de Profesorado Universitario) from the Spanish Ministry (Ministerio de Educación, Cultura y Deporte) and from European Project CGL2014-59616-R. The authors are grateful to María del Mar Abad Ortega, Isabel Sánchez Almazo and Concepción Hernández Castillo for their assistance at Microscopy services (Centro de Instrumentación Científica, University of Granada, Spain), and to Mare Scharfe for technical support at sequencing services (Genome Analytics, Helmholtz Centre for Infectious Diseases).

7. Supplementary material

Table S1. Fold-changes of most up-regulated transcripts at lag and early exponential phases in cells treated with 50 mM of Se(VI). Proteins of unknown function are not showed.

Modulated genes in lag phase	Fold change
Aklaviketone reductase	219,7
Flagellin FliC	162,7
Short-chain dehydrogenase	151,2
Multidrug RND efflux permease subunit	149,6
Lipoprotein NodT	132,5
Chemotaxis protein	129,7
Flagellin FliC	118,4
Chemotaxis protein	99,6
Stress response diiron-containing protein YciF	97,3
Glucoamylase	88,1
4,5-DOPA dioxygenase	80,0
Multidrug RND efflux periplasmic adaptor subunit	75,9
Hypothetical protein	75,5
Alpha-trehalose-phosphate synthase	71,6
TonB-dependent receptor BtuB	63,9
ErfK/YbiS/YcfS/YnhG family protein	57,2
Signal transduction histidine kinase CheA	54,3
Trehalose-6-phosphate phosphatase	51,6
Xanthine dehydrogenase family protein	51,5
FMN-dependent NADH-azoreductase	47,6
Outer membrane lipoprotein Blc	45,4
Catalase KatE-intracellular protease	44,5
UPF0391 membrane protein RPC 2356	43,8
DNA protection during starvation protein	38,2
ATP-dependent DNA ligase clustered with Ku protein	37,3
Oxidoreductase	35,5
UPF0337 protein YjbJ	34,7
UPF0391 membrane protein YtjA	28,6
ATP-dependent DNA ligase clustered with Ku protein	27,8
Xanthine dehydrogenase subunit M	27,3

Modulated genes in early exponential phase	Fold change
Respiratory nitrate reductase beta chain	180,1
Respiratory nitrate reductase gamma chain	154,0
Respiratory nitrate reductase alpha chain	152,3
Respiratory nitrate reductase delta chain	128,9
Catalase KatE-intracellular protease	113,2
Peptidyl-prolyl cis-trans isomerase PpiD	98,7
DNA protection during starvation protein	79,9
Xanthine dehydrogenase family protein	79,4
Nitrate/nitrite transporter NarK/NasA	76,5
Cytochrome d ubiquinol oxidase subunit II	63,9
TonB-dependent receptor BtuB	63,7
Oxygen-independent coproporphyrinogen III oxidase	60,2
Molybdopterin molybdenumtransferase MoeA	57,8
Molybdopterin synthase catalytic subunit MoaE	56,0
Glucoamylase	53,9
Sigma-fimbriae chaperone protein	51,8
Succinate-semialdehyde dehydrogenase	50,9
Cytochrome d ubiquinol oxidase subunit I CydA	50,1
Bacteriohemerythrin	49,6
Outer membrane protein W OmpW	47,6
Protease	46,7
Osmotically inducible protein	46,5
Universal stress protein family UpsA	46,2
Alpha-trehalose-phosphate synthase	45,6
Extracellular protease	43,6
Outer membrane lipoprotein Blc	42,2
Peroxiredoxin	42,0
Protein YciE	40,4
Nicotinamidase	39,8
Xanthine dehydrogenase subunit M	36,3

Table S2. Fold-changes of most up-regulated transcripts during middle-and late exponential phase in celss treated with 50 mM of Se(VI). Proteins of unknown function are not showed.

Modulated genes in middle exponential phase	Fold change
Methylmalonate-semialdehyde dehydrogenase	129,2
3-hydroxyisobutyryl-CoA hydrolase	85,6
Enoyl-CoA hydratase	66,2
3-hydroxyisobutyrate dehydrogenase	63,9
Potassium-transporting ATPase B chain	16,6
2-methylcitrate synthase	8,0
Chemosensory pili system protein ChpB	7,7
Chemotaxis protein histidine kinase CheA	7,1
Uncharacterized MFS-type transporter YhjE	7,1
Malate dehydrogenase	6,9
Cytochrome O ubiquinol oxidase subunit II	6,7
Inosine-5'-monophosphate dehydrogenase	6,2
Bacteriohemerythrin	6,0
Periplasmic serine protease DegQ	6,0
Type IV fimbrial biogenesis protein PilW	5,7
Ribonuclease P protein component	5,7
ATP synthase epsilon chain	5,3
Rhomboid family intramembrane serine protease	5,3
Bifunctional molybdenum cofactor biosynthesis MoaC/MoaB	5,1
Cyclic pyranopterin phosphate synthase MoaA	5,1
Iron ABC transporter permease subunit	5,0
ATP synthase beta chain	5,0
UDP-glucose 6-dehydrogenase	4,9
Molybdopterin molybdenumtransferase MoeA	4,9
Molybdopterin synthase catalytic subunit MoaE	4,8
Citrate synthase	4,8
Cytochrome O ubiquinol oxidase subunit I	4,8
3-ketoacyl-CoA thiolase	4,8
Cytochrome O ubiquinol oxidase subunit III	4,6
RND efflux system permease subunit	4,5

Modulated genes in late exponential phase	Fold change
Cold shock protein of CSP family	1,6
Glutathione S-transferase	-4,2
Phosphoenolpyruvate-protein phosphotransferase of PTS system	-4,3
TetR/AcrR family transcriptional regulator	-4,5
Heat-inducible transcription repressor HrcA	-4,6
Transcriptional regulator YerC	-4,6
AraC family transcriptional regulator	-4,8
Malate:quinone oxidoreductase	-4,9
Tn4651 auxiliary cointegrate resolution protein T	-5,1
Arsenic efflux ArsB protein	-5,2
Recombinase RecA	-5,2
Di-GMP-specific phosphodiesterase I	-5,5
Drug resistance transporter EmrB/QacA subfamily	-5,7
Probable FepA TonB-dependent receptor	-6,1
Esterase EstA	-7,2
Zinc chelation protein SecC	-7,3
ATP-dependent DNA helicase UvrD/PcrA	-7,6
ParA-like protein	-7,7
ATP-dependent zinc metalloprotease FtsH	-7,7
Metalloregulator ArsR/SmtB family transcription factor	-8,3
Glucose/arabinose dehydrogenase	-8,3
TetR/AcrR family transcriptional regulator	-8,8
Pyruvate dehydrogenase (quinone)	-10,8
Cytochrome c oxidase accessory protein FixG	-10,9
Thiazole synthase ThiG	-11,9
Type III secretion system protein PrgH	-13,8
Chorismate synthase	-14,0
ATP phosphoribosyltransferase	-17,0
Histidinol dehydrogenase	-18,2
Multisubunit Na+/H+ antiporter MnhE subunit	-40,6

DISCUSIÓN GENERAL

La capacidad de los microorganismos para tolerar altas concentraciones de contaminantes perjudiciales para el medio ambiente, tales como metales pesados y radionúclidos, es bien conocida en la actualidad. La presencia de estos contaminantes inorgánicos no degradables ha llevado al desarrollo de adaptaciones metabólicas en estos organismos debido al establecimiento de una serie de procesos de interacciones microorganismo-metal, entre las que destacan la biosorción, biotransformación, bioacumulación o biomineralización (López-Fernández et al., 2020; Merroun y Selenska-Pobell, 2008; Shukla et al., 2017). Estas interacciones son de gran interés en el ámbito de la biotecnología ambiental, ya que tienen como resultado cambios en la solubilidad y movilidad de los iones metálicos (Zammit et al., 2014). Es por ello que el estudio de cepas microbianas resistentes a metales pesados y radionúclidos se ha extendido recientemente por su potencial como agentes de biorremedio. El uso de microorganismos ofrece una amplia variedad de ventajas, como la obtención de grandes cantidades de biomasa de forma rápida y barata o menores consecuencias medioambientales, ofreciendo una alternativa prometedora a las técnicas convencionales (Selvakumar et al., 2018; Wei et al., 2019). El conocimiento de los mecanismos específicos llevados a cabo por estos microorganismos a nivel celular es crucial para el desarrollo y optimización de técnicas de bioremedio efectivas, obteniendo así el mayor rendimiento posible en el proceso. Sin embargo, aún se desconocen las bases moleculares y genéticas relativas a estos procesos.

En esta tesis doctoral se ha llevado a cabo la caracterización molecular y celular de los mecanismos de interacción de la nueva cepa bacteriana *Stenotrophomonas bentonitica* BII-R7 con uranio y selenio, para evaluar su potencial como agente de biorremedio. Esto se ha conseguido con la combinación de técnicas analíticas, microscópicas, espectroscópicas, bioquímicas y ómicas.

El estudio de la influencia de factores como el estado fisiológico de las células o el pH en la interacción de *S. bentonitica* con U ha puesto de manifiesto la capacidad de la cepa BII-R7 para eliminar U(VI) soluble de forma progresiva durante el tiempo de incubación. El mayor rendimiento de este proceso se ha obtenido a pH 7, incrementándose aún más cuando la cepa crecía en el medio mínimo, donde más del 90 % del U(VI) es eliminado durante las primeras 24 h de exposición. Este proceso va acompañado de la liberación paulatina de fosfato inorgánico como consecuencia de la

actividad fosfatasa de la cepa durante las primeras horas de incubación. La exposición al radionúclido provoca un efecto negativo en el crecimiento de BII-R7, existiendo una prolongación de la fase de adaptación a un mínimo de 36 h cuando la cepa se expone a 100 μM de U(VI). Estas observaciones indican que, durante la fase de adaptación, la cepa pone en marcha los mecanismos para lidiar con el metal tóxico. El perfil de ARN en esta fase refleja una alta actividad metabólica de la bacteria pese a la ausencia de crecimiento, lo que refuerza esta hipótesis. El análisis mediante microscopía (*high-angle anular dark field scanning transmission electron microscopy*, STEM-HAADF) confirmó estos resultados mediante la observación de acúmulos distribuidos principalmente a nivel extracelular y en la superficie celular, los cuales mostraron U y P en su composición mediante microanálisis de energía dispersiva de rayos X (*energy dispersive X-ray*, EDX).

Por otro lado, la combinación de técnicas espectroscópicas (*time-resolved laser-induced fluorescence spectroscopy*, TRLFS), microscópicas y analíticas (STEM-HAADF, EDX) permitió determinar la formación de fosfatos de U a diferentes pH cuando la cepa interacciona con el radionúclido en ausencia de crecimiento. Mientras que a pH 5.5 el U(VI) forma complejos con fosfato orgánico a nivel de la superficie celular, a pH 7 se observan dos tipos de interacciones distintas. En primer lugar, y durante las 2 primeras horas de contacto, el U(VI) se une rápidamente a la superficie celular formando complejos con grupos de fosfato orgánico en un proceso de biosorción. Esto proporciona sitios de nucleación para que tenga lugar un segundo proceso de biomineralización mediante la interacción del U(VI) adherido a la superficie con el fosfato inorgánico liberado mediante la actividad fosfatasa, dando lugar a fases de minerales de fosfatos de U(VI) con una estructura similar a meta-autunita, ($Ca(UO_2)_2(PO_4)_2 \cdot 10\text{-}12H_2O$). Estudios potenciométricos recientes han puesto de manifiesto la gran cantidad de fosfatos que se encuentran en la pared de la cepa *S. bentonitica* BII-R7 en comparación con otras especies bacterianas (Ruiz-Fresneda et al., 2020). Dada la importancia de estos grupos funcionales en los mecanismos de biosorción, estos resultados demuestran el elevado potencial de BII-R7 para llevar a cabo este proceso, tal y como se ha observado con otros radionúclidos como Cm(III) o Eu(III) (Ruiz-Fresneda et al., 2020). El proceso de biosorción previo ha sido descrito con anterioridad en bacterias capaces de biomineralizar U(VI), tales como *Bacillus subtilis* ATCC-6633 o *Bacillus cereus* 12-2 (Song et al., 2019; Zhang et al., 2018). Estos resultados evidencian la importancia de factores físico-químicos como el pH en la biomineralización de metales pesados y radionúclidos. El pH condiciona aspectos clave del proceso como la carga de los grupos funcionales de la superficie microbiana o

el nivel de actividad de enzimas fosfatasa, o la especiación química del metal, lo que podría explicar diferencias en cuanto a los mecanismos observados en ambos pH. Resultados similares han sido descritos en bacterias como *Serratia* sp. OT II 7 o cepas recombinantes de *Deinococcus radiodurans*, las cuales también incrementaron el rendimiento de la biomineralización a pH neutro. Además, los autores de estos estudios también evidenciaron el efecto del pH sobre la localización de los precipitados producidos, independientemente del compartimento celular en el que se encuentran las enzimas fosfatasas (Chandwadkar et al., 2018; Kulkarni et al., 2016).

En resumen, los resultados expuestos aquí ponen de manifiesto la importancia de conocer los parámetros, tanto físico-químicos como biológicos, que condicionan la biomineralización microbiana de U, con el fin de obtener los mayores rendimientos posibles. Además, la formación de complejos de meta-autunita por parte de *S. bentonitica* la convierte en una cepa interesante para su estudio como agente de biorremedio, ya que podría conducir a la inmovilización a largo plazo del U(VI) tóxico en el ambiente.

Los análisis transcriptómicos permitieron la determinación de la respuesta de *S. bentonitica* al crecimiento en presencia del radionúclido, así como la caracterización de los mecanismos de interacción a nivel molecular. Los resultados sugieren que el U(VI) provoca una alteración de la envuelta celular, ya que se produce la activación de mecanismos para restaurar la homeostasis de la membrana, tales como la síntesis de proteínas de membrana. Por otro lado, una mayor producción de LPS incrementa la cantidad de ligandos para la secuestración del metal a este nivel. La alteración de la membrana podría ocasionar cambios en la permeabilidad de la misma, dejando pasar los iones de U. Simultáneamente, la expresión de transportadores de metales como sistemas RND (*resistance-nodulation-cell division*) podrían exportar el U del interior celular. La presencia de actividad fosfatasa y la liberación de P_i detectados previamente se confirmó por la inducción de dos genes que codificaban para una fosfatasa ácida (PAP2) y otra alcalina (fosfoetanolamina transferasa). Dada la elevada expresión de estos genes durante la primera hora de exposición a U, la actividad fosfatasa de la cepa es mayor de la detectada mediante el ensayo bioquímico, ya que puede transcurrir un tiempo entre la transcripción y la síntesis de la proteína. Estos hallazgos también concuerdan con la eliminación de casi la totalidad del U(VI) durante las primeras 24 h de incubación. El papel de las fosfatasas tanto ácidas como alcalinas ha sido descrito con anterioridad en cepas como *E. coli*, *D. radiodurans*, *Sphingomonas* sp. S15-S1 o *Stenotrophomonas* sp. Br8 (Appukuttan et al., 2011; Kulkarni et al., 2016; Merroun et al., 2011; Sánchez-Castro

et al., 2020; Yung y Jiao, 2014). Estos resultados, junto con la observación de los precipitados mediante microscopía, sugieren de nuevo un mecanismo de interacción bifásico, mediado por la biosorción a nivel de la membrana, con la posterior biomineralización por la acción de las fosfatasas tanto ácida como alkalina.

Además del U, la producción de residuos con Se provenientes de su extensiva aplicación a nivel industrial, ocasiona gran preocupación al suponer un riesgo para la salud humana y de los ecosistemas. Los análisis proteómicos y transcriptómicos llevados a cabo en *S. bentonitica* revelaron que la exposición a las formas oxidadas de Se (IV y VI) origina una respuesta celular muy compleja, en la que diferentes mecanismos actúan de forma simultánea para lidiar con la presencia del metaloide. En esta cepa, el Se(IV) presentó una mayor toxicidad respecto al Se(VI). Tal y como demuestran estudios previos, el crecimiento de la cepa se ve afectado a tan sólo 2 mM de Se(IV), con una prolongación de la fase de adaptación de 48 h (Ruiz-Fresneda et al., 2018). Además, la duración de la fase de adaptación es independiente de la concentración inicial de Se(IV) en el cultivo (Ruiz-Fresneda et al., 2020). Por otro lado, la prolongación ocasionada por la exposición a 50 mM de Se(VI) fue de 8 h, y en el caso de este oxianión, la duración de esta fase es dependiente de la concentración inicial. Este fenómeno se explica por la expresión en ambos casos de la toxina RelE, que paraliza el crecimiento celular ante una situación de estrés (Kolodkin-Gal et al., 2009). La ausencia de crecimiento, junto a la mayor actividad metabólica observada, sugieren que durante esta fase tiene lugar la activación de mecanismos para hacer frente a la toxicidad del Se, gracias a los cuales inicia posteriormente la fase exponencial. Al igual que el U(VI), los resultados mostraron que las formas oxidadas de Se ocasionaron daños a nivel de la membrana celular, al hallarse la inducción de componentes de membrana tales como la lipocalina Bcl o la bactofilina CcmA, inducidos bajo estas condiciones (Campanacci et al., 2016; Taylor et al., 2020). La observación de las células mediante técnicas microscópicas (STEM-HAADF; *environmental scanning electron microscopy,* ESEM) confirmó la perturbación de la membrana, donde el Se(IV) provocó el desprendimiento de la membrana plasmática de la pared celular, mientras que el la presencia de Se(VI) originó cambios en la rugosidad de la superficie celular. Este fenómeno también ha sido descrito en otras bacterias como *Pseudomonas fluorescens* BA35SM1 y *Herbaspirillum* sp. WT00C (Cheng et al., 2019; Poirier et al., 2016).

Dichos mecanismos consisten básicamente en la reducción tanto de Se(IV) como Se(VI), y la mitigación del estrés oxidativo. Sin embargo, dadas las diferentes

características de ambos oxianiones, existen variaciones en los sistemas específicos que actúan en cada caso. La reducción de Se(IV) por BII-R7 se puso de manifiesto por la coloración rojiza que adoptaron los cultivos, tal y como se observó en estudios previos en la misma cepa (Ruiz-Fresneda et al., 2018, 2020). La observación de nanoesferas amorfas (a-Se) intracelulares a tiempos cortos de incubación mediante HAADF-STEM (Ruiz-Fresneda et al., 2018; capítulo III) indica que la reducción tiene lugar en el interior de la célula, siendo por tanto la captación de Se(IV) el primer paso del proceso. El análisis proteómico de *S. bentonitica* reveló la inducción de varios sistemas de transporte, entre los que se encuentran la lipoproteína NodT, el transportador de magnesio (Mg) MgtE o la porina OprP. Pese a tratarse de un elemento esencial, el Se carece de transporte específico, por lo que entra en la célula a través de transportadores de otros elementos (Tugarova y Kamnev, 2016). El transporte de Se(IV) también se ha relacionado anteriormente con porinas de la membrana externa o proteínas similares, tales como ExtI y ExtH en *Geobacter sulfurreducens* (González-Gil et al., 2016; Jahan et al., 2019). Por ello, es probable que la porina OprP esté involucrada en la captación de Se(IV). Sin embargo, es necesaria la realización de estudios específicos que confirmen su papel en el transporte del metaloide.

Una vez en el citoplasma, la gran cantidad de enzimas citoplasmáticas indica que la reducción tiene lugar mayoritariamente en este compartimento celular. Una de las enzimas inducidas en presencia de Se(IV) es la 3-oxoacil-ACP reductasa FabG, cuya actividad Se(IV) reductasa ha sido previamente descrita en *Pseudomonas moraviensis* subsp. stanleyae (Ni et al., 2015). Es importante destacar el metabolismo del glutatión (GSH) y otros grupos tiol como la tioredoxina (THX). Los resultados sugieren que el Se(IV) interacciona rápidamente durante las primeras horas de incubación con el *pool* de GSH reducido, produciendo Se(0). A medida que se oxida (GSSG), el GSH se repone por la actividad de las enzimas glutamato—cisteína ligasa, glutatión reductasa (GR) y glutatión sintetasa (GS). El papel del glutatión en la reducción microbiana de Se(IV) ha sido ampliamente reportado (Khoei et al., 2017; Nancharaiah y Lens, 2015; Tugarova y Kamnev, 2017). El papel del GSH y GR en la reducción de Se(IV) también se ha puesto de manifiesto por Antonioli et al. (2007) en *Stenotrophomonas maltophilia* SeITE02, donde además se destaca su importancia en las primeras fases de exposición al metaloide. Los grupos tiol y enzimas relacionadas también participan en el proceso de formación de especies volátiles de Se(-II). La inducción de la enzima tiorredoxina reductasa sugiere la formación de metil selenol, un posible intermediario de la síntesis de formas metiladas de

Se(-II) descrito previamente en *Methylococcus capsulatus* (Eswayah et al., 2019). Este proceso no sólo requiere la reducción de Se(0) a Se(-II), sino que además es necesaria la metilación por a través de metiltransferasas. Ruiz-Fresneda et al. (2020) detectaron recientemente la producción de formas metiladas volátiles de selenio, tales como dimetil diseleniuro (DMDSe) y dimetil selenil disulfuro (DMSeDS) en *S. bentonitica*. El selenio biometilado es una forma eficaz de eliminación de las formas solubles de Se a largo plazo, ya que presentan una toxicidad mucho menor que Se(IV) y Se(VI) (Eswayah et al., 2016). Por tanto, *S. bentonitica* es un candidato interesante para el bioremedio de ambientes contaminados con Se(IV).

Los análisis microscópicos (HAADF-STEM) demostraron la transformación de nanoesferas amorfas de Se(0) intracelulares a nanoestructuras cristalinas extracelulares de *t*-Se (Ruiz-Fresneda et al., 2018, 2020; capítulo III). Tras la reducción en el citoplasma las nanoesferas amorfas de Se(0) aumentan de tamaño progresivamente hasta que son liberadas al espacio extracelular mediante lisis celular a partir de las 48 h de incubación. Allí, las nanoesferas amorfas continúan agregándose, hasta dar lugar a estructuras cristalinas en forma de aguja y poligonales de diferentes tamaños. El análisis estructural de las formas cristalinas mediante la transformada rápida de Fourier (*Fast Fourier Transform*, FTT) y difracción de electrones (*selected-area electron diffraction*, SAED), detectó por primera vez en esta cepa la síntesis de nanoestructuras de *m*-Se a las 72 h, propuesta anteriormente como intermediario de la formación de *t*-Se (Ruiz-Fresneda et al., 2018, 2020), encontrado a mayores tiempos de incubación. Este proceso de biotransformación esta influenciado por proteínas, que permiten la estabilización de las nanoestructuras y controlan sus características físico-químicas. Las nanopartículas formadas en *S. bentonitica* presentan un recubrimiento de material orgánico formado principalmente por proteínas y aminoácidos (Ruiz-Fresneda et al., 2020). Estas proteínas pueden unirse a las nanopartículas en el citoplasma y/o durante la lisis celular (Fischer et al., 2020). De nuevo, los grupos tiol parecen estar involucrados en esta biotransformación, ya que se ha observado el enriquecimiento progresivo de las nanoestructuras. Del mismo modo, Ni et al. (2015) también sugirieron un importante papel de la GR en la estabilización y el control del tamaño de las nanopartículas formadas por *P. moraviensis* subsp. stanleyae. La formación de nanoesferas de Se(0) ha sido extensamente reportada en microorganismos filogenéticamente diversos. Por el contrario, la formación biológica de nanoestructuras de este tipo a temperatura ambiente apenas se ha observado anteriormente. Estos resultados indican que la formación de nanoestructuras de Se

reducido en *S. bentonitica* es ventajoso desde el punto de vista ambiental, ya que su mayor estabilidad coloidal hace que sean poco solubles y de menor toxicidad (Jain et al., 2017).

Como ya se ha mencionado, la exposición a Se(VI) desencadena una respuesta muy diferente a lo largo de las distintas fases de crecimiento, encontrándose una importante modulación de genes de rutas metabólicas muy diversas. La mayor inducción de la expresión génica se encontró con la concentración de 50 mM de Se(VI). A pesar de la ausencia de la coloración característica de la reducción del Se(VI) a esta concentración, cabe destacar la elevada actividad reductora encontrada. Aunque algunas de ellas podrían desarrollar un papel importante en la mitigación del estrés oxidativo, también proporciona indicios de un proceso de reducción del metaloide.

A diferencia del Se(IV), la captación del Se(VI) podría tener lugar a través del la lipoproteína de tipo RND NodT, el transportador de nitrato/nitrito NarK y/o a través del transportador de grupos tiol CydD. Antonioli et al. (2007) demostraron que existe una competición entre la captación de nitrato y selenito en *S. maltophilia* SeITE02, por lo que podría ocurrir lo mismo en el caso de BII-R7 para el Se(VI). Por otro lado, la implicación de transportadores de S en el transporte de Se(VI) ha sido previamente reportada, como sulfato permeasas de *E. coli* o *Mycobacterium tuberculosis* (Rosen y Liu, 2009; Zolotarev et al., 2008). Aunque el mecanismo de transporte de Se(VI) en *S. bentonitica* no está definido aún, los genes encontrados en este estudio proporcionan puntos de partida para posteriores estudios acerca de su papel en este proceso.

Durante la fase de adaptación se encontró un alto nivel de inducción de enzimas con actividad oxidorreductasa. Al igual que en el caso del Se(IV), oxidorreductasas NADP-dependientes y FabG también fueron detectadas, aunque esta última enzima podría estar relacionada con la sobreexpresión observada de flagelina, como describieron Filip'echeva et al. (2018) en *Azospirillum brasilense* Sp245. El operón *ars*, que otorga resistencia al As, también podría tener también un papel importante. La arsenato reductasa ArsC podría llevar a cabo la reducción de Se(VI) en el citoplasma celular, generando Se(IV). Dada la elevada toxicidad de este último, sería transportado al exterior a través de ArsB, junto con NodT (Hervás et al., 2012; Vorontsov et al., 2007), aunque también podría ser reducido por el glutatión a Se(0) o asimilado para su uso como cofactor enzimático (capítulo III, Staicu y Barton, 2017). Estos hallazgos sugieren una baja tasa de reducción de Se(VI) hasta su forma elemental, lo que explicaría la ausencia de color rojizo en este tratamiento.

Sin embargo, al alcanzar el crecimiento exponencial, se observa la alta inducción del clúster de genes *narH, narI, narG* and *narJ,* que codifican para la enzima nitrato reductasa respiratoria. La reducción de Se(VI) por este sistema como aceptor final de electrones ha sido reportado en bacterias como *Ralstonia eutropha, Paracoccus denitrificans* and *Paracoccus pantotrophus* (Sabati et al., 2001). Además, las selenato reductasas específicas descritas previamente parecen ser variantes de nitrato reductasas, lo que refuerza el papel de este sistema en la reducción de Se(VI) (Sabati et al., 2001; Shi et al., 2020). Al igual que ArsB y NodT, NarK también podría estar implicado en la exportación de Se(IV) al espacio extracelular. Por último, a mitad de la fase exponencial destacan enzimas del metabolismo del aminoácido valina, también relacionadas con el mantenimiento de la actividad antioxidante en *Herbaspirillum* sp. WT00C (Cheng et al., 2019).

Por otro lado, ningún gen fue inducido significativamente durante la exposición de *S. bentonitica* a 200 mM de Se(VI), lo que revela la alta toxicidad ejercida por esta concentración. El transcriptoma de la cepa en estas condiciones muestra una gran cantidad de genes con una marcada disminución de su expresión respecto a los tratamientos control. A pesar de ello, el cambio de coloración en el medio de cultivo demuestra la formación de Se(0). La reducción de la elevada concentración de Se(VI) daría lugar a una gran cantidad de Se(IV) tóxico, por lo que a diferencia de lo que ocurre a 50 mM, *S. bentonitica* llevaría a cabo su reducción hasta Se(0) de menor toxicidad. Para ello, la cepa emplearía mecanismos enzimáticos con niveles de expresión similares a los de los tratamientos control, y/o grupos tiol reducidos.

Las micrografías de HAADF-STEM y ESEM pusieron de manifiesto la presencia de nanoestructuras de Se(0), confirmando la reducción de Se(VI) a Se(0). Dichas estructuras se encuentran mayoritariamente en forma de nanotubos intracelulares y embebidos en la matriz de estructuras flagelares. La caracterización estructural mediante análisis espectroscópicos (FFT y SAED) permitieron determinar la presencia de *m*-Se y *t*-Se, sugiriendo un proceso de biotransformación hacia nanoestructuras de *t*-Se. La composición elemental refleja mayoritariamente Se, pero también S en menor medida, por lo que los grupos tiol podrían de nuevo ser clave para su formación. Sin embargo, este proceso parece ser muy diferente del descrito anteriormente para el Se(IV). La observación de nanotubos tras 24 h de incubación, junto con la ausencia de nanoesferas, indica que la agregación y síntesis de nanoestructuras ocurre con mayor rapidez en el caso del Se(VI). Además, en este último caso, la formación de nanoestructuras ocurre en el

espacio extracelular. Para esclarecer el mecanismo que tiene lugar en estas condiciones son necesarios estudios de los productos de reducción de Se(VI) a tiempos más cortos de incubación. Además, la cantidad de nanoestructuras parece decrecer a mayores tiempos de incubación. Estudios previos demostraron la producción de especies volátiles de Se(-II) cuando *S. bentonitica* creció en presencia de 100 mM de Se(VI) (Ruiz-Fresneda et al. 2021, trabajo en preparación). Por tanto, la disminución de las nanoestructuras podría deberse a la síntesis de estas formas de Se metiladas. Los microorganismos capaces de reducir Se(VI) forman generalmente como productos de reducción nanoesferas de Se(0), ya sea a nivel intracelular o extracelular, como *Comamonas testosteroni* S44, *Shewanella* e incluso *S. maltophilia* (Dungan et al., 2003; Soda et al., 2017; Tan et al., 2018). Hasta donde nosotros conocemos, la formación de nanotubos de *t*-Se a partir de Se(VI) es descrita en este estudio por primera vez, lo que de nuevo aumenta el valor de la cepa *S. bentonitica* como agente potencial para bioremedio.

En resumen, los estudios proteómicos y transcriptómicos indican que la resistencia a Se en *S. bentonitica* se debe principalmente a tres mecanismos que tienen lugar de manera sinérgica: (1) reducción tanto de Se(IV) como de Se(VI), dando lugar a especies más reducidas y de menor toxicidad, tales como nanoesferas de Se(0), (2) mitigación del estrés oxidativo derivado de los procesos de reducción (3) biotransformación de los productos de Se(0) para formar nanoestructuras de selenio monoclínico (*m*-Se) y trigonal (*t*-Se). Aunque el mecanismo de resistencia a ambas formas del metaloide en *S. bentonitica* aún no está clara, estos estudios reflejan el potencial de esta cepa para el biorremedio de ambientes contaminados con Se. Los genes y proteínas detectados aquí ofrecen un punto de partida importante para estudios posteriores que ayudarán a esclarecer estos mecanismos de interacción. Esto supone un avance no sólo hacia el desarrollo de técnicas efectivas de biorremedio, sino también sino también hacia la síntesis de nanoestructuras para diversos fines industriales de forma respetuosa con el medio ambiente.

CONCLUSIONES

Según los resultados obtenidos en esta Tesis Doctoral, se establecen las siguientes conclusiones:

1. La cepa de estudio *S. bentonitica* BII-R7 es capaz de eliminar altos porcentajes de U(VI) soluble en el medio de cultivo, a distintos pH y condiciones fisiológicas. El rendimiento a pH neutro fue mayor, especialmente cuando la bacteria crecía en el medio de cultivo, donde además el proceso va acompañado por una inducción de la actividad fosfatasa, tanto ácidas como alcalinas, y la liberación de fosfato inorgánico.

2. Análisis espectroscópicos (TRLFS) y microscópicos (STEM-HAADF) demuestran la complejación de U(VI) con fosfatos orgánicos a pH 5.5, mientras que a pH 7 tiene lugar una interacción inicial rápida de biosorción a fosfatos orgánicos en la superficie celular, con la posterior interacción con fosfatos inorgánicos, dando lugar a la biomineralización de U(VI) en forma de fosfatos de U(VI) con una estructura similar a meta-autunita.

3. Estudios transcriptómicos indicaron que el incremento de ligandos del metal mediante la síntesis de proteínas de la pared celular (como CreD) y LPS, junto con el flujo de U(VI) al exterior de la célula por sistemas de transporte (p. ej., sistemas de transporte RND), podrían ser mecanismos adicionales que contribuyen de manera sinérgica a la resistencia de *S. bentonitica* al U(VI).

4. La inmovilización efectiva de U(VI) por *S. bentonitica* BII-R7 en forma de fases minerales de fosfatos de U(VI) estables demuestra el potencial de la cepa como agente de biorremedio de ambientes contaminados con el radionúclido.

5. Los mecanismos de resistencia a Se están basados tres procesos principales: la la reducción del metaloide, la mitigación del estrés oxidativo y la formación de nanoestructuras cristalinas de *t*-Se.

6. El proteoma de la cepa sugiere el transporte del Se(VI) al citoplasma celular a través de transportadores de metales (NodT, MgtE) y/o porinas (OprP), así como el papel clave del metabolismo de grupos tiol (p. ej., glutatión reductasa y glutatión sintetasa) en la reducción y formación de especies insolubles de Se en forma de nanoesferas de Se(0) y compuestos volátiles de Se(-II).

7. Las nanoesferas de Se(0) producidas intracelularmente aumentan de tamaño hasta ser liberadas al exterior mediante lisis celular, donde los grupos tiol podrían influenciar su agregación y biotransformación a nanoestructuras de *m*-Se y finalmente a *t*-Se.

8. El mecanismo de resistencia a Se(VI) en *S. bentonitica* es dependiente de la concentración del mismo. A 50 mM es reducido a Se(IV), mientras que a 200 mM se reduce hasta Se(0), con la formación de nanotubos de *m*-Se y *t*-Se intracelulares y embebidos en la matriz de estructuras flagelares. La localización de estos nanotubos y la ausencia de nanoesferas indican que se trata de una biotransformación distinta a la observada en el caso del Se(IV).

9. Los análisis transcriptómicos demuestran posible el papel de enzimas NAD(P)H-oxidorreductasas, el operón *ars* de resistencia a arsénico y de la enzima nitrato reductasa respiratoria en la reducción de Se(VI) a Se(IV), además de los transportadores como NodT, de nitrito/nitrato NarK y de grupos thiol CydD en la captación y flujo al exterior del metaloide.

10. La gran diversidad metabólica de la cepa para llevar a cabo la reducción de tanto de Se(VI) y de Se(IV), como su inmovilización en formas insolubles y menos tóxicas de *t*-Se, indican de la aptitud de *S. bentonitica* para el diseño de estrategias de biorremedio de ambientes contaminados con Se, así como de la producción ecológica de nanomateriales de alto valor biotecnológico.

CONCLUSIONS

According to the results obtained in this Doctoral Thesis, the following conclusions are stablished:

1. The strain object of this study *S. bentonitica* BII-R7 is able to remove high percentages of soluble U(VI) from the culture medium, at different pH and physiological conditions. The yielding was higher at neutral pH, especially when the strain grew in the culture medium, with the induction of both acid and alkaline phosphatase activity and the release of inorganic phosphates.

2. Spectroscopic (TRLFS) and microscopic (STEM-HAADF) indicate that the cells of *S. bentonitica* BII-R7 bind U(VI) through organic phosphates at pH 5.5, while at pH 7 a first biosorption process to organic phosphates at the cell surface, followed by the interaction with inorganic phosphates, which leads to the biomineralization of U(VI)-phosphates structurally similar to meta-autunite.

3. Transcriptomics analyses indicated that the increase of the metal ligands through the synthesis of cell wall proteins (*e.g.,* CreD) and LPS, along with the U(VI) efflux outside the cells via transport systems (*e.g.,* RND efflux systems), could be additional mechanisms that contribute synergically to the *S. bentonitica* resistance to U(VI).

4. The effective immobilization of U(VI) by *S. bentonitica* BII-R7 in form of stable U(VI)-phosphate minerals evinced the potential of the strain as bioremediation agent for environments contaminated with this radionuclide.

5. The resistance mechanisms to Se are based in three main process: the reduction of the metalloid, the mitigation of oxidative stress and the synthesis of crystalline *t*-Se nanostructures.

6. The proteome of the strain suggest that Se(IV) uptake to the cytoplasm takes place through metal transporter (NodT, MgtE) and/or porines (OprP) , as well as the key role of metabolism of thiol groups (*e.g.,* glutathione reductase and glutathione synthetase) in reduction and synthesis of insoluble Se species in form of Se(0) nanospheres and volatile compounds of Se(-II).

7. The intracellular Se(0) nanospheres produced increase their size until the release to the extracellular media by cellular lysis, where thiol groups could influence the aggregation and biotransformation to *m*-Se nanostructures, and finally to *t*-Se.

8. The mechanism of resistance to Se(VI) in *S. bentonitica* is a metalloid concentration dependent process. At 50 mM of initial concentration, Se(VI) is reduced to Se(IV), while further reduction to Se(0) occurred when the initial concentration was 200 mM of Se(VI), with the synthesis of nanotubes of *m*-Se and *t*-Se in the cytoplasm and embedded in the matrix of flagella-like structures. The cellular location and the absence of nanospheres detected indicate a different biotransformation process than the observed in case of Se(IV).

9. The transcriptomics analyses revealed the possible rol of the NAD(P)H-oxidoreductases, *ars* operon for arsenic resistance and the respiratory nitrate reductase in the reduction of Se(VI) to Se(IV), as well as the NodT, nitrite/nitrate NarK and thiol groups CydD transporters in the uptake and efflux of the metalloid.

10. The great metabolic diversity of the strain to reduce both Se(VI) and Se(IV), with their immobilization into insoluble and less toxic forms of *t*-Se, demonstrate the suitability of *S. bentonitica* for the design of bioremediation strategies of Se contaminated environments, as well as the eco-friendly production of nanomaterials with high biotechnological value.

REFERENCIAS

Abin, C.A., Hollibaugh, J.T., 2018. Transcriptional response of the obligate anaerobe *Desulfuribacillus stibiiarsenatis* MLFW-2 ^{T} to growth on antimonate and other terminal electron acceptors. Environ Microbiol 1462-2920.14503. https://doi.org/10.1111/1462-2920.14503

Acharya, C., 2015. Uranium Bioremediation: Approaches and Challenges, in: Sukla, L.B., Pradhan, N., Panda, S., Mishra, B.K. (Eds.), Environmental Microbial Biotechnology, Soil Biology. Springer International Publishing, Cham, pp. 119–132. https://doi.org/10.1007/978-3-319-19018-1_7

Acharya, C., Apte, S.K., 2013. Novel surface associated polyphosphate bodies sequester uranium in the filamentous, marine cyanobacterium, Anabaena torulosa. Metallomics 5, 1595. https://doi.org/10.1039/c3mt00139c

Albino, V., 2014. Understanding the development trends of low-carbon energy technologies: A patent analysis. Applied Energy 19.

Ali, H., Khan, E., Ilahi, I., 2019. Environmental Chemistry and Ecotoxicology of Hazardous Heavy Metals: Environmental Persistence, Toxicity, and Bioaccumulation. Journal of Chemistry 2019, 1–14. https://doi.org/10.1155/2019/6730305

Amiro, B.D., 2001. Environmental Radioactivity. Encyclopedia of Physical Science and Technology 17.

Andrews, S.C., Robinson, A.K., Rodríguez-Quiñones, F., 2003. Bacterial iron homeostasis. FEMS Microbiol Rev 27, 215–237. https://doi.org/10.1016/S0168-6445(03)00055-X

Antonioli, P., Lampis, S., Chesini, I., Vallini, G., Rinalducci, S., Zolla, L., Righetti, P.G., 2007. Stenotrophomonas maltophilia SeITE02, a New Bacterial Strain Suitable for Bioremediation of Selenite-Contaminated Environmental Matrices. Appl. Environ. Microbiol. 73, 6854–6863. https://doi.org/10.1128/AEM.00957-07

Appukuttan, D., Seetharam, C., Padma, N., Rao, A.S., Apte, S.K., 2011. PhoN-expressing, lyophilized, recombinant Deinococcus radiodurans cells for uranium bioprecipitation. Journal of Biotechnology 154, 285–290. https://doi.org/10.1016/j.jbiotec.2011.05.002

Armengaud, J., 2016. Next-generation proteomics faces new challenges in environmental biotechnology. Current Opinion in Biotechnology 38, 174–182. https://doi.org/10.1016/j.copbio.2016.02.025

Banala, U.K., Indradyumna Das, N.P., Toleti, S.R., 2021. Uranium sequestration abilities of Bacillus bacterium isolated from an alkaline mining region. Journal of Hazardous Materials 411, 125053. https://doi.org/10.1016/j.jhazmat.2021.125053

Bao, P., Xiao, K.-Q., Wang, H.-J., Xu, H., Xu, P.-P., Jia, Y., Häggblom, M.M., Zhu, Y.-G., 2016. Characterization and Potential Applications of a Selenium Nanoparticle Producing and Nitrate Reducing Bacterium Bacillus oryziterrae sp. nov. Sci Rep 6. https://doi.org/10.1038/srep34054

Barkleit, A., Moll, H., Bernhard, G., 2009. Complexation of uranium(vi) with peptidoglycan. Dalton Transactions. https://doi.org/10.1039/b818702a

Barkleit, A., Moll, H., Bernhard, G., 2008. Interaction of uranium(vi) with lipopolysaccharide. Dalton Transactions. https://doi.org/10.1039/b715669c

Beazley, M.J., Martinez, R.J., Sobecky, P.A., Webb, S.M., Taillefert, M., 2009. Nonreductive Biomineralization of Uranium(VI) Phosphate Via Microbial Phosphatase Activity in Anaerobic Conditions. Geomicrobiology Journal 26, 431–441. https://doi.org/10.1080/01490450903060780

Beazley, M.J., Martinez, R.J., Sobecky, P.A., Webb, S.M., Taillefert, M., 2007. Uranium Biomineralization as a Result of Bacterial Phosphatase Activity: Insights from Bacterial Isolates from a Contaminated Subsurface. Environ. Sci. Technol. 41, 5701–5707. https://doi.org/10.1021/es070567g

Bhakat, K., Chakraborty, A., Islam, E., 2019. Characterization of arsenic oxidation and uranium bioremediation potential of arsenic resistant bacteria isolated from uranium ore. Environ Sci Pollut Res 26, 12907–12919. https://doi.org/10.1007/s11356-019-04827-6

Binet, R., Létoffé, S., Ghigo, J.M., Delepelaire, P., Wandersman, C., 1997. Protein secretion by Gram-negative bacterial ABC exporters – a review. Gene 192, 7–11. https://doi.org/10.1016/S0378-1119(96)00829-3

Bjørklund, G., Semenova, Y., Pivina, L., Dadar, M., Rahman, Md.M., Aaseth, J., Chirumbolo, S., 2020. Uranium in drinking water: a public health threat. Arch Toxicol 94, 1551–1560. https://doi.org/10.1007/s00204-020-02676-8

Bone, S.E., Dynes, J.J., Cliff, J., Bargar, J.R., 2017. Uranium(IV) adsorption by natural organic matter in anoxic sediments. Proc Natl Acad Sci USA 114, 711–716. https://doi.org/10.1073/pnas.1611918114

Boukhalfa, H., Icopini, G.A., Reilly, S.D., Neu, M.P., 2007. Plutonium(IV) Reduction by the Metal-Reducing Bacteria Geobacter metallireducens GS15 and

Shewanella oneidensis MR1. Appl. Environ. Microbiol. 73, 5897–5903. https://doi.org/10.1128/AEM.00747-07

Bradford, M.M., 1976. A rapid and sensitive method for the quantitation of microgram quantities of protein utilizing the principle of protein-dye binding. Analytical Biochemistry 72, 248–254. https://doi.org/10.1016/0003-2697(76)90527-3

Bradl, H.B., 2005. Chapter 1 Sources and origins of heavy metals, in: Interface Science and Technology. Elsevier, pp. 1–27. https://doi.org/10.1016/S1573-4285(05)80020-1

Briffa, J., Sinagra, E., Blundell, R., 2020. Heavy metal pollution in the environment and their toxicological effects on humans. Heliyon 6, e04691. https://doi.org/10.1016/j.heliyon.2020.e04691

Brooks, B.E., Buchanan, S.K., 2008. Signaling mechanisms for activation of extracytoplasmic function (ECF) sigma factors. Biochimica et Biophysica Acta (BBA) - Biomembranes 1778, 1930–1945. https://doi.org/10.1016/j.bbamem.2007.06.005

Brugge, D., Buchner, V., 2011. Health effects of uranium: new research findings. Reviews on Environmental Health 26. https://doi.org/10.1515/REVEH.2011.032

Buchs, B., Evangelou, M.W.H., Winkel, L.H.E., Lenz, M., 2013. Colloidal Properties of Nanoparticular Biogenic Selenium Govern Environmental Fate and Bioremediation Effectiveness. Environ. Sci. Technol. 47, 2401–2407. https://doi.org/10.1021/es304940s

Campanacci, V., Bishop, R.E., Blangy, S., Tegoni, M., Cambillau, C., 2006. The membrane bound bacterial lipocalin Blc is a functional dimer with binding preference for lysophospholipids. FEBS Lett 580, 4877–4883. https://doi.org/10.1016/j.febslet.2006.07.086

Carvalho, P.C., Hewel, J., Barbosa, V.C., Yates III, J.R., 2008. Identifying differences in protein expression levels by spectral counting and feature selection. Genet. Mol. Res. 7, 342–356. https://doi.org/10.4238/vol7-2gmr426

Celik, F., Camas, M., Kyeremeh, K., Sazak Camas, A., 2018. Microbial Sorption of Uranium Using Amycolatopsis sp. K47 Isolated from Uranium Deposits. Water, Air, & Soil Pollution 229. https://doi.org/10.1007/s11270-018-3766-5

Chandwadkar, P., Misra, H.S., Acharya, C., 2018. Uranium biomineralization induced by a metal tolerant *Serratia* strain under acid, alkaline and irradiated conditions. Metallomics 10, 1078–1088. https://doi.org/10.1039/C8MT00061A

Che, L., Xu, W., Zhan, J., Zhang, L., Liu, L., Zhou, H., 2019. Complete Genome

Sequence of Bacillus cereus CC-1, A Novel Marine Selenate/Selenite Reducing Bacterium Producing Metallic Selenides Nanomaterials. Curr Microbiol 76, 78–85. https://doi.org/10.1007/s00284-018-1587-9

Chen, C., Tian, J., Zhou, J., Ni, X., Lei, J., Wang, X., 2020. Bacterial growth, morphology, and cell component changes in *Herbaspirillum* sp. WT00C exposed to high concentration of selenate. J Basic Microbiol 60, 304–321. https://doi.org/10.1002/jobm.201900586

Chen, L., Hu, M., Huang, L., Hua, Z., Kuang, J., Li, S., Shu, W., 2015. Comparative metagenomic and metatranscriptomic analyses of microbial communities in acid mine drainage. The ISME Journal 9, 1579–1592. https://doi.org/10.1038/ismej.2014.245

Chimento, D.P., Kadner, R.J., Wiener, M.C., 2003. The Escherichia coli outer membrane cobalamin transporter BtuB: structural analysis of calcium and substrate binding, and identification of orthologous transporters by sequence/structure conservation. J. Mol. Biol. 332, 999–1014.

Choudhary, S., Islam, E., Kazy, S.K., Sar, P., 2012. Uranium and other heavy metal resistance and accumulation in bacteria isolated from uranium mine wastes. Journal of Environmental Science and Health, Part A 47, 622–637. https://doi.org/10.1080/10934529.2012.650584

Choudhary, S., Sar, P., 2015. Interaction of uranium (VI) with bacteria: potential applications in bioremediation of U contaminated oxic environments. Rev Environ Sci Biotechnol 14, 347–355. https://doi.org/10.1007/s11157-015-9366-6

Choudhary, S., Sar, P., 2011. Uranium biomineralization by a metal resistant Pseudomonas aeruginosa strain isolated from contaminated mine waste. Journal of Hazardous Materials 186, 336–343. https://doi.org/10.1016/j.jhazmat.2010.11.004

Collet, J.-F., Bardwell, J.C.A., 2002. Oxidative protein folding in bacteria: Oxidative protein folding in bacteria. Molecular Microbiology 44, 1–8. https://doi.org/10.1046/j.1365-2958.2002.02851.x

Debieux, C.M., Dridge, E.J., Mueller, C.M., Splatt, P., Paszkiewicz, K., Knight, I., Florance, H., Love, J., Titball, R.W., Lewis, R.J., Richardson, D.J., Butler, C.S., 2011. A bacterial process for selenium nanosphere assembly. Proceedings of the National Academy of Sciences 108, 13480–13485. https://doi.org/10.1073/pnas.1105959108

Dekker, L., Arsène-Ploetze, F., Santini, J.M., 2016. Comparative proteomics of Acidithiobacillus ferrooxidans grown in the presence and absence of uranium. Research

in Microbiology 167, 234–239. https://doi.org/10.1016/j.resmic.2016.01.007

Dessì, P., Jain, R., Singh, S., Seder-Colomina, M., van Hullebusch, E.D., Rene, E.R., Ahammad, S.Z., Carucci, A., Lens, P.N.L., 2016. Effect of temperature on selenium removal from wastewater by UASB reactors. Water Research 94, 146–154. https://doi.org/10.1016/j.watres.2016.02.007

Dobias, J., Suvorova, E.I., Bernier-Latmani, R., 2011. Role of proteins in controlling selenium nanoparticle size. Nanotechnology 22, 195605. https://doi.org/10.1088/0957-4484/22/19/195605

Duffus, J.H., 2002. Prepared for publication by. Pure and Applied Chemistry 15.

Dungan, R.S., Yates, S.R., Frankenberger, W.T., 2003. Transformations of selenate and selenite by Stenotrophomonas maltophilia isolated from a seleniferous agricultural drainage pond sediment. Environmental Microbiology 5, 287–295. https://doi.org/10.1046/j.1462-2920.2003.00410.x

Duntas, L.H., Benvenga, S., 2015. Selenium: an element for life. Endocrine 48, 756–775. https://doi.org/10.1007/s12020-014-0477-6

Dupierris, V., Masselon, C., Court, M., Kieffer-Jaquinod, S., Bruley, C., 2009. A toolbox for validation of mass spectrometry peptides identification and generation of database: IRMa. Bioinformatics 25, 1980–1981. https://doi.org/10.1093/bioinformatics/btp301

Edmonds, M., Mather, T.A., Liu, E.J., 2018. A distinct metal fingerprint in arc volcanic emissions. Nature Geoscience 11, 790–794. https://doi.org/10.1038/s41561-018-0214-5

Elahian, F., Reiisi, S., Shahidi, A., Mirzaei, S.A., 2017. High-throughput bioaccumulation, biotransformation, and production of silver and selenium nanoparticles using genetically engineered Pichia pastoris. Nanomedicine: Nanotechnology, Biology and Medicine 13, 853–861. https://doi.org/10.1016/j.nano.2016.10.009

Eliet, V., Bidoglio, G., Omenetto, N., Parma, L., Grenthe, I., 1995. Characterisation of hydroxide complexes of uranium(VI) by time-resolved fluorescence spectroscopy. Journal of the Chemical Society, Faraday Transactions 91, 2275–2285. https://doi.org/10.1039/FT9959102275

Equeenuddin, Sk.Md., Tripathy, S., Sahoo, P.K., Panigrahi, M.K., 2013. Metal behavior in sediment associated with acid mine drainage stream: Role of pH. Journal of Geochemical Exploration 124, 230–237. https://doi.org/10.1016/j.gexplo.2012.10.010

Eswayah, A.S., Hondow, N., Scheinost, A.C., Merroun, M., Romero-González,

M., Smith, T.J., Gardiner, P.H.E., 2019. Methyl Selenol as a Precursor in Selenite Reduction to Se/S Species by Methane-Oxidizing Bacteria. Appl Environ Microbiol 85, e01379-19, /aem/85/22/AEM.01379-19.atom. https://doi.org/10.1128/AEM.01379-19

Eswayah, A.S., Smith, T.J., Gardiner, P.H.E., 2016. Microbial Transformations of Selenium Species of Relevance to Bioremediation. Appl. Environ. Microbiol. 82, 4848–4859. https://doi.org/10.1128/AEM.00877-16

Etteieb, S., Magdouli, S., Zolfaghari, M., Brar, S., 2020. Monitoring and analysis of selenium as an emerging contaminant in mining industry: A critical review. Science of The Total Environment 698, 134339. https://doi.org/10.1016/j.scitotenv.2019.134339

Fath, M.J., Kolter, R., 1993. ABC transporters: bacterial exporters. Microbiol Rev 57, 995–1017.

FATHt, M.J., Kolter, R., n.d. ABC Transporters: Bacterial Exporters 23.

Filip'echeva, Y.A., Shelud'ko, A.V., Prilipov, A.G., Burygin, G.L., Telesheva, E.M., Yevstigneyeva, S.S., Chernyshova, M.P., Petrova, L.P., Katsy, E.I., 2018. Plasmid AZOBR_p1-borne *fabG* gene for putative 3-oxoacyl-[acyl-carrier protein] reductase is essential for proper assembly and work of the dual flagellar system in the alphaproteobacterium *Azospirillum brasilense* Sp245. Can. J. Microbiol. 64, 107–118. https://doi.org/10.1139/cjm-2017-0561

Fischer, S., Krause, T., Lederer, F., Merroun, M.L., Shevchenko, A., Hübner, R., Firkala, T., Stumpf, T., Jordan, N., Jain, R., 2020. Bacillus safensis JG-B5T affects the fate of selenium by extracellular production of colloidally less stable selenium nanoparticles. Journal of Hazardous Materials 384, 121146. https://doi.org/10.1016/j.jhazmat.2019.121146

Gadd, G.M., Fomina, M., 2011. Uranium and Fungi. Geomicrobiology Journal 28, 471–482. https://doi.org/10.1080/01490451.2010.508019

Gallois, N., Alpha-Bazin, B., Ortet, P., Barakat, M., Piette, L., Long, J., Berthomieu, C., Armengaud, J., Chapon, V., 2018. Proteogenomic insights into uranium tolerance of a Chernobyl's Microbacterium bacterial isolate. Journal of Proteomics 177, 148–157. https://doi.org/10.1016/j.jprot.2017.11.021

García-Ordiales, E., Esbrí, J.M., Covelli, S., López-Berdonces, M.A., Higueras, P.L., Loredo, J., 2016. Heavy metal contamination in sediments of an artificial reservoir impacted by long-term mining activity in the Almadén mercury district (Spain). Environ Sci Pollut Res 23, 6024–6038. https://doi.org/10.1007/s11356-015-4770-6

Gautam, P.K., Gautam, R.K., Banerjee, S., Chattopadhyaya, M.C., Pandey, J.D.,

n.d. HEAVY METALS IN THE ENVIRONMENT: FATE, TRANSPORT, TOXICITY AND REMEDIATION TECHNOLOGIES 30.

Gavrilescu, M., Pavel, L.V., Cretescu, I., 2009. Characterization and remediation of soils contaminated with uranium. Journal of Hazardous Materials 163, 475–510. https://doi.org/10.1016/j.jhazmat.2008.07.103

Geipel, G., Bernhard, G., Rutsch, M., Brendler, V., Nitsche, H., 2000. Spectroscopic properties of uranium(VI) minerals studied by time-resolved laser-induced fluorescence spectroscopy (TRLFS). Radiochimica Acta 88, 757–762. https://doi.org/10.1524/ract.2000.88.9-11.757

Geipel, Gerhard, Bernhard, G., Rutsch, M., Brendler, V., Nitsche, H., 2000. Spectroscopic properties of uranium(VI) minerals studied by time-resolved laser-induced fluorescence spectroscopy (TRLFS). Radiochimica Acta 88, 757–762. https://doi.org/10.1524/ract.2000.88.9-11.757

Gerber, U., Zirnstein, I., Krawczyk-Bärsch, E., Lünsdorf, H., Arnold, T., Merroun, M.L., 2016. Combined use of flow cytometry and microscopy to study the interactions between the gram-negative betaproteobacterium Acidovorax facilis and uranium(VI). Journal of Hazardous Materials 317, 127–134. https://doi.org/10.1016/j.jhazmat.2016.05.062

German, D.P., Weintraub, M.N., Grandy, A.S., Lauber, C.L., Rinkes, Z.L., Allison, S.D., 2011. Optimization of hydrolytic and oxidative enzyme methods for ecosystem studies. Soil Biology and Biochemistry 43, 1387–1397. https://doi.org/10.1016/j.soilbio.2011.03.017

Gómez-Gómez, B., Pérez-Corona, T., Mozzi, F., Pescuma, M., Madrid, Y., 2019. Silac-based quantitative proteomic analysis of Lactobacillus reuteri CRL 1101 response to the presence of selenite and selenium nanoparticles. Journal of Proteomics 195, 53–65. https://doi.org/10.1016/j.jprot.2018.12.025

Gonzalez-Gil, G., Lens, P.N.L., Saikaly, P.E., 2016. Selenite Reduction by Anaerobic Microbial Aggregates: Microbial Community Structure, and Proteins Associated to the Produced Selenium Spheres. Front. Microbiol. 7. https://doi.org/10.3389/fmicb.2016.00571

Gouveia, D., Grenga, L., Pible, O., Armengaud, J., 2020. Quick microbial molecular phenotyping by differential shotgun proteomics. Environ Microbiol 22, 2996–3004. https://doi.org/10.1111/1462-2920.14975

Grinter, R., Lithgow, T., 2019. The structure of the bacterial iron–catecholate

transporter Fiu suggests that it imports substrates via a two-step mechanism. J. Biol. Chem. 294, 19523–19534. https://doi.org/10.1074/jbc.RA119.011018

Hancock, V., Vejborg, R.M., Klemm, P., 2010. Functional genomics of probiotic Escherichia coli Nissle 1917 and 83972, and UPEC strain CFT073: comparison of transcriptomes, growth and biofilm formation. Mol Genet Genomics 284, 437–454. https://doi.org/10.1007/s00438-010-0578-8

Harrison, G., Curle, C., Laishley, E.J., 1984. Purification and characterization of an inducible dissimilatory type sulfite reductase from Clostridium pasteurianum. Arch. Microbiol. 138, 72–78. https://doi.org/10.1007/BF00425411

Hartmann, E.M., Allain, F., Gaillard, J.-C., Pible, O., Armengaud, J., 2014. Taking the Shortcut for High-Throughput Shotgun Proteomic Analysis of Bacteria, in: Vergunst, A.C., O'Callaghan, D. (Eds.), Host-Bacteria Interactions, Methods in Molecular Biology. Springer New York, New York, NY, pp. 275–285. https://doi.org/10.1007/978-1-4939-1261-2_16

Hayashi, K., Nakashima, R., Sakurai, K., Kitagawa, K., Yamasaki, S., Nishino, K., Yamaguchi, A., 2015. AcrB-AcrA Fusion Proteins That Act as Multidrug Efflux Transporters. J Bacteriol 198, 332–342. https://doi.org/10.1128/JB.00587-15

Hayoun, K., Gouveia, D., Grenga, L., Pible, O., Armengaud, J., Alpha-Bazin, B., 2019. Evaluation of Sample Preparation Methods for Fast Proteotyping of Microorganisms by Tandem Mass Spectrometry. Front. Microbiol. 10, 1985. https://doi.org/10.3389/fmicb.2019.01985

Hervás, M., López-Maury, L., León, P., Sánchez-Riego, A.M., Florencio, F.J., Navarro, J.A., 2012. ArsH from the Cyanobacterium Synechocystis sp. PCC 6803 Is an Efficient NADPH-Dependent Quinone Reductase. Biochemistry 51, 1178–1187. https://doi.org/10.1021/bi201904p

Horvath, A., Rachlew, E., 2016. Nuclear power in the 21st century: Challenges and possibilities. Ambio 45, 38–49. https://doi.org/10.1007/s13280-015-0732-y

Hu, P., Brodie, E.L., Suzuki, Y., McAdams, H.H., Andersen, G.L., 2005. Whole-Genome Transcriptional Analysis of Heavy Metal Stresses in Caulobacter crescentus. Journal of Bacteriology 187, 8437–8449. https://doi.org/10.1128/JB.187.24.8437-8449.2005

Huang, H.-H., Lin, Y.-T., Chen, W.-C., Huang, Y.-W., Chen, S.-J., Yang, T.-C., 2015. Expression and Functions of CreD, an Inner Membrane Protein in Stenotrophomonas maltophilia. PLOS ONE 10, e0145009.

https://doi.org/10.1371/journal.pone.0145009

Huang, Y.-W., Liou, R.-S., Lin, Y.-T., Huang, H.-H., Yang, T.-C., 2014. A Linkage between SmeIJK Efflux Pump, Cell Envelope Integrity, and σE-Mediated Envelope Stress Response in Stenotrophomonas maltophilia. PLoS ONE 9, e111784. https://doi.org/10.1371/journal.pone.0111784

Hunter, W.J., 2014. Pseudomonas seleniipraecipitans Proteins Potentially Involved in Selenite Reduction. Curr Microbiol 69, 69–74. https://doi.org/10.1007/s00284-014-0555-2

Ibrahim, M., Shi, Y., Qiu, H., Li, B., Jabeen, A., Li, L., Liu, H., Kube, M., Xie, G., Wang, Y., Sun, G., 2012. Differential Expression of In Vivo and In Vitro Protein Profile of Outer Membrane of Acidovorax avenae Subsp. avenae. PLoS ONE 7, e49657. https://doi.org/10.1371/journal.pone.0049657

Ikonen, J., Voutilainen, M., Söderlund, M., Jokelainen, L., Siitari-Kauppi, M., Martin, A., 2016. Sorption and diffusion of selenium oxyanions in granitic rock. Journal of Contaminant Hydrology 192, 203–211. https://doi.org/10.1016/j.jconhyd.2016.08.003

Islam, E., Sar, P., 2016. Diversity, metal resistance and uranium sequestration abilities of bacteria from uranium ore deposit in deep earth stratum. Ecotoxicology and Environmental Safety 127, 12–21. https://doi.org/10.1016/j.ecoenv.2016.01.001

J., S., P., B., R., O., 2002. Microbial transformation of elements: the case of arsenic and selenium. International Microbiology 5, 201–207. https://doi.org/10.1007/s10123-002-0091-y

Jahan, Mst.I., Juengwiwattanakitti, P., Izu, Y., Tobe, R., Imai, T., Mihara, H., 2019. Selenite uptake by outer membrane porin ExtI and its involvement in the subcellular localization of rhodanese-like lipoprotein ExtH in Geobacter sulfurreducens. Biochemical and Biophysical Research Communications 516, 474–479. https://doi.org/10.1016/j.bbrc.2019.06.037

Jain, R., Jordan, N., Tsushima, S., Hübner, R., Weiss, S., Lens, P.N.L., 2017a. Shape change of biogenic elemental selenium nanomaterials from nanospheres to nanorods decreases their colloidal stability. Environ. Sci.: Nano 4, 1054–1063. https://doi.org/10.1039/C7EN00145B

Jain, R., Jordan, N., Tsushima, S., Hübner, R., Weiss, S., L. Lens, P.N., 2017b. Shape change of biogenic elemental selenium nanomaterials from nanospheres to nanorods decreases their colloidal stability. Environmental Science: Nano 4, 1054–1063. https://doi.org/10.1039/C7EN00145B

Jauberty, L., Drogat, N., Decossas, J.-L., Delpech, V., Gloaguen, V., Sol, V., 2013. Optimization of the arsenazo-III method for the determination of uranium in water and plant samples. Talanta 115, 751–754. https://doi.org/10.1016/j.talanta.2013.06.046

Ji, G., Silver, S., 1995. Bacterial resistance mechanisms for heavy metals of environmental concern. Journal of Industrial Microbiology 14, 61–75. https://doi.org/10.1007/BF01569887

Jin, M., Xiao, A., Zhu, L., Zhang, Z., Huang, H., Jiang, L., 2019. The diversity and commonalities of the radiation-resistance mechanisms of Deinococcus and its up-to-date applications. AMB Express 9. https://doi.org/10.1186/s13568-019-0862-x

Kessi, J., 2006. Enzymic systems proposed to be involved in the dissimilatory reduction of selenite in the purple non-sulfur bacteria Rhodospirillum rubrum and Rhodobacter capsulatus. Microbiology 152, 731–743. https://doi.org/10.1099/mic.0.28240-0

Khalid, S., Bond, P.J., Carpenter, T., Sansom, M.S.P., 2008. OmpA: Gating and dynamics via molecular dynamics simulations. Biochimica et Biophysica Acta (BBA) - Biomembranes 1778, 1871–1880. https://doi.org/10.1016/j.bbamem.2007.05.024

Khoei, N.S., Lampis, S., Zonaro, E., Yrjälä, K., Bernardi, P., Vallini, G., 2017. Insights into selenite reduction and biogenesis of elemental selenium nanoparticles by two environmental isolates of Burkholderia fungorum. New Biotechnology 34, 1–11. https://doi.org/10.1016/j.nbt.2016.10.002

Kieliszek, M., Błażejak, S., Bzducha-Wróbel, A., Kot, A.M., 2019. Effect of Selenium on Lipid and Amino Acid Metabolism in Yeast Cells. Biol Trace Elem Res 187, 316–327. https://doi.org/10.1007/s12011-018-1342-x

Klein, G., Mathé, C., Biola-Clier, M., Devineau, S., Drouineau, E., Hatem, E., Marichal, L., Alonso, B., Gaillard, J.-C., Lagniel, G., Armengaud, J., Carrière, M., Chédin, S., Boulard, Y., Pin, S., Renault, J.-P., Aude, J.-C., Labarre, J., 2016. RNA-binding proteins are a major target of silica nanoparticles in cell extracts. Nanotoxicology 10, 1555–1564. https://doi.org/10.1080/17435390.2016.1244299

Koban, A., Geipel, G., Roßberg, A., Bernhard, G., 2004. Uranium(VI) complexes with sugar phosphates in aqueous solution. Radiochimica Acta 92, 903–908. https://doi.org/10.1524/ract.92.12.903.55114

Kolhe, N., Zinjarde, S., Acharya, C., 2018. Responses exhibited by various microbial groups relevant to uranium exposure. Biotechnology Advances 36, 1828–1846. https://doi.org/10.1016/j.biotechadv.2018.07.002

Kolodkin-Gal, I., Verdiger, R., Shlosberg-Fedida, A., Engelberg-Kulka, H., 2009. A Differential Effect of E. coli Toxin-Antitoxin Systems on Cell Death in Liquid Media and Biofilm Formation. PLoS ONE 4, e6785. https://doi.org/10.1371/journal.pone.0006785

Kónya, J., Nagy, N.M., 2018. Chapter 13 - Environmental Radioactivity, in: Kónya, J., Nagy, N.M. (Eds.), Nuclear and Radiochemistry (Second Edition). Elsevier, pp. 399–419. https://doi.org/10.1016/B978-0-12-813643-0.00013-5

Krafft, T., Bowen, A., Theis, F., Macy, J.M., 2000. Cloning and sequencing of the genes encoding the periplasmic-cytochrome B-containing selenate reductase of Thauera selenatis. DNA Seq 10, 365–377. https://doi.org/10.3109/10425170009015604

Krisko, A., Radman, M., 2013. Biology of extreme radiation resistance: the way of Deinococcus radiodurans. Cold Spring Harb Perspect Biol 5. https://doi.org/10.1101/cshperspect.a012765

Kulkarni, S., Ballal, A., Apte, S.K., 2013. Bioprecipitation of uranium from alkaline waste solutions using recombinant Deinococcus radiodurans. Journal of Hazardous Materials 262, 853–861. https://doi.org/10.1016/j.jhazmat.2013.09.057

Kulkarni, S., Misra, C.S., Gupta, A., Ballal, A., Apte, S.K., 2016. Interaction of Uranium with Bacterial Cell Surfaces: Inferences from Phosphatase-Mediated Uranium Precipitation. Applied and Environmental Microbiology 82, 4965–4974. https://doi.org/10.1128/AEM.00728-16

Kuroda, M., Yamashita, M., Miwa, E., Imao, K., Fujimoto, N., Ono, H., Nagano, K., Sei, K., Ike, M., 2011. Molecular Cloning and Characterization of the srdBCA Operon, Encoding the Respiratory Selenate Reductase Complex, from the Selenate-Reducing Bacterium Bacillus selenatarsenatis SF-1. Journal of Bacteriology 193, 2141–2148. https://doi.org/10.1128/JB.01197-10

Lakaniemi, A.-M., Douglas, G.B., Kaksonen, A.H., 2019. Engineering and kinetic aspects of bacterial uranium reduction for the remediation of uranium contaminated environments. Journal of Hazardous Materials 371, 198–212. https://doi.org/10.1016/j.jhazmat.2019.02.074

Lampis, S., Zonaro, E., Bertolini, C., Cecconi, D., Monti, F., Micaroni, M., Turner, R.J., Butler, C.S., Vallini, G., 2017. Selenite biotransformation and detoxification by Stenotrophomonas maltophilia SeITE02: Novel clues on the route to bacterial biogenesis of selenium nanoparticles. Journal of Hazardous Materials 324, 3–14. https://doi.org/10.1016/j.jhazmat.2016.02.035

Leskela, S., Kontinen, V.P., Sarvas, M., 1996. Molecular analysis of an operon in Bacillus subtilis encoding a novel ABC transporter with a role in exoprotein production, sporulation and competence. Microbiology 142, 71–77. https://doi.org/10.1099/13500872-142-1-71

Levicán, G., Ugalde, J.A., Ehrenfeld, N., Maass, A., Parada, P., 2008. Comparative genomic analysis of carbon and nitrogen assimilation mechanisms in three indigenous bioleaching bacteria: predictions and validations. BMC Genomics 9, 581. https://doi.org/10.1186/1471-2164-9-581

Li, D.-B., Cheng, Y.-Y., Wu, C., Li, W.-W., Li, N., Yang, Z.-C., Tong, Z.-H., Yu, H.-Q., 2014. Selenite reduction by Shewanella oneidensis MR-1 is mediated by fumarate reductase in periplasm. Sci Rep 4. https://doi.org/10.1038/srep03735

Li, F., Li, X., Hou, L., Shao, A., 2018. Impact of the Coal Mining on the Spatial Distribution of Potentially Toxic Metals in Farmland Tillage Soil. Scientific Reports 8, 14925. https://doi.org/10.1038/s41598-018-33132-4

Li, X., Ding, C., Liao, J., Du, L., Sun, Q., Yang, J., Yang, Y., Zhang, D., Tang, J., Liu, N., 2017. Microbial reduction of uranium (VI) by Bacillus sp. dwc-2: A macroscopic and spectroscopic study. Journal of Environmental Sciences 53, 9–15. https://doi.org/10.1016/j.jes.2016.01.030

Li, Z., Ma, Z., van der Kuijp, T.J., Yuan, Z., Huang, L., 2014. A review of soil heavy metal pollution from mines in China: Pollution and health risk assessment. Science of The Total Environment 468–469, 843–853. https://doi.org/10.1016/j.scitotenv.2013.08.090

Liang, X., Csetenyi, L., Gadd, G.M., 2016. Uranium bioprecipitation mediated by yeasts utilizing organic phosphorus substrates. Appl Microbiol Biotechnol 100, 5141–5151. https://doi.org/10.1007/s00253-016-7327-9

Liao, J., Wen, Z., Ru, X., Chen, J., Wu, H., Wei, C., 2016. Distribution and migration of heavy metals in soil and crops affected by acid mine drainage: Public health implications in Guangdong Province, China. Ecotoxicology and Environmental Safety 124, 460–469. https://doi.org/10.1016/j.ecoenv.2015.11.023

Lloyd, J.R., Macaskie, L.E., 2000. Bioremediation of Radionuclide-Containing Wastewaters, in: Environmental Microbe-Metal Interactions. John Wiley & Sons, Ltd, pp. 277–327. https://doi.org/10.1128/9781555818098.ch13

Lopez-Fernandez, M., Cherkouk, A., Vilchez-Vargas, R., Jauregui, R., Pieper, D., Boon, N., Sanchez-Castro, I., Merroun, M.L., 2015. Bacterial Diversity in Bentonites,

Engineered Barrier for Deep Geological Disposal of Radioactive Wastes. Microbial Ecology 70, 922–935. https://doi.org/10.1007/s00248-015-0630-7

López-Fernández, M., Fernández-Sanfrancisco, O., Moreno-García, A., Martín-Sánchez, I., Sánchez-Castro, I., Merroun, M.L., 2014. Microbial communities in bentonite formations and their interactions with uranium. Applied Geochemistry 49, 77–86. https://doi.org/10.1016/j.apgeochem.2014.06.022

Lopez-Fernandez, M., Jroundi, F., Ruiz-Fresneda, M.A., Merroun, M.L., 2020. Microbial interaction with and tolerance of radionuclides: underlying mechanisms and biotechnological applications. Microb. Biotechnol. 1751-7915.13718. https://doi.org/10.1111/1751-7915.13718

Lopez-Fernandez, M., Romero-González, M., Günther, A., Solari, P.L., Merroun, M.L., 2018. Effect of U(VI) aqueous speciation on the binding of uranium by the cell surface of Rhodotorula mucilaginosa, a natural yeast isolate from bentonites. Chemosphere 199, 351–360. https://doi.org/10.1016/j.chemosphere.2018.02.055

Loreggian, L., Sorwat, J., Byrne, J.M., Kappler, A., Bernier-Latmani, R., 2020. Role of Iron Sulfide Phases in the Stability of Noncrystalline Tetravalent Uranium in Sediments. Environ. Sci. Technol. 54, 4840–4846. https://doi.org/10.1021/acs.est.9b07186

Luke, N.R., Sauberan, S.L., Russo, T.A., Beanan, J.M., Olson, R., Loehfelm, T.W., Cox, A.D., St. Michael, F., Vinogradov, E.V., Campagnari, A.A., 2010. Identification and Characterization of a Glycosyltransferase Involved in Acinetobacter baumannii Lipopolysaccharide Core Biosynthesis. Infection and Immunity 78, 2017–2023. https://doi.org/10.1128/IAI.00016-10

Lütke, L., Moll, H., Bernhard, G., 2012. Insights into the uranium(vi) speciation with Pseudomonas fluorescens on a molecular level. Dalton Transactions 41, 13370–13378. https://doi.org/10.1039/c2dt31080e

Macaskie, L.E., Bonthrone, K.M., Yong, P., Goddard, D.T., 2000. Enzymically mediated bioprecipitation of uranium by a Citrobacter sp.: a concerted role for exocellular lipopolysaccharide and associated phosphatase in biomineral formation. Microbiology, 146, 1855–1867. https://doi.org/10.1099/00221287-146-8-1855

Marquez, B., 2005. Bacterial efflux systems and efflux pumps inhibitors. Biochimie 87, 1137–1147. https://doi.org/10.1016/j.biochi.2005.04.012

McBroom, A.J., Kuehn, M.J., 2007. Release of outer membrane vesicles by Gram-negative bacteria is a novel envelope stress response. Molecular Microbiology 63,

545–558. https://doi.org/10.1111/j.1365-2958.2006.05522.x

Merroun, M., Hennig, C., Rossberg, A., Reich, T., Selenska-Pobell, S., 2003a. Characterization of U(VI)-Acidithiobacillus ferrooxidans complexes using EXAFS, transmission electron microscopy, and energy-dispersive X-ray analysis. Radiochimica Acta 91, 583–592.

Merroun, M., Hennig, C., Rossberg, A., Reich, T., Selenska-Pobell, S., 2003b. Characterization of U(VI)-Acidithiobacillus ferrooxidans complexes using EXAFS, transmission electron microscopy, and energy-dispersive X-ray analysis. Radiochimica Acta 91, 583–592. https://doi.org/10.1524/ract.91.10.583.22477

Merroun, M.L., Nedelkova, M., Ojeda, J.J., Reitz, T., Fernández, M.L., Arias, J.M., Romero-González, M., Selenska-Pobell, S., 2011. Bio-precipitation of uranium by two bacterial isolates recovered from extreme environments as estimated by potentiometric titration, TEM and X-ray absorption spectroscopic analyses. Journal of Hazardous Materials 197, 1–10. https://doi.org/10.1016/j.jhazmat.2011.09.049

Merroun, M.L., Raff, J., Rossberg, A., Hennig, C., Reich, T., Selenska-Pobell, S., 2005a. Complexation of uranium by cells and S-layer sheets of Bacillus sphaericus JG-A12. Applied and Environmental Microbiology. https://doi.org/10.1128/AEM.71.9.5532-5543.2005

Merroun, M.L., Raff, J., Rossberg, A., Hennig, C., Reich, T., Selenska-Pobell, S., 2005b. Complexation of Uranium by Cells and S-Layer Sheets of Bacillus sphaericus JG-A12. Appl. Environ. Microbiol. 71, 5532–5543. https://doi.org/10.1128/AEM.71.9.5532-5543.2005

Merroun, M.L., Selenska-Pobell, S., 2008. Bacterial interactions with uranium: An environmental perspective. Journal of Contaminant Hydrology 102, 285–295. https://doi.org/10.1016/j.jconhyd.2008.09.019

Metzger, L.E., Raetz, C.R.H., 2009. Purification and Characterization of the Lipid A Disaccharide Synthase (LpxB) from *Escherichia coli* , a Peripheral Membrane Protein. Biochemistry 48, 11559–11571. https://doi.org/10.1021/bi901750f

Mishra, A., Malik, A., 2013. Recent Advances in Microbial Metal Bioaccumulation. Critical Reviews in Environmental Science and Technology 43, 1162–1222. https://doi.org/10.1080/10934529.2011.627044

Mitchell, A.M., Silhavy, T.J., 2019. Envelope stress responses: balancing damage repair and toxicity. Nature Reviews Microbiology 17, 417–428. https://doi.org/10.1038/s41579-019-0199-0

Modi, N., Bárcena-Uribarri, I., Bains, M., Benz, R., Hancock, R.E.W., Kleinekathöfer, U., 2015. Tuning the Affinity of Anion Binding Sites in Porin Channels with Negatively Charged Residues: Molecular Details for OprP. ACS Chem. Biol. 10, 441–451. https://doi.org/10.1021/cb500399j

Morcillo, F., Gonźalez-M̃unoz, M.T., Reitz, T., Romero-Gonźalez, M.E., Arias, J.M., Merroun, M.L., 2014. Biosorption and biomineralization of U(VI) by the marine bacterium Idiomarina loihiensis MAH1: Effect of background electrolyte and pH. PLoS ONE 9. https://doi.org/10.1371/journal.pone.0091305

Moulin, C., Laszak, I., Moulin, V., Tondre, C., 1998. Time-resolved laser-induced fluorescence as a unique tool for low-level uranium speciation. Applied Spectroscopy 52, 528–535. https://doi.org/10.1366/0003702981944076

Murahari, P., Anishetty, S., Pennathur, G., 2013. Understanding the lid movements of LolA in Escherichia coli using molecular dynamics simulation and in silico point mutation. Computational Biology and Chemistry 47, 71–80. https://doi.org/10.1016/j.compbiolchem.2013.06.005

Murphy, J., Riley, J.P., 1962. A modified single solution method for the determination of phosphate in natural waters. Analytica Chimica Acta 27, 31–36. https://doi.org/10.1016/S0003-2670(00)88444-5

Nakamoto, H., Bardwell, J.C.A., 2004. Catalysis of disulfide bond formation and isomerization in the Escherichia coli periplasm. Biochimica et Biophysica Acta (BBA) - Molecular Cell Research 1694, 111–119. https://doi.org/10.1016/j.bbamcr.2004.02.012

Nancharaiah, Y.V., Lens, P.N.L., 2015. Selenium biomineralization for biotechnological applications. Trends in Biotechnology 33, 323–330. https://doi.org/10.1016/j.tibtech.2015.03.004

Newsome, L., Morris, K., Lloyd, J.R., 2014. The biogeochemistry and bioremediation of uranium and other priority radionuclides. Chemical Geology 363, 164–184. https://doi.org/10.1016/j.chemgeo.2013.10.034

Ni, T.W., Staicu, L.C., Nemeth, R.S., Schwartz, C.L., Crawford, D., Seligman, J.D., Hunter, W.J., Pilon-Smits, E.A.H., Ackerson, C.J., 2015. Progress toward clonable inorganic nanoparticles. Nanoscale 7, 17320–17327. https://doi.org/10.1039/C5NR04097C

Nieboer, E., Richardson, D.H.S., 1980. The replacement of the nondescript term ‘heavy metals’ by a biologically and chemically significant classification of metal ions. Environmental Pollution Series B, Chemical and Physical 1, 3–26.

https://doi.org/10.1016/0143-148X(80)90017-8

Nies, D.H., 2003. Efflux-mediated heavy metal resistance in prokaryotes. FEMS Microbiology Reviews 27, 313–339. https://doi.org/10.1016/S0168-6445(03)00048-2

Nilgiriwala, K.S., Alahari, A., Rao, A.S., Apte, S.K., 2008. Cloning and Overexpression of Alkaline Phosphatase PhoK from Sphingomonas sp. Strain BSAR-1 for Bioprecipitation of Uranium from Alkaline Solutions. Applied and Environmental Microbiology 74, 5516–5523. https://doi.org/10.1128/AEM.00107-08

Nilsson, G., Belasco, J.G., Cohen, S.N., von Gabain, A., 1984. Growth-rate dependent regulation of mRNA stability in Escherichia coli. Nature 312, 75–77. https://doi.org/10.1038/312075a0

Noinaj, N., Guillier, M., Barnard, T.J., Buchanan, S.K., 2010. TonB-dependent transporters: regulation, structure, and function. Annu Rev Microbiol 64, 43–60. https://doi.org/10.1146/annurev.micro.112408.134247

Ojeda, J.J., Merroun, M.L., Tugarova, A.V., Lampis, S., Kamnev, A.A., Gardiner, P.H.E., 2020. Developments in the study and applications of bacterial transformations of selenium species. Critical Reviews in Biotechnology 40, 1250–1264. https://doi.org/10.1080/07388551.2020.1811199

Orellana, R., Hixson, K.K., Murphy, S., Mester, T., Sharma, M.L., Lipton, M.S., Lovley, D.R., 2014. Proteome of Geobacter sulfurreducens in the presence of U(VI). Microbiology 160, 2607–2617. https://doi.org/10.1099/mic.0.081398-0

Osredkar, J., 2011. Copper and Zinc, Biological Role and Significance of Copper/Zinc Imbalance. J Clin Toxicol s3. https://doi.org/10.4172/2161-0495.S3-001

Otsuka, O., Yamashita, M., 2020. Selenium recovery from wastewater using the selenate-reducing bacterium Pseudomonas stutzeri NT-I. Hydrometallurgy 197, 105470. https://doi.org/10.1016/j.hydromet.2020.105470

P1799_web.pdf, n.d.

Pan, X., Chen, Z., Chen, F., Cheng, Y., Lin, Z., Guan, X., 2015. The mechanism of uranium transformation from U(VI) into nano-uramphite by two indigenous Bacillus thuringiensis strains. Journal of Hazardous Materials 297, 313–319. https://doi.org/10.1016/j.jhazmat.2015.05.019

Panak, P.J., Raff, J., Selenska-Pobell, S., Geipel, G., Bernhard, G., Nitsche, H., 2000. Complex formation of U(VI) with Bacillus-isolates from a uranium mining waste pile. Radiochimica Acta 88, 71–76. https://doi.org/10.1524/ract.2000.88.2.071

Park, D.M., Jiao, Y., 2014. Modulation of Medium pH by Caulobacter crescentus

Facilitates Recovery from Uranium-Induced Growth Arrest. Appl. Environ. Microbiol. 80, 5680–5688. https://doi.org/10.1128/AEM.01294-14

Passmore, I.J., Dow, J.M., Coll, F., Cuccui, J., Palmer, T., Wren, B.W., 2020. Ferric Citrate Regulator FecR Is Translocated across the Bacterial Inner Membrane via a Unique Twin-Arginine Transport-Dependent Mechanism. J Bacteriol 202, e00541-19, /jb/202/9/JB.00541-19.atom. https://doi.org/10.1128/JB.00541-19

Pattanapipitpaisal, P., Mabbett, A.N., Finlay, J.A., Beswick, A.J., Paterson-Beedle, M., Essa, A., Wright, J., Tolley, M.R., Badar, U., Ahmed, N., Hobman, J.L., Brown, N.L., Macaskie, L.E., 2002. Reduction of Cr(VI) and Bioaccumulation of Chromium by Gram Positive and Gram Negative Microorganisms not Previously Exposed to CR-Stress. Environmental Technology 23, 731–745. https://doi.org/10.1080/09593332308618367

Perez-Riverol, Y., Zorin, A., Dass, G., Vu, M.-T., Xu, P., Glont, M., Vizcaíno, J.A., Jarnuczak, A.F., Petryszak, R., Ping, P., Hermjakob, H., 2019. Quantifying the impact of public omics data. Nature Communications 10, 3512. https://doi.org/10.1038/s41467-019-11461-w

Piacenza, E., Presentato, A., Zonaro, E., Lampis, S., Vallini, G., Turner, R.J., 2018. Microbial-Based Bioremediation of Selenium and Tellurium Compounds, in: Derco, J., Vrana, B. (Eds.), Biosorption. InTech. https://doi.org/10.5772/intechopen.72096

Pinel-Cabello, M., Jroundi, F., López-Fernández, M., Geffers, R., Jarek, M., Jauregui, R., Link, A., Vílchez-Vargas, R., Merroun, M.L., 2021. Multisystem combined uranium resistance mechanisms and bioremediation potential of Stenotrophomonas bentonitica BII-R7: Transcriptomics and microscopic study. Journal of Hazardous Materials 403, 123858. https://doi.org/10.1016/j.jhazmat.2020.123858

Pittman, M.S., Robinson, H.C., Poole, R.K., 2005. A Bacterial Glutathione Transporter (*Escherichia coli* CydDC) Exports Reductant to the Periplasm. J. Biol. Chem. 280, 32254–32261. https://doi.org/10.1074/jbc.M503075200

Poirier, I., Kuhn, L., Demortière, A., Mirvaux, B., Hammann, P., Chicher, J., Caplat, C., Pallud, M., Bertrand, M., 2016. Ability of the marine bacterium Pseudomonas fluorescens BA3SM1 to counteract the toxicity of CdSe nanoparticles. Journal of Proteomics 148, 213–227. https://doi.org/10.1016/j.jprot.2016.07.021

Porcelli, D., 2018. Radioactivity, in: White, W.M. (Ed.), Encyclopedia of Geochemistry: A Comprehensive Reference Source on the Chemistry of the Earth.

Springer International Publishing, Cham, pp. 1295–1298. https://doi.org/10.1007/978-3-319-39312-4_269

Pourret, O., 2018. On the Necessity of Banning the Term “Heavy Metal” from the Scientific Literature. Sustainability 10, 2879. https://doi.org/10.3390/su10082879

Prakash, D., Gabani, P., Chandel, A.K., Ronen, Z., Singh, O.V., 2013. Bioremediation: a genuine technology to remediate radionuclides from the environment. Microbial Biotechnology 6, 349–360. https://doi.org/10.1111/1751-7915.12059

Prăvălie, R., 2018. Nuclear energy: Between global electricity demand, worldwide decarbonisation imperativeness, and planetary environmental implications. Journal of Environmental Management 12.

Presentato, A., Piacenza, E., Anikovskiy, M., Cappelletti, M., Zannoni, D., Turner, R.J., 2018. Biosynthesis of selenium-nanoparticles and -nanorods as a product of selenite bioconversion by the aerobic bacterium Rhodococcus aetherivorans BCP1. New Biotechnology 41, 1–8. https://doi.org/10.1016/j.nbt.2017.11.002

Qu, C.-S., Ma, Z.-W., Yang, J., Liu, Y., Bi, J., Huang, L., 2012. Human Exposure Pathways of Heavy Metals in a Lead-Zinc Mining Area, Jiangsu Province, China. PLoS ONE 7, e46793. https://doi.org/10.1371/journal.pone.0046793

Rajta, A., Bhatia, R., Setia, H., Pathania, P., 2020. Role of heterotrophic aerobic denitrifying bacteria in nitrate removal from wastewater. Journal of Applied Microbiology 128, 1261–1278. https://doi.org/10.1111/jam.14476

Ranjard, L., Prigent-Combaret, C., Nazaret, S., Cournoyer, B., 2002. Methylation of Inorganic and Organic Selenium by the Bacterial Thiopurine Methyltransferase. JB 184, 3146–3149. https://doi.org/10.1128/JB.184.11.3146-3149.2002

Ridley, H., Watts, C.A., Richardson, D.J., Butler, C.S., 2006. Resolution of Distinct Membrane-Bound Enzymes from Enterobacter cloacae SLD1a-1 That Are Responsible for Selective Reduction of Nitrate and Selenate Oxyanions. AEM 72, 5173–5180. https://doi.org/10.1128/AEM.00568-06

Rosen, B.P., Liu, Z., 2009. Transport pathways for arsenic and selenium: A minireview. Environment International 35, 512–515. https://doi.org/10.1016/j.envint.2008.07.023

Rosenfeld, Y., Shai, Y., 2006. Lipopolysaccharide (Endotoxin)-host defense antibacterial peptides interactions: Role in bacterial resistance and prevention of sepsis. Biochimica et Biophysica Acta (BBA) - Biomembranes 1758, 1513–1522. https://doi.org/10.1016/j.bbamem.2006.05.017

Ruiz Fresneda, M.A., Delgado Martín, J., Gómez Bolívar, J., Fernández Cantos, M.V., Bosch-Estévez, G., Martínez Moreno, M.F., Merroun, M.L., 2018. Green synthesis and biotransformation of amorphous Se nanospheres to trigonal 1D Se nanostructures: impact on Se mobility within the concept of radioactive waste disposal. Environmental Science: Nano 5, 2103–2116. https://doi.org/10.1039/C8EN00221E

Ruiz-Fresneda, M.A., Eswayah, A.S., Romero-González, M., Gardiner, P.H.E., Solari, P.L., Merroun, M.L., 2020. Chemical and structural characterization of Se^{IV} biotransformations by *Stenotrophomonas bentonitica* into Se^{0} nanostructures and volatiles Se species. Environ. Sci.: Nano 7, 2140–2155. https://doi.org/10.1039/D0EN00507J

Ruiz-Fresneda, M.A., Gomez-Bolivar, J., Delgado-Martin, J., Abad-Ortega, M. del M., Guerra-Tschuschke, I., Merroun, M.L., 2019a. The Bioreduction of Selenite under Anaerobic and Alkaline Conditions Analogous to Those Expected for a Deep Geological Repository System. Molecules 24, 3868. https://doi.org/10.3390/molecules24213868

Ruiz-Fresneda, M.A., Gomez-Bolivar, J., Delgado-Martin, J., Abad-Ortega, M. del M., Guerra-Tschuschke, I., Merroun, M.L., 2019b. The Bioreduction of Selenite under Anaerobic and Alkaline Conditions Analogous to Those Expected for a Deep Geological Repository System. Molecules 24, 3868. https://doi.org/10.3390/molecules24213868

Ryan, R.P., Monchy, S., Cardinale, M., Taghavi, S., Crossman, L., Avison, M.B., Berg, G., van der Lelie, D., Dow, J.M., 2009. The versatility and adaptation of bacteria from the genus Stenotrophomonas. Nature Reviews Microbiology 7, 514–525. https://doi.org/10.1038/nrmicro2163

Sabaty, M., Avazeri, C., Pignol, D., Vermeglio, A., 2001. Characterization of the Reduction of Selenate and Tellurite by Nitrate Reductases. Appl. Environ. Microbiol. 67, 5122–5126. https://doi.org/10.1128/AEM.67.11.5122-5126.2001

Salome, K.R., Beazley, M.J., Webb, S.M., Sobecky, P.A., Taillefert, M., 2017. Biomineralization of U(VI) phosphate promoted by microbially-mediated phytate hydrolysis in contaminated soils. Geochimica et Cosmochimica Acta 197, 27–42. https://doi.org/10.1016/j.gca.2016.10.008

Sánchez-Castro, I., Bakkali, M., Merroun, M.L., 2017a. Draft Genome Sequence of *Stenotrophomonas bentonitica* BII-R7 ^{T} , a Selenite-Reducing Bacterium Isolated from Spanish Bentonites. Genome Announcements 5. https://doi.org/10.1128/genomeA.00719-17

Sánchez-Castro, I., Martínez-Rodríguez, P., Jroundi, F., Solari, P.L., Descostes, M., Merroun, M.L., 2020. High-efficient microbial immobilization of solved U(VI) by the Stenotrophomonas strain Br8. Water Research 183, 116110. https://doi.org/10.1016/j.watres.2020.116110

Sánchez-Castro, I., Ruiz-Fresneda, M.A., Bakkali, M., Kämpfer, P., Glaeser, S.P., Busse, H.J., López-Fernández, M., Martínez-Rodríguez, P., Merroun, M.L., 2017b. Stenotrophomonas bentonitica sp. nov., isolated from bentonite formations. International Journal of Systematic and Evolutionary Microbiology 67, 2779–2786. https://doi.org/10.1099/ijsem.0.002016

Santos-Beneit, F., 2015. The Pho regulon: a huge regulatory network in bacteria. Front. Microbiol. 6. https://doi.org/10.3389/fmicb.2015.00402

Sarria Carabalí, M.M., Cortés Páez, L.E., Martín Peinado, F.J., 2015. Evaluación de la recuperación de suelos contaminados por el vertido de Aznalcóllar. Acta Agronómica 64, 156–164. https://doi.org/10.15446/acag.v64n2.44265e

Sasaki, K., Blowes, D.W., Ptacek, C.J., 2008. Spectroscopic study of precipitates formed during removal of selenium from mine drainage spiked with selenate using permeable reactive materials. Geochem. J. 42, 283–294. https://doi.org/10.2343/geochemj.42.283

Schilling, K., Basu, A., Wanner, C., Sanford, R.A., Pallud, C., Johnson, T.M., Mason, P.R.D., 2020. Mass-dependent selenium isotopic fractionation during microbial reduction of seleno-oxyanions by phylogenetically diverse bacteria. Geochimica et Cosmochimica Acta 276, 274–288. https://doi.org/10.1016/j.gca.2020.02.036

Schmid, J., Heider, D., Wendel, N.J., Sperl, N., Sieber, V., 2016. Bacterial Glycosyltransferases: Challenges and Opportunities of a Highly Diverse Enzyme Class Toward Tailoring Natural Products. Front. Microbiol. 7. https://doi.org/10.3389/fmicb.2016.00182

Schröder, I., Rech, S., Krafft, T., Macy, J.M., 1997. Purification and Characterization of the Selenate Reductase from Thauera selenatis *. Journal of Biological Chemistry 272, 23765–23768. https://doi.org/10.1074/jbc.272.38.23765

Selvakumar, R., Ramadoss, G., Mridula P. Menon, Rajendran, K., Thavamani, P., Ravi Naidu, Megharaj, M., 2018. Challenges and complexities in remediation of uranium contaminated soils: A review. Journal of Environmental Radioactivity 192, 592–603. https://doi.org/10.1016/j.jenvrad.2018.02.018

Sharma, S., Tiwari, S., Hasan, A., Saxena, V., Pandey, L.M., 2018. Recent

advances in conventional and contemporary methods for remediation of heavy metal-contaminated soils. 3 Biotech 8. https://doi.org/10.1007/s13205-018-1237-8

Shen, Y., Zheng, X., Wang, X., Wang, T., 2018. The biomineralization process of uranium(VI) by Saccharomyces cerevisiae — transformation from amorphous U(VI) to crystalline chernikovite. Appl Microbiol Biotechnol 102, 4217–4229. https://doi.org/10.1007/s00253-018-8918-4

Shi, L.-D., Lv, P.-L., Niu, Z.-F., Lai, C.-Y., Zhao, H.-P., 2020a. Why does sulfate inhibit selenate reduction: Molybdenum deprivation from Mo-dependent selenate reductase. Water Research 178, 115832. https://doi.org/10.1016/j.watres.2020.115832

Shi, L.-D., Lv, P.-L., Wang, M., Lai, C.-Y., Zhao, H.-P., 2020b. A mixed consortium of methanotrophic archaea and bacteria boosts methane-dependent selenate reduction. Science of The Total Environment 732, 139310. https://doi.org/10.1016/j.scitotenv.2020.139310

Shukla, A., Parmar, P., Saraf, M., 2017. Radiation, radionuclides and bacteria: An in-perspective review. Journal of Environmental Radioactivity 180, 27–35. https://doi.org/10.1016/j.jenvrad.2017.09.013

Shuona, C., Hua, Y., Jingjing, C., Hui, P., Zhi, D., 2017. Physiology and bioprocess of single cell of Stenotrophomonas maltophilia in bioremediation of co-existed benzo[a]pyrene and copper. Journal of Hazardous Materials 321, 9–17. https://doi.org/10.1016/j.jhazmat.2016.09.002

Simate, G.S., Ndlovu, S., 2014. Acid mine drainage: Challenges and opportunities. Journal of Environmental Chemical Engineering 2, 1785–1803. https://doi.org/10.1016/j.jece.2014.07.021

Singh, A., Ulrich, K.-U., Giammar, D.E., 2010. Impact of phosphate on U(VI) immobilization in the presence of goethite. Geochimica et Cosmochimica Acta 74, 6324–6343. https://doi.org/10.1016/j.gca.2010.08.031

Singh, R., 2017. Microbial Biotransformation: A Process for Chemical Alterations. JBMOA 4. https://doi.org/10.15406/jbmoa.2017.04.00085

Singh Sidhu, G.P., 2016. Heavy Metal Toxicity in Soils: Sources, Remediation Technologies and Challenges. APAR 5. https://doi.org/10.15406/apar.2016.05.00166

Sivaswamy, V., Boyanov, M.I., Peyton, B.M., Viamajala, S., Gerlach, R., Apel, W.A., Sani, R.K., Dohnalkova, A., Kemner, K.M., Borch, T., 2011. Multiple mechanisms of uranium immobilization by Cellulomonas sp. strain ES6. Biotechnology and Bioengineering 108, 264–276. https://doi.org/10.1002/bit.22956

Skouri-Panet, F., Benzerara, K., Cosmidis, J., Férard, C., Caumes, G., De Luca, G., Heulin, T., Duprat, E., 2018. In Vitro and in Silico Evidence of Phosphatase Diversity in the Biomineralizing Bacterium Ramlibacter tataouinensis. Frontiers in Microbiology 8. https://doi.org/10.3389/fmicb.2017.02592

Smith, S.G.J., Mahon, V., Lambert, M.A., Fagan, R.P., 2007. A molecular Swiss army knife: OmpA structure, function and expression. FEMS Microbiology Letters 273, 1–11. https://doi.org/10.1111/j.1574-6968.2007.00778.x

Soda, S., Ma, W., Kuroda, M., Nishikawa, H., Zhang, Y., Ike, M., 2018. Characterization of moderately halotolerant selenate- and tellurite-reducing bacteria isolated from brackish areas in Osaka. Bioscience, Biotechnology, and Biochemistry 82, 173–181. https://doi.org/10.1080/09168451.2017.1406794

Song, D., Li, X., Cheng, Y., Xiao, X., Lu, Z., Wang, Y., Wang, F., 2017. Aerobic biogenesis of selenium nanoparticles by Enterobacter cloacae Z0206 as a consequence of fumarate reductase mediated selenite reduction. Sci Rep 7. https://doi.org/10.1038/s41598-017-03558-3

Song, J., Han, B., Song, H., Yang, J., Zhang, L., Ning, P., Lin, Z., 2019. Nonreductive biomineralization of uranium by Bacillus subtilis ATCC–6633 under aerobic conditions. Journal of Environmental Radioactivity 208–209, 106027. https://doi.org/10.1016/j.jenvrad.2019.106027

Sonntag, I., Schwarz, H., Hirota, Y., Henning, U., 1978. Cell envelope and shape of Escherichia coli: multiple mutants missing the outer membrane lipoprotein and other major outer membrane proteins. Journal of Bacteriology 136, 280–285. https://doi.org/10.1128/JB.136.1.280-285.1978

Sousa, T., Chung, A.-P., Pereira, A., Piedade, A.P., Morais, P.V., 2013. Aerobic uranium immobilization by Rhodanobacter A2-61 through formation of intracellular uranium–phosphate complexes. Metallomics 5, 390. https://doi.org/10.1039/c3mt00052d

Sowmya, S., Rekha, P.D., Arun, A.B., 2014. Uranium(VI) bioprecipitation mediated by a phosphate solubilizing Acinetobacter sp. YU-SS-SB-29 isolated from a high natural background radiation site. International Biodeterioration & Biodegradation 94, 134–140. https://doi.org/10.1016/j.ibiod.2014.07.009

Srivastava, N., Mukhopadhyay, M., 2015. Green synthesis and structural characterization of selenium nanoparticles and assessment of their antimicrobial property. Bioprocess Biosyst Eng 38, 1723–1730. https://doi.org/10.1007/s00449-015-1413-8

Staicu, L.C., Barton, L.L., 2017. Bacterial Metabolism of Selenium—For Survival

or Profit, in: van Hullebusch, E.D. (Ed.), Bioremediation of Selenium Contaminated Wastewater. Springer International Publishing, Cham, pp. 1–31. https://doi.org/10.1007/978-3-319-57831-6_1

Staicu, L.C., van Hullebusch, E.D., Lens, P.N.L., 2015. Production, recovery and reuse of biogenic elemental selenium. Environ Chem Lett 13, 89–96. https://doi.org/10.1007/s10311-015-0492-8

Sun, Y., Zhang, R., Ding, C., Wang, Xiangxue, Cheng, W., Chen, C., Wang, Xiangke, 2016. RETRACTED: Adsorption of U(VI) on sericite in the presence of Bacillus subtilis: A combined batch, EXAFS and modeling techniques. Geochimica et Cosmochimica Acta 180, 51–65. https://doi.org/10.1016/j.gca.2016.02.012

Suzuki, Y., Banfield, J.F., 2004. Resistance to, and Accumulation of, Uranium by Bacteria from a Uranium-Contaminated Site. Geomicrobiology Journal 21, 113–121. https://doi.org/10.1080/01490450490266361

Tan, H., Mo, H.-Y., Lau, A., Xu, Y.-M., 2018. Selenium Species: Current Status and Potentials in Cancer Prevention and Therapy. IJMS 20, 75. https://doi.org/10.3390/ijms20010075

Tan, Y., Wang, Yuantao, Wang, Yu, Xu, D., Huang, Y., Wang, D., Wang, G., Rensing, C., Zheng, S., 2018. Novel mechanisms of selenate and selenite reduction in the obligate aerobic bacterium Comamonas testosteroni S44. Journal of Hazardous Materials 359, 129–138. https://doi.org/10.1016/j.jhazmat.2018.07.014

Tan, Y., Yao, R., Wang, R., Wang, D., Wang, G., Zheng, S., 2016. Reduction of selenite to Se(0) nanoparticles by filamentous bacterium Streptomyces sp. ES2-5 isolated from a selenium mining soil. Microb Cell Fact 15, 157. https://doi.org/10.1186/s12934-016-0554-z

Tavares-Carreón, F., Fathy Mohamed, Y., Andrade, A., Valvano, M.A., 2015. ArnT proteins that catalyze the glycosylation of lipopolysaccharide share common features with bacterial *N* -oligosaccharyltransferases. Glycobiology cwv095. https://doi.org/10.1093/glycob/cwv095

Taylor, J.A., Bratton, B.P., Sichel, S.R., Blair, K.M., Jacobs, H.M., DeMeester, K.E., Kuru, E., Gray, J., Biboy, J., VanNieuwenhze, M.S., Vollmer, W., Grimes, C.L., Shaevitz, J.W., Salama, N.R., 2020. Distinct cytoskeletal proteins define zones of enhanced cell wall synthesis in Helicobacter pylori. eLife 9, e52482. https://doi.org/10.7554/eLife.52482

Tchounwou, P.B., Yedjou, C.G., Patlolla, A.K., Sutton, D.J., 2012. Heavy Metal

Toxicity and the Environment, in: Luch, A. (Ed.), Molecular, Clinical and Environmental Toxicology, Experientia Supplementum. Springer Basel, Basel, pp. 133–164. https://doi.org/10.1007/978-3-7643-8340-4_6

Thayer, J.S., Brinckman, F.E., 1982. The Biological Methylation of Metals and Metalloids, in: Stone, F.G.A., West, R. (Eds.), Advances in Organometallic Chemistry. Academic Press, pp. 313–356. https://doi.org/10.1016/S0065-3055(08)60524-9

Theodorakopoulos, N., Chapon, V., Coppin, F., Floriani, M., Vercouter, T., Sergeant, C., Camilleri, V., Berthomieu, C., Février, L., 2015. Use of combined microscopic and spectroscopic techniques to reveal interactions between uranium and Microbacterium sp. A9, a strain isolated from the Chernobyl exclusion zone. Journal of Hazardous Materials 285, 285–293. https://doi.org/10.1016/j.jhazmat.2014.12.018

Thorgersen, M.P., Lancaster, W.A., Ge, X., Zane, G.M., Wetmore, K.M., Vaccaro, B.J., Poole, F.L., Younkin, A.D., Deutschbauer, A.M., Arkin, A.P., Wall, J.D., Adams, M.W.W., 2017. Mechanisms of Chromium and Uranium Toxicity in Pseudomonas stutzeri RCH2 Grown under Anaerobic Nitrate-Reducing Conditions. Frontiers in Microbiology 8. https://doi.org/10.3389/fmicb.2017.01529

Troxell, B., Hassan, H.M., 2013. Transcriptional regulation by Ferric Uptake Regulator (Fur) in pathogenic bacteria. Front. Cell. Infect. Microbiol. 3. https://doi.org/10.3389/fcimb.2013.00059

Tu, H., Lan, T., Yuan, G., Zhao, C., Liu, J., Li, F., Yang, J., Liao, J., Yang, Y., Wang, D., Liu, N., 2019a. The influence of humic substances on uranium biomineralization induced by Bacillus sp. dwc-2. Journal of Environmental Radioactivity 197, 23–29. https://doi.org/10.1016/j.jenvrad.2018.11.010

Tu, H., Yuan, G., Zhao, C., Liu, J., Li, F., Yang, J., Liao, J., Yang, Y., Liu, N., 2019b. U-phosphate biomineralization induced by Bacillus sp. dw-2 in the presence of organic acids. Nuclear Engineering and Technology 51, 1322–1332. https://doi.org/10.1016/j.net.2019.03.002

Tugarova, A.V., Kamnev, A.A., 2017. Proteins in microbial synthesis of selenium nanoparticles. Talanta 174, 539–547. https://doi.org/10.1016/j.talanta.2017.06.013

Urík, M., Boriová, K., Bujdoš, M., Matúš, P., 2016. Fungal Selenium(VI) Accumulation and Biotransformation-Filamentous Fungi in Selenate Contaminated Aqueous Media Remediation: Water. Clean Soil Air Water 44, 610–614. https://doi.org/10.1002/clen.201500100

Verissimo, A.F., Daldal, F., 2014. Cytochrome c biogenesis System I: An intricate

process catalyzed by a maturase supercomplex? Biochimica et Biophysica Acta (BBA) - Bioenergetics 1837, 989–998. https://doi.org/10.1016/j.bbabio.2014.03.003

Vogel, M., Günther, A., Rossberg, A., Li, B., Bernhard, G., Raff, J., 2010. Biosorption of U(VI) by the green algae Chlorella vulgaris in dependence of pH value and cell activity. Science of the Total Environment 409, 384–395. https://doi.org/10.1016/j.scitotenv.2010.10.011

Vorontsov, I.I., Minasov, G., Brunzelle, J.S., Shuvalova, L., Kiryukhina, O., Collart, F.R., Anderson, W.F., 2007. Crystal structure of an apo form of Shigella flexneri ArsH protein with an NADPH-dependent FMN reductase activity. Protein Science 16, 2483–2490. https://doi.org/10.1110/ps.073029607

Wadhwani, S.A., Shedbalkar, U.U., Singh, R., Chopade, B.A., 2018. Biosynthesis of gold and selenium nanoparticles by purified protein from Acinetobacter sp. SW 30. Enzyme and Microbial Technology 111, 81–86. https://doi.org/10.1016/j.enzmictec.2017.10.007

Wang, P., Guo, Q., Ma, Y., Li, S., Lu, X., Zhang, X., Ma, P., 2015. DegQ regulates the production of fengycins and biofilm formation of the biocontrol agent Bacillus subtilis NCD-2. Microbiol. Res. 178, 42–50. https://doi.org/10.1016/j.micres.2015.06.006

Wang, S., Shi, X., 2001. Molecular mechanisms of metal toxicity and carcinogenesis. Mol Cell Biochem 222, 3–9.

Wang, T., Sun, H., Mao, H., Zhang, Y., Wang, C., Zhang, Z., Wang, B., Sun, L., 2014. The immobilization of heavy metals in soil by bioaugmentation of a UV-mutant Bacillus subtilis 38 assisted by NovoGro biostimulation and changes of soil microbial community. Journal of Hazardous Materials 278, 483–490. https://doi.org/10.1016/j.jhazmat.2014.06.028

Wang, T., Yang, L., Zhang, B., Liu, J., 2010. Extracellular biosynthesis and transformation of selenium nanoparticles and application in H2O2 biosensor. Colloids and Surfaces B: Biointerfaces 80, 94–102. https://doi.org/10.1016/j.colsurfb.2010.05.041

Wang, Y., 2002. The function of OmpA in Escherichia coli. Biochem. Biophys. Res. Commun. 292, 396–401. https://doi.org/10.1006/bbrc.2002.6657

Wang, Y., Shu, X., Hou, J., Lu, W., Zhao, W., Huang, S., Wu, L., 2018. Selenium Nanoparticle Synthesized by Proteus mirabilis YC801: An Efficacious Pathway for Selenite Biotransformation and Detoxification. IJMS 19, 3809. https://doi.org/10.3390/ijms19123809

Watts, C.A., Ridley, H., Condie, K.L., Leaver, J.T., Richardson, D.J., Butler, C.S.,

2003. Selenate reduction by *Enterobacter cloacae* SLD1a-1 is catalysed by a molybdenum-dependent membrane-bound enzyme that is distinct from the membrane-bound nitrate reductase. FEMS Microbiology Letters 228, 273–279. https://doi.org/10.1016/S0378-1097(03)00782-1

Wei, W., Ma, R., Sun, Z., Zhou, A., Bu, J., Long, X., Liu, Y., 2018. Effects of Mining Activities on the Release of Heavy Metals (HMs) in a Typical Mountain Headwater Region, the Qinghai-Tibet Plateau in China. IJERPH 15, 1987. https://doi.org/10.3390/ijerph15091987

Wei, Y., Chen, Z., Song, H., Zhang, J., Lin, Z., Dang, Z., Deng, H., 2019. The immobilization mechanism of U(VI) induced by Bacillus thuringiensis 016 and the effects of coexisting ions. Biochemical Engineering Journal 144, 57–63. https://doi.org/10.1016/j.bej.2019.01.013

Wells, M., McGarry, J., Gaye, M.M., Basu, P., Oremland, R.S., Stolz, J.F., 2019. Respiratory Selenite Reductase from *Bacillus selenitireducens* Strain MLS10. J Bacteriol 201, e00614-18, /jb/201/7/JB.00614-18.atom. https://doi.org/10.1128/JB.00614-18

Winkel, L.H.E., Vriens, B., Jones, G.D., Schneider, L.S., Pilon-Smits, E., Bañuelos, G.S., 2015. Selenium Cycling Across Soil-Plant-Atmosphere Interfaces: A Critical Review. Nutrients 7, 4199–4239. https://doi.org/10.3390/nu7064199

Xu, D., Yang, L., Wang, Y., Wang, G., Rensing, C., Zheng, S., 2018. Proteins enriched in charged amino acids control the formation and stabilization of selenium nanoparticles in Comamonas testosteroni S44. Sci Rep 8, 4766. https://doi.org/10.1038/s41598-018-23295-5

Xu, R., Wu, K., Han, H., Ling, Z., Chen, Z., Liu, P., xiong, J., Tian, F., Zafar, Y., Malik, K., Li, X., 2018. Co-expression of YieF and PhoN in Deinococcus radiodurans R1 improves uranium bioprecipitation by reducing chromium interference. Chemosphere 211, 1156–1165. https://doi.org/10.1016/j.chemosphere.2018.08.061

Yan, S., Cheng, K.Y., Ginige, M.P., Zheng, G., Zhou, L., Kaksonen, A.H., 2020. High-rate microbial selenate reduction in an up-flow anaerobic fluidized bed reactor (FBR). Science of The Total Environment 749, 142359. https://doi.org/10.1016/j.scitotenv.2020.142359

Yang, H.-C., Fu, H.-L., Lin, Y.-F., Rosen, B.P., 2012. Pathways of Arsenic Uptake and Efflux, in: Current Topics in Membranes. Elsevier, pp. 325–358. https://doi.org/10.1016/B978-0-12-394390-3.00012-4

Yang, H.-C., Rosen, B.P., 2016. New mechanisms of bacterial arsenic resistance.

Biomedical Journal 39, 5–13. https://doi.org/10.1016/j.bj.2015.08.003

Yang, T., Chen, M.-L., Wang, J.-H., 2015a. Genetic and chemical modification of cells for selective separation and analysis of heavy metals of biological or environmental significance. TrAC Trends in Analytical Chemistry 66, 90–102. https://doi.org/10.1016/j.trac.2014.11.016

Yang, T., Chen, M.-L., Wang, J.-H., 2015b. Genetic and chemical modification of cells for selective separation and analysis of heavy metals of biological or environmental significance. TrAC Trends in Analytical Chemistry 66, 90–102. https://doi.org/10.1016/j.trac.2014.11.016

Yang, X., Dai, X., Jin, H., Lin, G., Wang, Z., Song, Y., Zhang, W., Man, C., Jiang, Y., n.d. Physicochemical and transcriptomic responses of Lactobacillus brevis JLD715 to sodium selenite. Journal of the Science of Food and Agriculture n/a. https://doi.org/10.1002/jsfa.11073

Yung, M.C., Jiao, Y., 2014. Biomineralization of Uranium by PhoY Phosphatase Activity Aids Cell Survival in Caulobacter crescentus. Applied and Environmental Microbiology 80, 4795–4804. https://doi.org/10.1128/AEM.01050-14

Yung, M.C., Ma, J., Salemi, M.R., Phinney, B.S., Bowman, G.R., Jiao, Y., 2014. Shotgun Proteomic Analysis Unveils Survival and Detoxification Strategies by *Caulobacter crescentus* during Exposure to Uranium, Chromium, and Cadmium. J. Proteome Res. 13, 1833–1847. https://doi.org/10.1021/pr400880s

Yung, M.C., Park, D.M., Overton, K.W., Blow, M.J., Hoover, C.A., Smit, J., Murray, S.R., Ricci, D.P., Christen, B., Bowman, G.R., Jiao, Y., 2015. Transposon Mutagenesis Paired with Deep Sequencing of Caulobacter crescentus under Uranium Stress Reveals Genes Essential for Detoxification and Stress Tolerance. Journal of Bacteriology 197, 3160–3172. https://doi.org/10.1128/JB.00382-15

Zammit, C.M., Brugger, J., Southam, G., Reith, F., 2014. In situ recovery of uranium — the microbial influence. Hydrometallurgy 150, 236–244. https://doi.org/10.1016/j.hydromet.2014.06.003

Zhang, J., Song, H., Chen, Z., Liu, S., Wei, Y., Huang, J., Guo, C., Dang, Z., Lin, Z., 2018. Biomineralization mechanism of U(VI) induced by Bacillus cereus 12-2: The role of functional groups and enzymes. Chemosphere 206, 682–692. https://doi.org/10.1016/j.chemosphere.2018.04.181

Zhang, J., Wang, Y., Shao, Z., Li, J., Zan, S., Zhou, S., Yang, R., 2019. Two selenium tolerant Lysinibacillus sp. strains are capable of reducing selenite to elemental

Se efficiently under aerobic conditions. Journal of Environmental Sciences 77, 238–249. https://doi.org/10.1016/j.jes.2018.08.002

Zhang, X., Wu, W., Virgo, N., Zou, L., Liu, P., Li, X., 2014. Global transcriptome analysis of hexavalent chromium stress responses in Staphylococcus aureus LZ-01. Ecotoxicology 23, 1534–1545. https://doi.org/10.1007/s10646-014-1294-7

Zhang, Z., Adedeji, I., Chen, G., Tang, Y., 2018. Chemical-Free Recovery of Elemental Selenium from Selenate-Contaminated Water by a System Combining a Biological Reactor, a Bacterium–Nanoparticle Separator, and a Tangential Flow Filter. Environ. Sci. Technol. 52, 13231–13238. https://doi.org/10.1021/acs.est.8b04544

Zheng, H., Wisedchaisri, G., Gonen, T., 2013. Crystal Structure of a Nitrate/Nitrite Exchanger. Nature 497, 647–651. https://doi.org/10.1038/nature12139

Zhuang, P., Zou, B., Li, N.Y., Li, Z.A., 2009. Heavy metal contamination in soils and food crops around Dabaoshan mine in Guangdong, China: implication for human health. Environ Geochem Health 31, 707–715. https://doi.org/10.1007/s10653-009-9248-3